Katarzyna Ewa Lewińska MSc

Multi-scale detection of drought impact on the mountain forest of South Tyrol

DOCTORAL THESIS

to achieve the university degree of

Doktorin der technischen Wissenschaften

submitted to

Graz University of Technology

Supervisor

Univ.-Prof. Dr.rer.nat. Dipl.-Forstwirt Mathias Schardt

Institute of Geodesy
Working Group Remote Sensing and Photogrammetry

Faculty of Mathematics, Physics and Geodesy

Graz, December 2016

AFFIDAVIT

I declare that I have authored this thesis independently, that I have not used other than the declared sources/resources, and that I have explicitly indicated all material which has been quoted either literally or by content from the sources used. The text document uploaded to TUGRAZonline is identical to the present doctoral thesis.

Date

Signature

I almost wish I hadn't gone down the rabbit-hole
– and yet – and yet – it's rather curious, you know, this sort of life!
I do wonder what *can* have happened to me!

– Lewis Carroll, *Alice's Adventures in Wonderland*

Bolzano – Graz – Ispra – Biała Podlaska – Warsaw – London – Szczecin

CONTENTS

LIST OF FIGURES

LIST OF TABLES

1. INTRODUCTION

1.1. Climate change threads

Noticeable changes in the local and global weather patterns has been detected during the past century (EEA, 2012; IPCC, 2013). Observed transformation of temperature, precipitation and insolation results in prolonged climatic anomaly and has been highlighted in numerous studies (e.g., Breshears et al., 2005; Dai, 2011a, 2011b; EEA, 2009; Lloyd-Hughes & Saunders, 2002; Migliavacca et al., 2008; Philipona, Behrens, & Ruckstuhl, 2009; Schär et al., 2004) calling for attention and appropriate reception (EEA, 2012; IPCC, 2013). The most distinct alternation has been recognized for the global mean temperature (Dai, 2011a; Beniston, 2013), which between 1880 and 2012 increased by 0.85°C (land and ocean together) with the most prominent rise reported during the last thirty years (IPCC, 2013). Along with temperature, also precipitation patterns shifted extensively, revealing a worldwide rainfall decrease with considerable regionalization of drying as well as, wettening trends (Dai, 2011a). Consequently, arising aridity and elevated temperature result in increased number and scale of occurring dry periods and escalated extreme drought events (Dai, 2011b). According to recently made climatic predictions, further warming and rainfall scarcities concluding in advancing aridity are expected (Dai, 2011a). Sheffield and Wood (2007) suggest that by the end of the 21st century short-term drought events (4-6 months) will double their spatial extend and probability, whereas long-term drought events will become threefold more frequent.

Drought is one of the most common environmental disasters nowadays. It affects the largest number of people and the biggest area worldwide (Mishra & Singh, 2010; Ivits *et al.*, 2014), drawing attention of scientists, economists, policy makers, as well as the public (EEA, 2010a). Observed climate change, thus emerging drought impact is not uniform around the globe. According to Giorgi (2006) Europe and in particular the Mediterranean are regions of potentially the strongest climate alternation. Only since the year 2000 Europe suffered from three massive summer heat-waves of 2003 (Bréda *et al.*, 2006; Rebetez *et al.*, 2006, 2008; Granier *et al.*, 2007; Reichstein *et al.*, 2007), 2006 (Rebetez *et al.*, 2008; Ivits *et al.*, 2014) and 2010 (Barriopedro *et al.*, 2011; EEA, 2012; Ivits *et al.*, 2014), which had strong impact on the natural environment and agriculture, thus also on the society and economics of the continent (EEA, 2010a).

1.2. Drought definitions, measures and vegetation impact

Drought is a very complex and severe weather related natural hazard called by some a 'creeping phenomenon' due to its ambiguous inception and end (Mishra & Singh, 2010). Drought perception is relative and region dependant, the same as its course and impact, which leads to confusion, as well as problems in understanding and defining drought in unified terms at a global scale (Mishra & Singh, 2010).

A considerable majority of conceptual drought definitions (selected examples in Table 1) limits drought drivers only to precipitation, excluding temperature, insolation and wind that together shape water stress through evapotranspiration properties (Lloyd-Hughes & Saunders, 2002). Moreover, relative character of a drought phenomenon is frequently defined by divergence from local long-term normal conditions. Conversely, operational drought definitions provide less elusive,

mathematically based phenomenon description with identified onset, length, severity, intensity and frequency of the event. However, such precise definitions have only local application and in some cases work only under specific circumstances.

Table 1 Selected conceptual drought definitions (subjective selection).

Definition	Source
Drought is a recurring extreme climate event over land characterized by below-normal precipitation over a period of several months to several years or even a few decades.	(Dai, 2011b)
Drought is an 'absence of rainfall for a period of time long enough to result in depletion of soil water and injury to plants'	(Kramer, 1983)
Droughts are distinct from water scarcity, being a natural phenomenon defined as a sustained and extensive occurrence of below-average water availability.	(EEA, 2009b)
Drought stress occurs whenever soil water drops below a threshold inducing restrictions to growth and transpiration.	(Bréda *et al.*, 2006)
Drought is a natural phenomenon resulting from less than normal precipitation over a large area for an extended period of time.	(Feyen & Dankers, 2009)
Drought is a chronic, potential natural disaster characterized by a prolonged, abnormal water shortage.'	(Ghulam *et al.*, 2006)

Although drought almost always originates from precipitation shortfall, its relative character, in terms of perception and impacted environment, determines identification of four main drought concepts (Wilhite & Glantz, 1985):

- Meteorological drought, which occurs when precipitation amount in a given period is depleted comparing to the region specific climatological criteria;
- Hydrological drought, which is defined as precipitation deficit that results in reduced surface water resources and affects local water management;
- Agricultural drought, which is a period when soil moisture is insufficient to meet crops requirements resulting in vegetation stress and eventually crop failure (this type of drought redefines meteorological and hydrological conditions, putting vegetation condition as a reference);
- Socio-economic drought, which defines water supplies as an economic good, and whenever water demand exceeds supply (due to meteorological and or hydrological drought or simply elevated water use) a drought event is identified.

Mishra & Singh (2010) further extended this classification by a ground water drought, which is defined through diminished groundwater level, as well as lowered recharge and discharge amounts.

Due to a recognized economical, societal and environmental impact of arising aridity detailed drought monitoring became lately of high importance. Enhanced drought understanding is a key to identify, mitigate, predict or even prevent arising hazards. Diverse drought perceptions are reflected in multitude of related metrics, which through addressing selected event manifestations allow on phenomena detection,

description, quantification and monitoring. According to Niemeyer (2008) more than 80 drought indices can be easily identified, with twice as much metrics developed and published worldwide. Drought indices can be systematized with respect to employed datasets and a background domain into six main categories (after Niemeyer (2008)):

- Meteorological drought indices, which employ variables originally measured at meteorological stations such as precipitation amounts, temperature or insolation (e.g. Standardized Precipitation Index (SPI; Mckee et al., 1993) and Standardized Precipitation-Evapotranspiration Index (SPEI; Vicente-Serrano *et al.*, 2010));
- Comprehensive drought indices, which combine meteorological variables with local soil moisture information, accounting on local evapotranspiration conditions (e.g. Palmer Drought Severity Index (PDSI; Palmer, 1965) and its self-calibrating version (scPDSI; Wells *et al.*, 2004));
- Agricultural drought indices, which account mainly on evapotranspiration conditions and assess soil moisture capacity to foster agricultural crops (e.g. Soil Water Index (SWI; Gouveia *et al.*, 2009) and Crop Moisture Index (CMI; Palmer, 1968));
- Hydrological drought indices, which focus on stream-flow and discharge values, analyzing local water balance of a catchment (e.g. Surface Water Supply Index (SWSI; Doesken *et al.*, 1991));
- Remote sensing-based drought indices, which take an advantage of Earth Observation domain, and exploit, among others, photosyntetical vegetation response, vegetation moisture content, temperature, as well as ground moisture availability (e.g. Normalized Difference Vegetation Index (NDVI; Tucker, 1979), Normalized Difference Water Index (NDWI; Gao, 1996), FAPAR (Fraction of Absorbed Photosynthetically Active Radiation; Gobron *et al.*, 2006), Land Surface Temperature (LST; Ghulam *et al.*, 2006), Modified Perpendicular Drought Index (MPDI; Ghulam *et al.*, 2007) or Microwave Integrated Drought Index (MIDI; Zhang & Jia, 2013));
- Combined drought indices, which base on consolidation of traditional on-station meteorological measurements with remote sensed data (e.g. Vegetation Drought Response Index (VegDRI; Brown *et al.*, 2008).

Traditional implementations of meteorological or comprehensive drought measures, such as SPI or scPDSI, are based on long time series of on-station meteorological observations. Available records are used to inspect weather conditions at a given point, and statistically recognize 'normal' as well as 'extreme' meteorological events. Although these approaches provide a reliable relative drought assessment, especially when accounting on local evapotranspiration properties (Rebetez et al., 2006; Vicente-Serrano et al., 2010), they limit spatial understanding of the phenomenon. Spatial extrapolation of point values can be a solution; however goodness of calculation depends greatly on region complexity and density of measurements. Remote sensing techniques provide here considerable advantage, assuring consistent wall-to-wall observations with sensible time and space resolution. Variety of utilized electromagnetic spectra and sensors ensures, among others, information on precipitation, humidity, evapotranspiration, soil moisture and vegetation condition, which can be employed not only in remotely sensing-based drought indices, but also

serves for traditional meteorological or agricultural drought measures. Remarkably, vegetation oriented remote-sensed indicators yield direct information on actual vegetation status, which is an advantage comparing with meteorologically governed models of plant condition.

1.3. Vegetation drought impact from the optical remote sensing perspective

Considering vegetation drought impact, hot and arid conditions translate into decrease of vegetation water content and change of biochemical properties, concluding in diminished plant vigor, productivity as well as, depleted leaf area. These subtle changes are, among others, coupled with adjustments of vegetation reflectance properties. Water-stress hampered photosynthetical activity reveals in diminished absorption in the blue (450-495 nm) and red (620-750 nm) portion of the electromagnetic spectrum. As reflectance in these bandwidths increases, leafs discoloration from green to yellow, red and brown is observed. Moreover, drought driven lowered vegetation water content intensifies reflectance in the infrared portion of the electromagnetic spectrum (0.7-2.5 µm), whereas related cell structure changes are expressed in a decrease in the 0.7-1.1 µm bandwidth. In the worst case scenario, green vegetation dies out, which further alters the electromagnetic response. Moreover, drought related change in vegetation condition and density impacts also thermal and microwaves bands.

Aforementioned unique vegetation reflectance properties observed in the visible and infrared spectrum are employed in a wide collection of vegetation condition oriented indices. While some, such as FAPAR or NDVI aim on photosynthetic plant activity, the other explore cell structure and water content (e.g. Normalized Difference Infrared Index (NDII; Hardisky et al., 1983), Normalized Difference Water Index (NDWI; Gao, 1996) or Normalized Burn Ratio (NBR; van Wagtendonk et al., 2004) aka Normalized Burn Ratio Index (NBRI; Huang et al., 2010) or NDII7 (Normalized Difference Infrared Index band 7; Rahimzadeh Bajgiran *et al.*, 2009) which adopts MODIS band 7 short infrared information; see Appendix 1 for a review), or even amount of green matter (e.g. LAI (Chen *et al.*, 1997)).

Due to a great simplicity, robustness, as well as abundance of data, NDVI and various NDII indices gained high recognition in drought related vegetation monitoring. Despite some limitations such as saturation effect (Huete *et al.*, 2002), sensitivity to soil information (Gao, 1996), species dependent value range, and nonlinear correlation with precipitation (e.g. Peters *et al.*, 2002; Ji & Peters, 2003; Wang *et al.*, 2003; Gouveia *et al.*, 2009; Horion *et al.*, 2013) they are successfully applied in local, regional and wall-to-wall studies (e.g. Breshears et al., 2005; Gouveia et al., 2009; Ji and Peters, 2003; Lotsch et al., 2005; Rahimzadeh Bajgiran et al., 2009; Wang and Qu, 2009).

Many recent studies address vegetation condition and drought impact through MODIS and Landsat derived NDVI and NDII7 (aka NBRI) measures approximated as:

$$\mathrm{NDVI} = \frac{\rho 0.86 - \rho 0.67\mu\mathrm{m}}{\rho 0.86 + \rho 0.67\mu\mathrm{m}} \quad [1]$$

and

$$\mathrm{NDII7\ (aka\ NBRI)} = \frac{\rho 0.86\mu\mathrm{m} - \rho 2.2\mu\mathrm{m}}{\rho 0.86\mu\mathrm{m} + \rho 2.2\mu\mathrm{m}} \quad [2]$$

where the far infrared spectrum is not affected by the soil water content (Cheng *et al.*, 2007). Successful detection of pest-defoliation (e.g. Debeurs & Townsend, 2008; Spruce *et al.*, 2011) and drought induces productivity drop (Gu *et al.*, 2007; Caccamo *et al.*, 2011) proved MODIS efficiency considering long, as well as short-term drought monitoring (Caccamo *et al.*, 2011; Kharuk *et al.*, 2013). Landsat, although has lower temporal resolution, is also apt for drought disturbance detection (Volcani *et al.*, 2005; Dorman *et al.*, 2013), especially when taking advantage from high geometric resolution as well as long time series of observations (Cohen *et al.*, 2010; Kennedy *et al.*, 2010, 2014). Furthermore, comparable technical setup of Terra/Aqua and Landsat platforms as well as correspondence in MODIS and TM/ETM+ bands made it possible to fuse both datasets (e.g. Potapov *et al.*, 2008; Hwang *et al.*, 2011; Gevaert & García-Haro, 2015) taking advantage of MODIS acquisition frequency and Landsat resolution (Gao *et al.*, 2006; Gao, 2013).

1.4. Climate change and resulting drought in the Alpine forest

The Alps are not only a local hot-spot of climate change (Auer *et al.*, 2007), but also one of the most vulnerable to climate change regions in Europe (Theurillat & Guisan, 2001; Beniston, 2005; EEA, 2009a; EU, 2009; Rammig *et al.*, 2010). During the past century alone, the Alps experienced an average temperature rise of 2°C, which is twice as much as has been observed for the rest of the continent (Auer *et al.*, 2007). This elevated change can be explained through prolonged sunshine duration (Auer *et al.*, 2007; Wastl *et al.*, 2012) and drop in wind speed over the region (Matulla *et al.*, 2007), which combined with the global temperature increase result in this local extreme. Moreover, recent decades revealed regional variations of precipitation patterns with wettening trends for the North-West and drying tendencies in the South-East part of the Alps (Schmidli *et al.*, 2002; Auer *et al.*, 2005). All observed changes result in increasing dryness of the alpine climate (Calanca, 2007) with even more severe advance to come (Gebetsroither *et al.*, 2013; Zimmermann *et al.*, 2013a; Gobiet *et al.*, 2014). Climatic change model run for the Alps using the moderate scenario A1B (IPCC, 2000), projected further temperature increase of 3.3°C until the end of the 21st century (Gobiet *et al.*, 2014), with even higher amplitude for regions placed above 1500 m asl (EEA, 2009a). Foreseen precipitation patterns are also overall negative, although increase of snowfall on higher altitudes is expected (Beniston, 2012). Despite this, snow cover will decrease dramatically considering its duration as well as coverage (Beniston, 2012; Gobiet *et al.*, 2014).

All aforementioned are expected to result in further development of rainfall scarcity and drought risk over the Alps (e.g. Calanca, 2007; Gebetsroither *et al.*, 2013). An additional problem will be uneven precipitation distribution over a year with very dry period of early spring and summer (Beniston, 2012), which is considered as the most important for vegetation growth. As indicated by Gebetsroither *et al.* (2013) areas located on lower altitudes (valley floors and lower parts of slopes) will be especially exposed to rainfall decrease and heat waves occurring during the vegetation season. Although diverse climate models vary significantly among each other, most of them agrees on warming and drying trend of the changes (Zimmermann *et al.*, 2013a).

Despite the fact that alpine environment has a considerable natural change resistance capacity (Theurillat & Guisan, 2001), all aforementioned factors translate into an

increasing thread for reach biodiversity of the Alps (EEA, 2009a; Engler *et al.*, 2011). In fact, the alpine environment already undergoes climate change triggered uphill shift of vegetation belts (Gehrig-Fasel *et al.*, 2007; Vittoz *et al.*, 2008; Rigling *et al.*, 2013), an alternation of phenological phases (Theurillat & Guisan, 2001; Studer *et al.*, 2005, 2007), intensification of local dieback processes (e.g. Minerbi et al., 2006; Theurillat and Guisan, 2001), increased aridity and more frequent drought events (e.g. Gebetsroither *et al.*, 2013), as well as an overall sway of ecological balance (Körner, 2003; Courbaud *et al.*, 2010; Hanewinkel *et al.*, 2013; Bussotti *et al.*, 2014). Drought implications are particularly important for comprehensive monitoring of the alpine forest (Standing Forestry Committee Ad Hoc Working Group III on Climate Change and Forestry, 2010) – the biggest and the most biodiverse land cover of the Alps (Kapos and Iremonger 1998; Körner 2003 p 13).

Drought vegetation impact, although seemingly apparent, while considered in a long term scenario and on a regional to global scale, is still entangled and loaded with uncertainty (Schoene & Bernier, 2012). Forest drought influence is yet more complex because even though a primary dry spell does not directly lead to a dieback (e.g. Bigler et al., 2006; Dobbertin et al., 2005; Minerbi et al., 2006), it makes trees more vulnerable to secondary damages and disturbances such as windfalls, pest outbreaks (Battisti *et al.*, 2006) or fungus, parasites and pathogens infestations (Rigling *et al.*, 2013). Furthermore, trees response to drought stress is lagged (Bigler *et al.*, 2006; Pichler & Oberhuber, 2007; Etzold *et al.*, 2014) and governed by site-specific environmental conditions (Etzold *et al.*, 2014), not to mention inter- and intra- species differences (Lévesque *et al.*, 2014). This intricacy is a great hindrance not only for sustainable resource management and silviculture (Schoene & Bernier, 2012), but also for carbon sink efficiency modeling (Ma *et al.*, 2012; He *et al.*, 2014) and resulting climate change scenarios (Bonan, 2008). Consequently, vegetation water stress response analyses, with a particular insight on forest, are recently becoming a crucial aspect of comprehensive environmental monitoring (Standing Forestry Committee Ad Hoc Working Group III on Climate Change and Forestry, 2010; He *et al.*, 2014).

Although extensive environmental monitoring has a relatively long history in the Alps (Gobiet *et al.*, 2014), drought forest issue started to be frequently addressed only for the last 20 years, which coincides with extreme heat waves events and arising climate change awareness. Dense meteorological monitoring network with long observation records not only ensures a reliable data source for climatic analyses (Auer *et al.*, 2007; van der Schrier *et al.*, 2007), but also provides a solid background for dendrochronological surveys. The latter are especially crucial yielding information on trees development governed by drought stress conditions (e.g. Rigling *et al.*, 2001; Eilmann *et al.*, 2006; Pichler & Oberhuber, 2007; Weber *et al.*, 2007; Castagneri *et al.*, 2014). Although such surveys are important from a physiological viewpoint, they are limited to small sites or transects (Lévesque *et al.*, 2014), which restrain holistic understanding of the complex alpine forest environment. Especially essential are studies exploring vegetation competition (e.g. Eilmann *et al.*, 2006; Pichler & Oberhuber, 2007; Chauchard *et al.*, 2010; Rigling *et al.*, 2013) and comparing trees responses under diverse local environmental conditions (Pichler & Oberhuber, 2007; Weber *et al.*, 2012).

A remarkable number of recently conducted dendrochronological drought analyses focuses on Scots Pine (*Pinus sylvestris*) trees of dry inner-alpine valleys, which are observed to decline lately. Detailed studies revealed that this pioneer tree species populating sunny and xeric sites is highly sensitive to drought, and under water stress conditions suffer significant radial growth reduction (Rigling *et al.*, 2001; Leuzinger *et al.*, 2005; Eilmann *et al.*, 2006; Pichler & Oberhuber, 2007; Weber *et al.*, 2007; Lévesque *et al.*, 2014b) and an overall decline (Vacchiano *et al.*, 2012; Feichtinger *et al.*, 2014). Moreover, prolonged and severe dry spells in 00's have resulted in local Scots Pine diebacks (Dobbertin *et al.*, 2005; Minerbi *et al.*, 2006; Rigling *et al.*, 2013). Further inspection showed that Scots Pine trees located on lower elevations are more prone to suffer from aridity (Dobbertin *et al.*, 2005; Vacchiano *et al.*, 2012; Rigling *et al.*, 2013), especially when placed on north exposed slopes (Vacchiano *et al.*, 2012). In contrary, when considering higher elevations, sun-exposed locations revealed stronger decline (Pichler & Oberhuber, 2007; Vacchiano *et al.*, 2012). Moreover, some dendrochronological surveys highlight not straightforward Scots Pine performance in relation to precipitation and temperature variability, where trees growth depends on previous season conditions (Lévesque *et al.*, 2014), in particular on summer temperature (Pichler & Oberhuber, 2007). Importantly, tree mortality can occur even several years after a drought stress event (Bigler *et al.*, 2006).

Drought response investigated for other tree species present in the region showed strong diversification between xeric and mesic sites. While the latter were expected to foster usually increased productivity and growth responses (Lévesque *et al.*, 2014), the former were associated with reduced vitality and trees decline (Theurillat & Guisan, 2001; Eilmann *et al.*, 2006). On the other hand, some studies documented contradictory behavior, with the strongest drought impact observed for stands at mesic locations (European Beech - *Fagus sylvatica L*: Weber *et al.*, 2012; Castagneri *et al.*, 2014; Norway Spruce - *Picea Abies:* Castagneri *et al.*, 2014; Lévesque *et al.*, 2014*;* European Larch - *Larix deciduas*: Lévesque *et al.*, 2014). These observations can be explained through inadequate trees adaptation capacity to arising aridity conditions comparing with stands already living near their ecological limits. Moreover, additional factors such as CO_2 concentration (Leuzinger *et al.*, 2005) or tree competition (Eilmann *et al.*, 2006; Pichler & Oberhuber, 2007; Chauchard *et al.*, 2010; Giuggiola *et al.*, 2013; Rigling *et al.*, 2013) even further obscure straightforward understanding of the stress related with physiological processes.

Based on local dendrochronological and physiological studies regional projections and models of further forest development and mortality are conducted for the Alps (Manusch *et al.*, 2012). It is still arguable how climate change coincides with arising precipitation deficit, and how recurrent heat waves will influence the alpine forest. The uncertainty load is even greater as progressing alternation of weather patterns had already modified trees weather-growth dependence (Coppola et al., 2012).

As documented, temperature increase shifts trees physiological boundary upslope (Moser *et al.*, 2011), resulting in an increase of the forest area (Gehrig-Fasel *et al.*, 2007; Vittoz *et al.*, 2008). Although vegetation response on the treeline is a crucial indicator in the dendro-ecological studies (Körner 2003 p 88), it should be considered that the actual timberline is placed below the potential treeline (Pecher *et al.*, 2011; Vittoz *et al.*, 2013), thus some of the observed changes may not be triggered directly

by the climate alternation (Gehrig-Fasel *et al.*, 2007; Courbaud *et al.*, 2010; Castagneri *et al.*, 2014). Modification of precipitation and temperature patterns will also impact the lower ecological boundaries of plant occurrence, exposing lower placed regions to alien tree species invasion. Increasing aridity is naturally favorable for drought-resistant Mediterranean species such as Downy Oak (Rigling *et al.*, 2013), Hop Hornbeam (Theurillat & Guisan, 2001) and Manna Ash, which are expected to replace European Beech and Norway Spruce (Zimmermann *et al.*, 2013b). These new conditions will severely affect not only biodiversity of the alpine forest swaying existing ecological balance (Körner, 2003; Courbaud *et al.*, 2010; Hanewinkel *et al.*, 2013), but will also change its economic value and carbon sink capacity (Hanewinkel *et al.*, 2013; Rigling *et al.*, 2013). Although, the forest productivity is expected to increase at first (Jolly *et al.*, 2005; Reichstein *et al.*, 2007; Etzold *et al.*, 2014), in the long run trees strength will most probably reduce in the effect of dry conditions and secondary damages (Hanewinkel et al., 2013). Furthermore, elevated aridity leads to already increased fire thread (Wastl *et al.*, 2012; Ascoli *et al.*, 2013).

1.5. Motivation, objectives and outline

Climate alternation and resulting increasing frequency and intensity of extreme weather events govern an arising need for efficient and precise forest targeted drought monitoring in the Alps. Although there is a large number of single site studies that provide essential dendrochronological and physiological information (Moser *et al.*, 2011; Lévesque *et al.*, 2014b), comprehensive analyses covering the Alpine region as a whole, or its substantial part, are still in deficiency (BMU, 2007).

Addressing the emerging demand for better understanding of forest response to drought conditions and resulting productivity consequences (Standing Forestry Committee Ad Hoc Working Group III on Climate Change and Forestry, 2010), this thesis presents an approach for a large-scale alpine forest monitoring based on a synergy between meteorological observations and remotely sensed data explored using PCA decomposition. The study exploits MODIS and Landsat vegetation time series, coupled with the scPDSI. Analyses are conducted for the region of South Tyrol and focus on drought conditions between 2001 and 2012.

The following main research questions are investigated:

- is MODIS an appropriate data source for forest drought monitoring within complex mountain environment;
- can PCA decomposition be successful in identifying subtle drought induced forest status variability present in time series of remotely sensed vegetation indices, and under what conditions the convolution is the most effective;
- which satellite datasets ensure better recognition of subtle drought impact on the alpine forest environment: time series of enhanced temporal resolution and moderate spatial resolution (herein MODIS) or datasets with high spatial resolution but limited temporal repetition (herein Landsat).

Furthermore, the study ensures a general but also quite specific overview of identified drought impact on South Tyrolean forest.

The thesis comprises six chapters including the Introduction section.

Chapter 2 provides a general background for analyses. All datasets used in the study are presented here with detailed description of conducted preprocessing steps. This part includes also mathematical principles of PCA, as well as gives an overview of environmental conditions in South Tyrol.

In Chapter 3 drought conditions in South Tyrol are explored by the means of on-station precipitation and temperature measurements employed in the scPDSI. A synthesis of 2001-2012 meteorological conditions is attained through the S-mode PCA. The identified drought temporal variability provides a reference for the further remote sensing based analyses.

Chapter 4 presents 16-day MODIS NDVI and NDII7 2001-2012 time series analyzed using the S-mode PCA. Multiple method settings and data setups are investigated in a search for a vegetation response to the scPDSI-identified temporal drought variability. The most prominent results are spatially projected and further inspected regarding drought induced forest phenological changes.

In Chapter 5 forest drought condition in South Tyrol between 2001 and 2012 are investigated using the S-mode PCA of Landsat NDVI and NBRI time series. Due to data limitation and frequent cloud cover the survey is based on yearly composites assembled from summer acquisitions only. The resulting temporal variability is verified against the scPDSI patterns, with the most reliable scores spatially projected and further analyzed with respect to the forest phenology. The latter is done at 250 m MODIS resolution.

Finally, Chapter 6 presents a synthesis of results, addresses the research questions, as well as gives perspectives for forest drought monitoring in the Alps.

Results and findings presented in Chapters 1 to 4 compose the following publications:

- Lewińska K.E., Ivits E, Schardt M., Zebisch M., 2016, *Alpine forest drought monitoring in South Tyrol: PCA based synergy between scPDSI data and MODIS derived NDVI and NDII7 time series*, Remote Sensing, 8(8), DOI:10.3390/rs8080639
- Lewińska K.E., Ivits E, Schardt M., Zebisch M, *Drought impact on phenology and productivity of alpine forest – case study of South Tyrol 2001-2012 inspected with MODIS time series*, in preparation.

2. MATERIALS AND METHODS

2.1. Study area of South Tyrol – physical settings

South Tyrol, known also as Südtirol or Alto Adige, is a northmost province of the Italian Republic (Figure 1) with a capital in Bolzano. The region covers 7400 km^2 and is an autonomous area that shares its borders with Switzerland and Austria. Since 1996 it is a central part of Tyrol-South Tyrol-Trentino Euroregion.

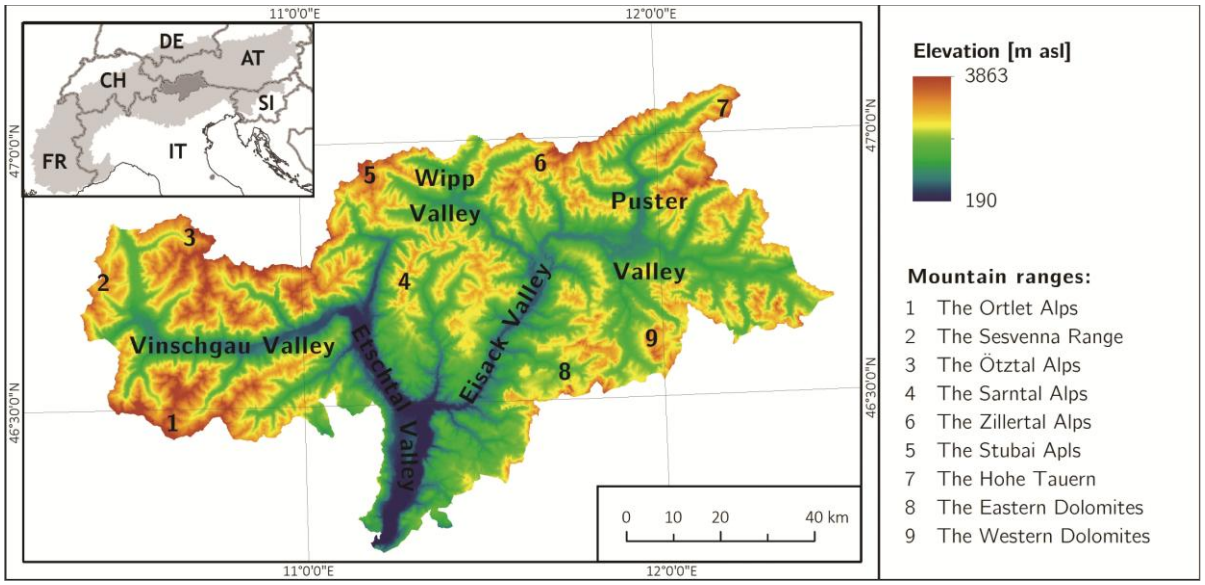

Figure 1 Upper left: South Tyrol location with respect to the national borders and the Alps defined according to the Alpine Convention (Ruffini *et al.*, 2007). Main plain: topography of the region with location of five main valleys and nine mountain ranges.

South Tyrol is located in the central part of the Alps, on a border between formations of the Central Eastern Alps and the Southern Limestone Alps. The land ranges here between 190 m asl (southern Etschtal Valley) and 3905 m asl (Mount Ortler, the highest peak of the Eastern Alps), with 86% of the area placed above 1000 m asl and over 40% above 2000 m asl. (*South Tyrol in figures*, 2012). It is a typical alpine region characterized by a complex and diverse orography. In topography of South Tyrol five main valleys can be identify (Figure 1): Vinschgau (Val Venosta), Etschtal (Etschtal/Val d'Adige), Eisack (Eisacktal/Valle Isarco), Wipp (Wipptal/Alta Val d'Isarco) and Puster (Pustertal/Val Pusteria).

From the geological viewpoint, the area of South Tyrol comprises mainly metamorphic rocks of Austroalpine nappes (Central Eastern Alps) in the North and West part, as well as magmatic and sedimentary Southalpine formations in the South and South-East (Southern Limestone Alps). Two are separated by the Periadriatic Seam – a prominent collision fault between the Apulian and European plates, which resulted in a still active orogen of the Alps (Stingl & Mair, 2005).

Nine main mountain ranges of South Tyrol (Figure 1) are grouped as follow:

- The Ortler Alps, the Sesvenna Range, the Ötztal Alps, the Sarntal Alps, the Zillertal Alps and the Stubai Alps belong to the Central Eastern Alps build out of, so called, Old Crystalline units of metamorphic rocks;
- The Hohe Tauern of the geological structure of the Hohe Tauern window in the Central Eastern Alps build out of gneiss and schist;
- The Eastern and Western Dolomites belonging to the Southern Limestone Alps and composed of permotriassic dolomite and limestone as well as quartz porphyries and granites in the West.

All but the Sarntal Alps have the highest peaks reaching above 3100 m asl. Mountain ranges are separated by a network of valleys, formed in the Messinian (last stage of the Miocen) and re-formed during the multiple glacial episodes. Nowadays, only trace of the last Ica Age called Wuerm Ice Age (110000-10000 YA) is visible in the landscape (Stingl & Mair, 2005). Due to intensive erosion processes bottoms of the main valleys are filled with quaternary residuum.

The Alps are a natural barrier between the Mediterranean climate of the Southern Europe and the temperate climate of the central Europe with the oceanic-continental gradient following the West-East direction. Local climate is additionally shaped through the local orography combined with altitudinal gradients of precipitation, temperature and solar radiation. The temperature gradient is probably the most important of all and governs average temperature decrease of 0.558°C for each 100 m of altitudinal change (Theurillat & Guisan, 2001). As decreasing temperature results in a reduction of moisture holding capacity of air, precipitation amount raises with elevation, reaching its maximum around 2000 m asl. This phenomenon is especially strong on windward mountain slopes, and additionally concludes in limited amount of clouds above a certain elevation. Moreover, as the atmosphere depth decreases with altitude and its isolation role is reduced, more solar radiation reaches the ground and more heat is irradiated in the night, which creates large daily temperature range.

All abovementioned conclude in a profound regionalization of the local climate, which is expressed first and foremost, in the altitudinal belts of weather conditions. Based on the Köppen-Kottek climate stratification (Kottek *et al.*, 2006) it is possible to identify in South Tyrol five main climatic regions:

- Humid subtropical climate with cold winters (January mean temperature of 0°C) and warm summers (July average temperature of 23°C) of the Etschtal valley, which is the driest and sunniest area;
- Oceanic climate with cold winters (-3°C to 1°C January mean) and mild summers (15°C to 21°C in July) is considerably richer in precipitation with high air humidity which leads very often to fog occurrence. It is observed in regions located between 300 m and 900 m asl.;
- Humid continental climate with very cold and potentially snowy winters (-8°C to -3°C in January) and mild summers (14°C to 19°C in July) is observed for regions located between 900 m and 1400 m asl. This zone is the largest in the area;
- Subarctic climate of very cold and snowy winters (-9°C to -5°C in January) and short and rainy summers (12°C in July) characterizes parts placed between 1400 m asl and 1700 m asl. It is the wettest zone in South Tyrol;

- Alpine tundra climate characterized regions above 1700 m asl where yearly average temperature oscillates around -5°C. Starting at 3000 m asl the Ice Cap climate with averaged January temperature of -14°C is observed.

Beside the altitude driven diversity of weather conditions, additional regionalization of climate can be spotted in the annual cumulative precipitation amounts recorded over the area. While the Vinschgau valley experiences yearly average rainfall below 500 mm (494.5 mm of normal rainfall amount in Schlanders, 698 m asl), in the Puster Valley annual precipitation reaches 1200 mm in the valley, and often 2000 mm on the mountain tops. Central part of the region is a transition zone with moderate to low yearly rainfall norms (707.3 mm, 711.6 mm and 663 mm for Merano, Bolzano and Brixen respectively; *South Tyrol in figures*, 2012). In general, South Tyrol is considered a rather arid region with inter-alpine climate.

Climatic drivers and orographic situation constitute diverse vegetation growth conditions. Mainly due to the altitudinal zonation, compression of multiple bioclimatic environments can be observed over a small area. Despite considerable similarities, altitudinal vegetation belts are much more complex comparing to the latitudinal vegetation zones. Importantly, vertical vegetation distribution in the Alps is additionally affected by local insolation conditions (Körner, 2003). It determines not only the lower and upper limits of subsequent zones, but often also species occurrence within strata. As a result, differences in elevation range of the same or similar plant communities can be observed between north and south exposed slopes, as well as the same vegetation belts can be composed of diverse vegetation groups on the north and south facing mountainsides.

Five climate-vegetation-soil zones can be identified in the Alps (Ozenda, 1988):

- Colline belt characteristic for big valleys and lower parts of slopes with mixed forest (an upper boundary on 800 m asl and 1000 m asl on the north and south slopes respectively);
- Mountain zone represented mainly by a coniferous forest (an upper boundary on 1400 m asl for north and 1800 m asl for south exposed slopes);
- Subalpine zone of dwarf trees and shrubs, which is a natural transition zone between the mountain and alpine vegetation belts (an upper range on roughly 2100 m asl on the north and 2500 m asl on the south facing mountainsides);
- Alpine zone is a region of meadow vegetation, which from a carpet distribution in the lower parts becomes more erratic and patchy moving towards the mountain tops (reaching up to 2700 m asl and 3200 m asl on the north and south exposed mountain slopes respectively);
- Nival level is an area of permanent (or almost permanent) snow and ice with sparse vegetation (above 2700-3200 m asl, upper boundary of this zone is not present in the Alps).

This zonation combined with landform feature naturally governs a horizontal structure of the land use in South Tyrol. Valley floors are extensively used for agriculture, expressed mainly in permanent crops of orchards and vineyards (5.3% of the total area). Flat or almost flat regions are favorable also for cities and bigger settlements (1.2%). Mountainsides are usually devoted to forest, which occupies around 43% of the

area of the province. Next in the altitudinal sequence is alpine vegetation of grasslands (roughly 17%) followed by bare rocks (19.6%) and glaciers (2.9%). Water bodies and semi-natural vegetation land cover classes do not follow elevation belts (Pütz *et al.*, 2011).

2.1.1. Forest

Forest occupies around 43% of the South Tyrol, which is exactly the number of the average forest share in the whole Alps (EEA, 2009a). The region is predominated by a coniferous woodland (2855.6 km^2; 38.6%) with an addition of mixed (231.5 km^2; 3.1%) and broadleaved (83.4 km^2; 1.1%) stands growing on lower elevations. Emerging from the climatic and biological conditions, South Tyrol comprises of three main forest regions (Figure 2): Central Inner Alps (Central Endalpica), Transitional Inner Alps (Transitional Endalpica) and Southern Inner Alps (Mesalpica) (Provincia Autonomica di Bolzano, 2010).

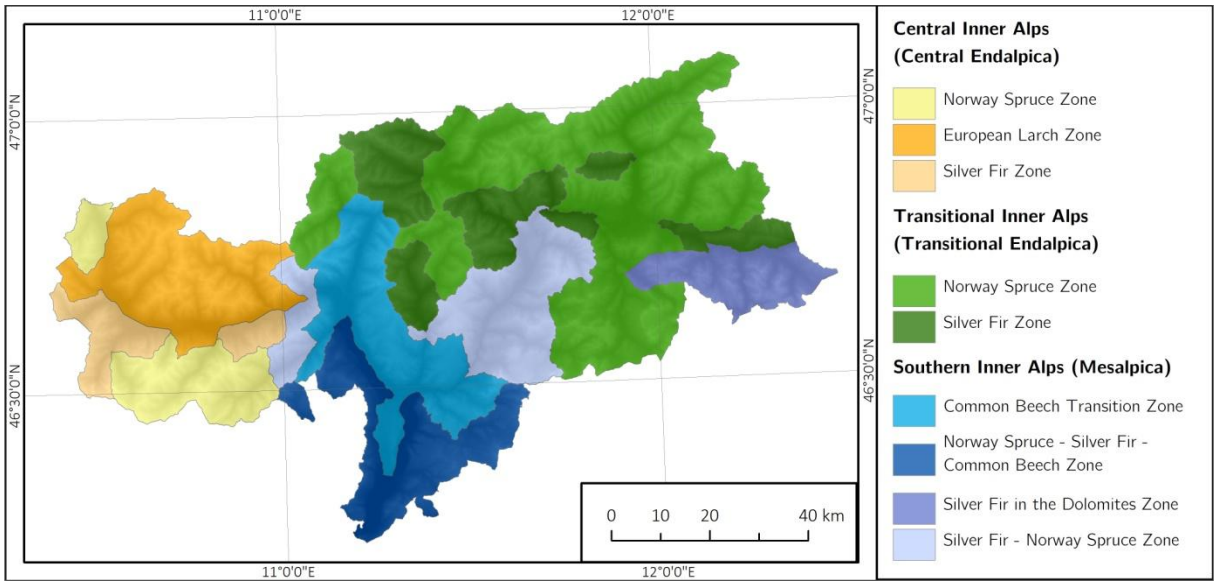

Figure 2 Forest regions map. Modified after Provincia Autonomica di Bolzano (2010, p. 17).

The Central Inner Alps are represented by the Vinschgau valley, and are characterized by a dry and continental climate with typical European Larch (*Larix decidua*) forest formation on the south exposed parts of the region. Norway Spruce (*Picea abies*) and Silver Fir (*Abies alba*) stands grow here on shadowy slopes with spruce trees more frequent nearer the valley floors and fir moving towards the higher altitudes. Downy Oak (*Quercus Petraea*) and Scots Pine (*Pinus sylvestris*) trees are present exclusively in the valley bottoms in the Colline alpine belt.

The zone of the Transitional Inner Alps occupies the northern part of South Tyrol with the Stubai Alps, Wipptal and a bigger part of Pustertal. Climate of this part is less continental comparing with the Central Inner Alps region. Norway Spruce forest dominates most of the region with exception of more shadowy places where it is partly replaced by Silver Fir. The driest locations are occupied by Scots Pine forest with local intrusion of European Larch (Wipp Valley, the Fundres Alps). Oak-Pine forest

formations are found here only on the fringe of forest, in the lowest and the warmest valleys parts.

The Southern Inner Alps region, unlikely the two others, is split into two with the main part located in the Etschtal and Eisack Valleys, and the second area placed in the Eastern Part of the Puster Valley. The main portion of the region is characterized by Hop Hornbeam (*Ostrya carpinifolia*), Manna Ash (*Fraxinus ornus*) and Downy Oak forest with local intrusions of Scots Pine, Sessile Oak (*Quercus pubescens*) and Sweet Chestnut (*Castanea sativa*) mixed stands. The higher slopes are a frequent location of mixed forest composed of Common Beech (*Fagus sylvatica*) trees accompanied by Silver Fir and Norway Spruce, which with increasing elevation becomes a coniferous spruce and/or fir forest.

For all the area, an upper forest boundary is made by Norway Spruce in the lower and European Larch with Arolla Pine (*Pinus cembra*) in the most elevated parts. This transition zone of subalpine forest is the most extensive in the Transitional Inner Alpine region, but is very limited in the Southern Inner Alps.

According to local-specific conditions (temperature, precipitation, insolatin, bedrock expressed indirectly in soil conditions), South Tyrolean forest is further delimitated into seven horizontal belts (Figure 3) (Provincia Autonomica di Bolzano, 2010):

- Lower Colline belt is in South Tyrol mostly assigned to the valley floors occupied by orchard and vineyards. Deciduous Oak forest with Hop Hornbeam and Manna Ash is a typical forest of this zone. Mediterranean species are present in the lowest and south-most parts of the region progressing along Etschtal and Eisack Valleys. Average annual temperature of this zone varies between 11°C and 12°C with precipitation amount between 500 mm and 730 mm. Maximum range of this strata is limited to 800 m asl in the Mesalpica region and 900 m asl in the Endalpica area;
- Upper Colline belt is a region of Oak forest, which in more favorable conditions of Mesalpica is mixed with Common Beech, while for more continental and drier locations incorporates Scots Pine. A mean temperature ranges here between 8°C and 10°C, and is accompanied by 500 mm (Vinschgau) to 800 mm of annual precipitation. High temperature and limited rainfall amounts make this region especially predisposed to drought conditions. This zone occupies area placed not higher than 1250 m asl (800 m if shaded);
- Sub-Mountain belt is dominated by Common Beech. This competitive specie is observed on a wide range of areas (also on poor soils) with exclusion of arid continental or regularly flooded sites, unstable soils and poorly ventilates spots. Beech habitat is delimitated by minimum annual precipitation of 500-600 mm and a minimum yearly averaged temperature of 5.5°C. On lower elevations Beech coexists with Downy Oak and Hop Hornbeam, while on higher altitudes comprises mixed forest stands with Norway Spruce and Silver Fir. Position of this belt varies greatly according to the local conditions. In general, for sunny slopes it can be defined from 750 m to 1150 m asl, and 600 m asl to 1000 m asl for less insolated locations;
- Medium-Mountain belt is much alike Sub-mountain zone, with extensive Common Beech presence, but also with significant and increasing with elevation share of coniferous species such as Silver Fir and Norway Spruce governed by

decreasing temperatures and shorter growing season combined with higher precipitation amount. The upper boundary of this forest belt is found on sunny slopes on average at 1350 m asl. For shaded locations, the Medium-mountain belt is placed between 700-800 m and 1200 m asl.

- Lower High-Mountain belt and Upper High-Mountain belt are considered here together. They span on average between 800 m and 1600 m asl. In the Central Endalpica region these zones are devoted to European Larch and Scots Pine on the sunny slopes, and Norway Spruce in the overshadowed locations. Rainfall shortages in Vinschgau limit occurrence of Silver Fir to north exposed slopes with annual precipitation exceeding 650 mm. As moisture is not a problem in the region of the Transitional Inner Alps (800-900 mm up to 1100-1200 mm per year) Norway Spruce and Silver Fir are no longer limited to lee slopes. However, snow cover and winter insolation patterns seems to restrict Silver Fir to humid north exposed sites. Although both High-Mountain forest belts are very alike, the Upper High-Mountain belt can be identified through yearly mean temperature of 4.5°C – 6.5°C, 4.5-6.5 months long growing season and 50-60% of precipitation occurring during the period of photosinthetical activity;

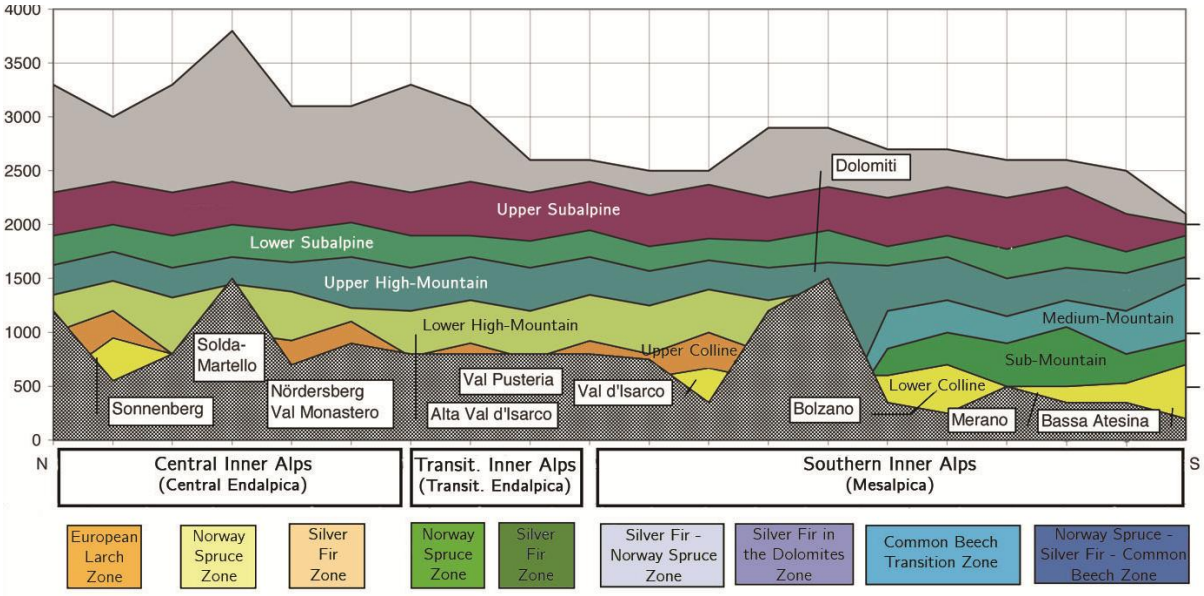

Figure 3 Forest types elevation belts. Modified after Provincia Autonomica di Bolzano (2010, p. 19).

- Lower Subalpine Belt is a zone spread between 1450 m and 1700 m asl for the north exposed slopes, and 1600 m to 1900 m asl on the intensively insolated sites. Forest stands are predominated by Norway Spruce, which in drier and more extreme locations is accompanied by European Larch. Harsh climatic conditions with long winters, short growing season (roughly three months), low temperatures (annual average of 2.5°C - 5°C) and intense snowfall (amount of total precipitation varies from 600 mm in the Central Endalpica region to 1200 mm in the Transitional Endalpica zone) limit favorable habitats, sometimes resulting in a sparse, detached stands;
- Upper Subalpine Belt is populated by European Larch and Arolla Pine, which gradually transition into dwarfed trees and shrubs. Climatic conditions are very

severe, with vegetation season rarely longer than 3 months, strong and chilling winds, and extreme negative temperatures during winter. Despite moderate precipitation amount (800 mm to 1200 mm a year) these regions are considered as rather dry. Weather conditions present in this zone often exceed physiological amplitude of tree species.

A quantitative dissemination of the South Tyrolean woodland according to the forest type (according to the *EL-04b* dataset of geoland2 (2012)), aspect, elevation (stratification after Theurillat and Guisan, (2001)) and slope classes, confirms dominance of regions placed between 1400 and 2100 m asl (Table 2). The next most represented altitudinal zone is the second elevation class (700-1400 m asl), whereas the lowest as well as the height regions contribute together to less than 8% of the total forest area. The lay of the land controls consequently forest distribution within the inclination strata, where the areas with 20-40 degrees of slopping are represented the most frequently. Remarkably, over 11% of the woodland growths on slopes with inclination exceeding 40 degrees. The majority of forest is located on north and west facing mountainsides, with only 21.73% of trees situated on the south exposed slopes. As aforementioned, forest in South Tyrol is predominated by coniferous tree species, with increasing share of broadleaved trees at lower elevations and valleys floors.

Table 2 Percentage forest allocation within forest type, aspect, elevation and slope classes.

	[%]
Coniferous	88.66
Broadleaved	4.32
Mixed	7.03
N	28.71
E	23.00
S	21.73
W	26.56
0-700 m asl	4.50
700-1400 m asl	33.60
1400-2100 m asl	59.48
2100-2500 m asl	2.41
0-10 deg.	6.37
10-20 deg.	17.58
20-30 deg.	30.74
30-40 deg	33.76
40-90 deg.	11.56

2.2. Data

2.2.1. Meteorological data

Meteorological service of South Tyrol maintains a dense grid of measurement stations with diverse history of observation records. In order to meet requirements posed by the scPDSI algorithm (Wells *et al.*, 2004) only stations with uninterrupted, minimum 25-year-long time series (taking December 2012 as the final record entry, meteorological observations had to date back to, at least, January 1988) of monthly precipitation cumulative and mean temperature records were selected from the WISKI

database of the Hydrographic Office of the Autonomous Province of Bolzano-Südtirol. These requirements were fulfilled by 26 stations evenly spread around the region (Figure 4). Aforementioned observation points represented diverse altitudinal zones and have various record lengths (Table 3).

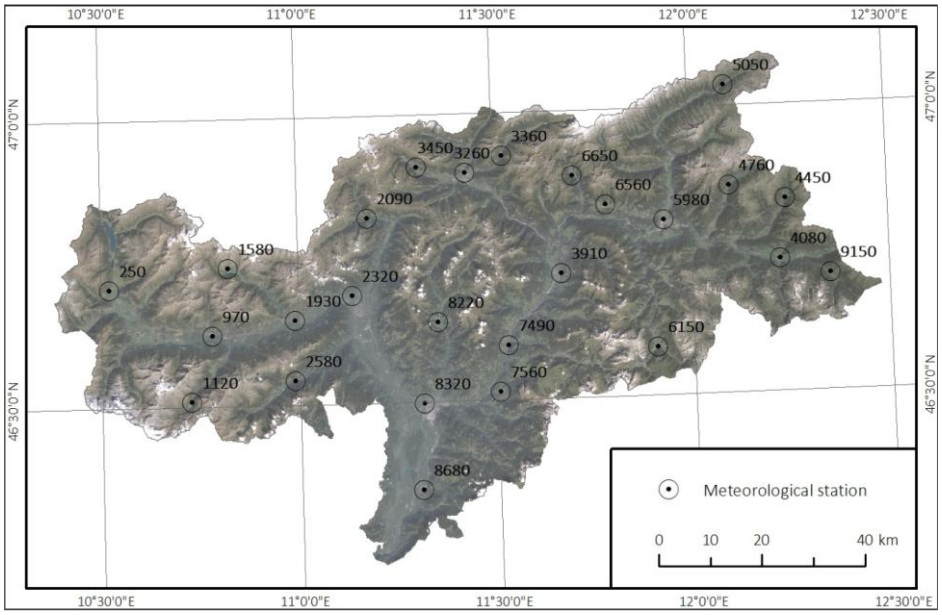

Figure 4 Location of 26 meteorological stations selected for the study. Station numbers follow WISKI database nomenclature and correspond with Table 3

Table 3 Complete list of meteorological stations used in the study with: station numbers (correspond with Figure 4), name of the location (in Italian), elevation and length of records used in the survey

Station no	Name (in Italian)	Elev. [m asl]	Records since	Station no	Name (in Italian)	Elev. [m asl]	Records since
250	Monte Maria	1310	1967	4450	S.Maddalena in Casies	1398	1967
970	Silandro	698	1988	4760	Anterselva di Mezzo	1236	1941
1120	Diga di Gioveretto	1851	1973	5050	Predoi	1449	1980
1580	Vernago - Finale	1950	1967	5980	Brunico	821	1986
1930	Naturno	541	1973	6150	La Villa in Badia	1390	1987
2090	Plata	1147	1936	6560	Terento	1349	1981
2320	Merano - Quarazze	330	1983	6650	Fundres	1159	1977
2580	Diga di Zoccolo	1144	1979	7490	Ponte Gardena	490	1984
3260	Vipiteno	948	1935	7560	Fie allo Sciliar	840	1956
3360	Diga di Vizze	1365	1973	8220	Sarentino	966	1977
3450	Ridanna	1350	1969	8320	Bolzano	254	1949
3910	Bressanone	560	1971	8680	Ora	250	1983
4080	Dobbiaco	1220	1967	9150	Sesto	1310	1956

2.2.1. Ancillary data

2.2.1.1. DEM

A Digital Elevation Model with 2.5 m resolution was obtained from the Autonomous Province of Bolzano. In order to adjust it to the satellite images used in the study, the original dataset was upscaled to 30 m and 250 m resolution (Landsat and MODIS

spatial resolution respectively) using bilinear reprojection method. Additional layers of slope and exposition were derived directly from the reprojected DEM datasets using the ArcGIS 10.1 software (ESRI, 2011).

2.2.1.2. Forest mask

Forest mask and forest type mask information were adopted from two core forest product of the EU's FP7 (Seventh Framework Programme) geoland2 project: *EL-04a* and *EL-04b* datasets for a demo site *EU05 Alpine Transect Munich-Innsbruck-Verona*which (geoland2, 2012). Information gaps, existing due to cloud cover and shadowing (in total 162 km² in South Tyrol only) were filled in using CORINE Land Cover 2006 dataset (EEA, 2010b). Despite different forest definitions, CLC2006 was the most appropriate supplementary information source, as both datasets share the same spatial resolution of 20m and were developed based on corresponding satellite images acquired in 2006 (± 1 year).

Resulting forest mask and forest type mask were initially reprojected from the LAEA (Lambert Azimuthal Equal Area) to the UTM 32N projection, and then adjusted from 20 m to the target resolutions of 30 m and 250 m. The scaling to the 30 m was a straightforward process employing nearest neighbor transformation.

A reprojection from 20 m to 250 m was based on a spatial averaging, where a new 250x250 m pixel was assigned to a 'forest' class only when at least 50% of its area was devoted to a forest within the core dataset. Following the geoland2 guidelines, pure coniferous or broadleaved forest type was defined only when a share of softwood or hardwood trees exceeded 75%.

2.2.2. MODIS data

MODIS (Moderate Resolution Imaging Spectroradiometer) is a versatile passive scanner constructed on a scientific heritage of AVHRR (Advanced Very High Resolution Radiometer), CZCS (Coastal Zone Color Scanner), Sea-WIFS (Sea-Viewing Wide Field-of-View Sensor), HIRS (High-resolution Infrared Sounder) and Landsat TM (Thematic Mapper) (Guenther *et al.*, 2002). Its uniqueness originates not only from a superb technical specification (Table 4), but also from a fact that MODIS flies on board two Earth Observing System (EOS) satellites: Terra (launched in December 1999) and Aqua (launched in May 2002). Furthermore, the MODIS Scientific Team supervises constant development of a wide suite of high quality scientific and operational products (Justice *et al.*, 2002) that are available free of charge.

One of the main concerns while working with medium resolution images is geometric accuracy. Officially assured geo-location precision of MODIS data reaches 50 m in native ISIN (Integrated Sinusoidal) projection (Wolfe *et al.*, 2002). However, an independent evaluation reported geometric accuracy at nadir as 113 meters (Knight *et al.*, 2006).

MODIS Vegetation Index product (MOD13Q1) is a standard Level 3 MODIS-Terra 16-day product coming in a 250 m resolution, a neat spatial structure of Integrated Sinusoidal Grid (Huete *et al.*, 1999) and HDF (Hierarchical Data Format) archives. The data are generated at regular time-steps of 16 days (23 composites per year), where all images acquired during a given time period contribute to a final composite

Table 4 Essential MODIS sensor specification after Guenther *et al.* (2002)

Parameters	
Orbit	705km, sun-synchronous, near-polar, circular, Terra: 10:30 descending node Aqua: 13:30 ascending node
Resolution	250 m (bands 1-2) 500 m (bands 3-7) 1000 m (bands 8-36)
Time resolution	overpass 12/24h, revisit 16 days
Radiometric resolution	12 bits
Number of bands	36
Spectral range	0.620 – 0.876 µm (1-2 visible/NIR channels) 0.459 – 2.155 µm (3-7 visible/NIR channels) 0.405 – 14.385 µm (8-36 visible/NIR/IR channels)

based on their quality (cloud contamination, sun elevation and sensor viewing angle), therefore a final product is possibly least corrupted by cloud cover or sensor misregistrations. The highest quality of data integration for each of the 16-day time periods is ensured for Collection 5 by an improved Constrained View angle – Maximum Value Composite (CV-MVC) algorithm (Solano *et al.*, 2010).

The original MOD13Q1 product comprises 12 bands with the NDVI and EVI vegetation indices at its core. They are accompanied by additional bands providing per-pixel information on zenith angle, sun elevation, relative azimuth angle and composite day of the year (DOY) as well as a bit quality information (QA) layer denoting overall pixel reliability. Moreover, MODIS bands 1, 2, 3 and 7 (red [620-670 nm], NIR [841-867 nm], blue [459-479 nm] and MIR [2105-2155 nm] respectively) are also incorporated into the product (Solano *et al.*, 2010). MOD13Q1 data are composed from datasets underwent an aerosol correction (Vermote *et al.*, 2002) and atmospheric correction based on the Second Simulation of a Satellite Signal in the Solar Spectrum Vector Code (6S) radiative transfer code (Feng *et al.*, 2012), hence are considered to have a limited atmospheric and topographic contamination, as the latter is addressed through the index quotients. As a result, no additional pre-processing steps are required.

Following the ISIN grid, South Tyrol is covered by a h18v04 granule. A complete 2000-2013 MOD13Q1 time series for this tile was acquired from the WIST[1] and EOSDIS[2] services, and comprises 309 scenes (23 scenes per year with only 10 tiles from 2000). All scenes came from MODIS Collection 5 processing scheme.

2.2.2.1. Preprocessing

All required preprocessing steps of MODIS data were performed in the MRT (MODIS Reprojection Tool; USGS EROS Data Center, 2002) and ENVI/IDL software (ENVI version 4.7 and 4.8, IDL version 7.0 and 8.0 respectively; Exelis Visual Information

[1] http://wist.echo.nasa.gov
[2] http://reverb.echo.nasa.gov

Solutions, Boulder, Colorado). Firstly, for each scene NDVI, QA, as well as band 2 (NIR: 0.840-0.876µm) and 7 (MIR: 2.105-2.155 µm) layers were extracted, subsetted to the region of interest and reprojected to the UTM 32N coordinate system using the MRT software (Figure 5). Subsequently, NDII7 was computed according to the formula:

$$NDII7 = \frac{band\ 2 - band\ 7}{band\ 2 + band\ 7} \quad [3]$$

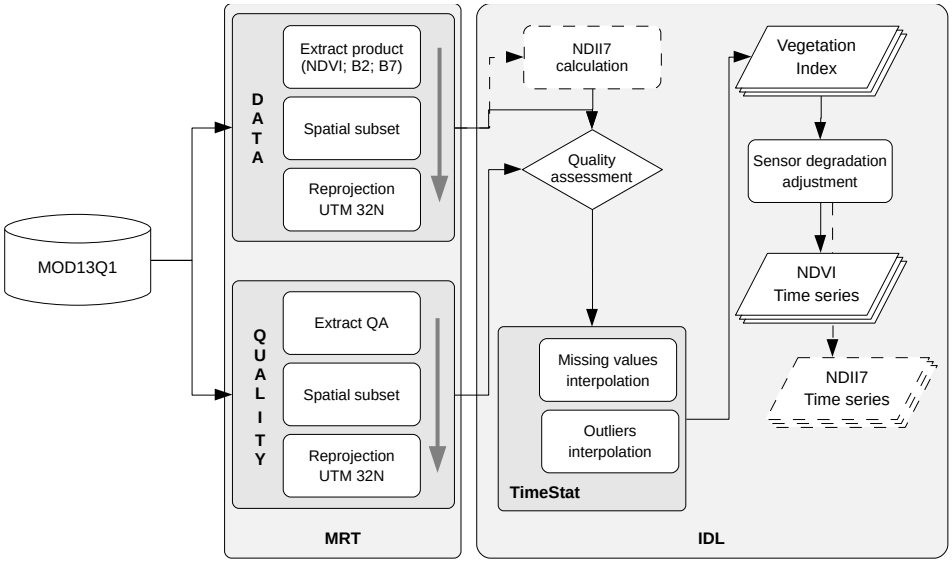

Figure 5 Preprocessing workflow of MOD13Q1 data

All pixels in the NDVI and NDII7 time series with QA-usefulness values below 'acceptable' were masked out following a suggestion of Colditz *et al.* (2008). Next, outliers (confidence level 0.95 according to Chebyshev's Theorem) and masked-out low quality pixels were replaced using a time-domain linear interpolation carried out in the TimeStats Software Tool (Udelhoven, 2011). To ensure the highest quality and limit amount of 'artificial' values introduced to the time series, the interpolation was performed only for a single observation gaps. (Table 5, Table 6). Longer gaps were not revised. As a result, a complete 2001-2013 NDII7 time series was available for 52009 forest pixels (out of 52394). NDVI spatial coverage was not affected. Finally, having in mind findings of Wang et al. (2012), proposed *ibid* adjustment for the sensor degradation was completed for both time series.

Subsequently, NDVI and NDII7 time series were further processed to ensure multiple data setups for the following PCA decomposition. The following were exploited:

- per-pixel time-domain noise removal using the Savitzky-Golay (SG) filtering of the second polynomial degree and a kernel of five (Chen *et al.*, 2004). This method assumes correctness of the upper signal envelope and filters abrupt drops in the time series, mitigating hence potential atmospheric contamination or other periodical disturbances;

Table 5 Number of forest pixels that underwent linear interpolation within the 2001-2013 MODIS derived NDVI time series. Complete forest mask comprises 52394 pixels.

com-	year												
posite	2001	2002	2003	2004	2005	2006	2007	2008	2009	2010	2011	2012	2013
1	6141	253	6137	18804	4389	6749	706	4263	8107	17031	3306	6067	1407
2	12602	547	3865	11249	3691	4095	9028	5683	18336	8245	1129	5522	11671
3	3275	429	1729	2259	2342	14171	1994	1230	16827	8130	461	8526	11023
4	2084	5654	372	10696	3750	7019	533	347	9445	7386	1259	1388	3682
5	1818	114	57	3503	245	2132	278	481	3172	2837	289	252	4141
6	1385	46	72	462	12	1329	776	1445	2021	1370	157	32	2676
7	2599	1474	173	510	166	819	40	11651	309	635	12	665	458
8	2675	51	27	200	95	193	30	326	154	374	1	697	44
9	243	113	53	108	1	39	0	894	7	4	35	28	39
10	119	3	71	0	1	3	528	66	7	6	110	70	122
11	7	4	0	3	0	2	4	122	4	5	4	3	1
12	246	12	16	8	0	0	89	3	205	0	0	36	67
13	6	41	0	50	5	23	0	0	0	43	124	0	1
14	0	37	6	0	0	103	0	9	3	0	2	0	0
15	0	0	1	4	8	0	1	6	1	1	0	0	2
16	0	108	0	0	32	2	0	15	0	1	8	0	0
17	6	1	0	0	0	0	0	2	3	0	1	0	0
18	0	4	4	0	0	0	0	0	1	0	0	96	2524
19	0	11	209	109	0	3	0	1	0	1003	0	0	1
20	0	1	426	125	30	157	3	344	183	195	11	182	312
21	53	3122	1333	70	2582	3393	792	727	268	11691	25	124	1277
22	269	2601	979	1219	14799	966	1698	28383	8105	9836	7759	7567	354
23	388	1643	10264	5991	12246	6749	760	10472	10140	7088	6995	5958	10527

Table 6 Number of forest pixels that underwent linear interpolation within the 2001-2013 MODIS derived NDII7 time series. Complete forest mask comprises 52394 pixels

com-	year												
posite	2001	2002	2003	2004	2005	2006	2007	2008	2009	2010	2011	2012	2013
1	864	7382	1362	149	1581	493	3717	2964	529	149	756	522	1188
2	422	6435	1444	300	1305	512	498	1099	79	289	1577	504	101
3	837	4266	1173	985	1307	586	1307	1801	155	157	2223	471	123
4	863	1673	2417	562	1548	250	1654	2953	299	363	1141	2241	305
5	775	5200	4947	1323	4212	668	3366	2448	1172	990	1796	3630	903
6	528	4849	5101	1509	6241	2272	861	2471	1476	1146	1231	3042	276
7	1124	955	3200	1458	2373	1045	2042	7426	347	1488	1633	796	436
8	283	1383	2819	2130	2175	1953	1845	1111	214	1362	596	718	654
9	351	2305	1158	1001	634	1848	176	2316	162	669	490	572	1740
10	353	780	368	920	371	467	1886	888	109	184	560	509	975
11	90	97	92	215	59	193	99	462	55	43	339	81	79
12	451	86	94	151	61	26	739	56	878	35	22	45	209
13	28	168	24	304	19	19	14	5	10	162	545	30	13
14	8	109	57	8	3	645	32	27	24	44	41	44	1
15	21	22	91	31	181	433	34	64	72	18	11	8	28
16	48	430	77	18	256	10	17	24	2	16	44	5	8
17	181	28	45	26	13	88	33	41	66	33	24	14	10
18	419	118	219	80	271	164	345	72	51	186	60	333	757
19	990	1639	464	774	1075	538	506	441	346	67	193	339	131
20	2839	2681	578	1644	1809	3336	1936	989	517	503	2041	478	546
21	3807	2111	1582	3601	2840	4399	1924	748	2344	364	3719	1201	957
22	5162	1876	2903	2158	279	1453	2684	15	372	530	1037	618	2193
23	6462	2478	1880	2033	562	3712	4448	425	620	708	899	352	573

- removal of seasonality through a per-pixel z-score normalization:

$$d = \frac{X_{ij} - \mu_{j-com}}{\delta_{j-com}} \quad [4]$$

where:
X_{ij} denotes a j-th composite ($j \in [1; 23]$) of an i-th year ($i \in [2001; 2013]$) of the complete time series;
$\mu_{j\text{-}com}$ stands for an average value for all j-th composites across all the years;
$\sigma_{j\text{-}com}$ is a standard deviation for all the j-th composite in the time series;
Normalization leaves out a 'common' data component, which for vegetation usually represents seasonality, allowing to focus on anomalies. This approach can result in much more informative datasets;
- three different lengths of NDVI and NDII7 time series (applied to the original and z-score normalized, as well as SG-filtered and not-filtered datasets), where beside the complete MODIS time series comprising all 23 annual composites (1-23), a vegetation season time series focusing on a period between end of April and mid-October (corresponding with 8th to 18th MODIS annual composites (8-18)) as well as high-season data (August to mid-September which coincides with composites 14th to 17th (14-17)) were exploited. While time series restricted to a vegetation season allow to exclude dormancy state signal and potential impact of snow cover, limiting thus an amount of redundant data, high-season datasets provide information only on vegetation status during potentially the highest drought vegetation stress period.

Aforementioned techniques were interlaced resulting in variety of NDVI and NDII7 datasets (Table 7 and Table 8 respectively). Remarkably, SG filtering was always performed before normalization and truncating.

Table 7 List of all produced NDVI time series setups. Ranges of corresponding MODIS 16-day composites are given in brackets.

Data z-score normalization	SG filtering	Annual time window (MODIS composites)	Dataset short name
no	no	full year (1-23)	$NDVI_{1\text{-}23}$
	no	veg. season (8-18)	$NDVI_{8\text{-}18}$
	yes	full year (1-23)	$NDVI_{SG1\text{-}23}$
	yes	veg. season (8-18)	$NDVI_{SG8\text{-}18}$
yes	no	full year (1-23)	$nNDVI_{1\text{-}23}$
	no	veg. season (8-18)	$nNDVI_{8\text{-}18}$
	no	high season (14-17)	$nNDVI_{14\text{-}17}$
	yes	full year (1-23)	$nNDVI_{SG1\text{-}23}$
	yes	veg. season (8-18)	$nNDVI_{SG8\text{-}18}$

Table 8 List of all produced NDII7 time series setups. Ranges of corresponding MODIS 16-day composites are given in brackets.

Data z-score normalization	SG filtering	Annual time window (MODIS composites)	Dataset short name
no	no	veg. season (8-18)	$NDII7_{8\text{-}18}$
yes	no	veg. season (8-18)	$nNDII7_{8\text{-}18}$
	no	high season (14-17)	$nNDII7_{14\text{-}17}$

Furthermore, based on the not-normalized high-season NDVI and NDII7 time series a yearly mean datasets were calculated (herein $NDVI_{HS}$ and $NDII7_{HS}$). These averages rendered information on vegetation status during the period of potentially the highest drought impact.

2.2.2.2. Phenological indicators

The complete, not normalized 2001-2013 MODIS NDVI time series ($NDVI_{1\text{-}23}$) was introduced to the *Phenolo* IDL-nested software developed at the EC Joint Research centre (Ivits *et al.*, 2013a). This pixel-bases algorithm derives a selection of yearly phenological parameters which provides information on vegetation dynamism, phenology and productivity. In this study, the focus was given to three vegetation productivity metrics: Cyclic Fraction (CF), approximation of Gross Primary Productivity (GPP); as well as two season information parameters: Season Length (SL, estimated length of vegetation season) and Season Begin Day (SBD, relative start of a season day). While Cyclic Fraction approximates annual seasonal growth between SBD and SED (Season End Day; Figure 6), Gross Primary Productivity estimates total accumulated biomass of permanent and seasonal vegetation produced during one annual vegetation cycle given by a time unit limited by two consecutive local minima observed on the vegetation index envelope.

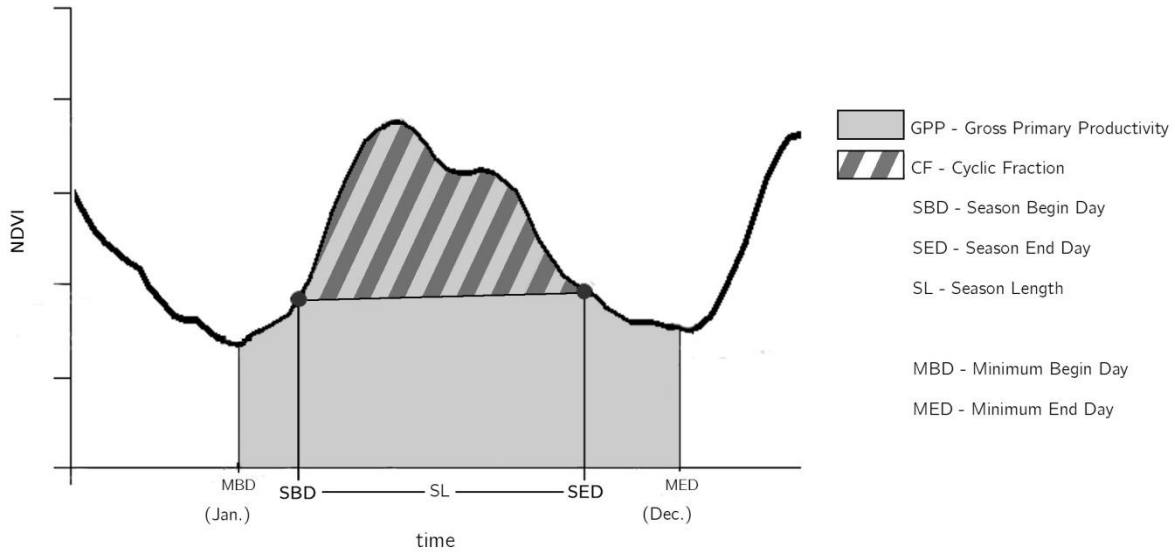

Figure 6 *Phenolo* conceptual scheme for selected productivity and phenology parameters. Modified after Ivits *et al.* (2013a).

Both productivity indices together with two phenology parameters provide extensive information on year-to-year vegetation variability (Ivits *et al.*, 2011, 2013b). NDVI data were selected here over the NDII7 time series due to more robust seasonality of the signal associated directly with plant 'greenness'. *Phenolo* algorithm is based on the moving average approach (Reed *et al.*, 1994), where an average phenological dynamism is computed independently for each pixel based on the available time series. Yearly vegetation growth defined as a histogram between two consecutive minima in the NDVI envelope (MBD – Minimum Begin Day and MED – Minimum End Day; Figure 6) determines annual mean and standard deviation. Conceptual, pixel-specific approximation of a season length for each year in a time series is a doubled standard deviation centered at a histogram barycentre.

Averaged yearly complements of season length approximations (i.e. length of non-vegetation season) gives a lag for moving average (in days). The original NDVI time series is next overlaid with the forward and backward lagged averaged NDVI curves. Intersections between both define SBD and SED respectively. Together with the yearly minima (MBD and MED), SBD and SED determine threshold days for all productivity and phenology parameters. Owing to a moving average principle of the approach, resulting time series comprised parameters only for the 2002-2012 period.

Due to a lack of ground-truth data for scaling, final time series of phenology measures were treated as indicators of relative changes, rather than absolute values.

2.2.3. Landsat

Initiated in 1972 the Landsat program is the longest running satellite earth observation project, and an irreplaceable source of environmental information on the global scale. Until today, seven Landsat satellites contributed to the enterprise, with the Landsat Data Continuity Mission (LDCM; Irons *et al.*, 2012) in service since 30 May 2013. Starting from 1982 the Landsat program continuously provides visible, near infrared and medium infrared datasets in a constant resolution of 30 meters. It has been possible thanks to the Thematic Mapper (TM) and the Enhanced Thematic Mapper Plus (ETM+) sensors (Table 9) flying on board Landsat 4, 5 and 7 satellites (Table 10). Landsat 6 with Enhanced Thematic Mapper (ETM) never got to its orbit.

Remarkable cohesion between consecutive Landsat platforms as well as their equipment, allowed to create unique and consistent data collection. Although between 1985 and 1999 Landsat 4 and Landsat 5 were transferred to the private sector, which negatively affected not only data availability, but also acquisition schemes (Williams *et al.*, 2006), recently made decisions including initiated in 2008 opening of the Landsat archives (Wulder *et al.*, 2012) aim to reintroduce to the public a complete global Landsat time series on a free-of-charge bases. Although the task is still incompleted due to abundance of data, an outlook for future Landsat based environmental analyses is promising and encouraging (Loveland & Dwyer, 2012; Wulder *et al.*, 2012, 2015).

Seizing the arising opportunity, the following survey employs a collection of Landsat Level 1T products (Standard Terrain Correction – the precision ortho corrected product, which provides systematic radiometric and geometric accuracy). To make it comparable with MODIS observations, foreseen time frame employed Landsat scenes

Table 9 Thematic Mapper (TM) and Enhanced Thematic Mapper Plus (ETM+) basic specification. After Loveland & Dwyer (2012).

	TM	ETM+
Platform	Landsat 4 Landsat 5	Landsat 7
Number of bands	7	8
Spectral ranges and resolutions		
Band 1	Blue: (0.45 - 0.52 µm) 30 m	Blue: (0.45 - 0.52 µm) 30 m
Band 2	Green: (0.52 - 0.60 µm) 30 m	Green: (0.52 - 0.60 µm) 30 m
Band 3	Red: (0.63 - 0.69 µm) 30 m	Red: (0.63 - 0.69 µm) 30 m
Band 4	NIR: (0.76 - 0.90 µm) 30 m	NIR: (0.77 - 0.90 µm) 30 m
Band 5	NIR: (1.55 - 1.75 µm) 30 m	NIR: (1.55 - 1.75 µm) 30 m
Band 6	Thermal: (10.40 - 12.50 µm) 120 m	Thermal: (10.40 - 12.50 µm) 60 m
Band 7	MIR: (2.08 - 2.35 µm) 30 m	MIR: (2.08 - 2.35 µm) 30 m
Band 8 (PAN)	-	PAN: (0.52 - 0.90 µm) 15 m

Table 10 Landsat 4, 5 and 7 platforms specifications. After Loveland & Dwyer (2012) and *Landsat 7 Science Data Users Handbook* (NASA)

	Landsat 4	Landsat 5	Landsat 7
Launched	16 July 1982	1 March 1982	15 April 1999
Deactivated	14 December 1994	5 June 2013	Ongoing
Additional information		TM operational imaging ended in November 2011	31 May 2003: Scan-line corrector (SLC) failure
Orbit	705 km, sun-synchronous, polar, Inclination: 98.2° 9:45 AM (±15 min), descending node	705 km, sun-synchronous, polar, Inclination: 98.2° 9:45 AM (±15 min), descending node	705 km, sun-synchronous, polar, Inclination: 98.2° 10:00 AM (±15 min), descending node
Time resolution	overpass 99 minutes, revisit 16 days	overpass 99 minutes, revisit 16 days	overpass 99 minutes, revisit 16 days
Sensors	TM, MSS	TM, MSS	ETM+

TM – Thematic Mapper; MSS – Multi Spectral Scanner; ETM – Enhanced Thematic Mapper Plus

acquired between 2001 and 2013. This condition determined use of images registered with TM and ETM+ sensors onboard on the Landsat 5 and Landsat 7 platforms respectively.

The area of South Tyrol is covered by four neighboring WRS-2 (World Reference System 2) tiles (Figure 7). Unfortunately, due to a technical problem of a disc-space limitation, only southern granules 192-028 and 193-028 were adopted for further investigation. This selection was governed by a fact that combination of both southern tiles covers the bigger part of the province, as well as comprises more diverse regions exposed to potentially stronger drought impact. Although Landsat archive has been

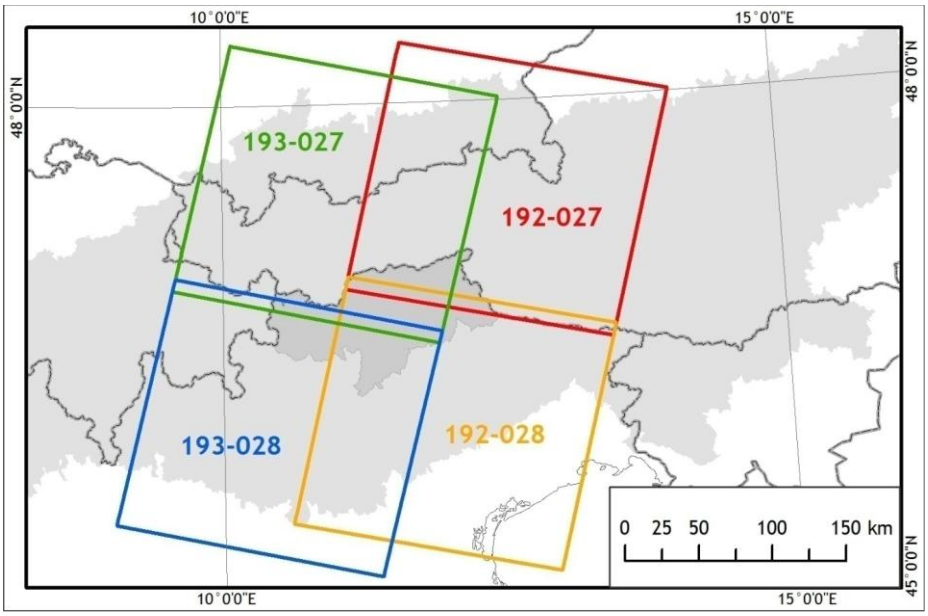

Figure 7 South Tyrol territory with the Landsat WRS-2 tile grid overlaid.

open since 2008 (Wulder *et al.*, 2012), at the moment of initializing this analysis (beginning of 2013) still not all Landsat scenes were available and transferred to the USGS archive[3] from the European ground segment. Moreover, additional limitation in data availability was recognized due to the end of Landsat 5 TM operational imaging in November 2011 as well as Landsat 7 SLC (Scan Line Corrector) failure in May 2003 (USGS, 2003). Furthermore, forest drought impact oriented character of the study additionally restricted employed datasets to the annual time-window of June-September, which corresponds with the period of complete crown development of deciduous trees, and potentially the strongest vegetation drought stress. All aforementioned, combined with high cloud cover probability over the study site, limited considerably data amount and resulted in an executive Landsat time series of summer acquisitions 2001-2011. During a dataset selection, only scenes with a maximum cloud cover of 80% were considered. Eventually, 24 images met the criteria for the 192-028 tile (Table 11). Granule 193-028 was represented by another 23 scenes (Table 11).

[3] U.S. Geological Survey, GloVis: http://glovis.usgs.gov

Table 11 Landsat 5 and 7 data availability for the 192-028 and 193-028 WRS-2 tiles tor the 2001-2011 period. Only June-September acquisitions with less than 80% cloud cover were considered.

192-028				193-028			
Dataset	Acquisition data			Dataset	Acquisition date		
LE71920282001158	2001	Jun	7	LE71930282001213	2001	Aug	1
LE71920282001206	2001	Jul	25	LE71930282002232	2002	Aug	20
LE71920282002209	2002	Jul	28	LE71930282002200	2002	Jul	19
LE71920282002225	2002	Aug	13	LT51930282003195	2003	Jul	14
LE71920282002241	2002	Aug	29	LE71930282003203	2003	Jul	22
LT51920282003220	2003	Aug	8	LT51930282003211	2003	Jul	30
LT51920282003236	2003	Aug	24	LT51930282003259	2003	Sep	16
LE71920282003260	2003	Sep	19	LT51930282004214	2004	Aug	1
LE71920282004247	2004	Sep	3	LE71930282005208	2005	Jul	27
LE71920282004263	2004	Sep	19	LE71930282005224	2005	Aug	12
LE71920282005201	2005	Jul	20	LT51930282006203	2006	Jul	22
LE71920282005217	2005	Aug	5	LT51930282006235	2006	Aug	23
LT51920282006244	2006	Sep	1	LT51930282007206	2007	Jul	25
LE51920282006252	2006	Sep	9	LT51930282007238	2007	Aug	26
LT51920282007199	2007	Jul	18	LE71930282008201	2008	Jul	19
LT51920282007231	2007	Aug	19	LT51930282009227	2009	Aug	15
LT51920282007247	2007	Sep	4	LT51930282009243	2009	Aug	31
LE71920282008242	2008	Aug	29	LE71930282010238	2010	Aug	26
LE71920282009228	2009	Aug	8	LT51930282010246	2010	Sep	3
LE71920282009244	2009	Sep	1	LE71930282010254	2010	Sep	11
LT51920282010255	2010	Sep	12	LT51930282010262	2010	Sep	19
LE71920282010263	2010	Sep	20	LT51930282011233	2011	Aug	21
LT51920282011226	2011	Aug	14	LE71930282011241	2011	Aug	29
LE71920282011234	2011	Aug	22				

2.2.3.1. Preprocessing

In the first step (Figure 8), all Landsat images were calibrated and atmospherically corrected in the LEDAPS processing software (version 1.0.6; Masek *et al.*, 2006). Next, each scene was subjected to the *f-mask* clouds and cloud shadows detection algorithm (Zhu & Woodcock, 2012). However, since even the in-house-adjusted f-mask algorithm version revealed unacceptable inaccuracy, a follow-up cloud and cloud shadow visual screening and digitalization was a must. Resulting masks were subsequently combined with automatically calculated no-data mask oriented on SLC stripes detection.

A wide annual data acquisition time-window of June-September concludes in variation of the sun elevation, hence terrain illumination properties. It is especially striking for mountainous regions, such as South Tyrol, where complex orography leads to extensive topographic shadows. This phenomenon is considerably affecting for multi-temporal surveys and time series analyses (Vanonckelen *et al.*, 2013).

Sun elevation profile calculated for Bolzano 10:00AM (local time, coincided with satellites overpass; Figure 9) revealed an overall absolute change of 21° between 15th June (local maximum of 54.36°) and 20th September (the latest available observation; 33.36°).

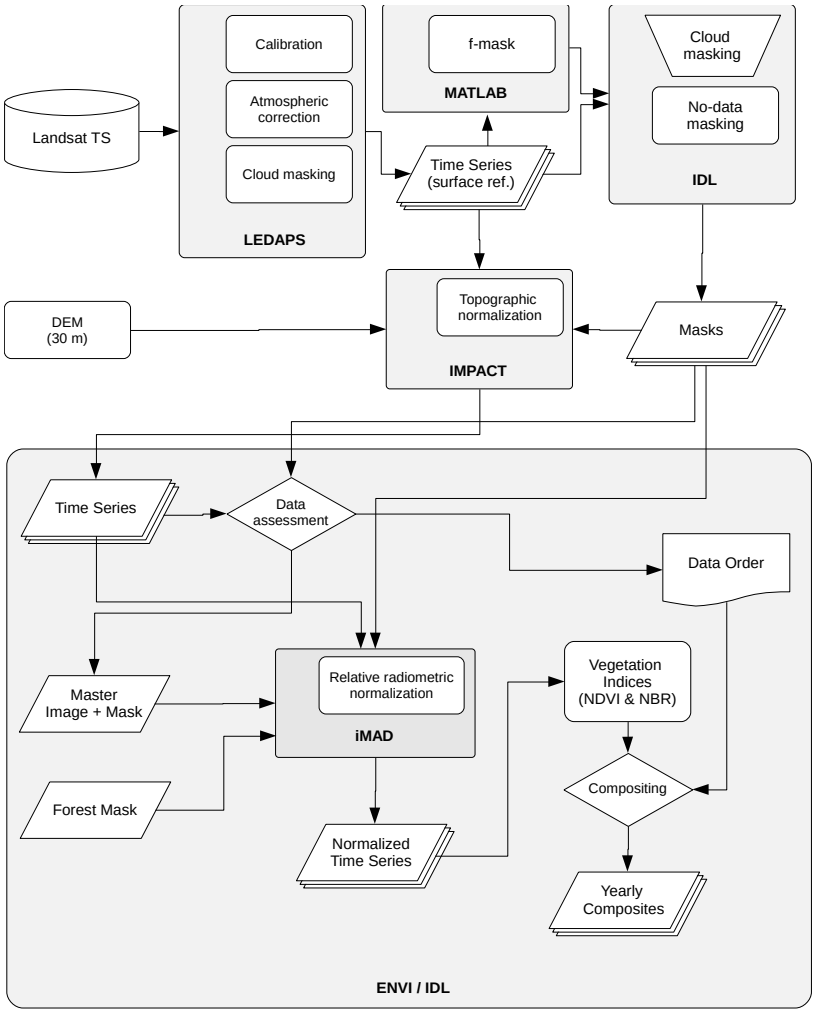

Figure 8 Landsat time series preprocessing workflow.

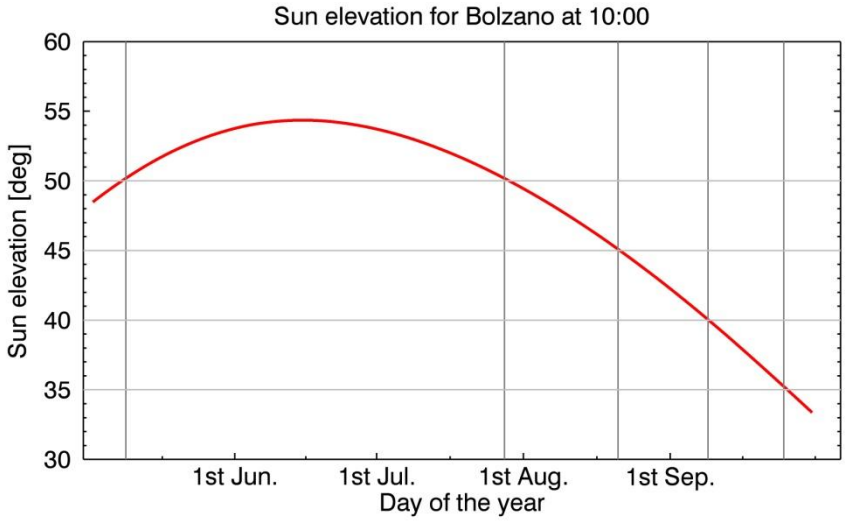

Figure 9 Sun elevation profile between 1st May and 31st September calculated for Bolzano 10:00AM local time. Maximum sun elevation is observed on 15th June (166 DOY; 54.36°). Above 50° values are reported between 9th May and 28th July (129 and 209 DOY respectively). During the sun inclination ascend 45°, 40° and 30° threshold values are crossed on 21st August (233 DOY), 9th September (252 DOY) and 25th September (268 DOY) respectively.

This variation translates into a strong solar radiation discrepancy between both dates (Figure 10), with smaller but still considerable differences among all the other observations. To properly address this issue a Minneart topographic correction implemented in the IMPACT software (Gallaun *et al.*, 2007) was performed for each Landsat scene. Computation was done using a 30 m resolution DEM of South Tyrol (please see section 2.2.1.1) additionally filtered with a 5x5 mean filter.

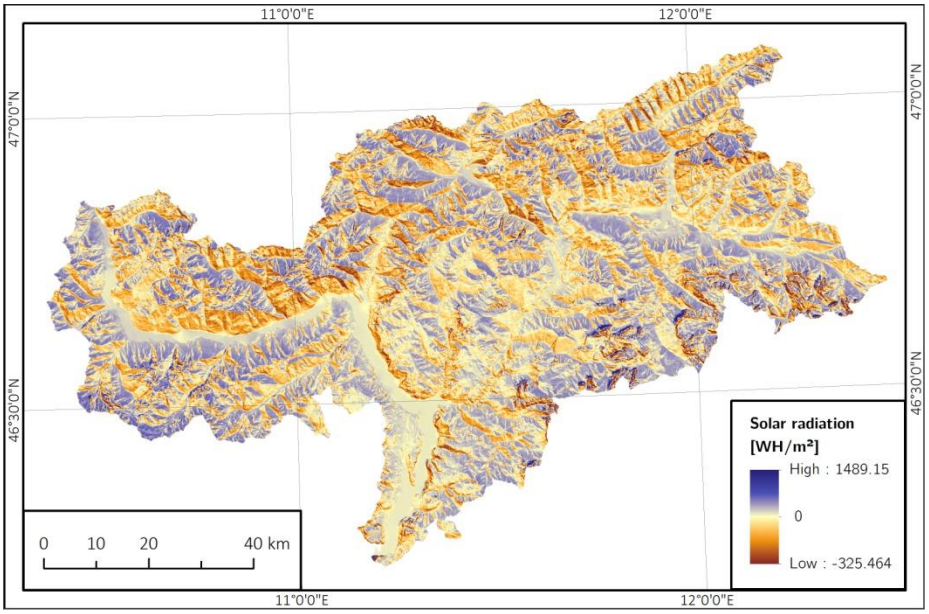

Figure 10 Solar radiation difference between 15th June and 20th September.

Following a suggestions of Riano *et al.* (2003), evaluation of topography corrected scenes was done through a comparison of the spectral characteristics of images, and inspection of standard deviation values calculated for selected regions in the pre- and post- corrected images. Due to a different extend of scenes, as well as cloud cover conditions, statistical training sites were identified separately for each dataset. As presented for the LE71930282002200 and LT51920282003220 images topography correction resulted in desired increase of homogeneity (Table 12 and Table 13 respectively). On the other hand, scenes acquired under low sun angel conditions (here example of LT51930282010262) revealed standard deviation increase (Table 14). Further inspection of the latter case showed that low sun inclination coupled with complex lay of the land, leads to hard shadows occurrence. Despite this, an overall quality of the topographic correction was assessed as good.

In order to ensure a reliable time series analyses, each considered pixel has to be represented by at least one value each year. Unfortunately, due to data scarcity, SLC stripping issue and frequent cloud cover, this assumption was very difficult to fulfill and severely restricted executive 2001-2012 spatial extend of the survey (Figure 11). Taking an advantage of the 192-028 and 193-028 tiles overlap, it was decided to combine both datasets together, increasing hence a number of observations available for the common area. This step allowed to broaden spatial coverage in the central part of the province.

Table 12 Reduction in standard deviation values after Minneart topography correction observed for the LE71930282002200 scene. Analysis performed for 2040 pixels.

	LE71930282002200			
	no topographic correction		topographically corrected	
	Mean	St. dev.	Mean	St. dev.
Band 1	144.34	71.84	160.22	67.47
Band 2	249.50	93.61	301.19	81.02
Band 3	157.72	83.92	184.26	71.97
Band 4	1682.34	464.85	2004.19	433.41
Band 5	658.65	276.34	805.66	250.54
Band 7	298.92	155.02	368.11	135.55

Table 13 Reduction in standard deviation values after Minneart topography correction observed for the LT51920282003220 scene. Analysis performed for 5473 pixels.

	LT51920282003220			
	no topographic correction		topographically corrected	
	Mean	St. dev.	Mean	St. dev.
Band 1	218.32	45.10	229.50	40.97
Band 2	301.17	59.64	334.38	45.09
Band 3	233.82	61.52	263.66	47.93
Band 4	1586.29	277.01	1854.02	215.47
Band 5	685.71	201.95	837.01	141.03
Band 7	333.10	117.09	413.05	89.25

Table 14 Increase in standard deviation values after Minneart topography correction observed for the LT51930282010262 scene. Analysis performed for 5173 pixels.

	LT51930282010262			
	no topographic correction		topographically corrected	
	Mean	St. dev.	Mean	St. dev.
Band 1	132.61	40.46	150.32	42.84
Band 2	223.60	56.05	290.16	53.43
Band 3	162.23	48.33	222.74	49.45
Band 4	1154.04	306.00	1703.89	284.43
Band 5	427.02	162.88	603.92	164.64
Band 7	185.18	87.31	256.00	89.28

In the following, 192-028 and 193-028 image collections were combined and reordered for each year according to data quality (cloud cover and SLC striping) and acquisition date. Scenes registered in August were the most favorable since they captured possibly the highest drought impact, and have limited cloud contamination (Table 15). During the assessment procedure, a so called 'master image' was selected. It became a reference dataset in a subsequent relative normalization process (Figure 8). Having in mind dry conditions present for the majority of the investigated years, it was decided based on meteorological records, to assume year 2002 as a period of 'normal weather conditions'. Moreover, reference to a period previous to, or at the beginning of the investigated vegetation stress, reduced potential negative drought impact rendered in the data. Among five scenes available for the year 2002 (Table 15), LE71920282002209

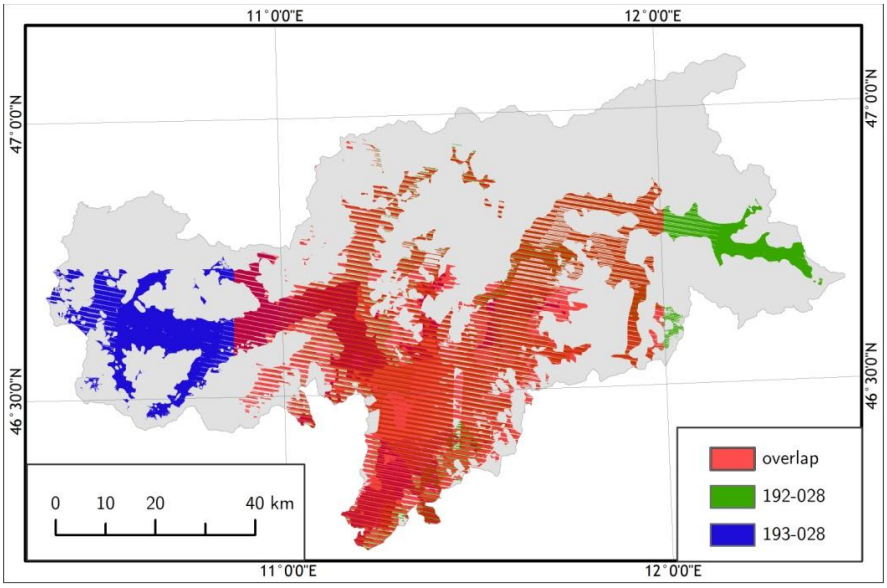

Figure 11 Pixels with a complete 2001-2012 Landsat data time series.

Table 15 Available 2001-2011 Landsat 192-028 and 193-028 datasets ordered for each year according to the acquisition date and overall quality. The bolded LE71920282002209 scene was selected as a reference (master) dataset in the iMAD normalization.

Dataset	Year	Date	Ordery
LE71920282001206	2001	Jul 25	1
LE71930282001213	2001	Aug 1	2
LE71920282001158	2001	Jun 7	3
LE71920282002209	**2002**	**Jul 28**	**1**
LE71930282002200	2002	Jul 19	2
LE71920282002225	2002	Aug 13	3
LE71930282002232	2002	Aug 20	4
LE71920282002241	2002	Aug 29	5
LT51920282003236	2003	Aug 8	1
LE71920282003260	2003	Sep 19	2
LT51930282003211	2003	Jul 30	3
LT51920282003220	2003	Aug 8	4
LE71930282003203	2003	Jul 22	5
LT51930282003259	2003	Sep 16	6
LT51930282003195	2003	Jul 14	7
LE71920282004247	2004	Sep 9	1
LE71920282004263	2004	Sep 19	2
LT51930282004214	2004	Aug 1	3
LE71920282005217	2005	Aug 5	1
LE71930282005224	2005	Aug 12	2
LE71930282005208	2005	Jul 27	3
LE71920282005201	2005	Jul 20	4

Dataset	Year	Date	Ordery
LT51930282006235	2006	Aug 23	1
LT51920282006244	2006	Sep 1	2
LE51920282006252	2006	Sep 9	3
LT51930282006203	2006	Jul 22	4
LT51930282007206	2007	Jul 25	1
LT51920282007199	2007	Jul 18	2
LT51920282007231	2007	Aug 18	3
LT51930282007238	2007	Aug 8	4
LT51920282007247	2007	Sep 4	5
LE71930282008201	2008	Jul 7	1
LE71920282008242	2008	Aug 8	2
LT51930282009227	2009	Aug 15	1
LE71920282009228	2009	Aug 8	2
LE71920282009244	2009	Sep 9	3
LT51930282009243	2009	Aug 31	4
LE71930282010238	2010	Aug 26	1
LT51930282010246	2010	Sep 3	2
LE71930282010254	2010	Sep 11	3
LT51920282010255	2010	Sep 12	4
LT51930282010262	2010	Sep 19	5
LE71920282010263	2010	Sep 20	6
LE71920282011234	2011	Aug 22	1
LT51930282011233	2011	Aug 21	2
LT51920282011226	2011	Aug 14	3
LE71930282011241	2011	Aug 29	4

image showed the highest quality comparing with remaining acquisitions, and therefore was selected as a 'master' scene.

Relative normalization to the LE71920282002209 dataset accounted on unification of forest phenological phase signal and was performed using the iMAD algorithm (Canty *et al.*, 2004). The process was done under a forest mask (see section 2.2.1.2) without division into forest ecosystems sub-domains. Further regionalization of already limited forest area could lead to excessive complexity and put into a question goodness of the overall normalization, as each sub-region would be characterized by a limited number of invariant pixels. Although vegetation phenology development is nonlinear (Helmer & Ruefenacht, 2007), the considered time-frame was narrow and excluded growth phase, making it possible to pass the linearity assumption.

Subsequently, NDVI and NDII7 indices were derived for each scene. The final compositing (Figure 8) was performed for each index separately using the previously defined data order. This practice was much alike in a composing module of the LandTrendr algorithm (Kennedy *et al.*, 2010) with one composite derived for each year. Following the pre-defined images order (Table 15) all data gaps in the primary scene were filled in employing information from the second the best scene. The procedure was continued with all the consecutive images of a given year until all gaps were filled-in or there was no more data to source from.

The aforementioned processing scheme resulted in a high quality 2001-2012 time series of NDVI and NBRI yearly composites, where cloud contamination and topography impact were minimized or excluded. Unfortunately, restricted amount of acquisitions as well as mountain-specific cloud cover formation process limited spatial coverage of both time series to 1336,053 km^2 (Figure 12), which represents only 42% of the forest are of South Tyrol.

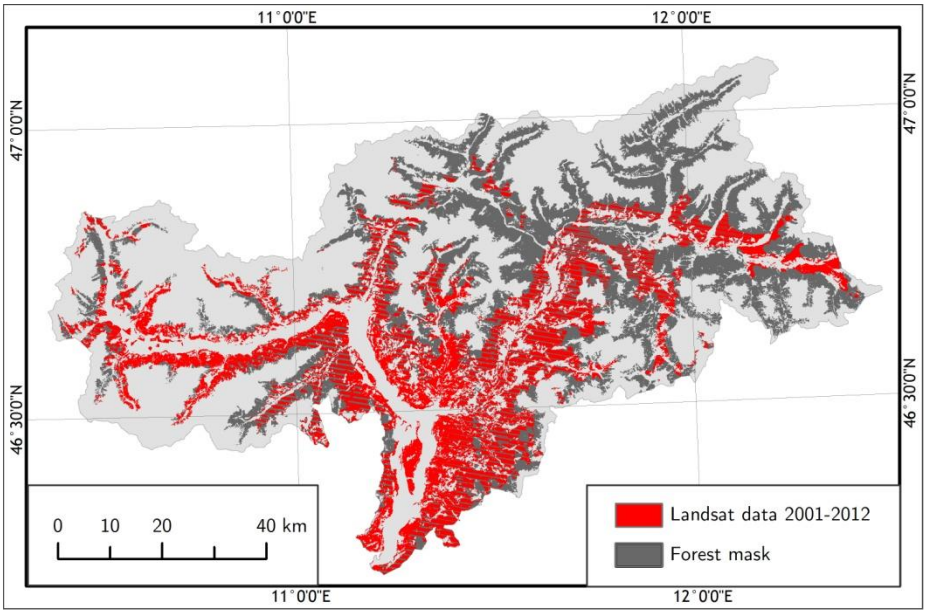

Figure 12 Final Landsat data coverage with respect to the forested area.

2.3. Principal Component Analysis (PCA)

Constant technology development results in a sustained increase in data collection. On one hand, richness of information allows on comprehensive investigation, hence deeper understanding of examined issues, but on the other hand, abundance of data imposes a need for more complex and efficient processing approaches.

A degree of convolution complexity increases with an increment of data dimensionality. Time series of satellite images is a good example of this phenomenon, as a feature space comprises not only the space and value, but also accounts on a time dimension. Multiple statistical and mathematical methods for multivariate analyses exist to mitigate the effect of data multidimensionality. Particularly interesting are variance oriented approaches that identify a dominant variability in space and/or time data domain (Venegas, 2001), which can be further related to processes or changes. Among these methods, Principal Component Analysis (PCA), Signal Value Decomposition (SVD), Common Factor Analysis (CFA) and Independent Components Analysis (ICA) are the best known and most frequently used ones.

The PCA, sometimes called also Empirical Orthogonal Functions (EOF; Wilks, 2006, p. 453), was introduced into the natural science in 1965 (Lorenz, 1956) and quickly gained wide recognition, especially in the meteorology and climate research (e.g. Singleton; Björnsson & Venegas, 1997; Venegas, 2001; Hannachi, 2004; Bordi *et al.*, 2006; Schrier *et al.*, 2007; Dai, 2011; Kim *et al.*, 2011; Tatli & Türkeş, 2011). Its robustness and straightforward calculation spurred further implementation for environmental studies (e.g. Studer *et al.*, 2005; Ivits *et al.*, 2013, 2014a) including a land cover classification (Lawley *et al.*, 2011) or time series analyses of remote sensed data (e.g. Eastman & Fulk, 1993; Lasaponara, 2006; Chen & Peter Ho, 2008; Small, 2012; Ivits *et al.*, 2013; Neeti & Ronald Eastman, 2014).

PCA identifies dominant components within a dataset investigating an inter-relationship between its elements. Depending on which dataset dimensions (space, time or field) are assigned as a variable and sample, PCA is performed in one of six unique modes (Richman Michael B., 1986; Preisendorfer, 1988). Since time series analyses focus either on time or space domain, appropriate PCA implementation accounts on the S- and T-mode respectively (Preisendorfer, 1988; Machado-Machado *et al.*, 2011). Once a data matrix is constructed, accordingly to the selected mode, dominant components are identified by solving the eigenproblem based either on covariance or correlation matrix, where the latter implies data standardization.

Mathematical principles of the S-mode covariance-matrix based PCA analysis are as follows (modified after: Björnsson & Venegas (1997) and Venegas (2001):

Taking an M x N dimensional data matrix F, where the M (rows) represents time and the N (columns) stands for locations, and M>N a covariance matrix F is formed by:

$$R_{FF} = F^t F \qquad [5]$$

where the F^t is a transpose of F, and the R_{FiFj} (a covariance between time series at i and j locations, where $i,j = 1...N$) is defined as:

$$R_{FiFj} = \frac{1}{N-1}\sum_{t=1}^{N} F_i(t) F_j(t) \qquad [6]$$

The R_{FF} covariance matrix is next decomposed into the E and Λ matrices through solving the eigenproblem (or the eigenvalue problem):

$$R_{FF}E = E\,\Lambda \quad [7]$$

The Λ is a diagonal N x N matrix of eigenvalues λ_N of R_{FF} where λ_N are usually sorted in decreasing order ($\lambda_1 > \lambda_2 > \ldots > \lambda_N$).

$$\Lambda = \begin{bmatrix} \lambda_1 & 0 & \cdots & 0 \\ 0 & \lambda_2 & \cdots & 0 \\ \cdots & \cdots & \cdots & \cdots \\ 0 & 0 & \cdots & \lambda_N \end{bmatrix} \quad [8]$$

The E is also an N x N dimensions matrix, with each column being an E^N eigenvector. Moreover, each non-zero eigenvalue λ_N corresponds with only one E^N eigenvector, and the eigenvectors are ordered according to the eigenvalues. Each eigenvalue λ_N informs about the proportion of the total variance in R_{FF} explained by the corresponding eigenvector E^N.

$$\%\ of\ explained\ variance\ of\ N = \frac{\lambda_N}{\sum_{i=0}^{N}\lambda_i} * 100 \quad [9]$$

Knowing that

$$\Lambda = E^tE = EE^t = I \quad [10]$$

where I is the Identity Matrix, eigenvectors are clearly orthogonal, thus uncorrelated over space.

Projection of E on the original dataset F

$$A = FE \quad [11]$$

gives an A^N – a time evolution of the E^N vector in time. This means that the F is now depicted by the spatial representations of E^N vectors called EOFs or loadings, and their time evolution A^N called principal components (PCs) or scores.

$$F = AE^t \quad [12]$$

Because a number of non-zero eigenvalues is usually $K \leq min(M,N)$, the effective amount of components reconstructing the original time series F is not greater than the minimal dimension of data matrix F. The equation [12] can be then given as:

$$F_N(t) = \sum_{k=1}^{K} A^k(t)\,E_N^k \quad [13]$$

where E is N x K, A is M x K, therefore F is M x N.

As aforementioned, EOF decomposition can be done based not only on a covariance but also on correlation matrix. The former is advisable when data are 'similar' or normalized *a-priori* because covariance matrix weights all observations equally. On the contrary, the correlation-matrix based approach is advisable for non-normalized data of different scales, as correlation matrix implements standardization of a dataset, which results in equal weights of all variables (Richman Michael B., 1986). In general, standardization allows on better identification of time/space patterns.

A correlation matrix is calculated through standardization of a covariance matrix

$$\mathcal{C}_{FiFj} = \frac{R_{FiFj}}{\sqrt{R_{FiFi}}\sqrt{R_{FjFj}}} \quad [14]$$

and the eigenproblem in [7] is posed as

$$\mathcal{C}_{FF}E = E\,\Lambda \quad [15]$$

All the further convolution steps stay the same.

The presented reasoning works efficiently only when N<M. An alternative solution for N>M introduces the eigenproblem in [7] as:

$$R_{FF}^{t}D = D\,\Lambda \quad [16]$$

where D is next projected on F in order to derive E

$$E = F\,D \quad [17]$$

Since F is M x N, R_{FF}^{t} is M x M, and D is M x M, resulting E has to be M x M, which means that not N, but only M eigenvectors are derived for this case. They correspond to the first M eigenvalues of Λ.

Independently of a standardization, covariance or correlation matrix is often additionally centered (or 'demeaned'; Venegas, 2001), which makes the variation relative to the mean. Importantly, centering done in the S-mode orientation (the mean is calculated for each location over time) detrends over space removing geographical differences. Conversely, when the centering is performed in the T-mode (the mean is calculated over space for each time step) results are detrended over time (Machado-Machado *et al.*, 2011).

As indicated by Richman Michael B. (1986), the PCA decomposition can be affected by domain shape dependence, instability of subdomains, and inaccuracy of EOFs (hence also PCs) desolation, which result in a misleading explanation of physical processes. These issues can be addressed through a rotation of a few first PCA loadings. The process strengthens and simplifies already detected patterns and maximizes the variance of EOFs, which leads to further clumping of similar modes. Additionally, regardless whether the orthogonal or oblique (procrustes) rotation model is applied, the physically unrealistic orthogonality hypothesis is released, which means new EOFs and PCs are correlated (Björnsson & Venegas, 1997). Due to this, the rotation is a controversial approach and according to Venegas (2001) should be considered individually for each dataset and intended application of PCA results.

The rotation can be realized through multiple transformations among which the most popular are Varimax (Kaiser, 1958) and Promax (Hendrickson & White, 1964) models for the orthogonal and oblique rotation respectively.

Although identification of an optimum number of factors to be rotated is an extremely crucial step, this selection is usually based on non-statistical approaches, therefore it is also the most elusive part of the process. The most frequently used stopping rules include (after Brown, 2009):

- Kaiser's stopping rule (Kaiser, 1960), which proposes to rotate all loadings with eigenvalue ≥ 1;
- Cattell's scree test (Cattell, 1966), in which the selection is based on a visual interpretation of the eigenvalues plot and identification of a transition point between an incline and leveled line. Because the transition point belongs to the

leveled part, only loadings of a lower order than the transition point are rotated. Cattell's scree test can be recognized as simplified graphical solution of the N rule (Preisendorfer, 1988);
- a-priori criterion, where a number of rotated factors is set beforehand;
- non-trivial factors approach, in which only these loadings are rotated that have at least 3 variables loadings above a certain threshold (customary 0.3);
- percent of cumulative variance criterion, in which rotated are these foremost loadings that eigenvalues sum up to a predefine value.

There is no clear recommendation of the stopping approach. Relatively neat Kaiser's rule, despite great popularity is considered as very inaccurate (Costello & Osborne, 2005). In contrast, seemingly inaccurate plot interpretation based scree test is considered a reliable approach for choosing a number of loadings for rotation.

PCA decomposition is a very powerful and versatile statistical method, but despite its popularity, it is sometimes implemented as an exploratory analysis, without correct exploitation of various PCA decomposition modes. Consequently, results might not be derived by the optimal PCA setup and next to general methodological constrains (Richman Michael B., 1986) they might be additionally affected by poor application. Importantly, there is no guaranty that derived scores and/or loadings have a true physical meaning and correspond to real processes (Hannachi, 2004). The main hindrance for this is the orthogonality assumption which can lead to redistribution of variance corresponding with recognizable physical variability between several uncorrelated EOF modes. Therefore only processes that act independently are possible to be successfully identified (Venegas, 2001). Whenever PCA is applied for identification of physically meaningful variability, it is advisable to evaluate results not only on a bases of eigenvalues, but also through associating the EOFs and/or PCs with known or expected process (Venegas, 2001). Moreover, it should be kept in mind that resulting loadings and scores have no arbitrary phase.

Due to all aforementioned, it is sometimes advised to explore several decomposition setups in a search for potentially the most accurate representation of expected variability. It is especially valid when the secondary rotation approach is implemented into the analysis (Venegas, 2001).

3. METEOROLOGICAL CONDITIONS IN SOUTH TYROL

3.1. Self-Calibrated Palmer Drought Severity Index (scPDSI)

Although drought originates mainly from rainfall deficit, co-occurring weather conditions that shape local evapotranspiration are equally important while estimating drought status. Due to this, among traditional drought indices based on long time series of on-station observations, comprehensive drought measures accounting on evapotranspiration conditions seem to be the most reliable ones (Vicente-Serrano *et al.*, 2010, 2014; Dai, 2011b; Ma *et al.*, 2012). The Palmer Drought Severity Index (PDSI; Palmer, 1965) with its variations (Dai, 2011b; van der Schrier *et al.*, 2013) is probably one of the most versatile and widely use comprehensive drought index to date. Furthermore, it was demonstrated to be well correlated with forest status (e.g. Büntgen *et al.*, 2010; Scharnweber *et al.*, 2011; Gillner *et al.*, 2013). Taking together, limited ground truth information and complexity of South Tyrol, scPDSI presents itself as the most comprehensive and reliable forest drought related index.

The PDSI is a simple 'bucket' model of water balance that estimates actual soil water availability with respect to the potential soil moisture. Beside precipitation and temperature records, it employs information on local soil holding capacity and climate driven moisture availability. The main flaw of the index is its setting on empirically derived constants, which were determined by Palmer for a restricted amount of locations and samples (Alley, 1984). Due to this, PDSI defines drought severity classes a bit arbitrary, without regard to the local climatic settings. Furthermore, the indicator employs the Thornthwaite equation (Thornthwaite, 1948) for a potential evapotranspiration model, and assumes precipitation to be always in a liquid phase (van der Schrier *et al.*, 2006). Due to this, although the PDSI is a robust drought index successfully implemented worldwide (e.g. Mika *et al.*, 2005; Dubrovsky *et al.*, 2009; Ram, 2012) and able to compare drought conditions on different location, it is not apt for comparisons between diverse climatic regions (Wells *et al.*, 2004; van der Schrier *et al.*, 2013).

To address the PDSI weaknesses several variants of the index have been established (Dai, 2011b; van der Schrier *et al.*, 2013). The self-calibrated Palmer Drought Severity Index (scPDSI) developed by Wells *et al.* (2004) takes an advantage of long time series of data (minimum 25 years) and substitutes empirical constants in the PDSI model with local-climate-based variables derived from the input dataset itself. This liberates the index from soil specific information that are not always available, and enhances accuracy of a between-climate comparison. Alike the PDSI, scPDSI is based on the Thornthwaite equation, and assumes liquid precipitation input. The computation is made most commonly on monthly bases and results in values assigned to predefined categories (Table 16), where scores follow the normal distribution predefined for introduced records. The statistical setup is designed to return extreme drought conditions with an approximate probability of 2% (Wells *et al.*, 2004).

The scPDSI has been successfully applied in numerous studies not only focusing on pure climate aspects (e.g. van der Schrier *et al.*, 2006, 2007, 2013; Briffa *et al.*, 2009; Potop *et al.*, 2012) but also investigating a climate-vegetation feedback (e.g. Drobyshev *et al.*, 2012; Fang *et al.*, 2012) with a particular focus on trees status (e.g. Büntgen *et*

al., 2010; Scharnweber *et al.*, 2011; Gillner *et al.*, 2013). Despite concerns indicated by Sheffield *et al.* (2012) and Vicente-Serrano *et al.* (2014), the PDSI and scPDSI models based on the Thornthwaite equation still remain solid indicators of drought severity (Dai, 2011a; Van Der Schrier *et al.*, 2011). Due to this, the scPDSI was selected for this study a primary index for the meteorological based drought examination in South Tyrol.

Table 16 Classification of the PDSI and scPDSI values (after Wells et al., 2004)

scPDSI value	scPDSI category
Above 4.00	Extreme wet spell
3.00 to 3.99	Severe wet spell
2.00 to 2.99	Moderate wet spell
1.00 to 1.99	Mild wet spell
0.50 to 0.99	Incipient wet spell
0.49 to -0.49	Normal
-0.50 to -0.99	Incipient drought
-1.00 to -1.99	Mild drought
-2.00 to -2.99	Moderate drought
-3.00 to -3.99	Severe drought
Below -4.00	Extreme drought

3.2. scPDSI calculation and analyses

The scPDSI algorithm developed by Wells *et al.* (2004) was used in this study. The model is distributed as a C++ code written within The GreenLeaf Project[4] (Wells, 2003), and with adequate input can provide scPDSI on monthly as well as weekly bases. Computation of scores was performed separately for each station based on the assembled monthly cumulative precipitation and mean temperature datasets (as described in section 2.2.1), hence ensured monthly scores.

All site-specific time series of different lengths were next collected and organized into one consistent structure. In order to match the time-span of MODIS time series, only the 2001-2012 scPDSI results were considered further. Subsequently, this collective dataset was introduced to the ENVI/IDL implemented correlation-matrix based S-mode PCA decomposition, which identified leading meteorological temporal variability in the region. Moreover, a yearly drought length (a total duration with the index below a certain threshold) and intensity (a mean value of the index below a certain threshold; after Mishra and Singh, (2010)) metrics were derived for each station for mild to extreme drought events (scPDSI<-1; Table 16). These values were subsequently regressed against stations elevation (Table 3) in order to check on possible interlink.

3.3. Results

The scPDSI calculated for 26 South Tyrolean meteorological stations revealed rather consistent weather variability between 2001 and 2012 (Figure 13).

[4] http://greenleaf.unl.edu

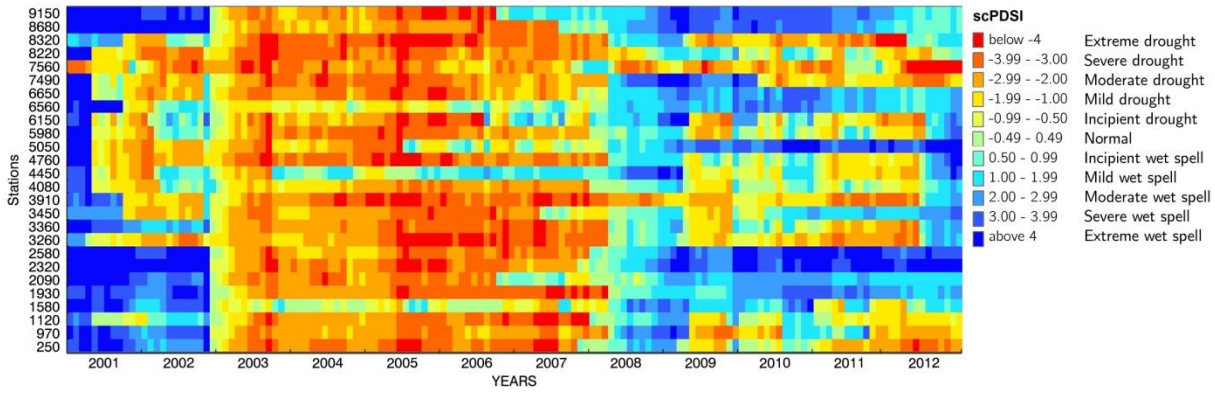

Figure 13 Distribution of scPDSI monthly values among the 26 stations (y axis) between January 2001 and December 2012 (x axis). Station identification numbers consist with Figure 4 and Table 3. scPDSI categories after (Wells, 2003).

Almost all stations showed at least moderate drought conditions between 2003 and 2007, with the most severe dry spells detected in 2003 and 2005. 11 out of 26 locations reported drought inception already in mid-2001, where 6 of them experienced a return of incipient or moderate wet conditions in 2002. The year 2008 was identified in all locations as rather moist period, but still not so wet as the beginning of the 00's. The last four years of the considered term revealed differences between stations, where some sites showed wet and very wet spells, while the others experienced dry conditions.

Spatial recognition indicated that stations located in the Vinschgau Valley (namely 250, 970, 1120, 1580, 1930, 2320 and 2580) experienced overall the least intense drought impact with commonly wet spell before and after the 2003-2007 anomaly. In contrary, central and eastern parts of the region (Eisack, Wipp and Puster Valleys) were much more affected by aridity, with drought inception already in mid-2001. Moreover, rainfall shortages and elevated temperatures were present there also beyond 2008. Especially extreme conditions were reported for two stations placed in the central part of the Eisack Valley and one in the Wipp Valley region (7560 - Fie allo Sciliar, 3910 - Bressanone, and 3260 - Vipiteno respectively).

The correlation-matrix based S-mode PCA analysis of the 2001-2012 monthly scPDSI time series provided a synthesis of the regional weather conditions. The first resulting PC (1scPDSI) accounted on 63%, of the total variance and depicted strong depression between 2003 and 2007, followed by an increase concluded in 2008 when values reached state observed in 2002 (Figure 14a). The second identified score (2scPDSI; Figure 14b) explained 9.95%, of the total variability and revealed a pattern with positive anomaly in 2001 and 2002 followed by lower and leveled values. The third principal component (3scPDSI; Figure 14c) described 7.36% of the overall signal variance demonstrating a leveled response until 2008 with two positive anomalies observed in 2002 and 2008. The following years revealed index decrease with an abrupt drop in 2009 and another decrease at a break of 2011 and 2012. The overall perception of this pattern suggested decreasing trend of $y=-0.0013x+0.0948$, $R^2=0.4378$ ($p=0.0000$). Finally, the fourth PC (4scPDSI; Figure 14d), which addressed 5.61% of data variability, demonstrated a subtle decrease between 2001 and 2008 followed by a strong positive anomaly in 2012. This response was defined by an overall insignificant trend of $y=-0.0001x+0.0104$,

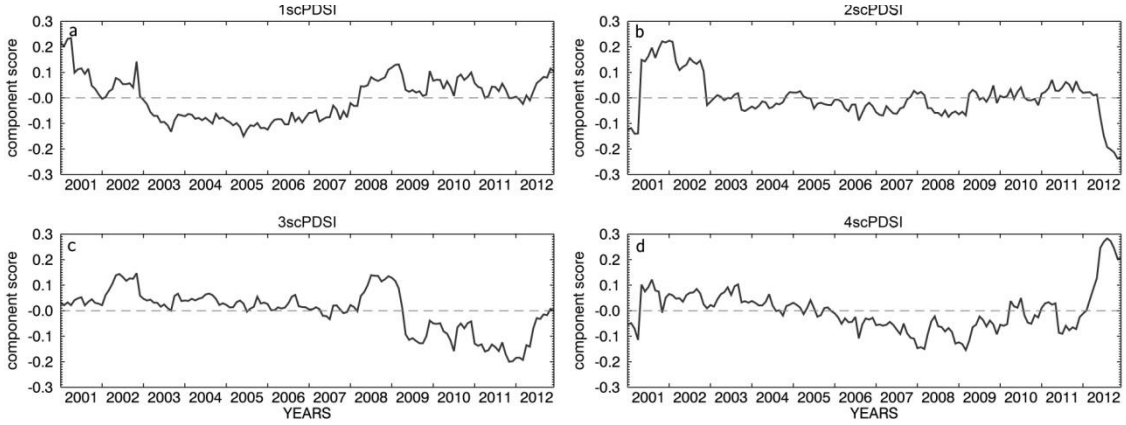

Figure 14 Four first PCs derived from the correlation-matrix based S-mode PCA of the 2001-2012 scPDSI time series: a) 1scPDSI, b) 2scPDSI, c) 3scPDSI and d) 4scPDSI. Presented scores explain 63%, 9.95%, 7.36% and 5.61% of the total scPDSI data variance respectively.

R^2=0.0052 (p=0.3892). However, focusing on the 2001-2007 period a decreasing tendency was described as y=-0.0015x+0.0701, R^2=0.429 with p<0.001. Principal Components of a higher order revealed no potentially meaningful temporal profiles, as well as obtained lower eigenvalues.

Annual station-specific drought intensity and length measures derived for scPDSI<-1 rendered main features of local dry spell conditions. Subsequently done year by year linear regression of both indicators against stations altitude did not reveal any meaningful relationships with most of the results insignificant at the level p<0.05 (Table 17). Furthermore, the overall on-station averaged drought intensity and length also revealed statistically insignificant connection to elevation, where, as expected, drought intensity demonstrated slightly positive trend of R^2=0.057 (p=0.238), while drought length revealed a minor negative tendency of R^2=-0.070 (p=0.193).

Table 17 Regression results performed for on-station yearly drought intensity and drought length metrics against stations altitude. All scPDSI observations greater than -1 were excluded from the analysis.

Year	Number of observations	Drought intensity		Drought length	
		regression	p-value	regression	p-value
2001	16	0.039	0.462	0.013	0.670
2002	16	0.153	0.134	0.012	0.683
2003	26	0.166	0.039	0.037	0.343
2004	24	0.148	0.064	0.041	0.344
2005	26	0.054	0.255	0.032	0.385
2006	25	0.115	0.097	0.252	0.011
2007	24	0.079	0.184	0.130	0.083
2008	12	0.248	0.099	0.076	0.385
2009	14	0.094	0.285	0.097	0.278
2010	16	0.011	0.693	0.482	0.003
2011	16	0.184	0.097	0.138	0.156
2012	16	0.204	0.079	0.002	0.884

3.4. Discussion and summary [5]

The presented scPDSI results provided an interesting and essential insight into the weather variability in South Tyrol between 2001 and 2012.

First of all, strong scPDSI drought condition was perceived in the region between 2003 and 2007 with the most severe dry spell in 2005 (Figure 13 and Figure 14a). Secondly, a clear positive anomaly was observed in 2008 for all on-stations scPDSI temporal profiles (Figure 13), and was well singled out in the 1scPDSI, 3scPDSI and also 4scPDSI scores (Figure 14a, c and d respectively). Next, the 2scPDSI, as well as 1scPDSI and 3scPDSI scores (Figure 14b, a and c respectively) highlighted above-average wet conditions for 2001 and 2002. Furthermore, the 3scPDSI indicated drought circumstances in 2009 and 2011 (Figure 14c), and an overall subtle decreasing trend. Finally, the 4scPDSI temporal pattern revealed a fine linear downturn between 2003 and 2007. Neither decreasing tendency was obvious in the original scPDSI dataset.

Interestingly, the most severe and prolonged drought impact was observed for the central and eastern part of the province, especially in the Eisack Valley, at Fie allo Sciliar (7560) and Bressanone (3910) stations, as well as in Bolzano (8320). This exceptional aridity supports climatic prediction of increasing drought thread in the floors and lower slopes of the main inter-alpine southern valleys (Gebetsroither *et al.*, 2013). On the contrary, the Vinschgau Valley – normally the driest area of South Tyrol; although reported drought influence between 2003 and 2007, revealed also a wet spell in 2001-2002 and overall moisture conditions from 2008 onwards. This result could be explained either by the relativistic nature of the scPDSI, or by indeed increasing humidity of the local Vinschgau climate (Schmidli et al., 2002; Auer et al., 2005).

The weakest drought stress was observed at stations: Vernago – Finale (1580), Santa Maddalena in Casies (4450), and Terento (6560; Figure 13). Although all three locations suffered limited drought conditions, they hardly followed the dry-spell variability between 2003 and 2007. Their disconnected localization excluded joint, regional-specific explanation of the phenomenon. Although the regression analyses showed no significant impact of the station altitude on neither drought severity nor length, comparison with neighboring locations performed for all three aforementioned sites suggests such dependency. Even though regression results indicated statistically uniform dry spell impact on all elevations, imposed regional differences in South Tyrolean weather patterns could obscure the impact of the elevation gradient. Moreover, conducted regression analyses are biased by the fact that all investigated meteorological stations are located below 2000 m asl (Table 3). Consequently, no solid conclusion on a local drought-elevation interlink should be drawn without further investigation.

Weather conditions during the last four years of the analyzed period varied fairly between sites. Stations in the central part of South Tyrol (Eisack and Wipp Valleys)

[5] All regional weather specific information used in this section was sourced from the CLIMAREPORT – an on-line publication of the Hydrographic Office of the Autonomous Province of Bolzano-Südtirol, Avalanche Prevention – Meteorological Service. Climareport numbers 63-204 (2001-2012) [URL: http://www.provincia.bz.it/meteo/climareport.asp]

revealed a tendency for higher scPDSI scores comparing with the rest of the province, which could be linked to the increasing aridity of the lower alpine valleys (Gebetsroither *et al.*, 2013).

Further investigation allowed to put the identified scPDSI variability in a broader context of European meteorological events. An inception of the strongest and most persistent drought conditions depicted by the 1scPDSI between 2003 and 2007 (Figure 14a) was in particular agreement with a very hot and dry summer of 2003, triggered by the pan-European summer heat wave of 2003 (e.g Rebetez et al., 2006). The consecutive year was also characterized by below-normal scPDSI values, which harmonized with drought conditions observed in the Western Europe and Mediterranean (Spinoni *et al.*, 2015). 2005 drought circumstances comprised an extremely arid spring culminated in a drought peak in May – June. These extreme conditions were attributed on exceptional setup of pressure system over Europe, and considerably affected the Iberian Peninsula and central Mediterranean Basin (García-Herrera *et al.*, 2007). An impact of the heat-wave of 2006, associated by Rebetez et al. (2008) mainly with Central and North Europe, was demonstrated in the analyses also for South Tyrol. Meteorological conditions showed here below-average rainfall sums and extreme temperatures from June onwards (Hydrographic Office of the Autonomous Province of Bolzano-Südtirol, 2006). Finally, drought conditions depicted in 2007 arose from averagely wet, but extremely hot spring and summer of 2007. These conditions were related to drought events observed in central Europe (EEA, 2012), Tyrol (Gruber *et al.*, 2010) as well as the Mediterranean region (August & Geiger, 2008). Comparing with the 2006 summer heatwave, which in South Tyrol revealed below-average rainfall sums and extreme temperatures only from June onwards, 2007 was richer in precipitation, but definitively much warmer in the first half of the year. Importantly, the extensive, five-year-long (2003-2007) persistent drought conditions identified in the study are in strong accordance with the drought response recognized for Central Europe by Ivits et al. (Ivits *et al.*, 2014). An earlier ingress of drought marked in the 1scPDSI (Figure 14a) and perceived in the southern and eastern parts of South Tyrol (Figure 14) could be linked to the Mediterranean drought of 2001-2002 (Ivits *et al.*, 2014).

Drought conditions in 2009 and 2011-2012 depicted in the 3scPDSI (Figure 14c) were perceived in the central and eastern part of South Tyrol (Figure 13) as well as the most western outskirts of the province. They correspond well with drought alerts in Central Europe (EEA, 2012) and drought in the western and central Mediterranean basin (Spinoni *et al.*, 2015). Moreover, the subtle scPDSI decreasing trend identified within the 3scPDSI temporal profile likely captured an on-going climate transformation and increasing aridity in the region, suggested by Auer et al. (Auer *et al.*, 2005). Alike observation was made for the 4scPDSI which indicated scPDSI decrease between 2003 and 2007 (Figure 14d).

Beside aforementioned drought events, identified meteorological variability indicated several periods with precipitation surplus. The scPDSI increase in 2008, depicted in the 1scPDSI and 3scPDSI (Figure 14a and c respectively), corresponds with a timing of Tropical Cyclone 'Emma', which hit Europe in the spring of 2008 and preceded a hot but rainy summer. Moreover, the excess of rainfall observed mainly in the northern part of South Tyrol in 2001 through 2002, and depicted in the 2scPDSI and 3scPDSI

(Figure 14b and c) is in strong accordance with the continental weather variability and flood events in Central Europe in 2002 (Eqecat, 2002). In addition, wetter than average meteorological condition denoted by the 1scPDSI and 3scPDSI during 2012 are also aligned with humid European weather patterns of that year.

Importantly, the North Hemisphere 2010 summer heat wave, which strongly impacted mainly eastern, northern and central Europe (Barriopedro *et al.*, 2011; EEA, 2012; Ivits *et al.*, 2014) did not constrain meteorological conditions in South Tyrol.

The S-mode PCA decomposition of the scPDSI time series worked well for identification of the dominant meteorological variability. Unlike in van der Schrier *et al.* (2013), resulting scores obtained high explanatory values, which supports their credibility. Importantly, the 1scPDSI PC came out robust and with very informative physical meaning (Figure 14a). The three following principal patterns also revealed interesting variability, which was strongly governed by pan-European, as well as more local meteorological conditions identified in other studies.

Potential shortcoming of the scPDSI use for the alpine forest monitoring originates from the algorithm assumption on the liquid phase of precipitation. This issue could be addressed through a scPDSI-incorporated snowmelt model (van der Schrier *et al.*, 2007). However, as snowfall and concluding snow cover affect mostly alpine and subalpine zones, leaving the colline and mountain forest under limited snow impact, it was decided to keep the original assumption. Nevertheless, this aspect should be mitigated for broader scPDSI use in the alpine environment. The second issue not discussed directly for the scPDSI, neither any other straightforward meteorological drought index, is a water discharge due to the land morphology. Slope steepness affects local water availability leading to faster runoff, but also implying additional water supply from the higher regions (from rainfall or snowmelt). It is a crucial factor, especially for the poor and shallow mountain soils with limited water holding capacity. Since the on-site scPDSI calibration excludes the inclination influence, results obtained for the steep locations are positively biased in comparison to the actual soil moisture conditions.

Another drawback of the presented analysis is a use of on-station measurements, which limits spatial understanding of drought variability that is especially complex and interesting in the mountains. However, due to a lack of high resolution spatial meteorological datasets covering the region of interest, as well as a reliable regional model for spatial interpolation of meteorological point measures, employed approach was the best possible.

The use of the Thornthwaite equation based scPDSI model can be questioned too, especially in a scope of analyses did by Dai (2011a), Sheffield *et al.* (2012) and Vicente-Serrano *et al.* (2014) who demonstrated that incorporation of diverse evapotranspiration approximations can lead to significantly different results. However, as highlighted in Sheffield *et al.* (2012) this inconsistency is concerning mainly for long-term trend analyses, and is not so crucial in rendering drought severity at a given moment, neither a series of moments, which was in fact the main purpose of this investigation. Therefore it is assumed that the above-presented results are not affected by this problem and provide a robust and valuable insight.

Demonstrated scPDSI based analyses ensure accurate approximation of local weather conditions. Presented variability not only highlighted the most prominent local patterns and tendencies, but most importantly, rendered well pan-European meteorological changeability, identified in other studies. This observation confirms not only a high utility of the scPDSI for drought monitoring, but also shows how dominant and extensive were discussed drought events.

Although the presented study focuses only on a simple scPDSI based synthesis analyzing weather conditions between 2001 and 2012, obtained results suggest presence of potentially broader and longer trends and relations. It could be very interesting to address the topic better, expanding the analysis in time in order to investigate long climatic trends in the region. Such a study could provide a better understanding of the meteorological variability in South Tyrol, and possibly also in the whole Alps.

4. FOREST DROUGHT ASSESSMENT THROUGH MODIS TIME SERIES ANALYSES

4.1. Design of the study

PCA decomposition of MODIS derived 2001-2012 NDVI and NDII7 time series was targeted at recognizing drought induced forest status variability, and identifying the most effective PCA method and data setups to do so. To meet this requirements the study design accounted on extensive S-mode PCA analyses (Figure 15) of multiple datasets (Table 7 and Table 8), correlation and covariance-matrix based PCA convolution as well as two rotation approaches.

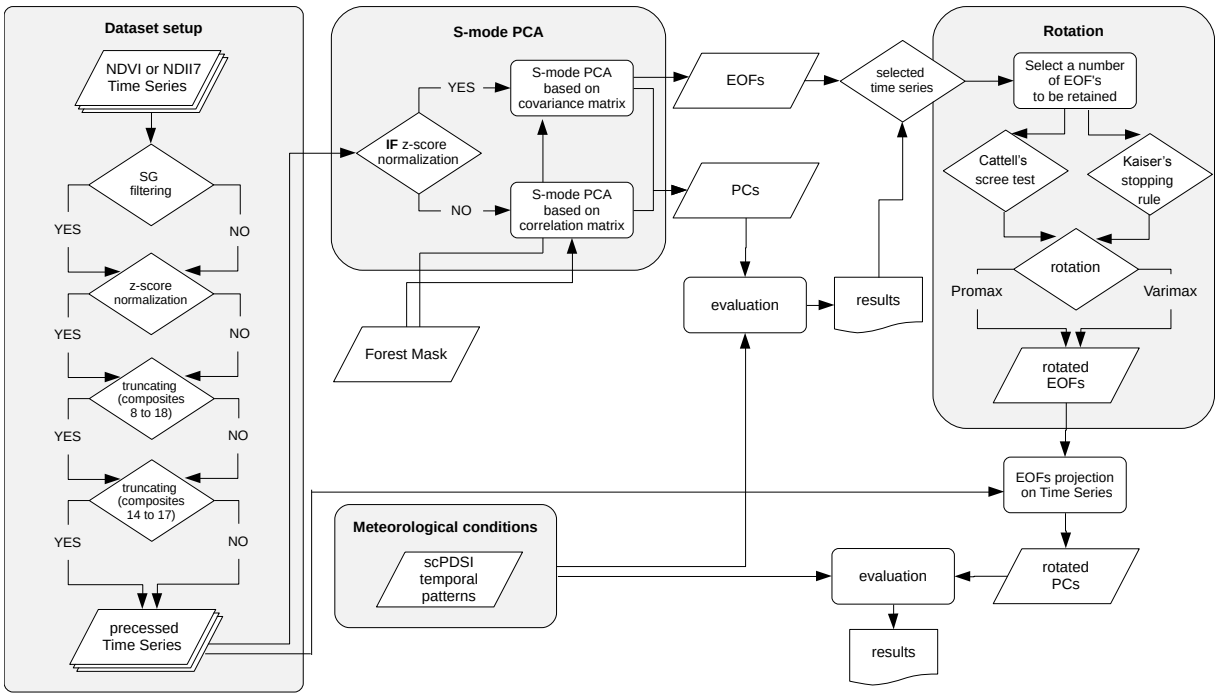

Figure 15 Conceptual flow chart of data and method setup for the PCA S-mode analyses of remotely sensed time series of vegetation indices. NDVI and NDII7 datasets were processed separately.

Altogether, 12 PCA decompositions of diverse setups (Table 18) were inspected. They aimed at a comparison among: two vegetation indices (namely NDVI and NDII7), SG-filtered and not-filtered data, z-score normalization of time series, different annual time-windows as well as correlation and covariance-matrix PCA results. Utility of the SG-filtering was examined only for NDVI, since this index better rendered phenology dynamism. Exploration of different length of annual time-windows was also focused mainly on NDVI time series. Following a suggestion of Eastman & Fulk (1993) a covariance-matrix based PCA was applied to z-score normalized time series, while not-normalized datasets were decomposed based on a correlation matrix. Remarkably, all S-mode PCA analyses were run under the forest mask.

Results of each tested PCA setup were evaluated through their PCs (scores) representing temporal profiles of identified changes. As proposed by Venegas (2001),

Table 18 Summary of the S-mode PCA design exploring utility of the NDVI and NDII7 time series, data z-score normalization, SG-filtering, diverse annual time windows, correlation and covariance-matrix based PCA setting, as well as loading rotation for detection of drought related changes in forest status.

Dataset	Index	z-score normalization	SG filtering	Time window (MODIS composites)	PCA matrix	Rotation
$NDVI_{1\text{-}23}$	NDVI	no	no	full year (1-23)	cor	no
$NDVI_{SG1\text{-}23}$	NDVI	no	yes	full year (1-23)	cor	no
$nNDVI_{1\text{-}23}$	NDVI	yes	no	full year (1-23)	cov	no
$nNDVI_{SG1\text{-}23}$	NDVI	yes	yes	full year (1-23)	cov	no
$NDVI_{8\text{-}18}$	NDVI	no	no	veg. season (8-18)	cor	no
$NDVI_{SG8\text{-}18}$	NDVI	no	yes	veg. season (8-18)	cor	no
$nNDVI_{8\text{-}18}$	NDVI	yes	no	veg. season (8-18)	cov	yes
$nNDVI_{SG8\text{-}18}$	NDVI	yes	yes	veg. season (8-18)	cov	no
$nNDVI_{14\text{-}17}$	NDVI	yes	no	high season (14-17)	cov	yes
$NDII7_{8\text{-}18}$	NDII7	no	no	veg. season (8-18)	cor	no
$nNDII7_{8\text{-}18}$	NDII7	yes	no	veg. season (8-18)	cov	yes
$nNDII7_{14\text{-}17}$	NDII7	yes	no	high season (14-17)	cov	no

Abbreviations: SG - Savitzky-Golay; veg. – vegetation; cor – correlation; cov – covariance

beside inspection of eigenvalues informing about robustness of each pattern, a correspondence with the scPDSI leading PCs was analyzed in order to draw a conclusion on an expected vegetation feedback. Only the first four PCs (scores), resulting from each of the tested PCA setup and representing temporal profiles of changes in forest vegetation status, were cross-compared against four identified scPDSI temporal patterns. Owing to inconsistent time steps (16-day vs. monthly) and annual windows (12 months vs. 23, 11 or 4 composites per year), vegetation indices based PCs and scPDSI temporal profiles were correlated for yearly averages. Since a sign of a resulting PCA score function is arbitrary and originates from the data variance based rotation of the original dataset, when needed, a sign of emerging PCs was subsequently adjusted to fit the scPDSI approximated meteorological variability. This step simplified interpretation and comparison between results. A limit to inspect only the first four resulting PCs of each PCA setup was governed by eigenvalues that indicate amount of dataset variance explained by a given loading and corresponding score. Since temporal and spatial patterns associated with higher variance are more likely to carry a physical meaning (Venegas, 2001), it was decided to focus only on the most prominent PCs.

The rotation was applied only to three PCA setups based on the $nNDVI_{8\text{-}18}$, $nNDII7_{8\text{-}18}$ and $nNDVI_{14\text{-}17}$ time series (Table 18). This selection was guided by the most auspicious drought temporal variability demonstrated among the first four resulting PCs of the lowest order obtained using z-score normalized vegetation season datasets. The additional inclusion of the high-season NDVI time series illustrated rotation impact on dataset with limited data variance. Varimax and Promax approaches were implemented for three aforementioned datasets. A number of EOFs to be retain for a

rotation was identified using Cattell's scree test and Kaiser's stopping rule. Also in a case of rotation, the investigation was limited to the first four emerging PCs.

Influence of Savitzky-Golay filtering on PCA decomposition results was assessed through a linear correlation run for corresponding PCA scores derived using filtered and non-filtered time series. It provided information on mutual similarity and potential advantages originating from noise reduction. Alike quantitative assessment procedure was undertaken for the rotation results where the similarity/disparity among rotated and original PCs, as well as eigenvectors emerging from diverse rotation approaches were investigated.

Each score potentially carrying information on drought impact on vegetation was subsequently correlated on pixel-bases with its original PCA-introduced vegetation index time-series. An emerging correlation map showed a spatial projection of a given temporal pattern and provided qualitative measure of its spatial representation. Unlike an EOF (loading), a correlation map ensures a quantitative resemblance assess thus a straightforward interpretation of the investigated temporal variation (Venegas, 2001).

Although the preselected PCs were derived using diverse datasets and PCA setups, they noticeably rendered similar temporal behavior. Therefore, all identified potentially drought related scores and their spatial representations were compared in order to identify the most reliable and informative patterns for further and detailed investigation. During the process PCs and their spatial representations were mutually examined using Pearson correlation analysis. Once the most representative potential forest drought patterns were selected, they were subsequently analyzed for real vegetation impact using time series of phenological indicators (section 2.2.2.2). Each selected spatial representation was classified into six drought severity classes using 5^{th}, 30^{th}, 50^{th}, 70^{th} and 95^{th} percentiles of the correlation values distribution. Class 1 (5^{th} percentile) represented regions with the most negative, whereas class 6 (95^{th} percentile) the most positive Pearson's correlation values. Only pixels with significance $p<0.1$ were taken into consideration. The threshold allowed to increase credibility of results simultaneously preserving a sensible amount of observations.

Firstly, significance of each classification was checked through the F-test based comparison between strata. Only then, a special insight was given to the areas with the strongest agreement with investigated drought temporal patterns (class 6), as well as their opposites (class 1). Drought impact assessment was done with yearly phenological indices using repeated ANOVA (Analysis of Variance) within factors of:

- forest type mask (coniferous, mixed, broadleaved);
- elevation (0-700 m asl, 700-1400 m asl, 1400-2100 m asl, 2100-2500 m asl; elevation stratification after Theurillat and Guisan, (2001));
- exposition (N, E, S, W);
- inclination (0°-10°, 10°-20°, 20°-30°, 30°-40°, 40°-90°).

4.2. Forest condition indicated by PCA of MODIS time series

4.2.1. NDVI time series

4.2.1.1. Full year time series: $NDVI_{1\text{-}23}$, $nNDVI_{1\text{-}23}$, $NDVI_{SG1\text{-}23}$ and $nNDVI_{SG1\text{-}23}$ [6]

The correlation-matrix based S-mode PCA of the complete NDVI time series ($NDVI_{1\text{-}23}$) revealed seasonality in all first four resulting PCs (Figure A2 1). This behavior was the most robust for the first score ($1CORNDVI_{1\text{-}23}$), which explained 63.23% of the total data variability. The following scores not only demonstrated more wobbly temporal profiles but also accounted on significantly smaller data variance (3.29%, 2.68 and 1.69% respectively for PCs two to four). The PCs showed limited similarity to the scPDSI temporal profiles where only the 2PC ($2CORNDVI_{1\text{-}23}$) and 3scPDSI, as well as 3PC ($3CORNDVI_{1\text{-}23}$) and 1scPDSI demonstrated significant moderate correlation on a yearly basis (Table A2 1). This accordance was however vague during a visual inspection of the PCs.

A seasonal component was clearly detectable in the four first scores of the correlation-matrix based S-mode PCA of the complete SG filtered NDVI time series ($NDVI_{SG1\text{-}23}$; Figure A2 2). The first PC ($1CORNDVI_{SG1\text{-}23}$) accounted on 70.86% of the total variance and distinctly followed phenological cycle. The consecutive scores revealed less prominent temporal behavior with intense spikes. They explained 3.51%, 2.71% and 1.77% of variability in the time series for the 2PC ($2CORNDVI_{SG1\text{-}23}$), 3PC ($3CORNDVI_{SG1\text{-}23}$) and 4PC ($4CORNDVI_{SG1\text{-}23}$) respectively. Moderate resemblance was indicated for the $2CORNDVI_{SG1\text{-}23}$ and $3CORNDVI_{SG1\text{-}23}$ that corresponded with the 3scPDSI and 1scPDSI scores respectively (Table A2 2). Visual comparison did not point to this concurrence. The overall similarity to the $NDVI_{1\text{-}23}$ based PCA results was very high (Table A2 3).

The full year, z-score normalized NDVI time series ($nNDVI_{1\text{-}23}$) introduced into the covariance-matrix S-mode PCA revealed temporal patterns with intense changes between consecutive observations (Figure A2 3). The first four PCs accounted together on 28% of the data variance with the first score ($1COVnNDVI_{1\text{-}23}$) explaining 18.55%. Correlation with the scPDSI temporal profiles, done for yearly averages, indicated a significant strong negative relation between the 2PC ($2COVnNDVI_{1\text{-}23}$) and 1scPDSI, as well as 3PC ($3COVnNDVI_{1\text{-}23}$) and 3scPDSI (Table A2 4). Due to unsteady temporal response of the NDVI based scores this relation was latent in the PCs.

The covariance-matrix implemented S-mode PCA of the complete, z-score normalized SG filtered NDVI dataset ($nNDVI_{SG1\text{-}23}$) resulted in scores of intense changeability, which partly blurred perception of overall trends (Figure A2 4). Alike it was observed for three other complete NDVI time series, a significant relation with the scPDSI patterns was demonstrated for the 2PC ($2COVnNDVI_{SG1\text{-}23}$) which related to the 1scPDSI score as well as the 3PC ($3COVnNDVI_{SG1\text{-}23}$) which correlated with the 3scPDSI (Table A2 5). Four first resulting scores explained together 34.12% of the total data variance where the 1PC ($1COVnNDVI_{SG1\text{-}23}$) accounted on 22.48%. The following scores addressed correspondingly 6.5%, 3.03% and 2.26% of data variability.

[6] Complementary information in the Appendix 2, Section A.2.1

Similarity between corresponding principal components of the S-mode PCA run for $nNDVI_{1\text{-}23}$ and $nNDVI_{SG1\text{-}23}$ time series was strong (Table A2 6).

4.2.1.2. Vegetation season time series: $NDVI_{8\text{-}18}$, $nNDVI_{8\text{-}18}$, $NDVI_{SG8\text{-}18}$ and $nNDVI_{SG8\text{-}18}$ [7]

The correlation-matrix S-mode PCA decomposition of the vegetation season NDVI time series ($NDVI_{8\text{-}18}$) left some periodic fluctuations in the PCs (Figure A2 5). It was especially strong in the first score, which explained 41.94% of the total data variance. Although not supported through a correlation with the scPDSI temporal profiles (Table A2 7), the 1PC ($1CORNDVI_{8\text{-}18}$) depicted diminished score envelope in 2003, 2006, 2007 and 2011. $NDVI_{8\text{-}18}$ derived PCs of the higher order addressed much smaller amount of the data variability, namely 4.77%, 3.04% and 2.68% respectively for scores two to four. Comparison with the scPDSI temporal profiles done on yearly bases indicated the 2PC ($2CORNDVI_{8\text{-}18}$) to be in high accordance with the 1scPDSI patter (Table A2 7). Despite positive statistics visual perception of this score presented some ambiguity due to various single-value anomalies that obscured the overall trend.

The first four principal components obtained from the correlation-matrix S-mode PCA of the SG filtered, vegetation-season NDVI ($NDVI_{SG8\text{-}18}$) indicated a seasonal component (Figure A2 6), which was particularly dominant in the 1PC ($1CORNDVI_{SG8\text{-}18}$). The pattern accounted on 52.88% of the total data variability and demonstrated diminished seasonal maxima of the score envelope in 2003, 2006 and 2007. This observation was not supported by correlation with the scPDSI (Table A2 8). Three consecutive PCs of the higher order, which explained 5.03%, 3.23% and 2.26% of data variance accordingly, demonstrated less robust response with several abrupt anomalies. Despite this, a strong relation was indicated between 2PC ($2CORNDVI_{SG8\text{-}18}$) and the 1scPDSI (Table A2 8), whereas the 3PC ($3CORNDVI_{SG8\text{-}18}$) was moderately correlated with the 2scPDSI. Correlation between corresponding scores that resulted from the $NDVI_{8\text{-}18}$ and $NDVI_{SG8\text{-}18}$ based PCA was strong only for a pair of the first PCs (Table A2 9). The following scores revealed moderate accordance which decreased with increasing PCs order.

The vegetation season z-score normalized NDVI time series ($nNDVI_{8\text{-}18}$) convoluted with the covariance matrix based S-mode PCA produced scores with intense variability between consecutive values (Figure A2 7). Dominance of the first PC ($1COVnNDVI_{8\text{-}18}$) was not so strong comparing with the $nNDVI_{8\text{-}18}$ based results, with the leading score explaining 15.25% of the data variance. A potential physical meaning of forest drought impact was observed in the 2PC ($2COVnNDVI_{8\text{-}18}$) that negatively correlated on yearly bases with the 1scPDSI and 2scPDSI. Furthermore, the 3PC ($3COVnNDVI_{8\text{-}18}$) depicted intense score drop in 2003 and was found in negative accordance with the 3scPDSI (Table A2 10). Both PCs explained 5.56% and 3.37% of the total data variance respectively (Figure A2 7).

The covariance-matrix based S-mode PCA of the SG filtered, vegetation season z-score normalized NDVI time series ($nNDVI_{SG8\text{-}18}$) fostered seasonality-free scores (Figure A2 8). Consequently, data variance was scattered with consecutive 1-4 principal components explaining 18.15%, 6.82%, 4.46% and 3.09% data variability respectively.

[7] Complementary information in the Appendix 2, section A.2.1

A correlation with the scPDSI patterns was significant only for the 2PC ($2COVnNDVI_{SG8\text{-}18}$) which was linked to the 1scPDSI and 2scPDSI scores, as well as the 3PC ($3COVnNDVI_{SG8\text{-}18}$) which was moderately correlated with the 3scPDSI (Table A2 11). Resemblance between corresponding $nNDVI_{8\text{-}18}$ and $nNDVI_{SG8\text{-}18}$ based PCA decomposition results were usual moderate with an exception of a pair of the third scores (Table A2 12).

4.2.1.3. High-season time series: $nNDVI_{14\text{-}17}$ [8]

Among the four first scores originating from the covariance-matrix S-mode PCA of the z-score normalized high-season NDVI time series ($nNDVI_{14\text{-}17;}$ Figure A2 9) only the 1PC ($1COVnNDVI_{14\text{-}17}$) and 4PC ($4COVnNDVI_{14\text{-}17}$) revealed significant correlation with the scPDSI variability, rendering 1scPDSI and 2scPDSI patterns respectively (Table A2 13). In both cases visual comparison suggested partial accordance with the scPDSI profiles. On the other hand, the 2PC ($2COVnNDVI_{14\text{-}17}$) as well as the 4PC ($4COVnNDVI_{14\text{-}17}$) depicted variability which was much alike the 4scPDSI, however this observation was not supported by the statistics (Table A2 13). The first four PCs explained accordingly 15.85%, 6.43%, 5.03% and 4.36% of the data variance (Figure A2 9) revealing limited dominance of the first principal component.

4.2.2. NDII7 time series

The $NDII7_{8\text{-}18}$ based PCA analyses were narrowed to three designs employing vegetation season and high-season time series (Table 18).

4.2.2.1. Vegetation season time series: $NDII7_{8\text{-}18}$, $nNDII7_{8\text{-}18}$ [9]

The vegetation season NDII7 ($NDII7_{8\text{-}18}$) was decomposed with the correlation-matrix based S-mode PCA. Resulting temporal profiles rendered vegetation seasonality of diverse level of complexity (Figure A2 10). Already the first extracted PC ($1CORNDII7_{8\text{-}18}$) showed a potentially meaningful response to drought conditions, demonstrating lowered score envelope between 2003 and 2007. This temporal profile was strongly consistent on a yearly bases with the 1scPDSI (Table A2 14), and represented 22.55% of the total data variance. Furthermore, the $1CORNDII7_{8\text{-}18}$ indicated moderate negative relation to the 3scPDSI (Table A2 14). Among the scores of a higher dimension significant 1scPDSI imprint was apparent in the third ($3CORNDII7_{8\text{-}18}$) and fourth ($4CORNDII7_{8\text{-}18}$) PCs that accounted on 4.40% and 2.68% of the total data variability respectively. Perception of those agreements was however limited due to intensive fluctuation in the $NDII7_{8\text{-}18}$ temporal profiles.

Principal components obtained through the covariance-matrix S-mode PCA decomposition of the z-score normalized vegetation season NDII7 time series ($nNDII7_{8\text{-}18}$) revealed intense anomalies (Figure A2 11). Although the 1PC ($1COVnNDII7_{8\text{-}18}$), which explained 11.98% of the data variance, revealed on a yearly basis strong negative correlation to the 1scPDSI (Table A2 15), their visual accordance was not so obvious. This score showed intense anomaly in 2003 and 2004 with a contrasting response at a break of 2006 and 2007. Although a PC of the fourth

[8] Complementary information in the Appendix 2, section A.2.1
[9] Complementary information in the Appendix 2, section A.2.2

dimension (4COVnNDII7$_{8\text{-}18}$) accounted on only 1.66% of the total data variance, it clearly resembled the 1scPDSI, which was further supported by correlation analysis done on a yearly bases (Table A2 15). Moreover, 4COVnNDII7$_{8\text{-}18}$ demonstrated also a moderate connection to the 4scPDSI (Table A2 15). Neither a 2PC (2COVnNDII7$_{8\text{-}18}$) nor 3PC (3COVnNDII7$_{8\text{-}18}$) revealed interesting temporal variability following any of the scPDSI profiles.

4.2.2.2. High-season time series: nNDII7$_{14\text{-}17}$ [10]

The z-score normalized high-season NDII7 time series (nNDII7$_{14\text{-}17}$) was analyzed with covariance-matrix implemented S-mode PCA. The first resulting PC (1COVnNDII7$_{14\text{-}17}$) demonstrated dominance over consecutive scores explaining 14.36% of the data variability (Figure A2 12). Its temporal profile moderately related to the 4scPDSI (Table A2 16). Three consecutive scores explained very similar fraction of the total data variability: 3.89%, 3.31% and 3.20% for PCs two, three and four respectively. They all showed visual analogy with the 1scPDSI. Yearly means based correlation with scPDSI suggested moderate connection between 4PC (4COVnNDII7$_{14\text{-}17}$) and 4scPDSI as well as detected the 3scPDSI based variability in 2PC (2COVnNDII7$_{14\text{-}17}$) and 3PC (3COVnNDII7$_{14\text{-}17;}$ Table A2 16).

4.2.3. Rotation

4.2.3.1. COVnNDVI$_{8\text{-}18}$ [11]

Following the Cattell's scree test the five first EOFs were used in rotation analyses of the COVnNDVI$_{8\text{-}18}$ dataset (Figure A3 1A). A convolution performed with Varimax (Figure A3 1B) and Promax (Figure A3 1C) algorithms produced very similar results (Table A3 1), although their visual comparison was not apparent. Among the Varimax scores, a significant moderate relation with scPDSI (on yearly bases) was recognized for 1PC (1COVnNDVI$_{8\text{-}18}$ROT5V) and 2scPDSI, as well as for 2PC (2COVnNDVI$_{8\text{-}18}$ROT5V) and 3scPDSI (Table A3 2). Promax rotation results had smoother temporal profiles and demonstrated better connection with the scPDSI patterns (Table A3 2). All four scPDSI temporal patterns were successfully recognized, where the 1scPDSI influenced 3PC (3COVnNDVI$_{8\text{-}18}$ROT5P), 2scPDSI controlled 1PC (1COVnNDVI$_{8\text{-}18}$ROT5P), 3scPDSI drove 2PC (21COVnNDVI$_{8\text{-}18}$ROT5P) and 3PC (3COVnNDVI$_{8\text{-}18}$ROT5P), whereas 4scPDSI governed 4PC (4COVnNDVI$_{8\text{-}18}$ROT5P). The rotation clearly altered variance of resulting temporal patterns where only the first PCs were strongly correlated with their not-rotated equivalent (Table A3 3).

Subsequently both rotations were performed using the four first EOFs retained based on Kaiser's stopping rule (Figure A3 1A). Also in this case, corresponding PCs produced using orthogonal and oblique rotation solutions (Figure A3 1D and E) were highly correlated (Table A3 4). Only two scores obtained through Varimax rotation demonstrated correspondence with meteorological variability (on yearly bases): 1PC (1COVnNDVI$_{8\text{-}18}$ROT4V), which indicted accordance with 2scPDSI, and 4PC (4COVnNDVI$_{8\text{-}18}$ROT4V), which was in line with 1scPDSI (Table A2 5). Temporal

[10] Complementary information in the Appendix 2, section 4.2.2.2
[11] Complementary information in the Appendix 3, section A.3.1

patterns derived using Promax solution supported 2scPDSI (2PC; 2COVnNDVI$_{8\text{-}18}$ROT4V) and 3scPDSI (2COVnNDVI$_{8\text{-}18}$ROT4V and 3COVnNDVI$_{8\text{-}18}$ROT4V). Notably, rotation performed using the four first EOFs demonstrated less intense alternation of variance within PCs (Table A3 6) than it was observed for scores based on the rotation of the five first scores. In the former case, regardless the rotation approach, all three first PCs showed high to moderate correlation with their uncorrelated equivalents. Differences between PCs produced based on five and four rotated EOFs were very small for Varimax (Table A3 7) as well as Prmax (Table A3 8) solutions.

4.2.3.2. COVnNDVI$_{14\text{-}17}$ [12]

The Cattell's scree test performed for the COVnNDVI$_{14\text{-}17}$ dataset indicated seven first EOFs (Figure A3 2 A) to be used for a rotation. First four PCs obtained for the Varimax (Figure A3 2 B) and Promax (Figure A3 2 C) approaches showed strong accordance on a statistical (Table A3 9) as well as visual level. Promax rotation results demonstrated smoother temporal profiles and narrower spectrum of changes. Correlation with the scPDSI variability performed for yearly averaged time series suggested for both rotation solutions a strong connection between 1scPDSI and 4PCs (Table A3 10; 4COVnNDVI$_{14\text{-}17}$ROT7V and 4COVnNDVI$_{14\text{-}17}$ROT7P). These scores highlighted an intense anomaly in 2002 followed by opposing deviation in 2004. Both 1PCs (1COVnNDVI$_{14\text{-}17}$ROT7V and 1COVnNDVI$_{14\text{-}17}$ROT7P) revealed 4scPDSI impact and emphasized a 2004-2005 anomaly that contrasted with a response in 2006-2007. Moreover, 1COVnNDVI$_{14\text{-}17}$ROT7V supported also 2scPDSI variability. On the other hand, Promax results demonstrated an interlink between 2PC and 4scPDSI, as well as 3PC and 3scPDSI. Regardless rotation approach, a strong 2003 anomaly was recognized in all 2PCs. Comparison among first four unrotated and rotated scores implied no relation (Table A3 11).

Following the Kaiser's rule rotation was done for 34 first PC's (Figure A3 2 A). Both algorithms returned highly correlated temporal profiles (Table A3 12) with one strong, isolated anomaly in each score (Figure A3 2 D and E for Varimax and Promax respectively). Drought related meteorological variability of the 1scPDSI was reflected in the 4PCs (Table A3 13). Moreover, a statistically significant connection was recognized between the two 2PCs (2COVnNDVI$_{14\text{-}17}$ROT34V and 2COVnNDVI$_{14\text{-}17}$ROT34P) and 4scPDSI, as well as Promax base 1PC (1COVnNDVI$_{14\text{-}17}$ROT34P) and 2scPDSI. A similarity between unrotated and rotated COVnNDVI$_{14\text{-}17}$ scores was limited and except from 3PCs and 1PCs revealed variance split (Table A3 14). Interestingly, a comparison run separately for Varimax (Table A3 15) and Promax (Table A3 16) resulting scores derived using seven and 34 EOFs showed moderate agreement, with an exception of 3PC's that were always highly correlated.

[12] Complementary information in the Appendix 3, section A.3.2

4.2.3.3. COVnNDII7$_{8\text{-}18}$ [13]

For the normalized vegetation season NDII7 time series the Cattell's scree test indicated to retain four first loadings (Figure A3 3A). Temporal patterns of the Varimax and Promax rotations (Figure A3 3B and C respectively) revealed very high mutual accordance (Table A3 17) where the latter solution demonstrated smoothed profiles with lower amplitude of change. In both cases the fourth resulting score was found strongly correlated to the 1scPDSI (Table A3 18). Significant negative relation was identified also for the 2scPDSI temporal pattern and a pair of the 1PCs (1CONnNDII7$_{8\text{-}18}$ROT4V and 1CONnNDII7$_{8\text{-}18}$ROT4P). Furthermore, 2003 anomaly was emphasized in the 1CONnNDII7$_{8\text{-}18}$ROT4V and 3CONnNDII7$_{8\text{-}18}$ROT4V. Accordance with corresponding not-rotated scores increased with a decrease of PC order, with orthogonal solution being more conservative (Table A3 19).

Subsequently, analyses were conducted for the first three scores selected using Kaiser's stopping rule (Figure A3 3 A). PCs derived from both inspected rotation approaches demonstrated very high mutual accordance (Table A3 20). Both first PCs (1CONnNDII7$_{8\text{-}18}$ROT3V and 1CONnNDII7$_{8\text{-}18}$ROT3P) showed variability correlated with the 1scPDSI (Table A3 21), where the first score from the Varimax solution revealed also statistical accordance with 3scPDSI. Furthermore, 2PC obtained through the oblique rotation (2CONnNDII7$_{8\text{-}18}$ROT3P) was associated with 2scPDSI. Due to only three EOFs retained for rotation, variance alternation in final PCs was very small (Table A3 22). Accordance between Varimax and Promax emerging scores obtained using first four (Table A3 23) and three (Table A3 24) EOFs was very high for 1PCs and 2PCs, and moderate for 3PCs.

4.3. Comparison of PCs identified as potential forest drought responses

A preliminary inspection of results of multiple S-mode PCA setups allowed to identify 53 scores that significantly correlated with the scPDSI drought related temporal patterns. However, due to inconsistent time-steps between the scPDSI and vegetation indices datasets, the comparison was done for yearly averages time series and failed to address intra-annual data variability. Consequently, despite high statistics some PCs showed temporal variability with strong anomalies that did not relate to recognized drought conditions. Therefore, statistical analyses were complemented by a visual evaluation of scores, where all erratic and 'noisy' patterns were excluded. PCs related exclusively to the 2scPDSI were rejected due to a non-drought-associated nature of this score. A correlation value minimum threshold for three remaining scPDSI patterns was set to 0.6. All aforementioned reduced the number of PCs with recognized potential drought vegetation impact, to 16 (Figure 16).

In order to simplify the further inspection, a phase of all scores rendering alike temporal variability were unified to match the appropriate scPDSI PC. All 16 selected scores were mutually compared (Table 19). When time-steps of two inspected PCs were inconsistent, a comparison was done for averaged yearly scores. Particularly interesting were similarities among principal components that showed alike temporal behavior governed by the same dominant scPDSI variability. Furthermore, spatial representations of identified PCs were also compared by the means of linear

[13] Complementary information in the Appendix 3, section A.3.3

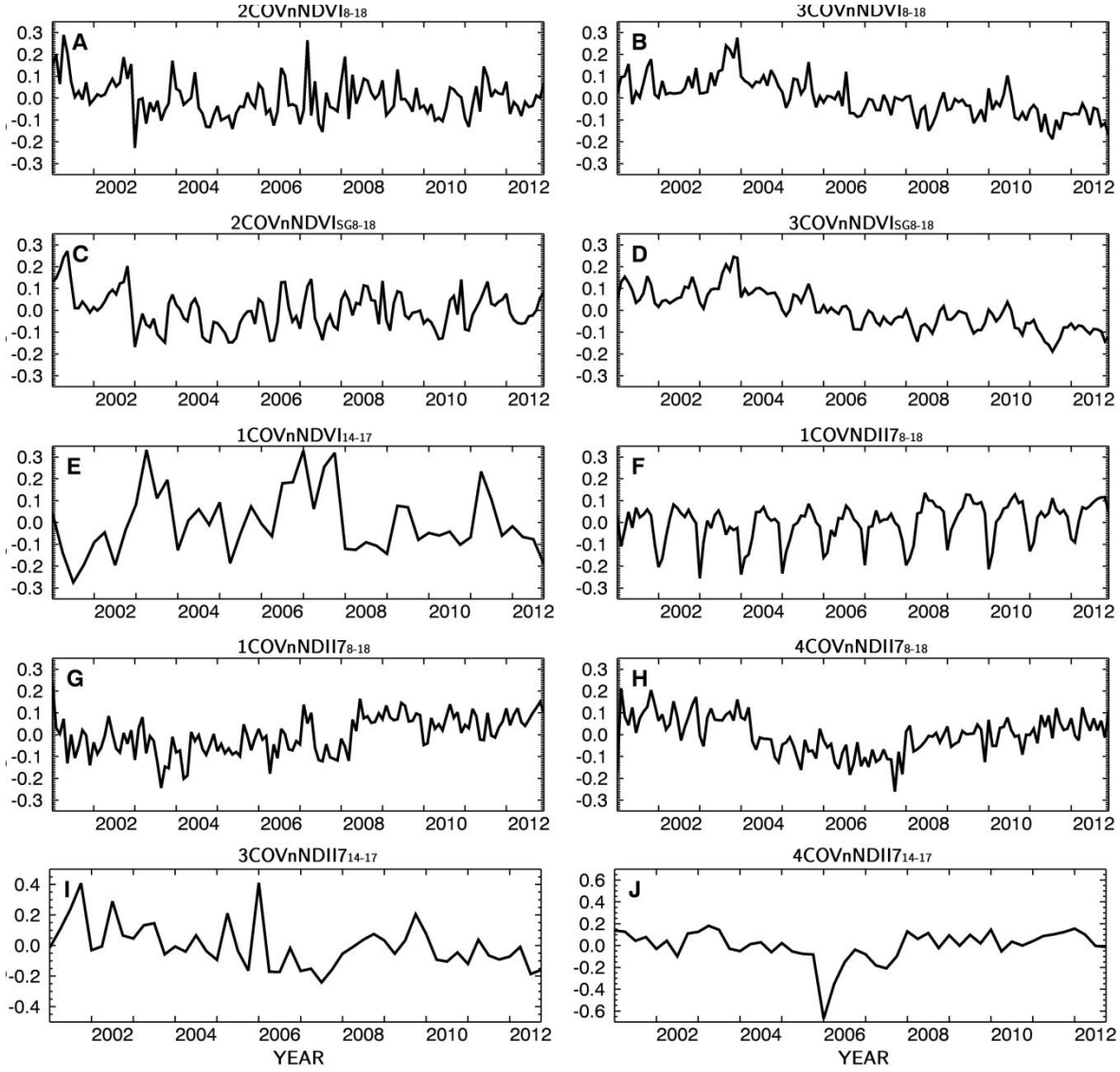

Figure 16 PCs that revealed potential physical meaning of forest drought impact: A: 2COVnNDVI$_{8\text{-}18}$ (the 2PC from correlation-matrix based PCA of NDVI$_{8\text{-}18}$ time series); B: 3COVnNDVI$_{8\text{-}18}$ (the 3PC from covariance based PCA of nNDVI$_{8\text{-}18}$ time series); C: 2COVnNDVI$_{SG8\text{-}18}$ (the 2PC from correlation-matrix based PCA of NDVI$_{SG8\text{-}18}$ time series); D: 3COVnNDVI$_{SG8\text{-}18}$ (the 3PC from covariance based PCA of nNDVI$_{SG8\text{-}18}$ data); E: 1COVnNDVI$_{14\text{-}17}$ (the 1PC derived through covariance based PCA of nNDVI$_{14\text{-}17}$); F: 1COVNDII7$_{8\text{-}18}$ (the 1PC obtained using correlation-based PCA of NDII7$_{8\text{-}18}$ dataset); G: 1COVnNDII7$_{8\text{-}18}$ (the 1PC from covariance-based PCA of nNDII7$_{8\text{-}18}$ data); H: 4COVnNDII7$_{8\text{-}18}$ (the 4PC derived from covariance-matrix based PCA of nNDII7$_{8\text{-}18}$ time series); I: 3COVnNDII7$_{14\text{-}17}$ (the 3PC from covariance-based PCA of nNDII7$_{14\text{-}17}$ time series); J: 4COVnNDII7$_{14\text{-}17}$ (the 4PC from covariance-based PCA of nNDII7$_{14\text{-}17}$ time series).

correlation (Table 20).

In total, nine PCs demonstrated primary resemblance to the 1scPDSI pattern: 2COVnNDVI$_{8\text{-}18}$, 2COVnNDVI$_{SG8\text{-}18}$, 1COVnNDVI$_{14\text{-}17}$, 1CORNDII7$_{8\text{-}18}$, 1COVnNDII7$_{8\text{-}18}$, 4COVnNDII7$_{8\text{-}18}$, 4COVnNDVI$_{8\text{-}18}$ROT4V, 4COVnNDII7$_{8\text{-}18}$ROT4V and 4COVnNDII7$_{8\text{-}18}$ROT4P (Figure 16 and Table 19 A, C, E, F, G, H, L, O and P respectively). Among them, the 2COVnNDVI$_{SG8\text{-}18}$ (Figure 16D) score obtained the

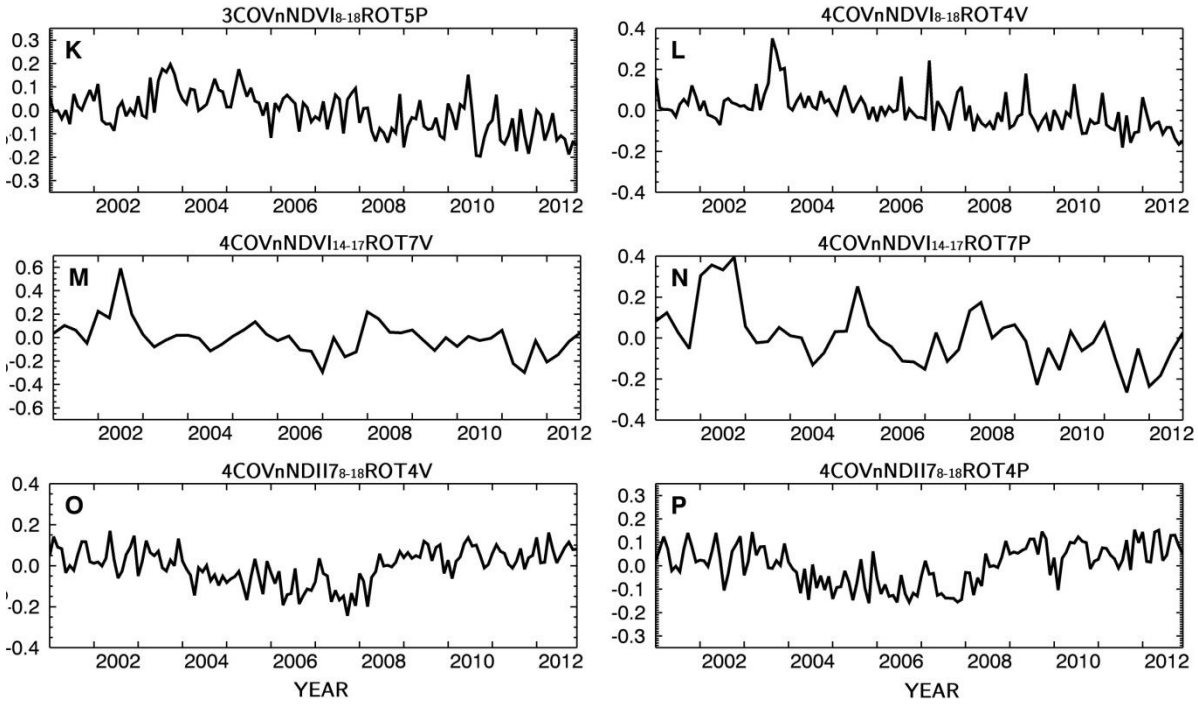

Figure 16 cont PCs that revealed potential physical meaning of forest drought impact: K: 3COVnNDVI$_{8\text{-}18}$ROT5P (3PC resulting from the Promax rotation of the five first PCs of covariance-matrix based PCA of nNDVI$_{8\text{-}18}$ time series); L: 4COVnNDVI$_{8\text{-}18}$ROT4V (4PC resulting from the Varimax rotation of the four first PCs of covariance-matrix based PCA of nNDVI$_{8\text{-}18}$ time series); M: 4COVnNDVI$_{14\text{-}17}$ROT7V (4PC resulting from the Varimax rotation of the seven first PCs of covariance-matrix based PCA of nNDVI$_{14\text{-}17}$ time series); N: 4COVnNDVI$_{14\text{-}17}$ROT7P (4PC resulting from the Promax rotation of the seven first PCs of covariance-matrix based PCA of nNDVI$_{14\text{-}17}$ time series); O: 4COVnNDII7$_{8\text{-}18}$ROT4V (4PC resulting from the Varimax rotation of the four first PCs of covariance-matrix based PCA of nNDII7$_{8\text{-}18}$ time series); P: 4COVnNDII7$_{8\text{-}18}$ROT4P (4PC resulting from the Promax rotation of the four first PCs of covariance-matrix based PCA of nNDII7$_{8\text{-}18}$ time series)

highest correlation with the 1scPDSI. Despite promising statistic and an abrupt anomaly in 2003, this PC presented no additional asset for the potential forest drought impact detection. The 2COVnNDVI$_{SG8\text{-}18}$ had very high accordance with the 2COVnNDVI$_{8\text{-}18}$ (Figure 16B), and alike it, showed no connection to any other principal component (Table 19). Spatial representation of both PCs (Figure A4 1 and Figure A4 3) showed the strongest correlation with identified scores in the central part of South Tyrol and along all main valleys. Negative correlation was observed at the highest outskirts of forested area. Similar distribution was recognized in a footprint of the 4COVnNDVI1$_{4\text{-}17}$ROT7V PC, which was primarily connected with the 4scPDSI (Table 20).

The 4COVnNDII7$_{8\text{-}18}$ROT4P (Figure 16P) also demonstrated very high correlation with the 1scPDSI and despite some anomalies in its temporal profile, the score revealed clear analogy to the dry spell of 2003-2007. Almost equally robust signal was produced for the 4COVnNDII7$_{8\text{-}18}$ROT4V PC (Figure 16O, Table 19), which even stronger emphasized dry conditions in 2006 and 2007. Both aforementioned scores emerged from variability detected in 4COVnNDII7$_{8\text{-}18}$ (Figure 16H), which was subsequently strengthened by the rotation. Mutual correlation among the original and rotated scores

Table 19 Mutual correlation between investigated potentially drought related PCs.. When timesteps of coupled datasets were inconsistent, comparison was done for averaged yearly scores. PCs index letters correspond with Figure 16.

	Index	PC															
		A	B	C	D	E	F	G	H	I	J	K	L	M	N	O	P
2COVnNDVI$_{8\ 18}$	**A**		0.000	0.795*	0.089	-0.569[1]	0.148	0.268*	0.302*	0.377[1]	-0.531[1]	-0.134	0.045	0.397[1]	0.355[1]	0.240*	0.197*
3COVnNDVI$_{8\ 18}$	**B**	0.000		-0.145	0.919*	0.115[1]	-0.207*	-0.422*	0.267*	0.826*[1]	0.138[1]	0.726*	0.753*	-0.458[1]	-0.557[1]	0.104	0.034
3COVnNDVI$_{SG8\ 18}$	**C**	0.795*	-0.145		0.000	-0.582*[1]	0.180*	0.332*	0.253*	0.243[1]	-0.533[1]	-0.323*	-0.184*	0.488[1]	0.474[1]	0.261*	0.246*
3COVnNDVI$_{SG8\ 18}$	**D**	0.089	0.919*	0.000		0.030[1]	-0.208*	-0.442*	0.295*	0.846*[1]	0.098[1]	0.686*	0.693*	-0.416[1]	-0.522[1]	0.084	0.001
1COVnNDVI$_{14\ 17}$	**E**	-0.569[1]	0.115[1]	-0.582*[1]	0.030[1]		0.459[1]	0.462[1]	-0.486[1]	-0.372*	-0.083	0.372[1]	0.405[1]	-0.256	-0.217	-0.520[1]	-0.448[1]
1CORNDII7$_{8\ 18}$	**F**	0.148	-0.207*	0.180*	-0.208*	0.459[1]		0.487*	-0.032	0.689*[1]	0.257[1]	-0.321*	-0.214*	-0.823*[1]	-0.866*[1]	0.278*	0.310*
1COVnNDII7$_{8\ 18}$	**G**	0.268*	-0.422*	0.332*	-0.442*	0.462[1]	0.487*		0.000	0.704*[1]	0.277[1]	-0.602*	-0.463*	-0.814*[1]	-0.855*[1]	0.611*	0.591*
4COVnNDII7$_{8\ 18}$	**H**	0.302*	0.267*	0.253*	0.295*	-0.486[1]	-0.032	0.000		0.120[1]	0.084[1]	0.058	0.125	0.642*[1]	0.544[1]	0.719*	0.659*
3COVnNDII7$_{14\ 17}$	**I**	0.377[1]	0.826*[1]	0.243[1]	0.846*[1]	-0.372*	0.689*[1]	0.704*[1]	0.120[1]		0.000	0.770*[1]	0.777*[1]	0.238	0.088	-0.238[1]	-0.300[1]
4COVnNDII7$_{14\ 17}$	**J**	-0.531[1]	0.138[1]	-0.533[1]	0.098[1]	-0.083	0.257[1]	0.277[1]	0.084[1]	0.000		0.144[1]	0.051[1]	-0.050	-0.044	0.001[1]	-0.059[1]
3COVnNDVI$_{8\ 18}$ROT5P	**K**	-0.134	0.726*	-0.323*	0.686*	0.372[1]	-0.321*	-0.602*	0.058	0.770*[1]	0.144[1]		0.894*	-0.705*[1]	-0.784*[1]	-0.202*	-0.255*
4COVnNDVI$_{8\ 18}$ROT4V	**L**	0.045	0.753*	-0.184*	0.693*	0.405[1]	-0.214*	-0.463*	0.125	0.777*[1]	0.051[1]	0.894*		-0.532[1]	-0.631*[1]	-0.059	-0.121
4COVnNDVI$_{14\ 17}$ROT7V	**M**	0.397[1]	-0.458[1]	0.488[1]	-0.416[1]	-0.256	-0.823*[1]	-0.814*[1]	0.642*[1]	0.238	-0.050	-0.705*[1]	-0.532*[1]		0.861*	0.852*[1]	0.906*[1]
4COVnNDVI$_{14\ 17}$ROT7P	**N**	0.355[1]	-0.557[1]	0.474[1]	-0.522[1]	-0.217	-0.866*[1]	-0.855*[1]	0.544[1]	0.088	-0.044	-0.784*[1]	-0.631*[1]	0.861*		0.788*[1]	0.856*[1]
4COVnNDII7$_{8\ 18}$ROT4V	**O**	0.240*	0.104	0.261*	0.084	-0.520[1]	0.278*	0.611*	0.719*	-0.238[1]	0.001[1]	-0.202*	-0.059	0.852*[1]	0.788*[1]		0.936*
4COVnNDII7$_{8\ 18}$ROT4P	**P**	0.197*	0.034	0.246*	0.001	-0.448[1]	0.310*	0.591*	0.659*	-0.300[1]	-0.059[1]	-0.255*	-0.121	0.906*[1]	0.856*[1]	0.936*	

* - significant at the level $p<0.05$

[1] - correlation done for yearly scores

Table 20 Correlation between footprints of investigated potentially drought related PCs. The index letters correspond with Figure 16 and Table 19.

PC footprint	Index	PC footprint															
		A	B	C	D	E	F	G	H	I	J	K	L	M	N	O	P
2COVnNDVI$_{8\ 18}$	**A**		0.002	0.958*	-0.117*	-0.434*	0.222*	0.213*	0.024*	0.070*	-0.079*	-0.170*	0.099*	0.524*	0.498*	-0.109*	-0.092*
3COVnNDVI$_{8\ 18}$	**B**	0.002		0.137*	0.952*	0.015*	-0.259*	0.117*	-0.011*	-0.209*	-0.026*	0.835*	0.818*	-0.199*	-0.246*	-0.378*	-0.378*
3COVnNDVI$_{SG8\ 18}$	**C**	0.958*	0.137*		0.000	-0.425*	0.173*	0.210*	0.041*	0.052*	-0.079*	-0.289*	-0.033*	0.502*	0.479*	-0.151*	-0.140*
3COVnNDVI$_{SG8\ 18}$	**D**	-0.117*	0.952*	0.000		0.077*	-0.255*	0.125*	-0.022*	-0.197*	-0.027*	0.796*	0.796*	-0.342*	-0.398*	-0.331*	-0.333*
1COVnNDVI$_{14\ 17}$	**E**	-0.434*	0.015*	-0.425*	0.077*		-0.262*	-0.355*	0.012*	-0.101*	0.027*	0.220*	0.127*	-0.619*	-0.435*	-0.077*	-0.121*
1CORNDII7$_{8\ 18}$	**F**	0.222*	-0.259*	0.173*	-0.255*	-0.262*		0.566*	-0.184*	0.108*	0.010	0.062*	0.119*	0.187*	0.156*	0.285*	0.374*
1COVnNDII7$_{8\ 18}$	**G**	0.213*	0.117*	0.210*	0.125*	-0.355*	0.566*		-0.078*	0.055*	-0.001	-0.259*	-0.189*	0.125*	0.043*	0.262*	0.398*
4COVnNDII7$_{8\ 18}$	**H**	0.024*	-0.011*	0.041*	-0.022*	0.012*	-0.184*	-0.078*		0.399*	0.440*	0.083*	0.122*	0.004	0.026*	0.625*	0.555*
3COVnNDII7$_{14\ 17}$	**I**	0.070*	-0.209*	0.052*	-0.197*	-0.101*	0.108*	0.055*	0.399*		-0.001	0.196*	0.227*	0.106*	0.090*	0.438*	0.417*
4COVnNDII7$_{14\ 17}$	**J**	-0.079*	-0.026*	-0.079*	-0.027*	0.027*	0.010	-0.001	0.440*	-0.001		0.050*	0.057*	-0.019*	-0.009	0.372*	0.341*
3COVnNDVI$_{8\ 18}$ROT5P	**K**	-0.170*	0.835*	-0.289*	0.796*	0.220*	0.062*	-0.259*	0.083*	0.196*	0.050*		0.933*	0.113*	0.207*	0.350*	0.337*
4COVnNDVI$_{8\ 18}$ROT4V	**L**	0.099*	0.818*	-0.033*	0.796*	0.127*	0.119*	-0.189*	0.122*	0.227*	0.057*	0.933*		0.222*	0.303*	0.356*	0.350*
4COVnNDVI$_{14\ 17}$ROT7V	**M**	0.524*	-0.199*	0.502*	-0.342*	-0.619*	0.187*	0.125*	0.004	0.106*	-0.019*	0.113*	0.222*		0.929*	0.032*	0.059*
4COVnNDVI$_{14\ 17}$ROT7P	**N**	0.498*	-0.246*	0.479*	-0.398*	-0.435*	0.156*	0.043*	0.026*	0.090*	-0.009*	0.207*	0.303*	0.929*		0.035*	0.051*
4COVnNDII7$_{8\ 18}$ROT4V	**O**	-0.109*	-0.378*	-0.151*	-0.331*	-0.077*	0.285*	0.262*	0.625*	0.438*	0.372*	0.350*	0.356*	0.032*	0.035*		0.964*
4COVnNDII7$_{8\ 18}$ROT4P	**P**	-0.092*	-0.378*	-0.140*	-0.333*	-0.121*	0.374*	0.398*	0.555*	0.417*	0.341*	0.337*	0.350*	0.059*	0.051*	0.964*	

* - significant at the level $p<0.05$

was moderate (Table 19) but the main envelope features were well preserved. An analogy was detected among spatial representations of all three discussed PCs (Table 20). They indicated a 2004-2007 NDII7 decrease in the Vinschgau Valley, north part of the Eisack Valley as well as western regions of the Western Dolomites (Figure A4 8, Figure A4 15 and Figure A4 16). The reversed response was observed in the central part of South Tyrol and along the Eisack and Puster Valleys.

Although the 1COVnNDII7$_{8\text{-}18}$ pattern (Figure 16G) demonstrated on a yearly bases very high correspondence with the 1scPDSI, as well as was found statistically related to the 4COVnNDII7$_{8\text{-}18}$ROT4V and 4COVnNDII7$_{8\text{-}18}$ROT4P, its actual temporal variability was more associated with the 3scPDSI and 4scPDSI. The latter observation was supported by an analogy with 3scPDSI and 4scPDSI governed PCs (Table 19). Next to signal anomalies in 2003 and 2004, 1COVnNDII7$_{8\text{-}18}$ showed lower values for 2001-2008, followed by raised NDII7 envelope. The spatial representation of the PC was a one sided correlation distribution (Figure A4 7) where the highest accordance with the principal component was found in the north part of the Eisack Valley, west outskirts of the Pustertal and south slopes of the Etschtal Valley. Only the 1CORNDII7$_{8\text{-}18}$ score footprint related to it moderately (Table 20).

The 1COVnNDVI$_{14\text{-}17}$ (Figure 16E) depicted intense positive anomalies in 2003 and 2007 parted with lower NDVI values, which was found in moderate agreement with the 1scPDSI. The score had no significant connection to any other PC but the 2COVnNDVI$_{SG8\text{-}18}$ (Table 19). Its spatial representation indicated the east part of the Puster Valley, Vinschgau and west exposed slopes of the Wipp Valleys as regions of the highest accordance with identified temporal variability of the score (Figure A4 5). This distribution was inversely related to the 4COVnNDVI$_{14\text{-}17}$ROT7V footprint (Table 20). Interestingly, correlation distribution of the 1COVnNDVI$_{14\text{-}17}$ was skewed towards negative values.

Despite a clear seasonal component, the 1CORNDII7$_{8\text{-}18}$ (Figure 16G) score was strongly associated with the 1scPDSI and rendered prolonged arid conditions before 2008, with two declines in the envelope in 2003 and 2007. Due to phenology signal, this PC was weakly correlated with all the other scores related to the 1scPDSI (Table 19), but demonstrated yearly-based agreement with 3scPDSI and 4scPDSI associated scores (Table 19). A spatial representation of the 1CORNDII7$_{8\text{-}18}$ (Figure A4 6) suggested potential drought impact mainly in the Northern and Western part of the province, which was in moderate agreement with the 1COVnNDII7$_{8\text{-}18}$ footprint (Table 20).

Although statistical alliance of the 4COVnNDVI$_{8\text{-}18}$ROT4V (Figure 16L) temporal patter was with the 1scPDSI, this PC demonstrated rather leveled response with several single anomalies, among which the 2003 peak was the most distinct. Correlation with other inspected scores demonstrated a significant relation mainly with 3scPDSI and 4scPDSI associated PCs (Table 19). A spatial footprint of the 4COVnNDVI$_{8\text{-}18}$ROT4V score indicated central part of South Tyrol, Eisack and Puster Valleys as areas with the strongest coincidence to the identified PC (Figure A4 12). This pattern corresponded well with spatial representations of the 3COVnNDVI$_{8\text{-}18}$, 3COVnNDVI$_{SG8\text{-}18}$ and 3COVnNDVI$_{8\text{-}18}$ROT5P (Table 20).

Decreasing NDVI and NDII7 tendencies, being significantly related to the 3scPDSI and 4scPDSI temporal variability were predominant in seven selected PCs:

$3COVnNDVI_{8\text{-}18}$, $3COVnNDVI_{SG8\text{-}18}$, $3COVnNDII7_{14\text{-}17}$, $4COVnNDII7_{14\text{-}17}$, $3COVnNDVI_{8\text{-}18}ROT5P$, $4COVnNDVI_{14\text{-}17}ROT7V$ and $4COVnNDVI_{14\text{-}17}ROT7P$ (Figure 16 and Table 19 B, D, I, J, K, M and N respectively).

The highest statistically defined accordance with the decreasing tendency of 4scPDSI was observed for $4COVnNDVI_{14\text{-}17}ROT7V$ and $4COVnNDVI_{14\text{-}17}ROT7P$ scores (Figure 16M and N respectively). Visual inspection of both PCs indicated the latter to have smoother and more robust temporal profile with clearer declining tendency, while the former revealed variability based mainly on strong anomaly in 2003. Both scores had strong mutual correlation and demonstrated strong yearly-averages-based accordance to $1CORNDII7_{8\text{-}18}$, $1COVnNDII7_{8\text{-}18}$, $4COVnNDII7_{8\text{-}18}$, $3COVnNDVI_{8\text{-}18}ROT5P$, $4COVnNDVI_{8\text{-}18}ROT4V$, $4COVnNDVI_{14\text{-}17}ROT7V$ and $4COVnNDVI_{14\text{-}17}ROT7P$ (Table 19). Resemblance in the time domain resulted in very high accordance in spatial representations of both scores (Table 20), which suggested a decreasing NDVI tendency to be predominant in the northern and eastern part of South Tyrol (Figure A4 13 and Figure A4 14). The southern, central and western portion of the province was characterized by negative correlation to both PCs which implied NDVI gain. Both footprints were moderately correlated with spatial representations of the $2COVnNDVI_{8\text{-}18}$ and $2COVnNDVI_{SG8\text{-}18}$ where the $4COVnNDVI_{14\text{-}17}ROT7V$ representation obtained higher statistics and demonstrated an additional negative link to the $1COVnNDVI_{14\ 17}$ footprint (Table 20).

Temporal variability recognized in the $3COVnNDII7_{14\text{-}17}$ PC (Figure 16I) was strongly correlated with the 3scPDSI and accounted on NDII7 decrease until 2007, followed by higher values. Unfortunately overall perception of this variability was obscured by strong positive anomalies in 2005 and 2006. The PC revealed significant yearly-based accordance with $3COVnNDVI_{8\text{-}18}$, $3COVnNDVI_{SG8\text{-}18}$, $1CORNDII7_{8\text{-}18}$, $1COVnNDII7_{8\text{-}18}$, $3COVnNDVI_{8\text{-}18}ROT5P$ and $4COVnNDVI_{8\text{-}18}ROT4V$ (Table 19). On the contrary, its spatial footprint showed no meaningful relation to any PC projection (Table 20). Produced correlation map depicted west and north-west part of the province to be related to the score temporal variability (Figure A4 9).

Despite visual similarity to the 1scPDSI, the $4COVnNDII7_{14\text{-}17}$ score (Figure 16J) was found to be significantly related to the 4scPDSI. The principal component showed deteriorated NDII7 envelope between 2004 and 2007 with intense abrupt drop in the first considered composite of 2006. This anomaly clearly predominated statistics. No numerical evidence supported a meaningful temporal or spatial based similarity of $4COVnNDII7_{14\text{-}17}$ with any other analyzed PC (Table 19), neither spatial footprint (Table 20). Depicted $4COVnNDII7_{14\text{-}17}$ spatial representation (Figure A4 10) revealed the highest correlation with the score in the Vinschgau region as well as on the East exposed sloped of the Etschtal and Puster Valleys.

Both the $3COVnNDVI_{8\text{-}18}$ and $3COVnNDVI_{SG8\text{-}18}$ (Figure 16B and D respectively) depicted NDVI decrease which was related to the 3scPDSI. PCs had very high mutual correlation (Table 19) and revealed significant positive relation to the $3COVnNDVI_{8\text{-}18}ROT5P$, $3COVnNDVI_{8\text{-}18}ROT4V$ and $3COVnNDII7_{14\text{-}17}$, where the latter was checked for the annual yearly scores (Table 19). The $3COVnNDVI_{8\text{-}18}$ and $3COVnNDVI_{SG8\text{-}18}$ spatial representations bore substantial accordance (Table 20) indicating the north exposed slopes in Vinschgau, Eisack, Wipp and Puster Valleys as especially prone to greenness deterioration (Figure A4 2 and Figure A4 4). On the

other hand, NDVI increase was suggested by both footprints in the central part of South Tyrol along the Eisack and Etschtal Valley. These spatial features were in line with the 3COVnNDVI$_{8\text{-}18}$ROT5P and 4COVnNDVI$_{8\text{-}18}$ROT4V footprints (Table 20).

The 3COVnNDVI$_{8\text{-}18}$ROT5P (Figure 16K) not only accounted on similar temporal variability as the 3COVnNDVI$_{8\text{-}18}$, which resulted in decreasing tendency correlated with the 3scPDSI, but also incorporated 1scPDSI alike component. The score revealed slightly erratic pattern which was proven to have considerable analogy with several inspected scores, including the 3COVnNDVI$_{8\text{-}18}$ and 3COVnNDVI$_{SG8\text{-}18}$ (Table 19). A 3COVnNDVI$_{8\text{-}18}$ROT5P spatial representation suggested NDVI decline to be the most common for the highest forest stands of the northern and western part of South Tyrol as well as south-east portion of the province (Figure A4 11). The stronger, opposite reaction of NDVI gradual increase was observed near the valley floors, particularly in the central part of South Tyrol and along the Etschta, Eisack and Puster Valleys. Alike tendencies were observed for the 3COVnNDVI$_{8\text{-}18}$ and 3COVnNDVI$_{SG8\text{-}18}$ and 4COVnNDVI$_{8\ 18}$ROT4V footprints (Table 20).

Considerable correlation among analyzed temporal patterns and their spatial projection was observed. It concerned not only mutual similarity between scores associated with the specific scPDSI identified drought temporal variability, but also proved overlaps between PCs following the 2003-2007 dry spell and increasing aridity patterns. Furthermore, three inspected principal components revealed significant impact of both drought variabilities.

Although scores obtained through the rotation revealed strong correlation with the scPDSI scores, their temporal responses were, in general, much more wobbly and with sudden peaks and lows, that had no support in the scPDSI, neither could be explained by forest processes. Roughness of time-profiles was also common among scores derived using the high-season time series. Finally, although the SG filtering reduced noise level presented in scores, the convolution ensured no considerable improvement. Taking together, having in mind physiological credibility and reliability of the identified NDVI and NDII7 forest responses as well as recognizing existing results overlap; three PCs were selected together with their footprints for further investigation:

- 1CORNDII7$_{8\text{-}18}$ which showed robust phenological component that corresponded with the 1scPDSI, and produced unique spatial correlation pattern;
- 4COVnNDII7$_{8\text{-}18}$ that also followed the 1scPDSI meteorological variability, but showed higher time-domain correspondence with other alike PCs, including rotation-retained scores. It demonstrated a coherent anomaly-based temporal representation with limited signal fluctuations or potential data artifacts that translated into the consistent footprint;
- 3COVnNDVI$_{8\text{-}18}$ which comprised all the most relevant features of the NDVI anomaly based PCs rendering the increasing/decreasing 'greenness' evolution. From all 3scPDSI and 4scPDSI related PC, this score was selected due to good correspondence with the other alike scores, and their spatial representations.

4.4. Assessment of drought impact on forest

Spatial projections of the three selected PCs rendering potential forest responses to drought conditions were subsequently classified using percentiles of their correlation

values distributions (Table 21). Only pixels that fulfilled the significance criterion ($p<0.1$) were considered in the further analyses. Pixels that fall between the 95th percentile and a maximum (class 6) had the strongest association with the considered score phase (Figure 16). On the contrary, all regions assigned to class 1 (minimum to 5th percentile) revealed opposite properties.

Table 21 Percentiles of correlation values of spatial projections of 1CORNDII7$_{8\text{-}18}$, 4COVnNDII7$_{8\text{-}18}$, and 3COVnNDVI$_{8\text{-}18}$ PCs considered as potential drought forest impact temporal responses. Indicated threshold values became limits of drought impact classes.

percentiles	impact class	spatial patterns		
		1CORNDII7$_{8\text{-}18}$	4COVnNDII7$_{8\text{-}18}$	3COVnNDVI$_{8\text{-}18}$
min	class 1	-0.610	-0.445	-0.632
5th	class 2	0.010	-0.203	-0.316
30th	class 3	0.338	-0.066	-0.109
50th	class 4	0.453	0.003	-0.004
70th	class 5	0.554	0.072	0.097
95th	class 6	0.714	0.218	0.284
max		0.893	0.514	0.600

Since PCs identified as potentially drought related had different temporal variability that addressed diverse stress-vegetation feedback, resulting spatial representations also depicted divergent regionalization of South Tyrol. Furthermore, when interpreted within multilevel factors of forest type, exposition, elevation and inclination, allocation of drought impact classes revealed interesting principles of behavior (Table 22; further examination and description in the following sections).

Table 22 Pixel distribution within factors levels inspected for the 1CORNDII7$_{8\text{-}18}$, 4COVnNDII7$_{8\text{-}18}$ and 3COVnNDVI$_{8\text{-}18}$ PCs spatial representations. Class 6 denotes regions with the strongest, whereas class 1 the weakest fit to the scores (Figure 16F, H and B).

	1CORNDII7$_{8\text{-}18}$		4COVnNDII7$_{8\text{-}18}$		3COVnNDVI$_{8\text{-}18}$	
[%]	**1**	**6**	**1**	**6**	**1(in)**	**6(d)**
Total (pixels)	2391	2391	692	692	1205	1205
Coniferous	92.30	94.65	91.04	95.38	76.10	96.85
Broadleaved	2.01*	0.59*	1.88*	0.58*	3.65*	0.33*
Mixed	5.69	4.64	7.08*	4.05*	20.25	2.82*
N	31.12	13.55	25.29	27.17	4.65	62.07
E	27.52	25.81	17.63	18.79	30.71	11.78
S	18.74	37.31	27.75	34.54	49.21	5.15
W	22.63	23.34	29.34	19.51	15.44	21.00
0-700 m asl	5.44	0.33*	1.88*	3.90*	13.11	0.50*
700-1400 m asl	20.91	8.99	33.38	54.77	63.24	31.29
1400-2100 m asl	54.12	89.00	64.74	33.96	20.66	68.13
2100-2500m asl	19.53	1.67*	-	7.37	2.99*	0.50*
0-10 deg.	9.45	8.66	18.50	3.76	14.27	3.90
10-20 deg.	33.71	27.39	34.54	20.38	36.43	20.08
20-30 deg.	38.39	41.36	36.56	51.01	40.91	56.85
30-40 deg	16.14	21.58	10.26	23.70	7.97	18.67
40-90 deg.	2.30	1.00*	0.14*	1.16*	0.41*	0.50*

* - category with less than 50 observations; in-increasing; d - decreasing

4.4.1. 1CORNDII7$_{8\text{-}18}$ spatial pattern

The 1CORNDII7$_{8\text{-}18}$ PC indicated depleted NDII7 seasonal scores priori to 2008 with the lowest maxima observed in 2003 and 2007 (Figure 16F). Regions significantly associated with this temporal response (Class 6 in Figure 17) were located mainly between 1400 and 2100 m asl (Table 22) in the Vinschgau and Wipp Valleys as well as in the Pustertal and the Etschtal Valley. The pattern addressed mainly coniferous stands, most often located on the south exposed slopes with moderate to high inclination. Class 1 accounted on pixels with very weak or negative correlation to the 1CORNDII7$_{8\text{-}18}$ score (Table 21). This response was identified mainly in the central and east part of South Tyrol, with a clear preference for upper forest limits and lower forest fringe (Figure 17). Furthermore, this class revealed preferences for north and east exposition and low to medium inclination (Table 22)

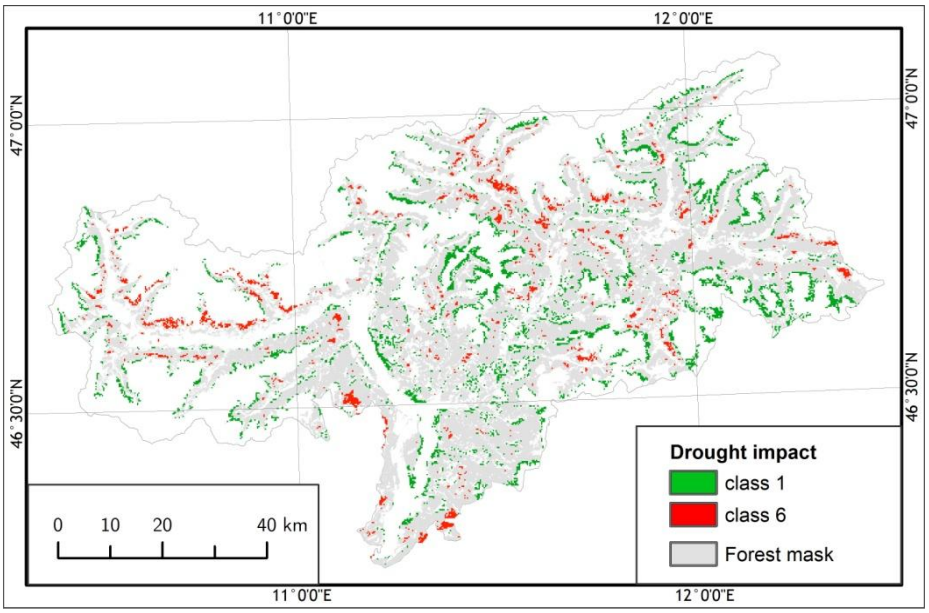

Figure 17 Spatial representation of the 1CORNDII7$_{8\text{-}18}$ PC limited to response of class 1 (green) and 6 (red). The forest mask marked in gray.

A significance of phenology and productivity[14] changes in time within recognized 1CORNDII7$_{8\text{-}18}$ response classes was tested with the within-subjects effects test of the repeated measures ANOVA performed with the Hujnh-Feldt adjustment. Results demonstrated statistically significant differences for time (Table 23) as well as combined factors of time and drought classes. Moreover, phenology diversity between factors levels was evaluated (Table 24) and demonstrated leading influence of elevation, with less evident diversification for slope, aspect and forest type.

Phenology and productivity changes observed within drought response classes 6 and 1 revealed for the former higher NDVI$_{HS}$ and NDII7$_{HS}$ scores (Figure 18e and f), with three considerable drops detected in 2003, 2007 and 2011. Alike timed declines were observed also for class 1, with an exception of the NDVI$_{HS}$ where 2007 decrease was

[14] Phenological indicators are dresribed in details in section 2.2.2.2.

Table 23 Within-subjects effects test of repeated measures ANOVA performed for the spatial representation of the $1CORNDII7_{8\text{-}18}$ PC. Test run with the Hujnh-Feldt adjustment returning results for the factor of time, and time combined with drought response class (6 levels) within selected phenology and productivity indicators.

	time			**time*response class**			**Error**
	df	F	p	df	F	p	df
CF	8.793	5443.52	0.000	43.963	57.787	0.000	420546.046
GPP	9.287	1646.97	0.000	46.436	26.187	0.000	444200.111
SBD	9.019	1565.92	0.000	45.097	14.181	0.000	431251.907
SL	9.320	1287.96	0.000	46.601	19.224	0.000	445777.326
$NDVI_{HS}$	9.565	8034.55	0.000	47.824	92.282	0.000	457478.427
$NDII7_{HS}$	9.668	9627.94	0.000	48.342	28.792	0.000	462430.924

Table 24 Effects of forest type, aspect, elevation and slope factors evaluated for phenology and productivity indices within the spatial representation of the $1CORNDII7_{8\text{-}18}$ PC using the test of between-subjects effects of repeated ANOVA.

	Forest type (df=2)		**Aspect (df=3)**		**Elevation (df=4)**		**Slope (df=4)**	
indicato	F	p	F	p	F	p	F	p
CF	24.810	0.000	1.417	0.236	116.669	0.000	5.024	0.000
GPP	0.154	0.858	5.065	0.002	153.635	0.000	3.093	0.015
SBD	3.360	0.035	8.037	0.000	31.595	0.000	0.974	0.420
SL	0.350	0.705	11.737	0.000	6.889	0.000	9.513	0.000
$NDVI_{HS}$	50.281	0.000	9.455	0.000	70.970	0.000	24.480	0.000
$NDII7_{HS}$	12.691	0.000	2.299	0.075	38.563	0.000	20.112	0.000

substituted by a drop in 2006. Both strata demonstrated an increasing significant linear trend, which was found particularly strong for the $NDII7_{HS}$ (Table 25). Potentially drought affected sites of class 6 revealed the lowest CF (Figure 18a). Regardless the response class, seasonal productivity reported an abrupt increase in 2003 followed by gradual decline, which for class 6 lasted until 2007. A consecutive peak was observed again in both strata around 2008-2009. Overall linearity of CF change was insignificant for area of class 6, but strong and meaningful within class 1 (Table 25). Conversely, GPP (Figure 18b) showed higher values for sites consistent with the $1CORNDII7_{8\text{-}18}$ PC variability, where overall productivity increase was observed (Table 25). A decreasing GPP tendency between 2002 and 2010 was detected within class 6, whereas class 1 rendered strong GPP decline between 2008 and 2010. SBD showed a vast amplitude of changes (Figure 18c) where sites aligned the strongest with the $1CORNDII7_{8\text{-}18}$ score experienced always sooner vegetation onset. This overall tendency for earlier season begin (Table 25) was disturbed in 2008-2010. Associated SL values depicted a very subtle and statistically significant increase for class 6 (Table 25), but with no direct link to the SBD variability (Figure 18d). Moreover, respective regions experienced lower spectrum of inter-annual SL changes.

Forest stands demonstrating the strongest accordance with the $1CORNDII7_{8\text{-}18}$ variability, hence also drought impact, were analyzed further with repetitive ANOVA

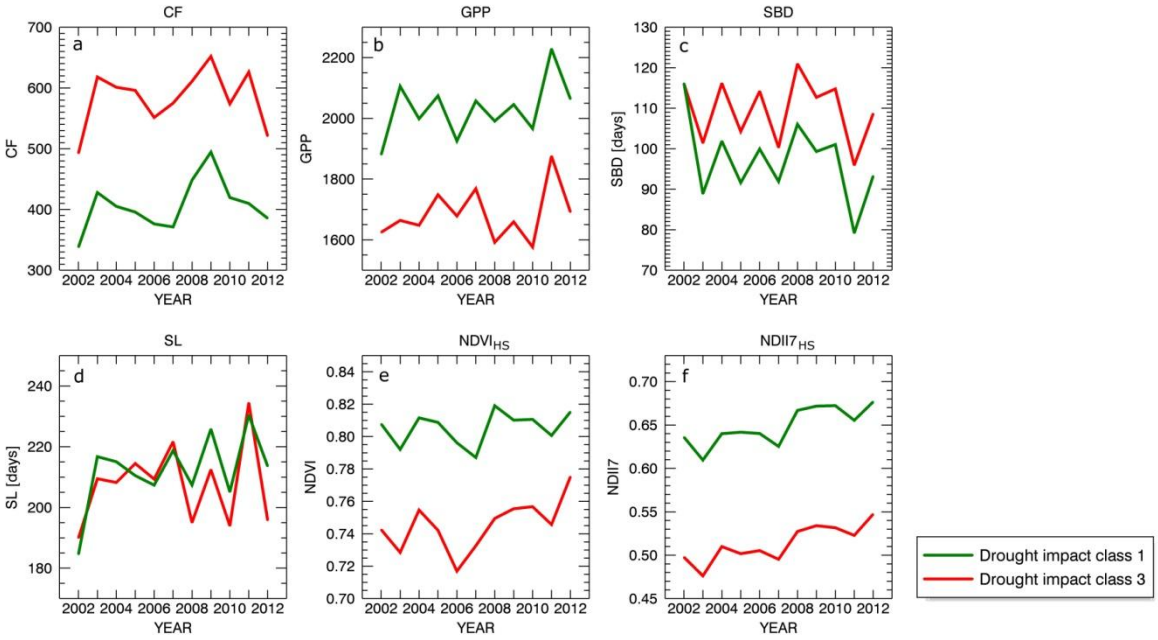

Figure 18 Year-to-year variability observed within drought impact classes 1 and 6 of the 1CORNDII7$_{8\text{-}18}$ PC footprint: a) CF, b) GPP, c) SBD, d) SL, e) NDVI$_{HS}$ and f) NDII7$_{HS}$.

Table 25 Strength of overall linear trends identified for phenology and productivity indicators within response classes 1 and 6 derived for the spatial representation of the 1CORNDII7$_{8\text{-}18}$ PC. Assessment done using the within subject contrasts test of repeated ANOVA.

	Class 1		**Class 6**	
indicator	F	p	F	p
CF	12.728	0.000	1.694	0.193
GPP	11.578	0.001	13.245*	0.000
SBD	14.917	0.000	4.990	0.026
SL	3.580	0.059	7.533*	0.006
NDVI$_{HS}$	54.301	0.000	34.776	0.000
NDII7$_{HS}$	177.909*	0.000	227.867*	0.000

* - the strongest trend of all tested contrast order

measures. Firstly, statistical significe of time driven differences of phenological measures were confirmed with the within-subjects effect test (Table A5 1). Subsequently, combined effect of time and site-specific characteristics was tested, and revealed significant and meaningful differences only for CF, NDVI$_{HS}$ and NDII7$_{HS}$ for a combination of time and elevation (Table 26).

Further insight into phenological changes observed within the forest type, aspect, elevation and slope levels, was provided for area associated with the 1CORNDII7$_{8\text{-}18}$ response class 6 by detailed temporal profiles of repetitive ANOVA measures (Figure A6 1). Forest type classes revealed the strongest diversification for NDVI$_{HS}$, NDII7$_{HS}$ and CF, where coniferous strands obtained always the lowest scores. Moreover, needle-leaved woodland revealed the strongest NDVI$_{HS}$ decrease between 2003 and 2007. GPP productivity demonstrated alike values for all forest types. Notably, mixed

Table 26 Effect of elevation factor in time on distinction between productivity indices tested for the response class 6 derived for the spatial representation of the $1CORNDII7_{8\text{-}18}$ PC. Analyses performed using within-subjects effects test of repeated ANOVA. Only measures with significant statistics are shown ($p<0.001$).

	time*elevation	
	df	**F**
CF	27.809	2.385
$NDVI_{HS}$	28.995	4.524
$NDII7_{HS}$	35.055	3.460

forest reported a bit later vegetation onset between 2003 and 2007, which however did not translate into shorter SL. Broadleaved stands were not considered due to insufficient representation (Table 22). Exposition had limited impact on phenology, where only north exposed sites revealed outstanding responses. Those regions showed the highest $NDVI_{HS}$, $NDII7_{HS}$ and GPP scores, but the lowest CF. Moreover, $NDVI_{HS}$ change spectrum observed within the north facing slopes was the highest. Conversely, CF dynamism seemed to increase with a shift towards south exposition. A tendency towards earlier SBD was observed, with the most intense shift at north facing sites between 2003 and 2005. Despite this, north slopes experienced the shortest SL. Diversification between three remaining strata was limited. Due to a poor representation, only 700-1400 m asl and 1400-2100 m asl elevation zones were considered in this part (Table 22). They demonstrated very alike $NDVI_{HS}$ and $NDII7_{HS}$ responses rendering the same temporal features. The same was valid for GPP profiles that indicated regions placed on 700-1400 m asl to show a smooth increasing trend only mildly interrupted in 2005 and 2010. Stands growing on lower altitudes demonstrated lower CF and limited time driven changes. Elevation increase translated not only into CF increment, but also emphasized inter-annual variability. SBD revealed limited elevation dependence, where however the 700-1400m asl class showed smoother and more persistent tendency towards earlier vegetation onset. Related response was observed for SL, where aforementioned elevation class depicted a robust prolongation trend of vegetation season. Conversely, despite SBD decrease, the upper elevation strata showed more persistent SL behavior, altered mainly in the second part of the observation period. Slope, as expected, showed more favorable vegetation conditions for regions with the lowest inclination – the highest $NDVI_{HS}$, $NDII7_{HS}$ and GPP score were observed here. In contrast, the same locations revealed the lowest CF with less intense inter-annual variability. Although SBD demonstrated considerable differences and intense inter-annual dynamism among inclination classes no clear relation was detected. Conversely, SL response was rather coherent. Importantly, signal difference among diverse factor classes was much more intense before 2007 than later on.

4.4.2. $4COVnNDII7_{8\text{-}18}$ spatial pattern

Spatial pattern associated with the $4COVnNDII7_{8\text{-}18}$ PC (Figure 16H) was composed of relatively small number of pixels, which was a consequence of the correlation p-value criterion (Table 22). Sites recognized as experiencing diminished foliage water content between 2004 and 2007 and aggregated in class 6 were located in the west and central part of South Tyrol (Figure 19). They were represented almost exclusively by

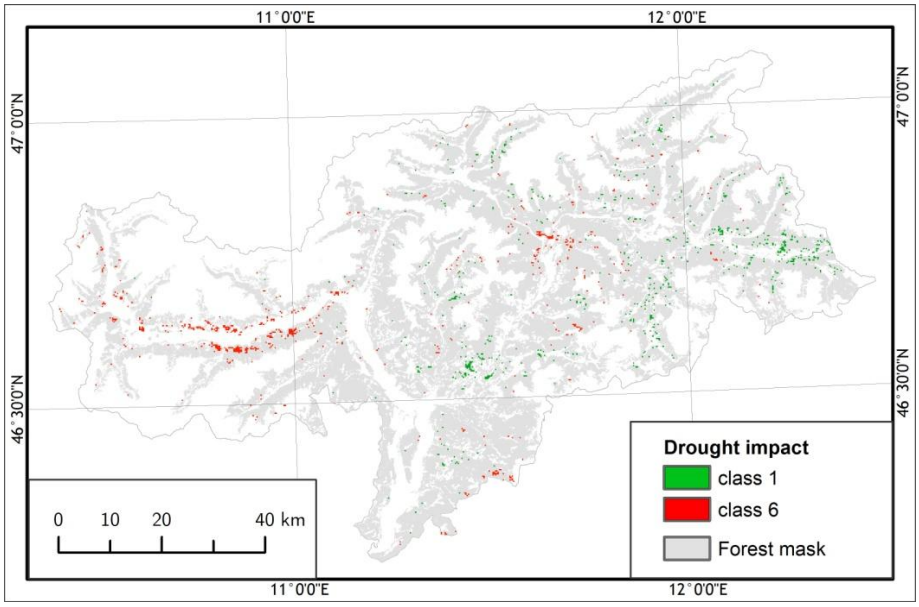

Figure 19 Spatial representation of the 4COVnNDII7$_{8\text{-}18}$ PC limited to response of class 1 (green) and 6 (red). The forest mask marked in gray.

coniferous stands growing mainly between 700 and 2100 m asl, which reflected rather well the general lay of the land. A mild preference for south exposition and moderate inclination was observed within this class. The opposite response of class 1, was recognized principally in the Eisack Valley and the east-most part of the Pustertal. This pattern was more common for west and south facing slopes of mid to high altitudes and low to moderate inclination (Table 22).

Year-to-year phenology and productivity variability observed within the 4COVnNDII7$_{8\text{-}18}$ footprint over the 2002-2012 period was not only significant in time, but also revealed significant time-controlled differences among six considered drought impact classes (Table 27; repeated measures ANOVA performed with Hujnh-Feldt adjustment). NDII7$_{HS}$ showed the strongest diversification among drought impact classes. Lower, but still robust differences were observed for NDVI$_{HS}$ and CF, whereas SL, GPP and SBD were the least affected by variability suggested in the PC. Moreover, the forest response was proven to be governed by elevation, slope, aspect and forest type (Table 28), where the influence of altitude was the strongest, while exposition and inclination were found less dominant, with even insignificant impact on CF and GPP. Forest factor was statistically irrelevant for GPP and SL.

Although the 4COVnNDII7$_{8\text{-}18}$ PC showed a decrease between 2004 and 2007, areas associated with this score reported diminished NDVI$_{HS}$ and NDII7$_{HS}$ starting already from 2003 (Figure 20e and f). A decrease was observed in both envelopes until 2007 with an intense increase afterwards. Regions indicated by the response class 1 revealed usually higher values of phenological indices with significant linear tendency (Table 29) and highlighted negative anomalies in 2003 and 2011. Moreover, the NDVI$_{HS}$ time series observed for class 1 showed additional decrease in 2006-2007. SBD reported for both strata rather complex responses. While an overall perception of the signal within class 6 suggested a decreasing SBD tendency (Figure 20c, Table 29), vegetation onset between 2003 and 2008 showed progressively later inception. On the other hand, forest

Table 27 Within-subjects effect test of repeated measures ANOVA performed for the spatial representation of the 4COVnNDII7$_{8\text{-}18}$ PC. Test run with the Hujnh-Feldt adjustment returning results for factor of time and time combined with impact class (6 levels) within selected phenology and productivity indicators.

	time			**time*response class**			**Error**
	df	F	p	df	F	p	df
CF	8.781	1494.70	0.000	43.907	40.477	0.000	8705.347
GPP	9.202	475.511	0.000	46.009	4.284	0.000	127454.137
SBD	9.024	410.723	0.000	45.120	5.183	0.000	124991.028
SL	9.353	355.989	0.000	46.766	5.303	0.000	129551.833
NDVI$_{HS}$	9.507	2252.72	0.000	47.537	68.155	0.000	131687.247
NDII7$_{HS}$	9.683	2711.45	0.000	48.413	256.943	0.000	134113.119

Table 28 Effects of forest type, aspect, elevation and slope factors evaluated for phenology and productivity indices within the spatial representation of the 4COVnNDII7$_{8\text{-}18}$ PC using the test of between subjects effects of repeated ANOVA.

	Forest type (df=2)		**Aspect (df=3)**		**Elevation (df=4)**		**Slope (df=4)**	
	F	p	F	p	F	p	F	p
CF	28.261	0.000	1.805	0.144	64.356	0.000	1.784	0.129
GPP	0.860	0.423	2.404	0.065	115.223	0.000	1.131	0.340
SI	4.443	0.012	3.793	0.010	35.461	0.000	4.524	0.001
SBD	6.555	0.001	4.825	0.002	36.370	0.000	0.204	0.936
SL	2.197	0.111	4.841	0.002	2.864	0.022	3.994	0.003
NDVI$_{HS}$	21.981	0.000	4.860	0.002	84.364	0.000	4.767	0.001
NDII7$_{HS}$	3.061	0.047	0.543	0.653	46.848	0.000	4.652	0.001

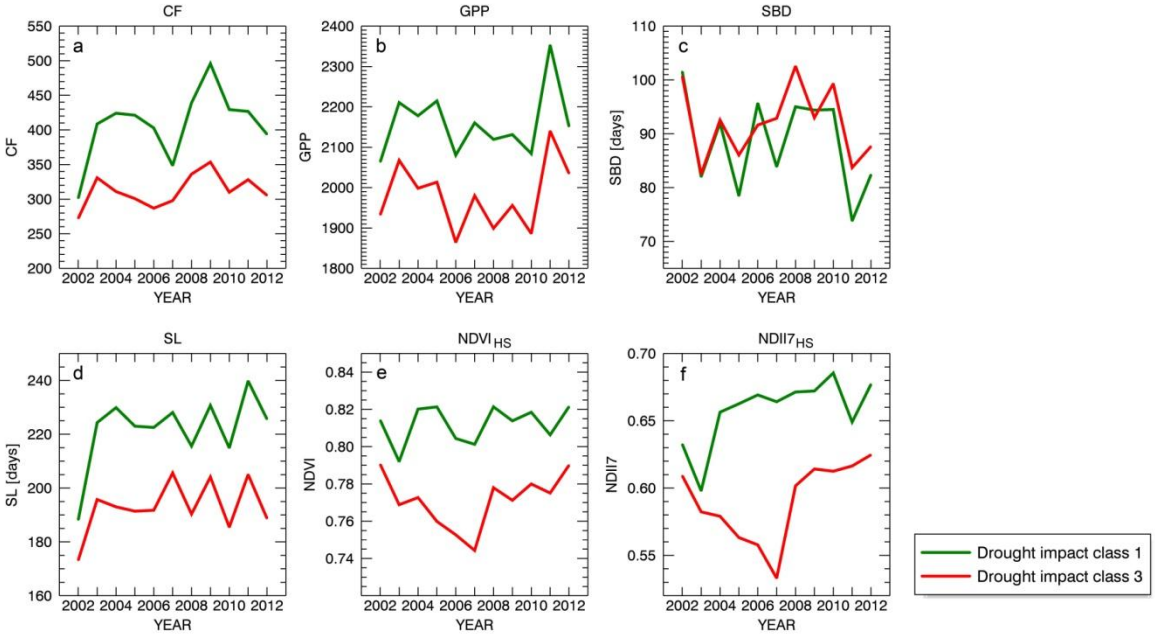

Figure 20 Year-to-year variability observed within drought impact values 1 and 5 of the 4COVnNDII7$_{8\text{-}18}$ PC footprint: a) CF, b) GPP, c) SBD, d) SL, e) NDVI$_{HS}$ and f) NDII7$_{HS}$.

Table 29 Strength of overall linear trends identified for phenology and productivity indicators within response classes 1 and 6 derived for the spatial representation of the $4COVnNDII7_{8\text{-}18}$ PC. Assessment done using the within subject contrasts test of repeated ANOVA.

	Class 1		**Class 6**	
	F	p	F	p
CF	11.034	0.001	0.013	0.911
GPP	5.534*	0.019	4.479	0.035
SBD	1.618	0.204	2.480	.0116
SL	5.225*	0.023	0.076	0.783
$NDVI_{HS}$	41.501	0.000	15.287	0.000
$NDII7_{HS}$	183.333	0.000	62.645	0.000

* - the strongest trend of all tested contrast orders

associated with class 1 revealed wobbly SBD signal with three single-year positive peaks and a massive positive anomaly between 2008 and 2010. Although the visual interpretation suggested an overall decreasing tendency, this linear relation was statistically insignificant (Table 29). SL revealed strong differences between classes with the shortest vegetation period denoted for the response class 6 (Figure 20d). Importantly, a moderate significant tendency for longer SL was observed in both classes (Table 29). Conversely, GPP within class 6 depicted an overall moderate decrease until 2010 with an intense rise afterwards (Figure 20b), whereas regions belonging to class 1 had not only higher productivity, but also experienced less distinct decrease between 2002 and 2010. CF observed within both considered response classes revealed contrasting signal between 2004 and 2007 (Figure 20a). While stands associated with class 6 showed decreasing CF, areas with the opposite response denoted much higher values with an initial increase concluded in a local drop in 2007. During the second part of the investigated period both CF signals had alike variability with an apparent positive peak centered at 2009. The overall perception of both responses suggested linear tendencies, which was statistically confirmed only for class 1 (Table 29).

A further investigation of the $4COVnNDII7_{8\text{-}18}$ drought related response of class 6 was performed with the within-subjects effects test of repeated ANOVA measures with Hujnh-Feldt correction. The analysis confirmed for all metrics significant time governed differences (Table A5 2). Time combined with elevation factor revealed statistically significant differences only for CF, $NDVI_{HS}$ and $NDII7_{HS}$ (Table 30).

Table 30 Effect of elevation factor in time on distinction between productivity indices tested for the response class 6 derived for the spatial representation of the $4COVnNDII7_{8\text{-}18}$ score. Analyses performed using within-subjects effects test of repeated ANOVA. Only measures with significant statistics are shown ($p<0.001$).

	time*elevation	
	df	F
CF	30.000	3.122
$NDVI_{HS}$	32.670	6.493
$NDII7_{HS}$	36.000	3.963

Detailed insight on phenology and productivity variability within forest type, aspect, elevation and slope classes was analyzed only for stands affected by diminished plant water content (class 6).

While altitude increase translated on almost linear decrease in $NDII7_{HS}$, $NDVI_{HS}$, GPP as well as delayed vegetation onset, it had a positive effect on CF (Figure A6 2). Regions placed at higher elevations, reported in 2003 CF, $NDII7_{HS}$ and $NDVI_{HS}$ rise, which was soon followed by depletion of all three measures. Even though CF and $NDVI_{HS}$ revealed subsequent increase already in 2007, $NDII7_{HS}$ recovered not until 2008. Drought conditions had no effect on CF of stands growing below 1400 m asl, but resulted there in lower $NDII7_{HS}$ and $NDVI_{HS}$. GPP calculated for the regions placed between 700 and 1400 m asl showed diminished values for 2004 through 2010, which contrasted with a 2002-2007 GPP rise reported for the highest elevation class. A distinct shift towards earlier vegetation onset was observed only for the 700-1400m asl strata. It had no clear relation with the SL though. Diversification of SL within elevation zones was suggested until 2006, where the highest areas experienced prolongation of the vegetation season. Starting from 2007, SL differences were irrelevant.

Exposition had limited impact on phenology and productivity variability under diminished foliage water content conditions. All aspect classes reported comparable $NDII7_{HS}$ and $NDVI_{HS}$ temporal responses of general 2002-2007 downturn, where the south facing regions were characterized by the lowest values (Figure A6 2). Noticeable similarity among exposition classes was also observed for GPP. The south-facing regions revealed here the smallest, while the west-oriented slopes, the biggest GPP variability spectrum. CF provided the best distinction among the aspect classes. West and south facing locations reported the lowest seasonal productivity, but also the most intense CF decline under drought conditions. In general, west exposition experienced the earliest vegetation onset, whereas south facing stands showed the latest SBD. The greatest disparity in season start was reported before 2007 and in 2011. All classes but S, revealed general SBD delay tendency between 2003 and 2008. This trend was not translated into SL profiles that revealed wobbly temporal variability with the greatest disparity observed between 2004 and 2006. The most intense SL change was observed on west-exposed areas. Discrepancy among aspect classes were reduced after 2007.

Inclination showed no significant role in governing $NDVI_{HS}$, $NDII7_{HS}$ nor CF drought related responses (Figure A6 2). In all three cases slope levels depicted alike temporal variability where leaning increase leaded to $NDVI_{HS}$ and $NDII7_{HS}$ drop, but apparently CF rise. Conversely, an inclination-specific response was observed for GPP, where steepness increase leaded to nonlinear productivity changes. GPP disparity among slope classes was the greatest for 2003 and 2004. Diminished foliage water content conditions leaded to modest shift towards an earlier vegetation onset within regions of 10-40 degrees inclination. On the other hand, sites with leaning of less than 10 degrees revealed clear 2002-2009 SBD decrease tendency temporally hampered in 2004-2005. The greatest differences in vegetation season length were noted from 2003 through 2006, where the change variability decreased with slope increment.

Since neither broadleaved nor mixed stands were represented by a sufficient number of pixels (Table 22; Figure A6 2), forest type was excluded from the consideration.

4.4.3. 3COVnNDVI$_{8\text{-}18}$ spatial pattern

The 3COVnNDVI$_{8\text{-}18}$ PC (Figure 16B) implied a gradual decrease in forest 'greenness' initiated with a 2003 NDVI increase. Response correlated with this variability was recognized for coniferous forest (Table 22) growing in majority on north exposed sites in the central, north and west parts of South Tyrol (Figure 21). Discussed stands occupied usually medium to high altitudes with a clear preference for 1400-2100m asl strata and moderate sloping. The reversed response was fostered by class 1 and comprised a NDVI drop in 2003 followed by gradual NDVI increase. The rising tendency was identified most often in the central part of South Tyrol and the Eisack Valley (Figure 21) at medium elevations as well as on south and east exposed slopes (Table 22). It was characteristic mainly for coniferous stands, with addition of mixed forest growing on slopes with low to moderate inclination.

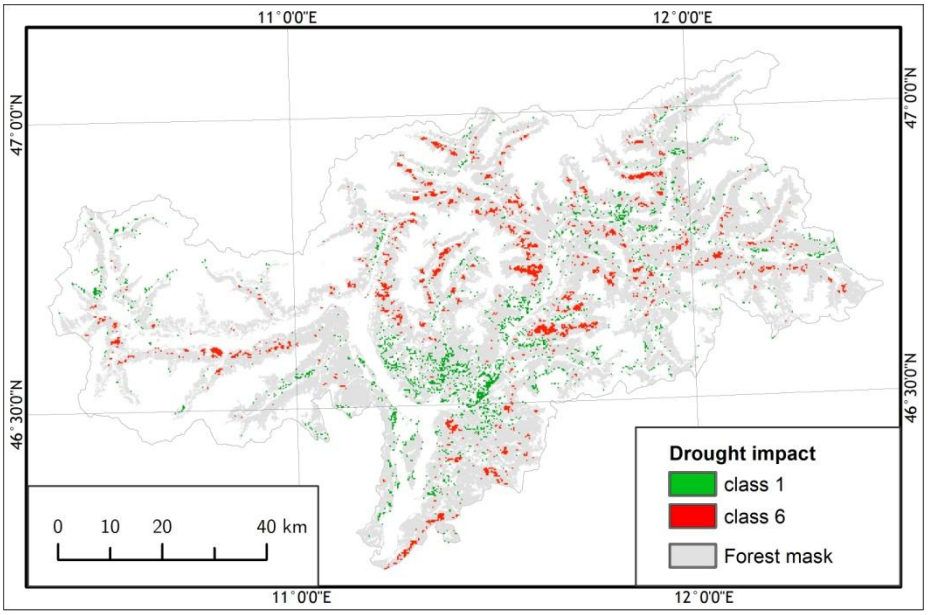

Figure 21 Spatial representation of the 3COVnNDVI$_{8\text{-}18}$ PC limited to response of class 1 (green) and 6 (red). The forest mask marked in gray.

Significance of phenology and productivity changes observed in the region was confirmed using the within-subjects effects test of the repeated measures ANOVA performed with the Hujnh-Feldt adjustment (Table 31). Furthermore, differences among six drought impact classes were also significant in time, with the greatest disparity observed for NDVI$_{HS}$. The effect of site-specific characteristics on local phenology was inspected, and revealed the leading impact of elevation (Table 32). Aspect and slope were found less influential, whereas forest type showed significant relation only for CF and NDVI$_{HS}$.

The alpine forest revealing nNDVI decrease between 2003 and 2012 (class 6) showed an overal NDVI$_{HS}$ decline (Table 33) with two local minima in 2007 and 2011 (Figure 22e). On the contrary, NDII7$_{HS}$ revealed rather levelled response with a minor reduction in 2003, and two drops in 2007 and 2011 separated by higher NDII7$_{HS}$ values

Table 31 Within-subjects effects test of repeated measures ANOVA performed for the spatial representation of the 3COVnNDVI$_{8\text{-}18}$ PC. Test run with the Hujnh-Feldt adjustment returning results for the factor of time, and time combined with response class (6 levels) within selected phenology and productivity indicators.

	time			**time*response class**			**Error**
	df	F	p	df	F	p	df
CF	8.896	2279.982	0.000	44.478	89.880	0.000	214427.103
NPP	9.316	742.959	0.000	46.581	73.776	0.000	224568.362
SBD	9.012	627.540	0.000	45.062	32.252	0.000	217242.288
SL	9.365	533.215	0.000	46.823	48.752	0.000	225734.212
NDVI$_{HS}$	9.905	3923.234	0.000	49.493	929.866	0.000	238759.726
NDII7$_{HS}$	9.723	5432.021	0.000	48.613	244.681	0.000	232420.809

Table 32 Effects of forest type, aspect, elevation and slope factors evaluated for phenology and productivity within the spatial representation of the 3COVnNDVI$_{8\text{-}18}$ PC using the test of between subjects effects of repeated ANOVA.

	Forest type (df=2)		**Aspect (df=3)**		**Elevation (df=4)**		**Slope (df=4)**	
	F	p	F	p	F	p	F	p
CF	14.228	0.000	0.027	0.994	64.442	0.000	2.898	0.021
GPP	0.394	0.674	1.725	0.160	83.772	0.000	2.772	0.027
SBD	1.941	0.144	10.885	0.000	17.933	0.000	1.543	0.187
SL	0.801	0.449	5.993	0.000	3.150	0.013	6.861	0.000
NDVI$_{HS}$	29.905	0.000	5.908	0.001	44.437	0.000	13.420	0.000
NDII7$_{HS}$	9.399	0.000	1.762	0.152	22.774	0.000	9.798	0.000

Table 33 Strength of overall linear trends observed for phenology and productivity indicators within response classes 1 and 6 derived for the spatial representation of the 3COVnNDVI$_{8\text{-}18}$ PC. Assessment done using the within subject contrasts test of repeated ANOVA.

	Class 1		**Class 6**	
	F	p		F
CF	25.981	0.000	3.581	0.059
GPP	91.100	0.000	0.909	0.341
SBD	38.053	0.000	0.568	0.451
SL	4.700	0.030	2.182	0.140
NDVI$_{HS}$	401.204*	0.000	156.622	0.000
NDII7$_{HS}$	385.796*	0.000	8.559	0.004

* - the strongest trend of all tested contrast orders

(Figure 22f). A no clear tendency could be identified for SBD observed within those regions (Figure 22c; Table 33). Vegetation onset varied greately between consecutive years, with earlier SBD in 2003, 2005, 2007 and 2011. Although SL also demonstrated considerable variation (Figure 22d) its relation with vegetation onset was limited. Despite a downturn in the 3COVnNDVI$_{8\text{-}18}$ envelope, CF demonstrated increasing tendency with two intense gains in 2003 and 2009 (Figure 22a), as well as clear gradual

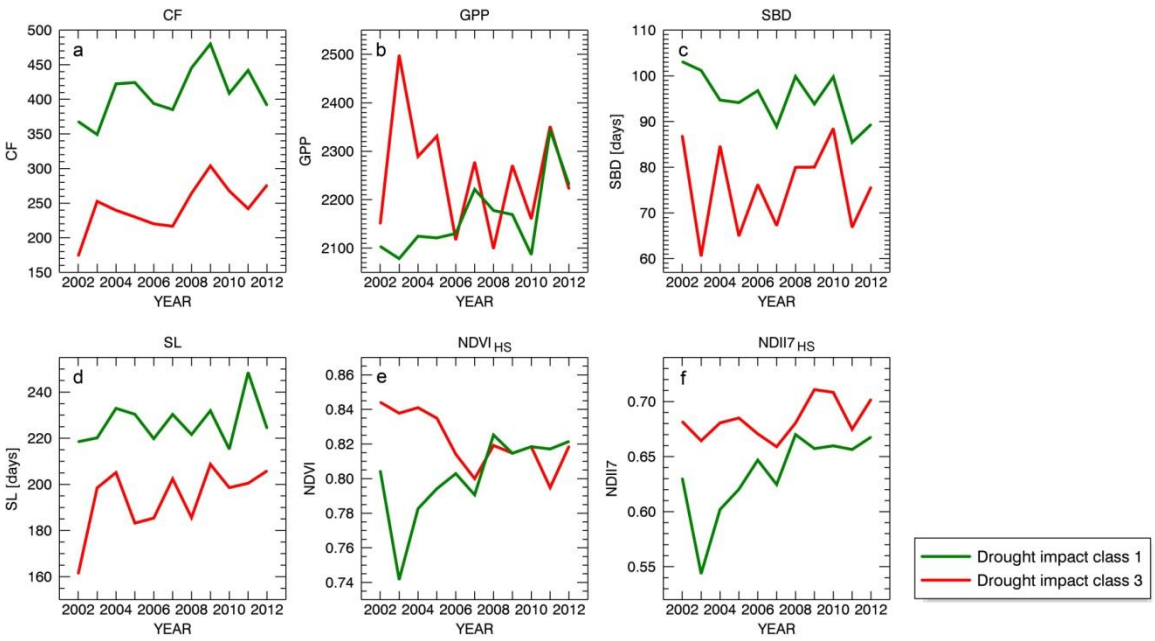

Figure 22 Year-to-year variability observed within drought impact classes 1 and 6 of the 3COVnNDVI$_{8\text{-}18}$ PC footprint: a) CF, b) GPP, c) SBD, d) SL, e) NDVI$_{HS}$ and f) NDII7$_{HS}$.

decline from 2003 through 2007. GPP temporal profile accounted on a massive increase in 2003 followed by equaly strong productivity drop terminated in 2006 (Figure 22b). Consecutive years revealed strong GPP variabilit with slightly increasing tendency.

Drought impact within class 1 opposed the 3COVnNDVI$_{8\text{-}18}$ PC, implying nNDVI increase after the initial negative anomaly in 2003. Associated forest stands demonstrated for NDVI$_{HS}$ and NDII7$_{HS}$ massive decreases in 2003 followed by a progressive increment (Figure 22e and f respectively; Table 33). Both temporal profiles were usually below envelopes depicted for class 6, and highlighted small, secondary drops in 2007 as well as smooth and levelled response beyound the year 2008. Start of the season occurred on average 19.6 days later than within class 6 (Figure 22c) and revealed clear 2002-2007 shift towards ealrier onset (Table 33). In contrast, despite some minor fluctuation SL showed no apparent long term trends (Table 33) and was roughly 32.6 days longer comparing with the opposing impact class (Figure 22d). CF revealed an overal increasing tendency (Table 33) comprising drops in 2003, 2006-2007 and 2010, as well as local maxima of 2004-2005 and 2009-2010 (Figure 22a). Derived values were considerably higher than seasonal productivity within stands associated with class 6. An initial GPP increment observed since 2003 reversed after 2007 into a decline halted in 2010 (Figure 22b). On the other hand an abrupt GPP increase in 2011 gave an impression of overall upturn (Table 33).

Phenology changes within the 3COVnNDVI$_{8\text{-}18}$ class 6 response were not always positively evaluated for the factor of time with the within-subjects effects test of repetitive ANOVA measures (Table A5 3). Corresponding analyses performed for combinations of time with four environmental factors revealed significant differences for coupling with elevation and forest type only for CF measure (Table 34).

Table 34 Effect of elevation factor in time, as well as, forest type in time on distinction between phenological indices tested for the response class 6 derived for the spatial representation of the $3COVnNDVI_{8\text{-}18}$ score. Analyses performed using within-subjects effects test of repeated ANOVA. Only measures with significant statistics are shown ($p<0.001$).

	time*elevation		**time*forest type**	
	df	F	df	F
CF	29.464	1.960	19.642	2.094

In-depth factors-specific inspection of phenology and productivity within stands following the nNDVI decline (class 6) shed some light on temporal variability observed within forest type, aspect, elevation and slope levels (Figure A6 3).

Elevation increase drove $NDVI_{HS}$ and GPP decline, as well as SBD delay but has positive effect on $NDII7_{HS}$, SL and CF (Figure A6 3; based on two altitude classes). Overall nominal differences between elevation classes were small for $NDVI_{HS}$ and $NDII7_{HS}$. Conversely, CF showed clear disparity between strata. Regions placed at 1400-2100 m asl revealed an increasing tendency comprising strong productivity gain in 2003 and a second local maxima in 2009. The lower elevation class showed very limited CF changes over time. GPP disparity between altitudinal classes was apparent in 2002 and 2006 through 2008. Forest growing within the higher altitudinal zone depicted an abrupt GPP rise in 2003 followed by steady decline until 2008. Temporal variability observed between 700 and 1400 m asl, although more subtle, implied an overall productivity downturn shortly interrupted in 2007. SBD revealed moderate link to elevation. Fluctuation in vegetation onset were more frequent at 1400-2100 m asl, whereas the lower class depicted shift towards considerably earlier vegetation onset between 2004-2005, followed by progressing SBD delay. No straightforward relation between SBD and SL was detected. Vegetation season length was more constant at higher altitudes, where also intense SL prolongation in 2003 was observed.

Although aspect affected $NDVI_{HS}$ and $NDII7_{HS}$ values, all exposition-specific temporal profiles followed alike, index-specific variability (Figure A6 3), with south facing-slopes revealing the lowest $NDVI_{HS}$ and $NDII7_{HS}$. Moreover, south and west exposed locations demonstrated the highest amplitude of $NDII7_{HS}$ changes highlighting three intense drops in 2003, 2007 and 2010. CF revealed a clear disparity among expositions classes. All regions showed productivity gain in 2003, with the greatest CF rise observed for north and east facing regions. Aspect clearly governed forest resistance to prolonged drought conditions where east-exposed stands were the first to report substantial relative productivity decline. The most apparent GPP deterioration after an initial rise in 2003 was observed at north and west exposed sites. Although SBD and SL showed no mutual relation, both revealed not only strong temporal variability, but also a considerable disparity among aspect classes after 2004. Solely north exposed stands rendered an overall uneven shift towards later SBD, whereas three remaining classes indicated intense year-to-year vegetation onset changes with the earliest SBD observed in 2005-2007.

Inclination had no impact on $NDVI_{HS}$ nor CF diversification under decreasing 'greenness' conditions (Figure A6 3) and temporal profiles obtained for those indices demonstrated a limited disparity among slope classes. On the contrary, $NDII7_{HS}$ was

clearly driven by land leaning, but the steepness increase was not linearly related to the index values. The fourth steepness class (30-40 deg) revealed here the lowest $NDII7_{HS}$ with an outstanding local maximum in 2008. GPP, SBD and SL showed enhanced inclination-induced differences from 2005 onward. The strongest year-to-year GPP and SBD variability was observed for two zones with the lowest inclination. It revealed a distinct shift towards earlier vegetation onset in 2005 through 2007. Relation between SBD and SL was vague.

Consideration of forest types was hindered by insufficient representation of pixels associated with broadleaved and mixed stands (Table 22; Figure A6 3).

Since the reversed, increasing tendency of the $3COVnNDVI_{8\text{-}18}$ PC also presented interesting, potential drought induced forest status evolution, phenology and productivity variability within the impact class 1 were also inspected in detail. The within-subjects effect test evaluated positively significance of phenology alternation in time (Table A5 4). Furthermore, class 1 demonstrated also significant phenology differences for a combination of time and elevation factors (Table 35)

Table 35 Effect of elevation factor in time on distinction between phenology and productivity indices tested for the response class 1 derived for the spatial representation of the $3COVnNDVI_{8\text{-}18}$ score. Analyses performed using within-subjects effects test of repeated ANOVA. Only measures with significant statistics are shown ($p<0.001$).

	time*elevation	
	df	F
CF	25.458	7.765
GPP	29.086	2.919
SBD	25.005	3.131
$NDVI_{HS}$	31.845	5.051
$NDII7_{HS}$	34.015	2.434

A multilevel investigation revealed limited elevation impact on $NDII7_{HS}$ where a distinction among altitude levels was hardly possible (Figure A6 4). Although also $NDVI_{HS}$ revealed alike temporal variability for all three considered classes, regions placed the highest were characterized by noticeably lower index values. CF depicted a disparity between forest productivity below and above 1400 m asl. While the former area marked lower CF with suppressed temporal variability and productivity decline in 2003, the latter revealed not only significantly higher CF, but also more intense changes and stronger overall upturn initiated with a clear increase in 2003-2004. Conversely, the 1400-2100 m asl elevation class reported the lowest GPP with the strongest drop in 2010 and following peak in 2011. Moreover, unlike stands at lower elevation, considered forest revealed modest GPP increases in 2005 and 2007. SBD showed a minor and nonlinear relation to altitude with the earliest vegetation onset observed between 700 and 1400 m asl. The third elevation class was here the only one experiencing an earlier SBD in 2003 as well as delayed start of the season in 2008-2009. The most apparent, although still rather small SL differences were noted before 2006. The third elevation zone, as the only one, implied prolonged vegetation season in 2003.

Aspect governed phenology and productivity, but did not alter forest response to nNDVI upturn (Figure A6 4). The best distinction among expositions was ensured for $NDII7_{HS}$ and CF, where, in both cases, north-facing regions revealed the highest values. GPP demonstrated recognition between south-west and north-east aspects, with the former having higher productivity yield. Diversification among aspect classes was very limited for $NDVI_{HS}$ and SL, and showed no apparent drought stress changes. Aspect-specific SBD discrepancies were observed only before 2006 and comprised moderate 2002-2007 shift towards earlier onset. Only north-facing stands hampered this tendency with a modest SBD increase in 2005.

Alike aspect, also inclination shaped forest phenology and productivity, but had no apparent effect on response to long-term nNDVI change. A relation between slope and inspected measures was nonlinear (Figure A6 4). The highest $NDVI_{HS}$ and $NDII7_{HS}$ were observed within the first inclination class (0-10 deg.). Moreover, those regions experienced the earliest SBD, the longest vegetation season and the highest GPP. Areas leaning between 30 and 40 degrees were in perfect opposition. The clearest disparity among inclination classes was observed for SBD between 2003 and 2004. Temporal profiles implied here strong shift towards earlier vegetation onset within the first slope class.

Forest type analyses comprised coniferous and mixed stands (Figure A6 4). Both levels followed alike temporal variability with the former having lower $NDVI_{HS}$, $NDII7_{HS}$ and GPP but higher CF and in general later SBD. The most distinct disparity between responses of both forest types was observed in 2003, when mixed woodland revealed abrupt CF decline and modestly delayed SBD, which contrasted with responses depicted for coniferous stands.

4.5. Summary and discussion

Condition of the South Tyrolean forest was extensively investigated in relation to the local meteorological variability between 2001 and 2012. Analyses were based on the time series of MODIS derived NDVI and NDII7 indices, and focused on identification of potential drought stress driven vegetation status changes. The S-mode PCA decomposition was the primary exploration method applied to 15 different datasets and convolution setups (Table 18). PCA results were evaluated against the dominant scPDSI temporal patterns (Chapter 3, Figure 14), which allowed not only to identify the most reliable drought related temporal profiles and their footprints, but also determined most suitable PCA setups for alpine forest stress monitoring. Moreover, extensive phenology and productivity based investigation of three selected responses provided detailed information on changes taking place at drought affected sites.

4.5.1. Utility of diverse S-mode PCA setups and EOFs rotation for forest vegetation status monitoring

Applied multiple S-mode PCA settings and data setups (Table 18) produced variety of NDVI and NDII7 based temporal patterns among which many scores demonstrated considerable accordance with drought conditions identified through the scPDSI analysis.

The length of the annual time window composing a time series was recognized as a principal factor driving PCA results. Presented analyses indicated that for the alpine forest, vegetation response registered during the dormancy state is inessential for drought related investigation and can even blur anticipated variability. Moreover, late autumn to early spring images can have high probability of snow occurrence, which can produce anomalies and outstanding signal that is able to predominate a time series. In addition, due to more frequent cloud cover and other registration issues, 1^{st} to 7^{th} and 19^{th} to 23^{rd} yearly composites need more preprocessing in terms of gap-interpolation (Figure 5 and Figure 6). Exclusion of those composites, realized through data truncating to the vegetation season and high-season time series, ensured datasets of higher quality and limited variation present in the data to relevant minimum. Consequently, PCA decomposition was more efficient in addressing subtle drought induced vegetation changes. On the other hand, high-season time series restrict understanding of intra-seasonal variability, including only late summer information. Although this period is a time of potentially the highest drought impact on vegetation, and resulting PCA scores showed good accordance to the scPDSI derived meteorological profiles, importance of the late spring and early summer weather stress should not be overlooked.

The z-score normalization of a time series was also an important controlling factor in the PCA decomposition. Implemented data z-score normalization combined with the covariance-matrix based S-mode PCA outperformed the correlation-matrix based decomposition of not-normalized time series. Although the correlation matrix approach implies data standardization the process is based on a global mean, whereas the applied z-score method uses composite mean assuring hence more exact anomalies. As a result a normalized time series carries more precise information on disparity from 'normal' condition, which more accurately refers to the drought concept. This approach reduces total variance of a time series being introduced into PCA, hence allows on more efficient exploration of drought related signal. Moreover, the time-specific expression of anomalies corresponds better with conceptual drought definitions as well as computation schemes of drought indices, including the scPDSI. The correlation-based PCA of not-normalized time series preserved a seasonal component, which controlled resulting temporal profiles and governed very high eigenvalues of first PCs. The drought related signal was here either incorporated into the dominant patterns, or hidden in the principal components of the higher order. Conversely, PCA implementation based on the covariance-matrix and z-score normalized datasets generated loadings and scores with more dispersed variability, and less dominant leadings patterns.

Although time series after the Savitzky-Golay filtering obtained higher eigenvalues and smoother PCs profiles comparing to non-filtered time series, beforehand noise reduction had a very limited impact on temporal as well as spatial representation of identified drough responses. Mutual comparison of scores and their spatial projections derived for coupled SG-filtered and non-filtered time series showed very strong correlation. Importantly, impact of SG filtering was so subtle, that it does not altered variance distribution and did not lead to disparate principal components identification.

A beneficial impact of rotation on strengthening drought related vegetation response was selective. Although some temporal patterns came out more robust in terms of

correlation with the scPDSI scores, temporal variability of rotated PCs often comprised more intense variability with multiple anomalies. Resulting scores tended to depict separated anomalies rather than a coherent temporal development. Differences between orthogonal Varimax and oblique Promax solutions were limited, but showed the latter to produce smoother temporal profiles that better resembled identified meteorological conditions. Variability of resulting PCs was strictly governed by a number of rotated EOFs. With one exception, Kaiser's stopping rule and Cattell's scree test retained a very similar number of loadings to be rotated, which implied limited differences of emerging PCs. Performed analyses were insufficient to conclude on potential inaccuracy of the Kaiser's approach (Costello & Osborne, 2005). The Cattell's scree test was rather consistent in nominating only a few first EOFs, but was much more ambiguous to conduct.

Due to diverse NDVI and NDII7 design and properties, both indices addressed different but complementary drought governed forest changes. While the NDVI focuses on 'greenness' rendering a straightforward canopy status, the NDII7 addresses plant water content and cell structure. Although both demonstrated vast information load, each index tended to depict selected drought related phenomenon. NDVI was more prone to indicate patterns of gradual decline (PCs: $3COVnNDVI_{8\text{-}18,}$ $3COVnNDVI_{SG8\text{-}18}$, $3COVnNDVI_{8\text{-}18}ROT5P$ and $4COVnNDVI_{14\text{-}17}ROT7P$), whereas NDII7 rendered temporal variability of prolonged decrease between 2003 and 2007 (PCs: $1CORNDII7_{8\text{-}18}$, $4COVnNDII7_{8\text{-}18}$, $4COVnNDII7_{8\text{-}18}ROT4V$ and $4COVnNDII7_{8\text{-}18}ROT4P$).

Importantly, multiple PCA setups resulted in similar temporal variability, which confirms the method consistency, dominant character of weather stress conditions, as well as aptness of applied vegetation related measures. Despite subtle character of investigated changes, obtained results provided interesting insight and allowed for further identification and investigation of drought impacted forest sites.

4.5.2. Selection and evaluation of PCA results associated with scPDSI-defined drought conditions

Preliminary examination of results of 15 S-mode PCA setups was targeted at identification of temporal patterns related to the scPDSI established meteorological drought variability (Chapter 3). Despite severe dry conditions in 2003-2007 demonstrated by the scPDSI analyses, documented negative drought impact on forest vegetation was limited in South Tyrol to diminished trees productivity and local discolorations, with only one recorded small-scale dieback event in the Eisack Valley (Minerbi *et al.*, 2006). The dry spell in question was translated into lower plant water content and crown fitness, which although extensive, were very subtle. Due to this, absolute changes in NDVI and NDII7 values were suppressed and addressed only narrow variability in the time series. Scarcity of site-specific information on feedback between water-stress and forest status or productivity, enforced a rest on an assumption upon direct link between drought conditions and NDVI and NDII7 changes. Consequently, all PCA resulting scores were linearly correlated with the scPDSI derived meteorological variability, where owing to the disparity in length and annual time-scope of datasets, the comparison was based on yearly averages. This approach clearly inhibited a perception of intra-annual variability, as well as

identification of more complex forest responses to drought conditions accounting on physiologically lagged reaction of some trees species (Pichler & Oberhuber, 2007; Lévesque *et al.*, 2014), or site specific differences (Primicia *et al.*, 2015). Inconsistency of time steps between the scPDSI and MODIS time series was an important hindrance for a qualitative assessment. Although the correlation usually provided sensible estimate, additional visual assess between the NDVI and NDII7 scores, and the scPDSI temporal patterns was required. Only this synergy ensured identification of scores of statistical credibility and physiological feasibility.

Interestingly, most of the 1scPDSI associated NDII7 PCs showed drought induced score decrease not until 2004, while the dry spell started in South Tyrol already in 2003. On the other hand, a strong 2003 anomaly was clearly detected in numerous PC based on the NDII7 as well as, NDVI time series. This distinction could be governed, among others, by different vegetation perception of drought incept and persistent aridity stress, which is controlled by environmental conditions (e.g. Vacchiano *et al.*, 2012; Lévesque *et al.*, 2014), tree species (e.g. Scherrer *et al.*, 2011a; Hanewinkel *et al.*, 2013; Zimmermann *et al.*, 2013a) and local tree competition (e.g. Eilmann *et al.*, 2006; Pichler & Oberhuber, 2007; Chauchard *et al.*, 2010; Giuggiola *et al.*, 2013; Rigling *et al.*, 2013; Primicia *et al.*, 2015).

Mutual comparison among 16 identified PCs and their spatial representations demonstrated a considerable overlap between scores following the same scPDSI variability. This observation supported credibility of identified temporal patterns, as well as their footprints. Although, yearly-averages based correlation used for PCs of different length restricted comparison of inter-annual variability, an emerging bias was negligible.

Although the $3COVnNDVI_{8\text{-}18}$ and $4COVnNDII7_{8\text{-}18}$ PCs selected for further analyses did not have the strongest statistical connection to the scPDSI, their temporal variability had high potential credibility of reliable forest responses to identified drought conditions. The $1CORNDII7_{8\text{-}18}$ score was incorporated into the analysis due to its unique seasonal component. All three identified patterns addressed variety of PCA setups, and demonstrated hardly any mutual overlap of spatial footprints.

4.5.3. Forest vegetation response to drought[15]

Drought impact on forest in South Tyrol implied by three selected PCs was analyzed in detail using four vegetation productivity metrics and two phenology indicators, all employed into repeated ANOVA measures. The main concern was usually given to the regions the strongest associated with recognized drought temporal variability. The examination ensured site-specific insight into phenological changes governed by underlying dry spell conditions.

4.5.3.1. $1CORNDII7_{8\text{-}18}$ spatial pattern

The $1CORNDII7_{8\text{-}18}$ PC rendered NDII7 seasonality with clearly diminished seasonal maxima before 2008 and three distinct declines in the envelope in 2003, 2007 and 2010 (Figure 16F). Irrespective of seasonal component, the signal was the most characteristic for alpine and subalpine forest comprising Norway Spruce, Silver Fir

[15] All forest specific information are sourced from Provincia Autonomica di Bolzano, (2010)

with Scots Pine, Arolla Pine and European Larch growing on drier locations. Although an initial response to the dry-spell involved intense productivity increase, forest growth capacity was soon depleted (Figure 18), most surely, due to water shortages and elevated temperature. While the drought related temperature increase combined with priori moist conditions in 2002 acted as a catalyst for coniferous trees growth at high elevation (Jolly *et al.*, 2005; Primicia *et al.*, 2015), next-year decline illustrated delayed response to arising aridity (Theurillat & Guisan, 2001; Pichler & Oberhuber, 2007; Castagneri *et al.*, 2014). Despite the dry-spell, $NDII7_{HS}$ revealed an overall rise, implying increase in plant foliage water capacity. $NDVI_{HS}$ reported for 2004-2005 an increase with respect to 2003 and 2006 lows, which contrasted with the $1CORNDII7_{8\text{-}18}$ score. SBD decrease observed between 2003 and 2006 was most probably governed by temperature, alike the overall SL prolongation, which translated into moderate GPP increase (Table 25). Positive feedback between the seasonality governed PC and coniferous stands could be explained through abundance of Larch trees as well as low crown density and frequent presence of signal originating from shrubs or grasslands. On the other hand, depicted CF values were small, hence it is possible that they illustrate actual seasonality of coniferous trees.

Areas associated with the $1CORNDII7_{8\text{-}18}$ class 1 response comprised a wide spectrum of correlation from strongly negative up to values around zero (Table 21). This inconsistency obscured statistics and hindered clarity of results. Spatial projection of drought impact class 1 indicated lower forest fringe composed of Common Beech, Downy Oak, Sessile Oak, Hop Hornbeam, Manna Ash and Sweet Chestnut, as well as, upper forest border with Silver Fir, European Larch and Arolla Pine. Discussed regions, also demonstrated the heat-wave triggered productivity increase, but unlike for class 6, the rising tendencies in GPP and SL lasted until 2007, and were proceeded by strong negative anomaly clearly governed by delayed SBD (Figure 18). This observation is supported by better adjustment of hardwood trees to increasing aridity (Scherrer *et al.*, 2011; Hanewinkel *et al.*, 2013; Zimmermann *et al.*, 2013a) as well as beneficial effect of temperature increase on forest vegetation productivity at higher elevations (Jolly *et al.*, 2005; Coppola *et al.*, 2012; Primicia *et al.*, 2015). Moreover, depicted changes can be presumably attributed on dominance of north-exposed slopes among discussed area. However, it has to be kept in mind that phenology scores were averaged over a variety of response to the $1CORNDII7_{8\text{-}18}$ PC, including the upper fringe of the forest border, which in its definition incorporates sparsely wooded zones of grasslands with drafted trees and shrubs. Therefore presented results could carry some uncertainty.

Interestingly, an anomaly of 2010 observed in the $1CORNDII7_{8\text{-}18}$ score and not explained by the scPDSI variability, was also visible in the phenologyl time series.

4.5.3.2. $4COVnNDII7_{8\text{-}18}$ spatial pattern

Diminished foliage water content between 2004 and 2007 indicated by the $4COVnNDII7_{8\text{-}18}$ PC, was the most apparent in mountain and subalpine forests composed of Norway Spruce, Silver Fir and Downy Oak with regional inclusion of Scots Pine and European Larch trees on the most arid locations of south exposed slopes, as well as the upper tree line. Considered stands were often located on poor mountain soils developed on silicate rocks (Provincia Autonomica di Bolzano, 2010).

Forest enclosed in the class 1 response comprised Norway Spruce with addition of Downy Oak and Common Beech. It frequently grew on north and west exposed, richer silt and carbonate soils (Provincia Autonomica di Bolzano, 2010). Phenological response of those areas accounted on higher than for class 6 productivity and vegetation status (Figure 20), which can be attributed on more frequent presence of hardwood tree species.

Drought governed disparity between phenology and productivity of two considered classes were the most apparent for $NDII7_{HS}$, $NDVI_{HS}$ and CF. The initial response to drought ingress in 2003 was similar within both classes. Despite $NDVI_{HS}$ and $NDII7_{HS}$ drops, GPP and CF productivity increase was observed that year. The latter could be explained not only by the earlier SBD and longer SL, but also intensified vegetation growth at higher altitudes, which is normally constrained by the elevation gradient (Jolly *et al.*, 2005; Primicia *et al.*, 2015). Subsequently observed mutual divergence between forest productivity of both classes can be related to site-specific differences and environmental conditions such as soil structure, elevation and forest species distribution (Scherrer *et al.*, 2011; Castagneri *et al.*, 2014; Lévesque *et al.*, 2014b). Despite class 6 was in majority detected in the Vinschgau Valley, which is the driest region in South Tyrol, expected higher drought adjustment of trees was not observed as shown by Feichtinger *et al.* (2014). Conversely, depicted response indicated downturn in forest status. Although the presented data did not suggest any long-term trends in forest decline, depicted GPP downturn, especially clear for class 6, implies aridity impose forest weakening. It is feasible that longer or more intense drought event(s) could exceed adaptation and mitigation abilities of selected forest communities and lead local diebacks (Theurillat & Guisan, 2001; Jump & Penuelas, 2005).

In contrast with forest productivity, phenology measures revealed limited drought related diversification between impact classes.

4.5.3.3. $3COVnNDVI_{8\text{-}18}$ spatial pattern

Decreasing nNDVI, associated with the $3COVnNDVI_{8\text{-}18}$ class 6 response was the most common for mountain Norway Spruce forest (Provincia Autonomica di Bolzano, 2010) growing in majority at north-exposed slopes. Although Norway Spruce has moderate drought tolerance, particularly at lower altitudes (Hartl-Meier *et al.*, 2014), its preference for moisture habitats at higher elevations could partly mitigate impact of arising aridity (Pichler & Oberhuber, 2007). Consequently, beneficial effect of released temperature gradient constrain (e.g. Theurillat & Guisan, 2001; Jolly *et al.*, 2005; Castagneri *et al.*, 2014), leaded to the initial productivity increase in 2003. The following years demonstrated however CF and GPP decline, where the latter revealed particularly massive deterioration. This observation is in line with findings of Pasho *et al.*, (2011) who indicated that forest drought response at mesic sites can be stronger than at xeric locations. Furthermore, due to shallow root system as well as poor soils and rocky bedrock conditions, Norway Spruce is susceptible to elevated temperature and depleted soil moisture (Castagneri *et al.*, 2014).

Despite $NDVI_{HS}$ and GPP decline, discussed forest sites showed overall CF upturn. This decoupled response could be partly explained by prolonging SL. A gradual vegetation type change is also a probable interpretation, however has to be confirmed through other analyses.

The nNDVI increase featured in the $3COVnNDVI_{8\text{-}18}$ class 1 response, highlighted regions dominated by Downy Oak, Sessile Oak, Hop Hornbeam, Sweet Chestnut, Manna Ask and Common Beach trees, with Scots Pine in dry and hot locations, as well as Downy Oak and Norway Spruce forests on higher and shadowy regions (Provincia Autonomica di Bolzano, 2010). Most of the discussed stands grows at lower altitudes that are more prone to temperature increase and rain decline (Gebetsroither *et al.*, 2013), whereas endemic, poor silicate soils cannot mitigate arid conditions. Consequently, the observed overall productivity increase and earlier vegetation onset tendency suggest upturn in hardwood trees status, which agrees with their overall better adjustment to drought (Scherrer *et al.*, 2011; Rigling *et al.*, 2013). Furthermore, field observations and documented local Scots Pine dieback (Minerbi *et al.*, 2006) has demonstrated drought induced change in competition between coniferous and broadleaved trees, where better adjusted hardwood understory species such as Downy Oak and Hop Hornbeam replaced evergreen trees withered after the 2003 heat-wave. Alike transitions were already observed in other alpine valleys (e.g. Bigler et al., 2006; Rigling et al., 2013) and are often attributed on climate change (Hanewinkel *et al.*, 2013; Zimmermann *et al.*, 2013a). A tendency towards earlier vegetation onset revealed within this class is in line with other studies (Theurillat & Guisan, 2001; Studer *et al.*, 2005, 2007), but interestingly, had no impact on SL.

4.5.3.4. Drought impact within elevation, slope, aspect and forest type

Elevation was the most important factor driving forest phenology and productivity, also under drought conditions. Its impact varied among three considered spatial patterns. Although Ciais et al. (2005) demonstrated Pan-European forest productivity decline in 2003, this study revealed GPP and CF drop only within stands indicated by the $3COVnNDVI_{8\text{-}18}$ class 1 response and growing below 1400 m asl. Conversely, forest at higher elevations showed clear GPP and CF increase in 2003 and also partly in 2004. Moreover, in a case of the $1CORNDII7_{8\text{-}18}$ and $3COVnNDVI_{8\text{-}18}$ class 6 responses productivity gain due to the heat-wave conditions was spotted already above 700 m asl. The abovementioned discrepancy could arise from higher resolution data, as well as wider range of elevation covered used in this study. Furthermore, above presented findings agree with demonstrated by Hartl-Meier et al. (2014) diverse effect of elevation increase on different tree species under heat wave conditions, as well as reported productivity increase observed for higher alpine regions due to released elevation gradient (Dobbertin *et al.*, 2005; Jolly *et al.*, 2005; Vacchiano *et al.*, 2012; Gebetsroither *et al.*, 2013; Rigling *et al.*, 2013). Next, an apparent shift towards earlier vegetation onset revealed for woodlands growing below 1400 m asl (the $3COVnNDVI_{8\text{-}18}$ class 6 was an exception here) potentially reflects climate alternation towards warmer and dryer conditions (Zimmermann *et al.*, 2013a), which is particularly vivid at lower altitudes (Gebetsroither *et al.*, 2013). Finally, the counterintuitive relation between elevation and CF could be partly explained by increasing contribution of larch trees in the mountain and subalpine forest. However, forest canopy openings being more frequent towards the upper tree line could also lead to false perception of increased CF. Remarkably, upturn in seasonal productivity was not coupled with prolongation of the vegetation season.

Drought impact on forest productivity showed moderate diversification in relation to exposition. In most of the cases, all aspect classes followed alike, index-specific temporal variability and revealed only minor differences in intensity and timing of changes during the meteorological stress period. Those disparities presumably originate from species-specific conditions as well as exposition governed water scarcity (Pichler & Oberhuber, 2007; Lévesque *et al.*, 2014b). The greatest differences were noted for SBD and SL. Disparity among exposition classes enhanced under drought stress conditions (from 2004 onwards, as well as between 2003-2006 and in 2011 respectively) with no link between aspect-specific responses derived for both spatial patterns. Since Swidrak et al. (2013) showed SBD to be controlled by temperature rather than precipitation, as well as highlighted influence of photoperiod on growth and competitive strategies of various tree species, observed disparity was assumed to emerge from stand composition and site-specific conditions governing survival strategies under extreme conditions (Brunner *et al.*, 2015). This presumption is supported by CF variability, nevertheless should be further confirmed by site-specific surveys, and in a case of SL additionally evaluated for drought induced earlier senescence.

Since inclination governs water discharge and soil formation processes hence moisture availability, one would expect an apparent relation between steepness increase and deterioration of productivity and phenology indicators (e.g. Rigling et al., 2013). However, the presented variability not always followed this assumption, demonstreting very complex and often irregular temporal patterns of conterintuitive transition. The leading reason for this inconsistence could be very complex and elevation-independent allocation of slope classes. Consequently, one inclination strata comprises variety of climate-vegetation-soil horizontal belts, which hinders interpretation of potential differences among inclination classes.

Insufficient spatial representation limited analysis of forest type specific variability to coniferous and mixed stands recognized within the $3COVnNDVI_{8\text{-}18}$ class 1 footprint. Both forest types revealed adjacent temporal phenology and productivity evolution, with an exception in 2003. While coniferous woodland demonstrated that year earlier SBD combined with CF increase, mixed stands not only revealed a later vegetation onset and considerable CF decline, but also diminished GPP. Initial negative response to drought inception fostered by mixed woodland could emerged from the aformenetioned unexpected delay in SBD, as well as heatwave conditions that exceeded trees mitigation abilities and in the most extreme cases leaded to local diebacks of coniferous species (Minerbi *et al.*, 2006) wilting and earlier senescence. Furthermore, following horizontal distribution of vegetation belts, mixed forests are located at lower altitudes, which subjects them to more intense drought impact (Gebetsroither *et al.*, 2013; Gobiet *et al.*, 2014). Persistent stress conditions during the following years pressumably enforced drought adaptation strategies (e.g. increase in root biomass (Brunner *et al.*, 2015)) leading to expected rise of vitality and productivity. As stated before, higher CF reported for coniferous stands comparing to mixed stands can be a result of forest openings, as well as extended larch presence.

Notably, the greatest disparities between factors levels were mostly recognized between 2002 and 2007, as well as in 2011, that is under drought stress conditions. This observation implies differences in forest response to aridity governed by local biotic

(forest structure, density, competition (Scherrer *et al.*, 2011)) and abiotic (slope, exposition, soil (Pasho *et al.*, 2011; Rigling *et al.*, 2013)) qualities.

4.5.4. General remarks to MODIS derived forest drought response

While comparing the $NDVI_{HS}$ and $NDII7_{HS}$ time series probed within footprints of three PCs identified as drought impact on forest (Figure 18, Figure 20 and Figure 22), three global negative anomalies were identified in 2003, 2007 and 2011. While the first one is clearly associated with the pan-European heat wave of 2003 (e.g. Granier et al., 2007; Rebetez et al., 2006; Reichstein et al., 2007) depicted also by the scPDSI (Figure 14), two others have more complex and local origins. The anomaly of 2007 was supported by the scPDSI analysis and arose from extraordinarily hot spring and summer. Noticeably, forest $NDVI_{HS}$ and $NDII7_{HS}$ responded more negatively to the hot spring of 2007 than to arid summer of 2006. The last anomaly of 2011 was not detected in the scPDSI time series, neither was distinct in the PCA scores, but considerably affected $NDVI_{HS}$ and $NDII7_{HS}$ envelopes. It originated from a local phenomena observed at the beginning of September 2011 (Hydrographic Office of the Autonomous Province of Bolzano-Südtirol, 2011). While the first half of the month was exceptionally hot, with mean temperatures even two or more degrees above the long-term means, the end of the month brought massive precipitation events, which for some locations exceeded twofold or more normal rainfall amounts. Although averaged temperature and precipitation sums balanced well in the monthly scPDSI, earlier senescence triggered by this short heatwave was clearly detectible in the remote-sensed data. Beside this exception, year 2011 was considered as favorable even with increased GPP productivity.

Based on presented results, very hot summer of 2010, which was recognized in eastern and north Europe as the extreme heat-wave (Barriopedro *et al.*, 2011; EEA, 2012; Ivits *et al.*, 2014), had limited impact in South Tyrol. Although its potential imprint was visible in the $3COVnNDVI_{8\text{-}18}$, $3COVnNDVI_{SG8\text{-}18}$ and $3COVnNDVI_{8\text{-}18}ROT5P$ PCs (Figure 16 B, C, and K respectively) and leaded to leafs discoloration and local wilting (Minerbi, personal communication), potentially related scPDSI anomaly was visible only in the 3scPDSI score. Particularly interesting is also a fact that spring weather conditions reported for the province in 2010 were favorable and could not explain delayed SBD. A potential interpretation of this phenomenon could be linked with the 2010 eruptions of Eyjafjallajökull in Island, which beginning from 14th April started to produce an ash cloud that severely contaminated the atmosphere over Europe (Pappalardo *et al.*, 2013). Increased aerosol optical thickness not only limited sun energy reaching the ground and being available for vegetation, but also biased remote sensing observations, possibly further depleting NDVI envelope and leading to corrupted phenological measures.

In contrast to the scPDSI analysis, regional perception of all three identified drought vegetation responses recognized the Vinschgau Valley as the area of forest status decline. This observation highlights relativity of weather conditions, local environment capacity as well as tree species specific drought adaptation strategies.

Despite recognized meteorological aridity, $NDII_{HS}$ showed increasing trends within regions associated with drought related temporal variability, as well as within the opposite responses. This striking observation could not be explicitly justified based on

available datasets and information. Beside actual rise in the plant water content, shown variability could had been potentially introduced during the sensor degradation adjustment (Wang *et al.*, 2012). However since the $NDVI_{HS}$ time series showed no suspicious changeability, the latter is unlikely.

Although some identified phenological tendencies support climate change projections and emerging vegetation transformation trends (Theurillat & Guisan, 2001), the presented results are in itself no solid evidence of local climate alternation and following vegetation response. Demonstrated forest phenological variability is in line with local and continental trends (e.g. Zimmermann *et al.*, 2013b) and observations. However, due to a short observation period, as well as extraordinary meteorological conditions present during this time, shown results could be biased. Furthermore, phenological analyses focus on a very small portion of South Tyrol (topmost canopy), leaving tendencies within the bigger part of the South Tyrolean forest unrevealed. Confirmed uneven perception of climate alternation in the province and complexity of the local environment, exclude a possibility of region-wide generalization of presented results and call upon further investigation.

4.5.5. Approach limitations

Performed analyses provided complex information on alpine forest status and phenology in relation to meteorological variability of prolonged drought conditions. During the investigation several aspects emerged.

Firstly, structure of the forest in South Tyrol is very complex in terms of species allocation and stands distribution. Both are addressed by the forest mask. According to the GEOLAND standards (geoland2, 2012), a pure coniferous or broadleaved stand is identified when a dominant tree type occupies minimum 75% of the area. In other words, some stands identified as coniferous can have a considerable share of hardwood trees (and the other way round) that affect the spectral response. Moreover, while intensive and extensive management practices result in sharp, but jagged lower forest boundary, the upper forest fringe is usually a transition zone of drafted trees, shrubs and grass. Furthermore, due to local conditions, such as inter- and intra-species competition, coniferous forest is thinning out making room for broadleaved trees and bushes of an understory. Finally, Larch, a typical alpine coniferous species shows a broadleaved-alike phenological response. All aforementioned could influence the coniferous forest response, making it more alike to mixed and broadleaved communities. Even if this issue can be addressed in high resolution studies, resolution decrease leads obviously to generalization and loss of accuracy. Therefore, applied in this study forest mask upscaling from 20 m to 250 m resolution implies very low chances for spectrally pure pixels. Moreover, the moderate majority threshold used in the rescaling could incorporate fraction of non-forest regions into the forest mask. Although, a more restricted criterion would result in 'clearer' response, it would also limit greatly the forest area, hence desired dynamism of the environment could not be demonstrated properly.

Secondly, due to the MODIS pixel size, as well as crown opening and locally diminished density of investigated forest stands, top-most canopy response of reduced greenness and water content can be potentially compensate by understory, undergrowth or even bedrock signal (for the steepest locations). This can be

particularly true when the lower forest levels are overshadowed, and populated by species with higher water stress tolerance.

Subsequently, lack of site-specific surveys on tree species response to drought stress limited interpretation of the obtained PCA scores only to approximated weather variability. Trees response to stress condition is however much more complex than that, and not only depends on species physiology and plasticity but also on local distribution (Lévesque *et al.*, 2014) and environmental conditions (e.g. Pichler & Oberhuber, 2007; Pasho *et al.*, 2011; Rigling *et al.*, 2013; Etzold *et al.*, 2014). The aforementioned combined with diverse intensity of aridity, can introduce a certain lag to forest response (Bigler *et al.*, 2006; Pichler & Oberhuber, 2007; Castagneri *et al.*, 2014; Etzold *et al.*, 2014). Unfortunately, shortage of ancillary dendrological data and a mismatch between temporal resolution of the scPDSI and MODIS time series, restricted feasible analyses to a direct interaction of meteorological conditions on forest phenology neglecting an impact of meteorological conditions in the preceding year(s)/season(s). Furthermore, deficiency of reference information hampered 'backward' interpretation where variability in obtained PC and its footprint could be explained and evaluated according to local woodland condition.

Moreover, although the scPDSI is well correlated with forest status (e.g. Büntgen *et al.*, 2010; Scharnweber *et al.*, 2011; Gillner *et al.*, 2013), coupling of temperature and precipitation variability obscures identification of more specific, interannual trees variability (Coppola *et al.*, 2012; Castagneri *et al.*, 2014; Lévesque *et al.*, 2014). However, since the study analyzes more general, reional forest response to drought conditions, merging of both measurements is not particularly hindering.

Next, considering lay of the land, SBD, thus also CF and SL measures can be inaccurate for the highest elevations due to snow cover (Jönsson *et al.*, 2010). Although a snowmelt is expected to be in line with the end of the dormancy state and onset of phenological activity, snow occurrence importantly decreases wintertime NDVI, resulting in falsely high signal increase in spring (Studer *et al.*, 2007), which predictably leads to elevated annual productivity measures. Because due to a lack of ground truth data used phenological indices were anyway treated as a between-years change trackers rather than absolute indicators of productivity, as well as related snow cover issue was observed only for relatively limited number of pixels, presented analyses are not significantly hampered by this issue.

Furthermore, many factors shape forest phenology and plant vitality, potentially contributing to the PCA identified variability. However, the most probable damage causes that could result in drought-alike response, such as pest infestations or fungal attacks, are considered a secondary damage agents, attacking drought weakened trees (Rigling *et al.*, 2013). Secondly, such attacks have in South Tyrol always a local character, thus could not impact significantly the presented results. Performed crosscheck with available large-scale calamites reports revealed no overlay with investigated strata, confirming hence exclusive drought variability impact on the PCA results.

Finally, MODIS data not only have their embedded limitations, but also are influenced by inaccuracies originating from data preprocessing. Although the composition process of the MOD13Q1 product mitigates, among others, an impact of the sensor viewing

geometry, sun position or atmospheric optical depths (Solano *et al.*, 2010), these processing steps are characterized by certain level of inaccuracy (Vermote & Vermeulen, 1999; Mao *et al.*, 2015). Moreover, the sensor calibration also has its limitations (Vermote & Vermeulen, 1999). Even though the impact of those uncertainties is limited, and was partly further suppressed through the implemented QA screening and outliers interpolation, its presence should be kept in mind. An additional flaw of MODIS acquisitions emerges from their geometric accuracy (Wolfe *et al.*, 2002) and resolution disparity among bands. The latter is concerning for the NDII7 time series. Although consecutive MODIS collections improve geolocation accuracy, this issue should not be neglected, especially in mountain regions. Finally, an additional source of possible errors was recognized in the data reprojection, which, despite being a geometric convolution, could enhanced and propagate geolocation inaccuracy of the data. However, since the study was based on multiple data sources, reprojection of data was inevitable.

Despite potential limitations, presented results demonstrate high capacity of the S-mode PCA for identification of subtle drought related vegetation variability in MODIS derived NDVI and NDII7 time series. Selected principal components addressed diverse aspects of forest feedback, while extensive phenology and productivity based investigation allowed to identify scientifically supported explanation of those responses. Captured variability revealed to be site-specific, as well as reflected broader climate change induced changes. The study provided comprehensive and exhaustive information on South Tyrolean forest condition between 2001 and 2012, simultaneously highlighting still existing information shortage and necessity for extensive and multidisciplinary environmental monitoring.

5. FOREST DROUGHT INVESTIGATION USING LANDSAT TIME SERIES

5.1. Design of the study

2001-2011 time series of yearly Landsat NDVI and NBRI composites, hereafter called $_{L}$NDVI and $_{L}$NBRI respectively, were the secondary datasets used for investigation of drought impact on forest in South Tyrol. Despite limited spatial coverage and no information on intra-annual vegetation status variability, Landsat data ensure robust forest condition information at the 30 meters resolution. Increased spatial resolution comparing with the MODIS datasets is the most important asset of Landsat images.

Alike for the MODIS analyses (Chapter 4), also the Landsat time series were processed using the S-mode PCA decomposition (method description in section 2.3). Since each of the $_{L}$NDVI and $_{L}$NBRI time series comprised 11 composed scenes (one image per year), no seasonality component was present in the data. Consequently, a-priori normalization was not needed and the S-mode PCA decomposition was based on the correlation-matrix (Eastman & Fulk, 1993), which standardized time series. Evaluation and further processing of results was carried out alike in the case of MODIS time series, where resulting PCs were compared to the scPDSI derived weather dynamism averaged to yearly values. Subsequently, the most promising and potentially the most drought related temporal variabilities were correlated against the appropriate original $_{L}$NDVI or $_{L}$NBRI time series. Each resulting spatial representation was further classified into six response classes using 5^{th}, 30^{th}, 50^{th}, 70^{th} and 95^{th} percentiles of the correlation values distribution. Pixels allocated within class 1 (minimum to 5^{th} percentile; representing regions with the most negative response to a given phase of the selected score), and class 6 (95^{th} percentile to maximum; indicating the most positive Pearson's correlation values) were next investigated in relation to their location and natural environment.

Subsequently, spatial representations of identified Landsat-based PCs showing potential impact of drought conditions were converted to the resolution of 250 m. The adaptation was done separately for each Landsat-derived drought impact footprint using the MODIS Point Spread Function (PSF) model (Huang *et al.*, 2002). This step allowed not only on a straightforward comparison between MODIS and Landsat drought impact footprints, but also enabled further investigation of Landsat-based drought footprints, which was assured by MODIS derived phenology and productivity indices (section 2.2.2.2). All mModeled 250 m projections of Landsat drought representations were classified using 5^{th}, 30^{th}, 50^{th}, 70^{th} and 95^{th} percentiles. Also here, special attention was given to classes 1 (minimum-5^{th} percentile) and 6 (95^{th} percentile-maximum). Phenology temporal variability was investigated within both strata using repeated ANOVA performed for factors of:

- forest type mask (coniferous, mixed, broadleaved);
- elevation (0-700 m asl, 700-1400 m asl, 1400-2100 m asl, 2100-2500 m asl; elevation stratification after Theurillat and Guisan, (2001));
- exposition (N, E, S, W);
- inclination (0°-10°, 10°-20°, 20°-30°, 30°-40°, 40°-90°).

5.2. Forest conditions indicated by PCA of $_{L}$NDVI and $_{L}$NBRI time series

5.2.1. $_{L}$NDVI time series [16]

The correlation-matrix based S-mode PCA of the $_{L}$NDVI time series produced PCs with suppressed dominance of scores of the lowest order (Table A7 1). The first PC (1COR$_{L}$NDVI) explained 16.43% of the total variance present in the dataset (Table A7 1), and demonstrated intense $_{L}$NDVI decrease in 2003 and 2004, which was followed by a steady increase culminated in 2008 (Figure A7 1). This response alluded to the 1scPDSI (Table 36), showing however shorter drought impact and emphasizing greenness recovery. An increase in vegetation status was also revealed in the second PC (2COR$_{L}$NDVI), which presented a steady increase that peaked in 2008 (Figure A7 1). This score accounted on 14.81% of the data variability and clearly contrasted with the identified regional weather patterns (Table 36).

Scores of the higher order demonstrated dynamic responses, but with limited accordance with the scPDSI meteorological variability. They explained 12.85% and 10.74% of the data variance for the third and fourth PC respectively. Any connection to the 2scPDSI was neglected due to non-drought related character of this score.

Table 36 Correlation among the scPDSI scores and first four PC obtained for the S-mode correlation-matrix based PCA of the $_{L}$NDVI 2001-2011 time series (in columns). Comparison was done for yearly averages.

	COR$_{L}$NDVI			
	1PC	2PC	3PC	4PC
1scPDSI	0.643, p=0.033	-0.211, p=0.532	-0.052, p=0.879	0.575, p=0.064
2scPDSI	-0.146, p=0.667	-0.910, p<0.000	0.183, p=0.590	-0.040, p=0.916
3scPDSI	0.421, p=0.197	-0.447, p=0.168	-0.050, p=0.883	0.618, p=0.043
4scPDSI	-0.075, p=0.827	-0.832, p=0.001	0.282, p=0.400	-0.362, p=0.274

5.2.2. $_{L}$NBRI time series [17]

The $_{L}$NBRI time series subjected to the correlation-matrix based S-mode PCA revealed in the first and second PC (1COR$_{L}$NBRI and 2COR$_{L}$NBRI respectively) temporal variability of potentially high weather related origins (Figure A7 2). While the former score highlighted gradual decrease being in strong accordance with the 4scPDSI (Table 37), the latter depicted depleted $_{L}$NBRI values between 2003 and 2007 that were in line with the 1scPDSI (Table 37). They explained 14.8% and 13.55% of the total data variance respectively (Table A7 2).

The third PC explained 11.45% of the data variability and revealed a response highlighting the 2008 anomaly. Although potentially interesting, this pattern had no significant support in any of the scPDSI scores (Table 37). The fourth principal component, which still accounted on more than 10% of data variance (Figure A7 2), revealed two strong anomalies in 2004 and 2008 and demonstrated no potentially weather related feedback (Figure A7 2).

[16] Complementary information in the Appendix 7, section A.7.1
[17] Complementary information in the Appendix 7, section A.7.2

Table 37 Correlation among the scPDSI scores and first four PC obtained for the S-mode correlation-matrix based PCA of the $_{L}$NBRI 2001-2011 time series (in columns). Comparison was done for yearly averages.

	COR$_{L}$NBRI			
	1PC	2PC	3PC	4PC
1scPDSI	0.121, p=0.722	0.839, p=0.001	0.305, p=0.361	0.136, p=0.690
2scPDSI	0.934, p<0.001	0.198, p=0.559	-0.02, p=0.952	0.132, p=0.698
3scPDSI	0.315, p=0.345	0.666, p=0.025	0.386, p=0.241	0.270, p=0.422
4scPDSI	0.929, p<0.001	-0.136, p=0.689	-0.243, p=0.471	0.022, p=0.948

5.3. Assessment of drought impact on forest

Preliminary inspection of the S-mode PCA results for the $_{L}$NDVI and $_{L}$NBRI time series indicated in total four scores being well related to scPDSI principal components and depicting drought variability in the region. The 1COR$_{L}$NDVI pattern (Figure 23A) demonstrated diminished NDVI in 2003-2004 which was consist with the onset of the 2003/4–2007 dry spell. Moreover, the score highlighted two positive anomalies in 2001-2002, and in 2008. The 2COR$_{L}$NDVI presented an overall increasing tendency with a positive peak in 2008 (Figure 23B). Although this variability was in opposition to the 4scPDSI (Table 36) it strongly resembled the 3COVnNDVI$_{8\text{-}18}$ MODIS based score. Alike the 2COR$_{L}$NDVI also the 1COR$_{L}$NBRI PC followed a monotonic increasing/decreasing trend (Figure 23C). Also in this case the increasing tendency was promoted based comparison to MODIS results. The 2COR$_{L}$NBRI score strictly adopt the 1scPDSI temporal profile (Table 37), rendering soundly not only diminished plant water content between 2003 and 2007, but also a moisture peak in 2008.

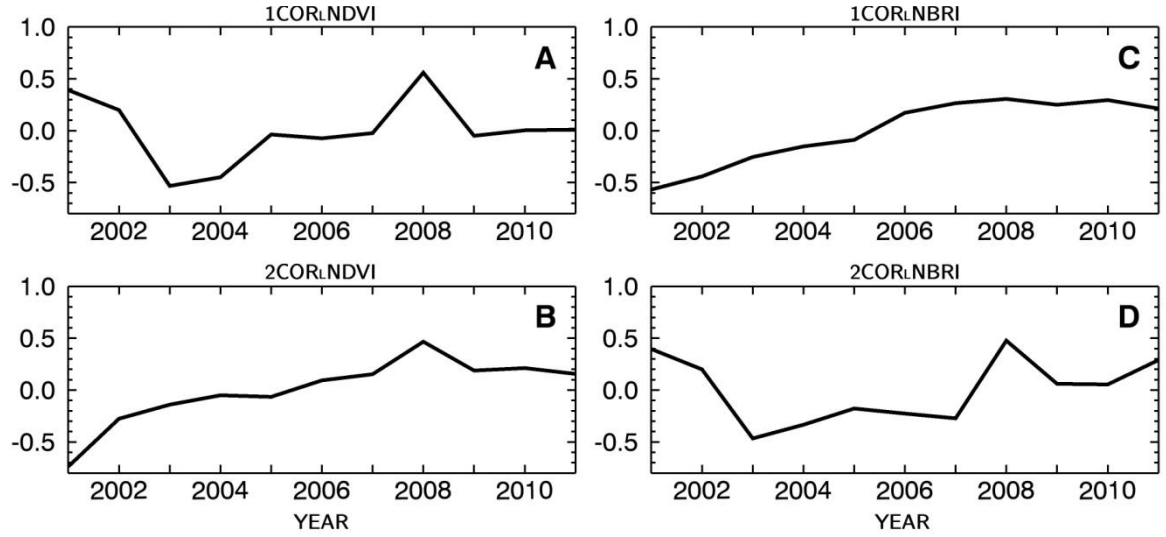

Figure 23 PCs that revealed potential physical meaning of forest drought impact: A: 1COR$_{L}$NDVI (the 1PC from the correlation-matrix based S-mode PCA of $_{L}$NDVI time series), B: 2COR$_{L}$NDVI (the 2PC from the correlation-matrix based S-mode PCA on $_{L}$NDVI time series), C: 1COR$_{L}$NBRI (the 1PC from the correlation-matrix based S-mode PCA on $_{L}$NBRI time series), and D: 2COR$_{L}$NBRI (the 2PC from the correlation-matrix based PCA on $_{L}$NBRI time series).

Each of the identified scores was next projected by the means of pixel-based correlation against its original, PCA-introduced time series (Appendix 8). Emerging patterns were classified using percentiles of the correlation values into six response classes (Table 38).

Table 38 Percentiles of correlation values for all four spatial projection of $1COR_LNDVI$, $2COR_LNDVI$, $1COR_LNBRI$ and $2COR_LNBRI$ PCs considered as temporal responses of potential drought forest impact. Indicated threshold became limits of drought impact classes.

percentiles	impact class	synthetic MODIS-like spatial patterns			
		$1COR_LNDVI$	$2COR_LNDVI$	$1COR_LNBRI$	$2COR_LNBRI$
min	class 1	-0.975	-0.975	-0.976	-0.979
5th	class 2	-0.555	-0.566	-0.597	-0.547
30th	class 3	-0.138	-0.178	-0.177	-0.172
50th	class 4	0.109	0.047	-0.051	0.047
70th	class 5	0.349	0.278	0.275	0.269
95th	class 6	0.718	0.683	0.653	0.640
max		0.985	0.988	0.992	0.985

Obtained representations (Appendix 8) showed spatial footprints of identified vegetation stress conditions. Diversity in temporal profiles of scores governed disparity among footprints. Further inspection of pixels allocation within forest type, exposition, elevation and slope classes, was done only for response classes 1 and 6. It allowed to shed some more light on potential drought impact hotspots and their opposites (Table 39; further examination and description in the following sections).

Table 39 Pixel distribution within factors levels inspected for the $1COR_LNDVI$, COR_LNDVI, $1COR_LNBRI$ and $2COR_LNBRI$ PCs spatial representations. Class 6 denotes regions with the strongest, whereas class 1 the weakest fit to the scores in Figure 23.

	$1COR_LNDVI$		**$2COR_LNDVI$**		**$1COR_LNBRI$**		**$2COR_LNBRI$**	
[%]	**1**	**6**	**1**	**6**	**1**	**6**	**1**	**6**
Total (pixels)	72746	72746	72746	72746	72746	72746	72746	72746
Coniferous	96.74	48.15	89.04	74.87	80.97	88.92	91.54	67.22
Broadleaved	2.17	27.71	6.72	14.51	11.55	6.14	5.15	18.80
Mixed	1.09	24.15	4.25	10.62	7.48	4.94	3.31	13.98
N	24.31	25.89	25.27	28.08	28.44	21.28	31.06	18.98
E	22.53	20.04	21.86	21.47	21.86	26.45	20.72	23.01
S	31.23	18.80	28.85	22.23	24.12	32.32	22.36	26.79
W	21.92	35.28	24.02	28.21	25.58	19.95	25.87	31.22
0-700 m asl	0.97	33.61	3.07	16.65	5.61	7.14	1.71	23.07
700-1400 m asl	23.05	54.60	35.67	47.25	36.80	52.63	27.03	56.08
1400-2100 m asl	72.92	11.71	59.52	35.74	55.30	39.96	68.20	20.57
2100-2500m asl	3.05	0.08	1.74	0.37	2.29	0.27	3.05	0.28
0-10 deg.	8.80	3.62	9.34	7.21	9.29	5.89	9.26	4.71
10-20 deg.	22.13	10.12	24.06	15.89	22.86	14.22	21.42	12.67
20-30 deg.	35.95	23.36	33.62	28.28	33.53	29.88	34.67	28.06
30-40 deg	28.42	39.15	26.42	37.15	26.99	40.30	28.99	36.39
40-90 deg.	4.70	23.75	6.56	11.48	7.33	9.71	5.66	18.18

5.3.1. 1COR$_L$NDVI spatial pattern

The 1COR$_L$NDVI PC (Figure 23A) response class 6 marked the central part of South Tyrol, namely in the Eisack and Etschtal Valleys and their smaller joining valleys (Figure 24). These locations were in half devoted to coniferous forest with another half almost evenly divided between broadleaved and mixed stands. They were placed mainly on medium (700-1400 m asl) and low (0-700 m asl) altitudes (Table 39), where the latter was overrepresented comparing with the overall forest allocation pattern. The aspect distribution promoted west exposed locations, while inclination showed preferences for the higher inclination strata.

The drought impact class 1 highlighted almost exclusively coniferous forest stands in the Vinschgau, Wipp and Puster valleys (Figure 24). Considered woodland grew at higher and medium elevation of intermediate inclination (20-40 degrees; Table 39), which rather well renders orography of the region. Allocation within aspect classes revealed preference for the south exposed locations.

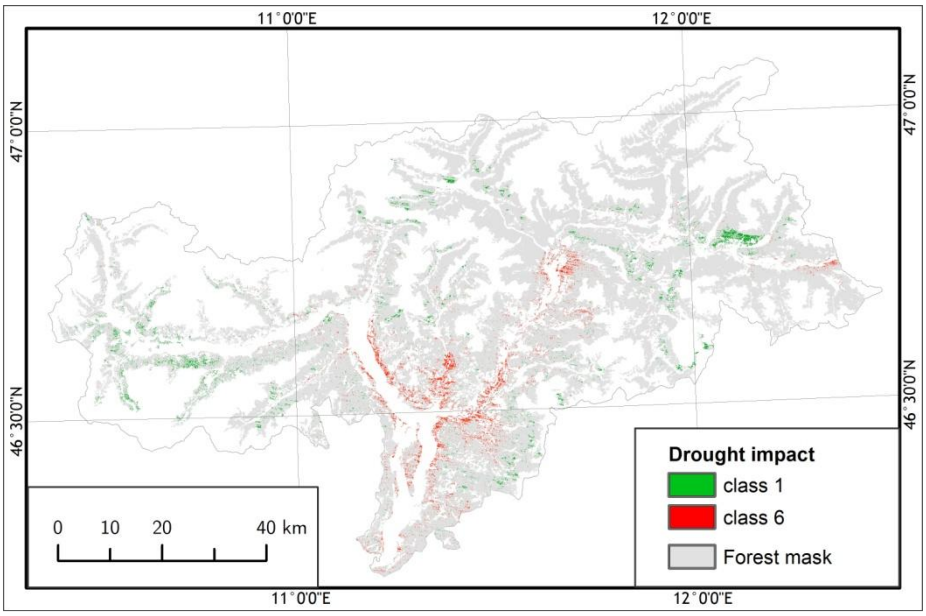

Figure 24 Spatial representation of the 1COR$_L$NDVI PC limited to response class 1 (green) and 6 (red). The forest mask is marked in gray.

5.3.2. 2COR$_L$NDVI spatial pattern

The 2COR$_L$NDVI score (Figure 23B) suggested an overall 'greenness' increase. Spatial allocation of this response, associated with class 6, indicated north Etschtal Vallye, south-west part of the Eisack Valley as well as Puster Valley (Figure 25). Forest structure accounted there on three-fourths of needle leaved dominated stands, and a quarter of broadleaved and mixed forests (Table 39). Almost half of class 6 was placed between 700 and 1400 m asl. Among the aspect classes west and north exposed slopes were in majority. Inclination demonstrated preferences for medium and high steepness.

The 2COR$_L$NDVI response class 1, which implied gradual decrease of $_L$NDVI was unevenly distributed throughout South Tyrol with the most prominent hotspots in the central part of the region, as well as the Vischgau Valley (Figure 25). Considered woodland grew mainly between 700 and 2100 m asl with 59.52% of the stands placed

between 1400 and 2100 m asl. This response was the most often for slopes of intermediate inclination (20-40 degrees, Table 39), which well fostered orography of the region. Allocation within aspect classes revealed minor preference for the south exposed locations.

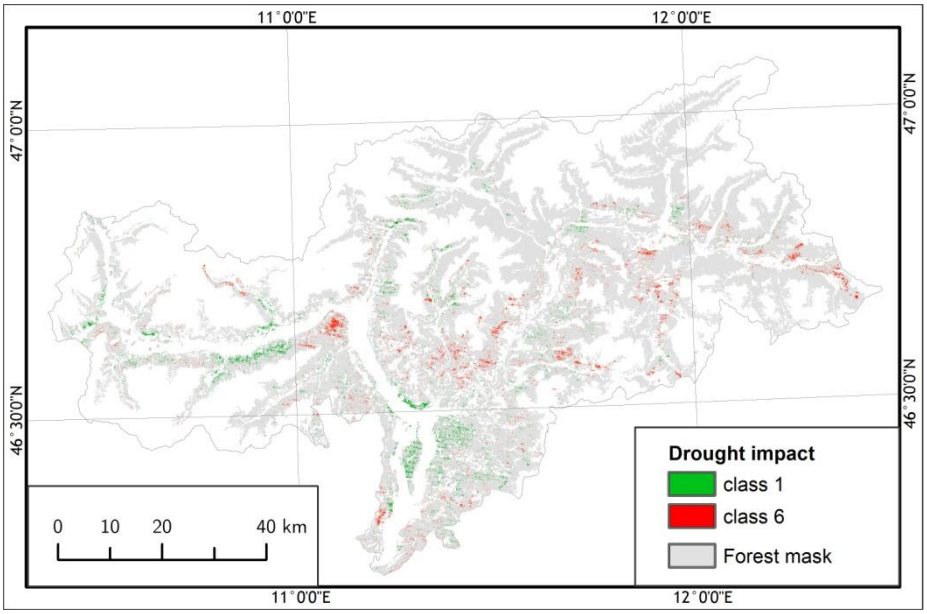

Figure 25 Spatial representation of the 2COR$_L$NDVI PC limited to response class 1 (green) and 6 (red). The forest mask is marked in gray.

5.3.3. 1COR$_L$NBRI spatial pattern

A gradual vegetation water content increase depicted by the 1COR$_L$NBRI PC and associated with class 6, highlighted disperse stands located mainly in the central part of South Tyrol and along the Vinschgau and the Puster Valleys (Figure 26). It accounted mostly on coniferous trees, with an above average share of broadleaved forest (Table 39). Recognized stands occurred most frequently at moderate and high elevations (700-1400 and 1400-2100 m asl respectively), and on the south and east exposed slopes. No inclination preferences were spotted as pattern allocation followed the general lay of the land.

The antagonistic response mapped as the 1COR$_L$NBRI class 1 indicated mainly forest in the Vinschgau Valley, as well as some isolated locations in the Puster Valley and southern part of the Eisack Valley (Figure 26). Stand structure revealed a dominance of needle-leaved stands, but with considerable addition of broadleaved and mixed woodland (Table 39). Neither aspect, nor inclination preferences were identified. On the contrary, elevation revealed very strong dominance of zones placed between 700 and 2100 m asl.

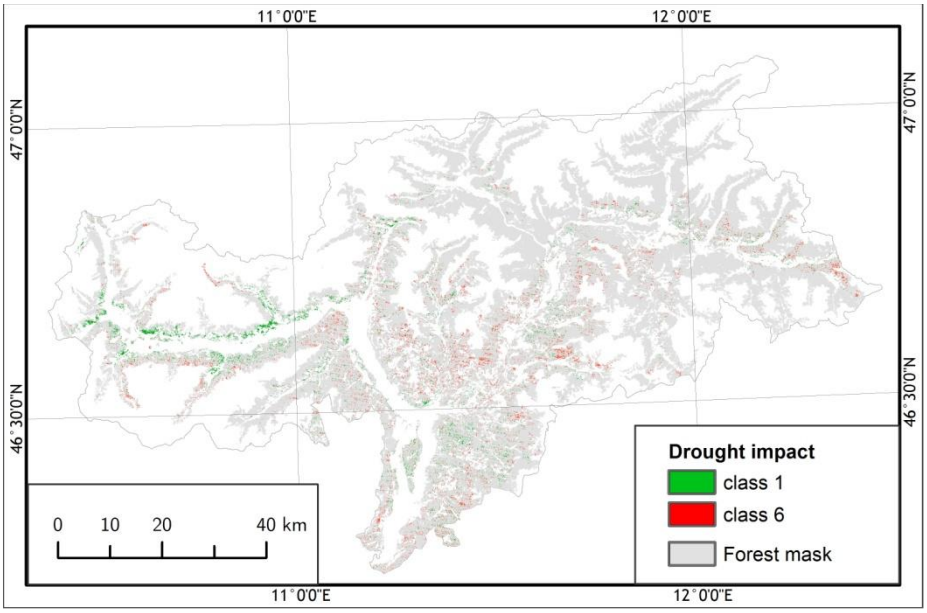

Figure 26 Spatial representation of the 1COR$_L$NBRI PC limited to response class 1 (green) and 6 (red). The forest mask is marked in gray.

5.3.4. 2COR$_L$NBRI spatial pattern

The 2COR$_L$NBRI principal component, which depicted diminished plant water content between 2003 and 2007 (Figure 23D), had the strongest response in the medium elevated regions (Table 39) of the Eisack and Etschtal Valleys (Figure 27). The pattern was especially firm for west and south exposed slopes and accounted on an above-average share of broadleaved and mixed stands. Inclination within the response class 6 revealed a tendency towards steeper locations.

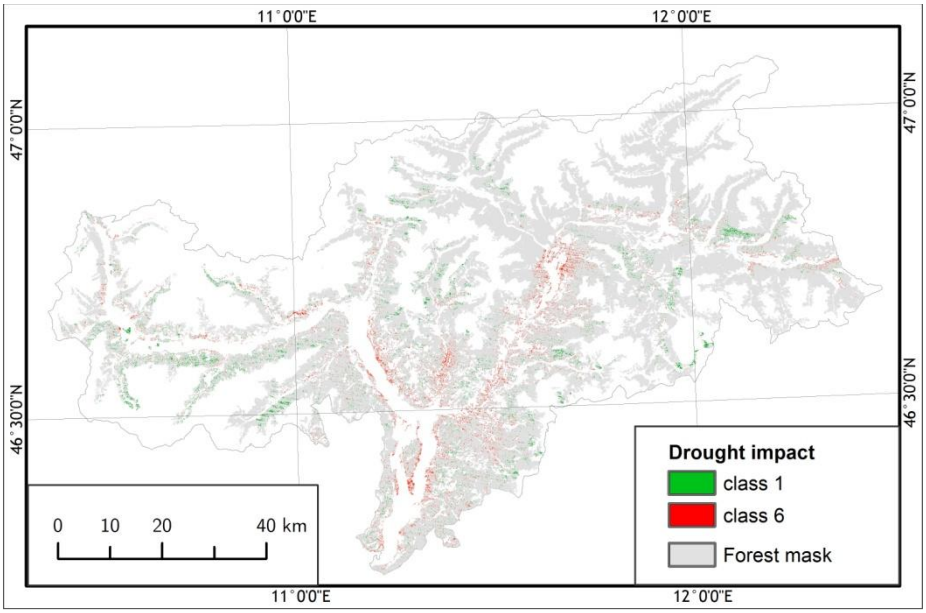

Figure 27 Spatial representation of the 2COR$_L$NBRI PC limited to response class 1 (green) and 6 (red). The forest mask is marked in gray.

The 2COR$_L$NBRI PC response class 1 highlighted multiple regions located mainly in the Vinschgau and Puster Valleys, as well as smaller hotspots in the Wipp Valley and in the higher elevated parts of the Eisack Valley (Figure 27). Considered areas were devoted mostly to the coniferous stands and covered high and medium elevation zones (1400-2100 m and 700-1400 m asl respectively). North exposed locations of low to medium inclination were the most characteristic for this response.

5.4. Modeling synthetic MODIS-like data on Landsat derived spatial representations

In order to compare Landsat results with MODIS derived footprints of drought impact as well as, further investigate Landsat-identified drought related variability using the time series of phenology and productivity indices, all obtained spatial patterns were converted from 30 to 250 m resolution.

Considerable similarities in technical setups of Landsat 5, Landsat 7 and Terra platforms (Table 4 and Table 10) as well as, TM, ETM+ and MODIS spectral bands design that facilitates inter-sensor comparison (Price, 2003) were a great asset in the process. Although several Landsat-MODIS synergy applications assume perfect rendering of ground reflectance from a pixel footprint where a bigger pixel is calculated through aggregation of corresponding small pixels within its footprint and further linear regression to model an exact value (Feng *et al.*, 2012; e.g. STARFM by Gao *et al.*, (2006) or ESTARFM from Zhu *et al.*, (2010)), this straightforward assumption is too idealistic and neglects wide spectrum of MODIS viewing angles (Boccardo *et al.*, 2006) and sensor's point spread function (PSF; Huang *et al.*, 2002) as well as, additional atmosphere effect. The difference between results obtained with a simple spatial average filter and PSF convolution are particularly apparent for heterogeneous areas and regions with complex morphology (Feng *et al.*, 2012).

Implemented simulation of MODIS data from Landsat derived information was therefore based on proposed by Huang *et al.*, (2002) MODIS PSF model working under an additional assumption of negligible TM and ETM+ PSF deviation (Tan *et al.*, 2006). The MODIS PSF was firstly modeled for 30x30 m resolution grid (Figure 28) and subsequently represented as a 23x23 pixels kernel of a moving-window filter (Figure 29). Notably, the 7x7 core part of the kernel roughly corresponded to the central MODIS pixel of a footprint, accounted on 60% of response.

Knowing the MODIS pixel grid in South Tyrol, a geometric center of each pixel was calculated and overlaid with the Landsat datasets in order to identify corresponding middle-point pixels. Those pixels were subsequently used to center the MODIS PSF kernel, and determined values of synthetic MODIS-like Landsat-derived pixels. Importantly, calculation was enabled only when at least 50% of the kernel cells had non-zero values as well as, the kernel's core was represented by minimum 39 pixels (80% out of 49 cells). Otherwise, when the kernel was dominated by no-data, or the core was underrepresented, synthetic MODIS-like pixel was assigned a '0' value. These conditions were particularly important when working with Landsat dataset which not only enclosed heterogeneous coverage and jagged forest borderlines, but also was characterized by data gaps. The adopted approach increased credibility and accuracy of final aggregation results.

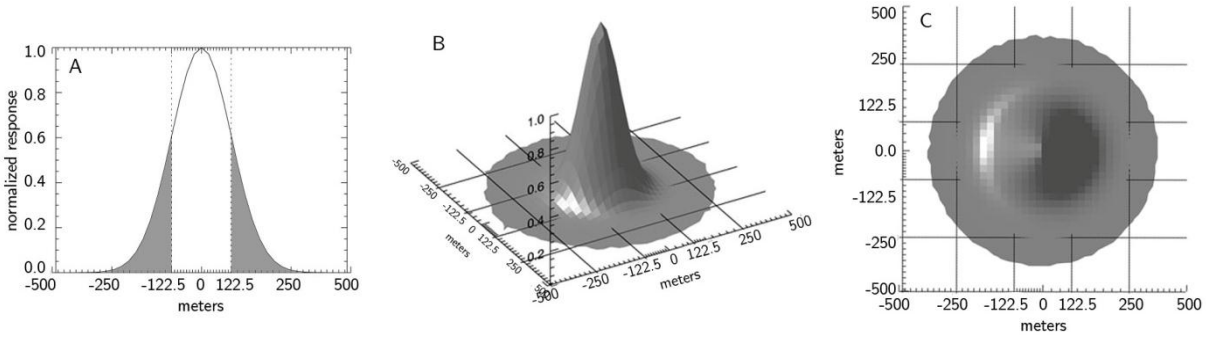

Figure 28 MODIS PSF modeled for 30 m resolution Landsat based grid: A: an actual MODIS PSF. In gray response from the adjacent area outside the 250x250 m MODIS pixel; B: a top-side view of the MODIS PSF simulated for 30m resolution pixels with respect to 250x250 m greed; C: a top view of the MODIS PSF simulated for 30m resolution pixels with respect to 250x250 greed.

0.000	0.000	0.000	0.000	0.000	0.000	0.000	0.000	0.000	0.001	0.001	0.001	0.001	0.001	0.000	0.000	0.000	0.000	0.000	0.000	0.000	0.000	0.000
0.000	0.000	0.000	0.000	0.000	0.000	0.001	0.001	0.001	0.002	0.002	0.002	0.002	0.002	0.001	0.001	0.001	0.000	0.000	0.000	0.000	0.000	0.000
0.000	0.000	0.000	0.000	0.000	0.001	0.002	0.003	0.004	0.006	0.007	0.008	0.007	0.006	0.004	0.003	0.002	0.001	0.000	0.000	0.000	0.000	0.000
0.000	0.000	0.000	0.000	0.001	0.002	0.005	0.008	0.012	0.017	0.020	0.021	0.020	0.017	0.012	0.008	0.005	0.002	0.001	0.000	0.000	0.000	0.000
0.000	0.000	0.000	0.001	0.003	0.006	0.012	0.020	0.031	0.041	0.050	0.053	0.050	0.041	0.031	0.020	0.012	0.006	0.003	0.001	0.000	0.000	0.000
0.000	0.000	0.001	0.002	0.006	0.013	0.026	0.044	0.067	0.090	0.108	0.115	0.108	0.090	0.067	0.044	0.026	0.013	0.006	0.002	0.001	0.000	0.000
0.000	0.001	0.002	0.005	0.012	0.026	0.050	0.085	0.130	0.175	0.210	0.223	0.210	0.175	0.130	0.085	0.050	0.026	0.012	0.005	0.002	0.001	0.000
0.000	0.001	0.003	0.008	0.020	0.044	0.085	0.146	0.223	0.301	0.360	0.382	0.360	0.301	0.223	0.146	0.085	0.044	0.020	0.008	0.003	0.001	0.000
0.000	0.001	0.004	0.012	0.031	0.067	0.130	0.223	0.339	0.458	0.548	0.582	0.548	0.458	0.339	0.223	0.130	0.067	0.031	0.012	0.004	0.001	0.000
0.001	0.002	0.006	0.017	0.041	0.090	0.175	0.301	0.458	0.618	0.741	0.786	0.741	0.618	0.458	0.301	0.175	0.090	0.041	0.017	0.006	0.002	0.001
0.001	0.002	0.007	0.020	0.050	0.108	0.210	0.360	0.548	0.741	0.887	0.942	0.887	0.741	0.548	0.360	0.210	0.108	0.050	0.020	0.007	0.002	0.001
0.001	0.002	0.008	0.021	0.053	0.115	0.223	0.382	0.582	0.786	0.942	1.000	0.942	0.786	0.582	0.382	0.223	0.115	0.053	0.021	0.008	0.002	0.001
0.001	0.002	0.007	0.020	0.050	0.108	0.210	0.360	0.548	0.741	0.887	0.942	0.887	0.741	0.548	0.360	0.210	0.108	0.050	0.020	0.007	0.002	0.001
0.001	0.002	0.006	0.017	0.041	0.090	0.175	0.301	0.458	0.618	0.741	0.786	0.741	0.618	0.458	0.301	0.175	0.090	0.041	0.017	0.006	0.002	0.001
0.000	0.001	0.004	0.012	0.031	0.067	0.130	0.223	0.339	0.458	0.548	0.582	0.548	0.458	0.339	0.223	0.130	0.067	0.031	0.012	0.004	0.001	0.000
0.000	0.001	0.003	0.008	0.020	0.044	0.085	0.146	0.223	0.301	0.360	0.382	0.360	0.301	0.223	0.146	0.085	0.044	0.020	0.008	0.003	0.001	0.000
0.000	0.001	0.002	0.005	0.012	0.026	0.050	0.085	0.130	0.175	0.210	0.223	0.210	0.175	0.130	0.085	0.050	0.026	0.012	0.005	0.002	0.001	0.000
0.000	0.000	0.001	0.002	0.006	0.013	0.026	0.044	0.067	0.090	0.108	0.115	0.108	0.090	0.067	0.044	0.026	0.013	0.006	0.002	0.001	0.000	0.000
0.000	0.000	0.000	0.001	0.003	0.006	0.012	0.020	0.031	0.041	0.050	0.053	0.050	0.041	0.031	0.020	0.012	0.006	0.003	0.001	0.000	0.000	0.000
0.000	0.000	0.000	0.000	0.001	0.002	0.005	0.008	0.012	0.017	0.020	0.021	0.020	0.017	0.012	0.008	0.005	0.002	0.001	0.000	0.000	0.000	0.000
0.000	0.000	0.000	0.000	0.000	0.001	0.002	0.003	0.004	0.006	0.007	0.008	0.007	0.006	0.004	0.003	0.002	0.001	0.000	0.000	0.000	0.000	0.000
0.000	0.000	0.000	0.000	0.000	0.000	0.001	0.001	0.001	0.002	0.002	0.002	0.002	0.002	0.001	0.001	0.001	0.000	0.000	0.000	0.000	0.000	0.000
0.000	0.000	0.000	0.000	0.000	0.000	0.000	0.000	0.000	0.001	0.001	0.001	0.001	0.001	0.000	0.000	0.000	0.000	0.000	0.000	0.000	0.000	0.000

Figure 29 Spatial representation of the MODIS PSF simulated for 30m resolution pixels. Values round-off to the 3 digits precision. Each cell of the 23x23 kernel represents one 30x30m Landsat pixel and has a normalized response assigned with respect to the central pixel. Corresponding MODIS pixel grid is marked in yellow. The 'core' kernel of 7x7 Landsat pixels (210x210m; in red) accounts on 60% of the signal rendered in resulting MODIS pixel.

The model presented above was consecutively applied to Landsat derived unclassified spatial representations of four selected PCs. This approach allowed to inspect capacity of Landsat data to capture drought impact, rather than model MODIS scenes with Landsat acquisitions. The process resulted in new correlation footprints of 250 m resolution called herein: $1COR_{L250}NDVI$, $2COR_{L250}NDVI$, $1COR_{L250}NBRI$ and $2COR_{L250}NBRI$. Although emerging maps rendered almost exact space perception as the original impact projections (Appendix 8), convolution affected correlation distribution. Consequently, all four newly produced correlation maps were individually classified into response classes using the 5^{th}, 30^{th}, 50^{th}, 70^{th} and 95^{th} percentiles (Table 40; Appendix 9).

Table 40 Percentiles of correlation values for synthetic MODIS-like spatial representations of $1COR_LNDVI$, $2COR_LNDVI$, $1COR_LNBRI$ and $2COR_LNBRI$ PCs recognized as potential drought governed forest response. Indicated threshold values were being limits of impact classes.

percentiles	impact class	synthetic MODIS-like spatial patterns			
		$1COR_{L250}NDVI$	$2COR_{L250}NDVI$	$1COR_{L250}NBRI$	$2COR_{L250}NBRI$
min		-0.761	-0.786	-0.800	-0.700
5th	class 1	-0.388	-0.379	-0.293	-0.315
30th	class 2	-0.067	-0.107	-0.047	-0.076
50th	class 3	0.107	0.041	0.055	0.042
70th	class 4	0.277	0.201	0.154	0.162
95th	class 5	0.586	0.511	0.347	0.411
max	class 6	0.825	0.839	0.740	0.786

Change in resolution as well as, principles of the convolution leaded to some alternation in aspect, elevation, slope and forest type classes distribution comparing with the original Landsat patterns (Table 41).

Table 41 Pixel distribution within factors levels inspected for the $1COR_{L250}NDVI$, $2COR_{L250}NDVI$, $1COR_{L250}NBRI$ and $2COR_{L250}NBRI$ spatial representations. Class 6 denotes regions with the strongest, whereas class 1 the weakest fit to the scores in Figure 23

	$1COR_{L250}NDVI$		**$2COR_{L250}NDVI$**		**$1COR_{L250}NBRI$**		**$2COR_{L250}NBRI$**	
	1	**6**	**1(d)**	**6(in)**	**1 (d)**	**6 (in)**	**1**	**6**
Total (pixels)	1054	1054	1054	1054	1054	1054	1054	1054
Coniferous	98.76	43.99	72.89	93.27	86.02	91.58	97.44	52.18
Broadleaved	0.48*	19.68	9.48	1.71*	3.74*	1.49*	1.04*	15.56
Mixed	0.76*	36.33	17.63	5.02	10.25	6.93	1.52*	32.26
N	28.69	20.81	31.47	26.45	30.56	17.52	34.16	12.05
E	15.63	21.67	17.54	18.96	14.75	29.60	14.52	30.27
S	33.56	14.66	21.61	28.25	20.50	39.50	23.81	23.34
W	22.12	42.86	29.38	26.35	34.20	13.37	27.51	34.35
0-700 m asl	0.19*	46.74	23.51	1.42*	6.70	3.96*	0.09*	40.89
700-1400 m asl	13.44	50.05	41.90	29.48	28.35	50.10	11.76	54.17
1400-2100 m asl	84.56	3.22	34.50	68.15	60.54	45.35	85.10	4.93
2100-2500m asl	1.81*		0.09*	0.95*	4.41*	0.59*	3.04*	-
0-10 deg.	10.01	5.77	9.38	9.38	9.58	6.53	9.49	6.36
10-20 deg.	37.27	23.65	20.09	34.98	20.98	15.94	29.41	21.92
20-30 deg.	44.52	41.82	42.94	42.84	45.02	45.15	48.58	43.07
30-40 deg	8.10	25.92	26.16	12.42	16.95	31.78	12.24	24.67
40-90 deg.	0.10*	2.84*	1.42*	0.38*	0.57*	0.59*	0.28*	3.98*

* - category with less than 50 observations; in – increasing; d – decreasing

5.4.1. $1COR_{L250}NDVI$ spatial pattern

A spatial representation of the $1COR_{L250}NDVI$ drought impact response (Figure 30) was much alike the $1COR_LNDVI$ footprint (Figure 24). However, due to the resolution change, allocation within factors' levels was altered. A footprint of class 6 marked decrease in coverage of coniferous and broadleaved stands that accounted now on 43.99% and 19.68% respectively. In contrast, share of mix stands increased up to 36.33% (Table 41). Considered area was placed almost exclusively below 1400 m asl on

slopes with moderate to high inclination. Among aspect classes west-exposed areas were in strong majority. The opposite response depicted by the impact class 1 was almost exclusively devoted to needle leaved stands growing between 1400 and 2100 m asl. Alike for the $1COR_{L}NDVI$ spatial pattern, class 1 response was the most common on south facing slopes with north exposition being the second most frequent. Inclination allocation revealed a shift towards less steep locations, especially considering the 10-20 and 20-30 degrees strata (Table 41).

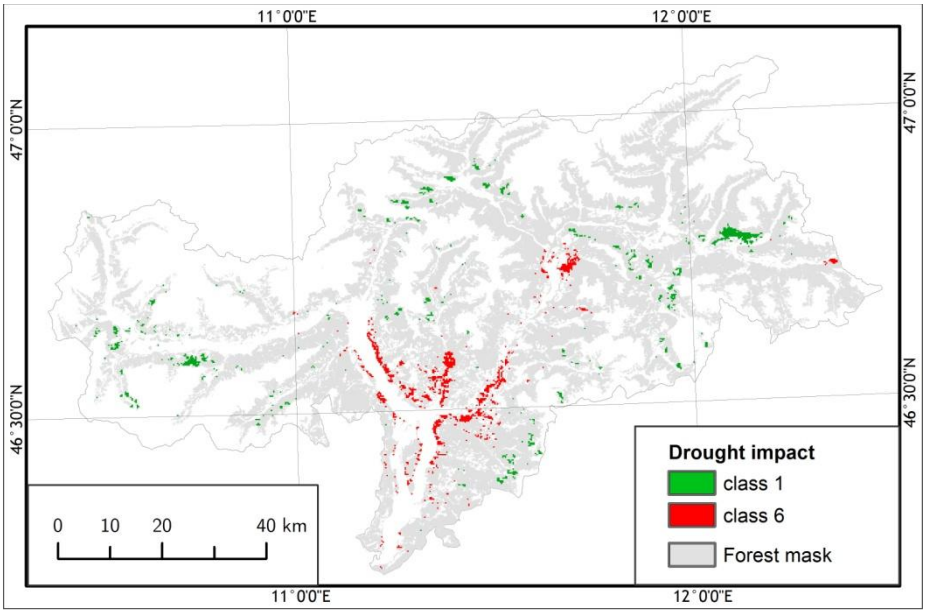

Figure 30 Spatial representation of the $1COR_{L}NDVI$ PC converted into MODIS-like response $1COR_{L250}NDVI$. Only response class 1 (green) and 6 (red) are plotted. The forest mask is marked in gray.

Statistical significance of time governed phenology and productivity changes observed within the $1COR_{L250}NDVI$ drought pattern was inspected using the within-subjects effects test of the repeated measures ANOVA performed with the Hujnh-Feldt adjustment (Table 42). The same approach confirmed significant influence of time on changeability of all six investigated metrics within drought response classes. Subsequently, impact of site-specific characteristics on phenology and productivity was analyzed. The superior influence of elevation was demonstrated (Table 43) along weaker and selective impact of aspect, slope and forest type levels.

Changes in forest status following the $1COR_{L}NDVI$ PC variability were associated with the $1COR_{L250}NDVI$ drought response class 6. It reported deteriorate $NDVI_{HS}$ values between 2003 and 2007 with local minima in 2003 and 2007 (Figure 31). A massive $NDVI_{HS}$ increase was revealed in 2008. The same years were marked by drops and rises in the $NDII7_{HS}$ envelope, however unlike for the $NDVI_{HS}$, $NDII7_{HS}$ has a clear and statistically significant (Table 44) increasing tendency. Forest response after 2008 was characterized by high values with some minor fluctuations among which the 2011 negative anomaly was the strongest one. Although the $NDVI_{HS}$ depicted for the class 1 fostered the same timing and character of anomalies, local minima were observed there

Table 42 Within-subjects effects test of repeated measures ANOVA performed for the $1COR_{L250}NDVI$ spatial representation. Test run with the Hujnh-Feldt adjustment returning results for the factor of time, and time combined with response class within selected phenology and productivity indicators.

	time			time*correlation class			Error
	df	F	p	df	F	p	df
CF	9.158	1283.13	0.000	45.790	45.148	0.000	189828.830
GPP	9.440	417.107	0.000	47.233	21.265	0.000	195807.460
SBD	9.348	424.326	0.000	46.738	8.947	0.000	193758.122
SL	9.572	363.261	0.000	47.860	13.522	0.000	198408.155
$NDVI_{HS}$	8.719	2838.74	0.000	43.597	120.109	0.000	184003.798
$NDII7_{HS}$	9.594	4740.68	0.000	47.971	51.333	0.000	202064.995

Table 43 Effects of forest type, aspect, elevation and slope factors evaluated for phenology and productivity indices within the $1COR_{L250}NDVI$ spatial representation using the test of between subjects effects of repeated ANOVA.

	Forest type (df=2)		Aspect (df=3)		Elevation (df=4)		Slope (df=4)	
indicator	F	p	F	p	F	p	F	p
CF	40.892	0.000	1.126	0.337	58.043	0.000	0.516	0.724
GPP	1.577	0.207	1.284	0.278	96.532	0.000	4.661	0.001
SBD	8.303	0.000	4.025	0.007	13.878	0.000	0.505	0.732
SL	1.358	0.257	5.289	0.001	3.773	0.005	2.298	0.057
$NDVI_{HS}$	27.950	0.000	10.010	0.000	61.486	0.000	7.340	0.000
$NDII7_{HS}$	0.723	0.485	1.374	0.249	38.349	0.000	10.036	0.000

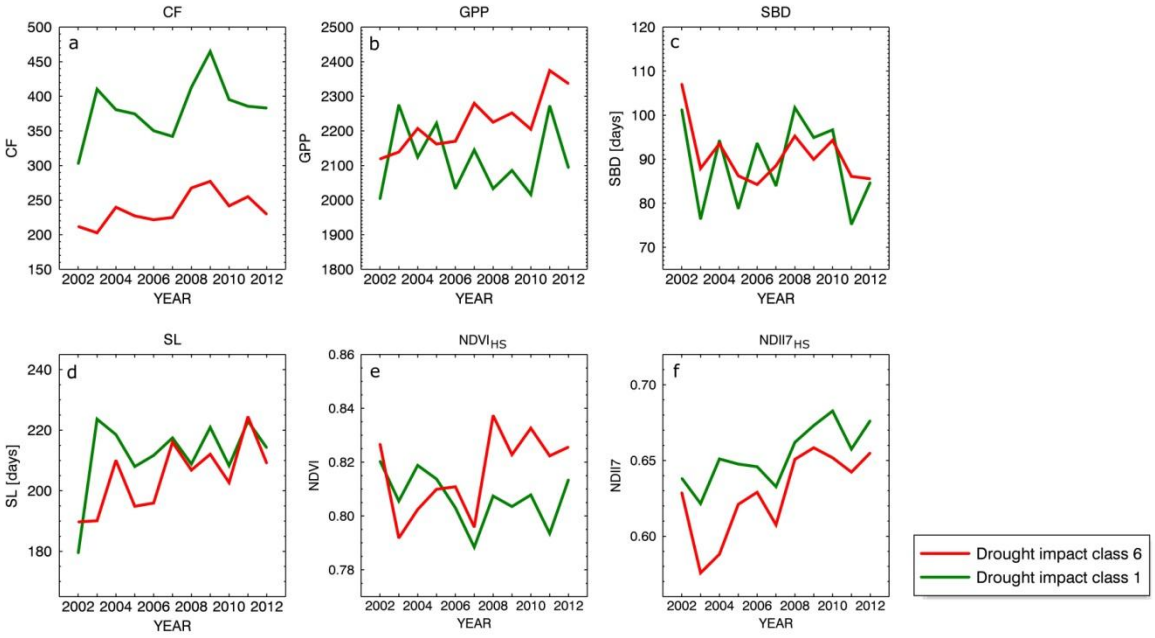

Figure 31 Year-to-year variability observed within drought impact classes 1 and 6 of the $1COR_{L250}NDVI$ spatial representation of the $1COR_{L}NDVI$ PC: a) CF, b) GPP, c) SBD, d) SL, e) $NDVI_{HS}$ and f) $NDII7_{HS}$.

in 2007 and 2011 with much smaller drop in 2003. On the contrary, $NDII7_{HS}$ within class 1 showed variability adjacent to the response of class 6, but with smaller change spectrum, hence weaker increasing tendency (Table 44). Forest stands associated with variability of class 6 revealed before 2007 distinct change towards an earlier vegetation onset, which was interrupted in the following years by SBD. An overall change tendency was insignificant (Table 44). Although SL did not adopt SBD changes immediately, a general season length perception revealed significant extension of the vegetation season (Table 44). SBD and SL observations made for the drought impact class 1 revealed rather shaky profile of vegetation onset as well as, trendless and elevated SL. The most profound differences between investigated drought responses were observed for CF. Regions of high correlation with the $1COR_{L}NDVI$ PC revealed low but steadily increasing CF. Despite small drops in 2003, 2006-2007 and after 2010, this tendency was statistically significant (Table 44). In contrast, response within class 1 not only had higher seasonal growth which achieved its local maxima in 2003 and 2009, but also depicted massive CF decrease between 2003 and 2007. GPP changes observed for class 6 supported CF variability and depicted increasing productivity tendency (Table 44) with local peaks in 2004, 2007 and 2011. A reversed manner was presented for class 1, where after elevated yield in 2003, GPP declined until 2010. This response was however not identified as statistically significant linear trend (Table 44).

Table 44 Strength of overall linear trends observed for phenology and productivity indicators within response classes 1 and 6 derived for the $1COR_{L250}NDVI$ footprint. Assessment done using the within subject contrasts test of repeated ANOVA.

	Class 1		**Class 6**	
	F	p	F	p
CF	5.456	0.020	40.316*	0.000
GPP	0.445	0.505	14.790	0.000
SBD	0.139	0.710	2.529	0.112
SL	0.462	0.497	8.410*	0.004
$NDVI_{HS}$	1.120	0.290	152.218*	0.000
$NDII7_{HS}$	50.230*	0.000	386.024*	0.000

* - the strongest trend of all tested contrast orders

Phenology and productivity response within class 6 was further inspected with the within-subjects effects test of repeated ANOVA measures with Hujnh-Feldt correction. Generated results showed a significant impact of time factor on observed variability (Table A10 1). Furthermore, moderate but significant influence of elevation in time was revealed for CF and $NDVI_{HS}$. Combined factors of aspect and time governed $NDVI_{HS}$ and $NDII7_{HS}$, whereas combinations of slope and time, as well as forest type and time factors, had limited impact diversification of CF values (Table 45).

Variability in forest status observed within the class 6 of the $1COR_{L250}NDVI$ spatial representation was deeper inspected within diverse levels of forest type, aspect, elevation and slope factors using repeated ANOVA measures plots (Figure A11 1). According to derived visualizations, coniferous stands revealed the least intense

Table 45 Effect of elevation, aspect, slope and forest type factors in time on distinction between productivity indices tested for the response class 6 derived of the $2COR_{L250}NDVI$ spatial representation. Analyses performed using subjects effects test of repeated ANOVA. Only measures with significant statistics are shown ($p<0.001$)

	time*elevation		**time*aspect**		**time*slope**		**time*forest**	
indicator	df	F	df	F	df	F	df	F
CF	20	5.269			40	2.123	20	2.216
$NDVI_{HS}$	21.939	2.449	32.909	2.167				
$NDII7_{HS}$			36.000	3.016				

variability with the lowest CF, SL and $NDVI_{HS}$. The most intense change amplitudes were observed for mixed forest, which was especially visible in GPP and SBD profiles. Moreover, SBD response was the only example of disparity between coniferous and mixed forest in drought stress reaction, where the former showed the soonest onset in 2005 and 2006, whereas the latter depicted SBD drop in 2004. Forest type revealed a limited impact on $NDII7_{HS}$ with broadleaved stands having the highest score. Aspect study indicated a positive relation between southern exposition and increase in CF and SL values. On the contrary, north-facing sites had more favorable $NDVI_{HS}$ and $NDII7_{HS}$ conditions, with the smallest change amplitude. The latter observation did not relate to GPP, SBD and SL where profound peaks were detected for north-exposed locations. Particularly intriguing was a massive 2002-2007 SBD depression centered at 2004. Despite this, remaining strata followed mutually alike temporal variability. Altitude impact on phenology under drought conditions was rather complex. Although elevation increase was positively correlated with $NDII7_{HS}$, no other index followed this relation. Apparent distinction was also observed for CF, with the lowest elevation zone showing the best productivity. Inclination role was not utterly explicit. Although the lowest sloping zones obtained the highest CF, SBD and SL results, inclination increase did not translate on linear decrease of aforementioned metrics. Moreover, $NDVI_{HS}$ and $NDII7_{HS}$ revealed very limited differences between inclination levels, which indirectly translated on complex response of remaining measures that, in most of the cases, followed mutually similar temporal profiles.

5.4.2. $2COR_{L250}NDVI$ spatial pattern

Although the $2COR_{L250}NDVI$ (Figure 32) originated from the spatial distribution of the $2COR_{L}NDVI$ PC (Figure 25), allocation of $2COR_{L250}NDVI$ drought severity classes within factors levels was altered due to different resolution and exclusion of some regions governed by the spatial aggregation principles (Table 41). Areas associated with the drought impact class 6 showed slightly weaker dominance of coniferous stands and stronger share of mixed woodland comparing with the $2COR_{L}NDVI$ footprint (Table 41). North and west exposed slopes, of moderate to high inclination (0°-40°) were the most common for these stands. Medium and high elevation was favored, but the lowest altitude class accounted on 23.51% of the response. On the contrary, class 1 addressed almost exclusively coniferous forest stands. Aspect allocation revealed small dominance of south exposition. 68.15% of the area of class 1 was placed between 1400 and 2100 m asl, with another 29.48% between 700 and 1400 m asl. Sloping preferences

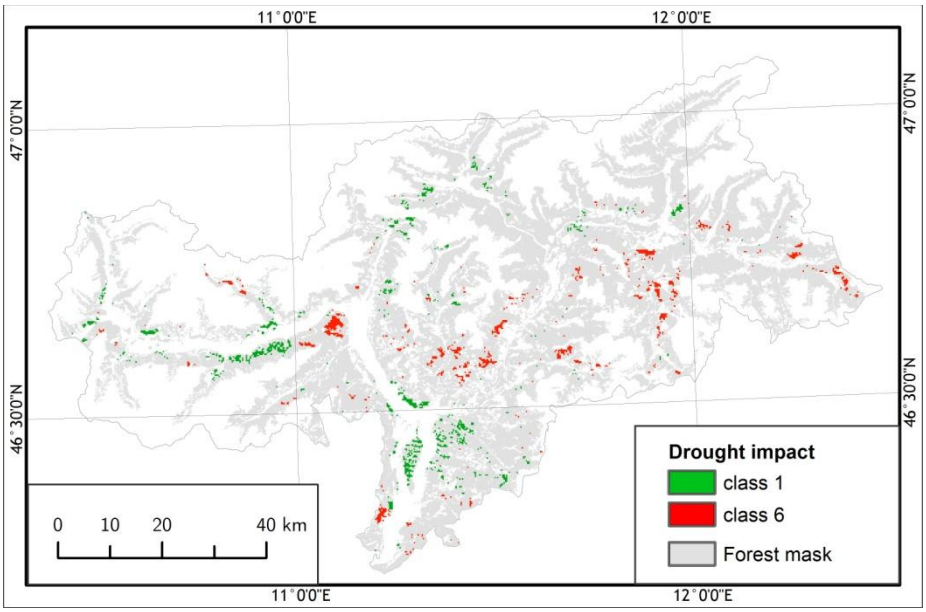

Figure 32 Spatial representation of the $2COR_{L}NDVI$ PC converted into MODIS-like response $2COR_{L250}NDVI$. Only response class 1 (green) and 6 (red) are plotted. The forest mask is marked in gray

revealed this response to be the most prominent at sides with moderate inclination (10-30 degrees).

Significance of time dependent phenology and productivity changes observed within the $2COR_{L250}NDVI$ spatial pattern were tested with the within-subjects effects test of the repeated measures ANOVA performed with the Hujnh-Feldt adjustment. Statistics confirmed significance of changes of forest status in time (Table 46), as well as a valid influence of combined factors of time and drought impact classes within all six considered indices. Furthermore, a relation between environmental features and phenology-productivity was inspected, and revealed statistically significant connection to elevation (Table 47). Differences between aspect, slope and forest type classes were less evident, or even irrelevant.

Table 46 Within-subjects effects test of repeated measures ANOVA performed for the $2COR_{L250}NDVI$ spatial representation. Test run with the Hujnh-Feldt adjustment returning results for the factor of time, and time combined with response class within selected phenology and productivity indicators.

	time			**time*correlation class**			**Error**
	df	F	p	df	F	p	df
CF	9.109	1204.587	0.000	45.543	14.512	0.000	192236.359
GPP	9.433	447.711	0.000	47.165	5.042	0.000	199085.480
SBD	9.346	425.088	0.000	46.732	3.021	0.000	197254.942
SL	9.566	383.409	0.000	47.831	4.054	0.000	201896.726
$NDVI_{HS}$	8.623	2761.485	0.000	43.115	48.301	0.000	181989.787
$NDII7_{HS}$	9.567	4460.367	0.000	47.833	25.397	0.000	201501.175

Table 47 Effects of forest type, aspect, elevation and slope factors evaluated for phenology and productivity indices within the $2COR_{L250}NDVI$ spatial representation using the test of between subjects effects of repeated ANOVA.

	Forest type (df=2)		Aspect (df=3)		Elevation (df=4)		Slope (df=4)	
indicator	F	p	F	p	F	p	F	p
CF	40.885	0.000	1.125	0.337	58.043	0.000	0.516	0.000
GPP	1.579	0.206	1.285	0.278	96.542	0.000	4.661	0.001
SBD	8.302	0.000	4.025	0.007	13.878	0.000	0.505	0.732
SL	1.355	0.258	5.289	0.001	3.772	0.005	2.297	0.057
$NDVI_{HS}$	27.951	0.000	10.009	0.000	61.492	0.000	7.340	0.000
$NDII7_{HS}$	0.723	0.485	1.374	0.249	38.355	0.000	10.036	0.000

Forest indicated by the $2COR_{L250}NDVI$ impact classes 6 and 1, associated with the increasing and decreasing NDVI tendency respectively, revealed very similar temporal responses of all six investigated indices (Figure 33). Both strata demonstrated $NDII7_{HS}$ drop in 2003, followed by a strong increasing tendency (Table 48) inhibited shortly in 2007 and 2011. Remarkably, class 6 had higher $NDII7_{HS}$ and showed smaller decrease between 2002 and 2003, and more intense increase between 2003 and 2013 comparing with class 1. $NDVI_{HS}$ observed for areas of inclining greenness reported lower scores with less intense variability. The only exception was here 2008. Both temporal profiles highlighted drop in 2003, 2007 and 2011 as well as rise in 2008 and 2012. Regions associated with class 1 experienced much more intense decrease between 2001 and 2007 and weaker gain in 2008 than class 6. (Figure 33). Although both drought response classes revealed between 2002 and 2007 a tendency for earlier vegetation onset, class 1 demonstrated a smoother envelope (Figure 33). The overall tendency was insignificant due to 2008-2010 SBD increase (Table 48). Although SL demonstrated alike, wobbly

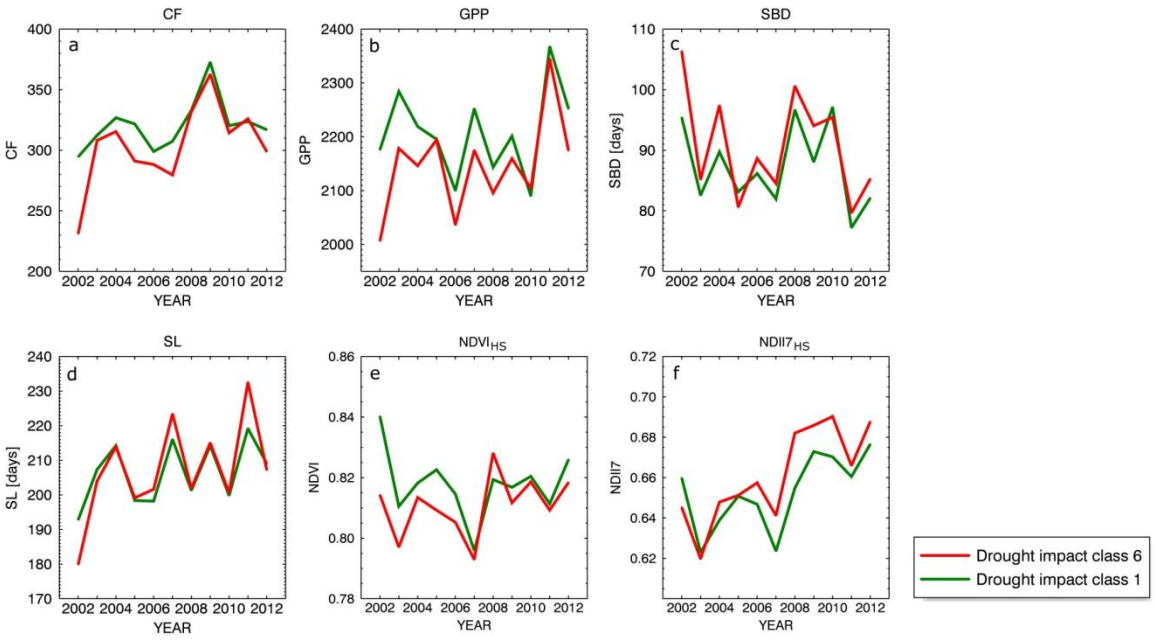

Figure 33 Year-to-year variability observed within drought impact classes 1 and 6 of the $2COR_{L250}NDVI$ spatial representation of the $2COR_{L}NDVI$ PC: a) CF, b) GPP, c) SBD, d) SL, e) $NDVI_{HS}$ and f) $NDII7_{HS}$.

response for both classes, only class 6 showed overall significant linear relation (Table 48). Interestingly, 2003 and 2004 brought longer vegetation period within both strata, which resulted in elevated CF. Productivity rise lasted only until 2004, and was followed by CF decline concluded in 2006 and 2007 for class 1 and 6 respectively. Despite these deteriorations, the overall CF changeability suggested increasing tendencies, which was governed mainly by a massive rise in 2008-2009. GPP demonstrated limited correlation to CF. Drought impact class 6 obtained here lower productivity scores, with slightly decreasing tendency between 2005 and 2010 hampered by elevated GPP in 2011. Regions supporting NDVI decline showed more intense variability with stronger decrease before 2010, but equally intense rise in 2011 (Figure 33).

Table 48 Strength of overall linear trends observed for phenology and productivity indicators within response classes 1 and 6 derived for the $2COR_{L250}NDVI$ spatial representation. Assessment done using the within subject contrasts test of repeated ANOVA.

	Class 1		**Class 6**	
	F	p	F	p
CF	4.213	0.004	5.567	0.019
GPP	9.201	0.002	6.985*	0.008
SBD	2.651	0.104	2.424	0.120
SL	1.590	0.208	4.602	0.032
$NDVI_{HS}$	15.498	0.000	87.803*	0.000
$NDII7_{HS}$	137.504*	0.000	224.821*	0.000

* - the strongest trend of all tested contrast orders

Subsequently, drought response within class 6 was investigated deeper through the within-subjects effects test of repeated ANOVA measures with Hujnh-Feldt correction. Significance of time governed changes was confirmed for all phenology and productivity measures (Table A10 2). Further analyses performed for time combined with four environmental factors revealed significant but limited impact of elevation and time on CF, $NDVI_{HS}$ and $NDII7_{HS}$ variability (Table 49). Furthermore slope and time factors were found relevant for $NDVI_{HS}$ and $NDII7_{HS}$.

Table 49 Effect of elevation and slope factors in time on distinction between productivity indices tested for the response class 6 derived for the $2COR_{L250}NDVI$ spatial representation. Analyses performed using within-subjects effects test of repeated ANOVA. Only measures with significant statistics are shown ($p<0.001$).

	time*elevation		**time*slope**	
indicator	df	F	df	F
CF	29.948	3.366		
$NDVI_{HS}$	32.696	4.778	43.595	2.281
$NDII7_{HS}$	36.000	2.771	48.000	2.083

Comprehensive information on drought governed phenology and productivity changes within regions of class 6 inspected for forest type, aspect, elevation and slope classes

was ensured through repeated ANOVA measures plots (Figure A11 2). Following the obtained results coniferous stands showed usually the lowest GPP, $NDVI_{HS}$ and $NDII7_{HS}$ scores. Interestingly, needle-leaved forest had the highest CF with a positive peak in 2003 followed by a productivity decline lasting until 2006, and a massive increase between 2007 and 2009. On the contrary broadleaved and mixed stands reported drop in 2003 with a steady productivity rise peaked in 2009. This behavior was not transferred on GPP, where hardwood and mixed stands reported light productivity incline, whereas needle-leaved forest demonstrated leveled and lower scores. Robust differences in SBD were observed between forest types before 2008, with coniferous trees revealing earlier vegetation onset for 2003-2008. While mixed stands demonstrated overall SBD decrease briefly interrupted in 2008-2010, broadleaved forest experienced an abrupt SBD drop between 2004 and 2006, followed by later vegetation onset. $NDII7_{HS}$ indicted alike patterns for all three classes with the highest index values reported for mixed and hardwood forests. The same observation was made for the $NDVI_{HS}$. SL seemed to be species independent with an exception of 2005-2008 period when broadleaved forest experienced shorter vegetation. The north exposition rendered the highest $NDVI_{HS}$ and $NDII7_{HS}$ with all aspect classes following alike temporal profiles. A strong diversification among aspect classes was observed for SBD where south and west facing regions experienced the latest vegetation onset, but the clearest declining tendency. Very limited differences were observed for SL, where north facing forest stands revealed the strongest amplitude of changes. Furthermore, north exposed regions experienced CF decline in 2004. GPP on south facing slopes was suppressed but revealed a clear increase. Elevation gain leaded to $NDVI_{HS}$, CF and GPP decrease, with the highest variability observed within the lowest altitudinal class. All measures suggested increasing trends over time. Interestingly, no linear relation was spotted between elevation and SBD neither SL, where the latter revealed the biggest differences between factor levels for 2002-2007. The highest $NDII7_{HS}$ was reported for stands growing at moderate elevation (700-1400 m asl). The fourth altitudinal class was not considered due to insufficient representation (Table 41). Inspection of phenological changes driven by inclination demonstrated no straightforward relations. Although SL seemed to decline with increasing steepness, it did not translate onto other indices. Areas of the lowest inclination demonstrated the lowest CF. The most intense differences between classes were observed between 2002 and 2007. Inclination class 5 was not considered due to limited representation.

5.4.3. $1COR_{L250}$NBRI spatial pattern

The $1COR_{L250}$NBRI pattern (Figure 34) rendered alike spatial features as the $1COR_{L}$NBRI footprint (Figure 26), but due to change in resolution and associated spatial aggregation approach, its allocation within factors levels transformed (Table 41). Regions that followed the increasing tendency of the $1COR_{L}$NBRI PC (response class 6) were the most common at south and east exposed slopes of moderate to high inclination, which differ slightly from the $1COR_{L}$NBRI footprint settings. Considered class was located on medium to high altitudes with preference of the former, whereas species distribution indicated dominance of coniferous stands with small addition of mixed forest and neglected share of broadleaved woodland. The opposite

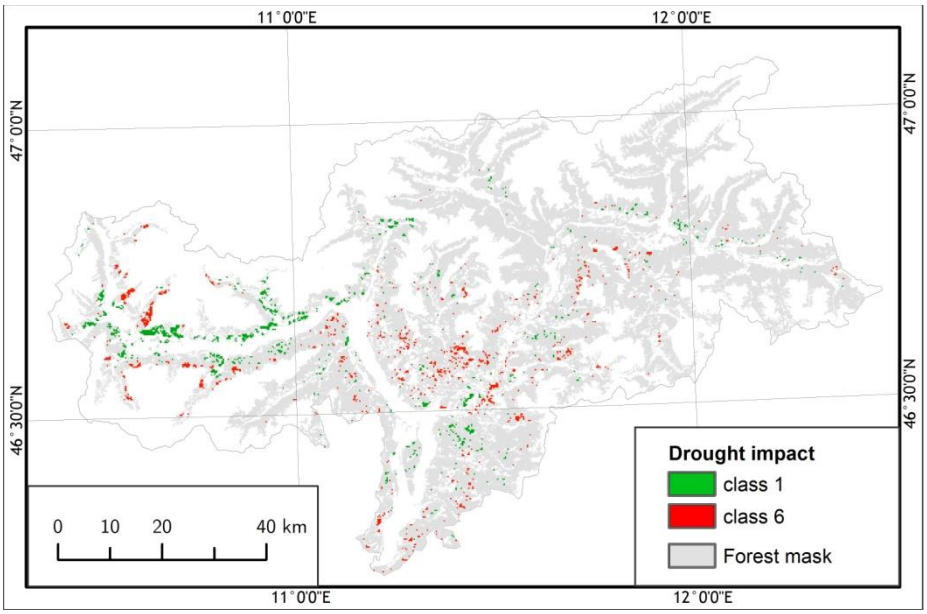

Figure 34 Spatial representation of the $1COR_{L}NBRI$ PC converted into MODIS-like response $1COR_{L250}NBRI$. Only response class 1 (green) and 6 (red) are plotted. The forest mask is marked in gray.

response of class 1 that suggested increasing NBRI was represented by coniferous forest with addition of mixed stands. They were located mainly on west and north exposed locations of inclination between 10° and 40°. Elevation distribution followed the South Tyrolean lay of the land with minor underestimation of the 700-1400 m asl strata.

Significance of time in phenology and productivity changes, as well as diversification between drought response classes in time was confirmed by the within-subjects effects test of the repeated measures ANOVA performed with the Hujnh-Feldt adjustment (Table 50). Moreover, expected leading influence of elevation on phenology changes was confirmed through the between subjects effects test (Table 51). Importance of forest type, aspect and slope on forest growth was less relevant and not always significant.

Table 50 Within-subjects effects test of repeated measures ANOVA performed for the $1COR_{L250}NBRI$ spatial representation. Test run with the Hujnh-Feldt adjustment returning results for the factor of time, and time combined with response class within selected phenology and productivity indicators.

	time			**time*correlation class**			**Error**
	df	F	p	df	F	p	df
CF	9.121	1245.76	0.000	45.603	21.615	0.000	189013.873
GPP	9.434	437.153	0.000	47.134	3.502	0.000	195505.602
SBD	9.345	421.075	0.000	46.724	2.548	0.000	193661.760
SL	9.564	343.228	0.000	47.818	4.836	0.000	198196.865
$NDVI_{HS}$	8.678	2628.95	0.000	43.420	69.568	0.000	179966.116
$NDII7_{HS}$	9.561	4285.03	0.000	47.839	43.519	0.000	196226.031

Table 51 Effects of forest type, aspect, elevation and slope factors evaluated for phenology and productivity indices within the $1COR_{L250}NBRI$ spatial representation using the test of between subjects effects of repeated ANOVA.

	Forest type (d2=2)		Aspect (df=3)		Elevation (df=4)		Slope (df=4)	
indicator	F	p	F	p	F	p	F	p
CF	41.216	0.000	1.522	0.207	93.588	0.000	0.640	0.634
GPP	1.608	0.200	1.302	0.272	153.785	0.000	5.530	0.010
SBD	7.796	0.000	4.544	0.003	28.905	0.000	0.690	0.599
SL	1.635	0.195	4.773	0.003	3.565	0.014	2.408	0.047
$NDVI_{HS}$	28.137	0.000	7.586	0.000	87.890	0.000	9.140	0.000
$NDII7_{HS}$	0.637	0.529	2.209	0.085	47.493	0.000	11.356	0.000

Forest stands convergent with the increasing $1COR_LNBRI$ PC and represented by class 6, demonstrated $NDII7_{HS}$ decline in 2003 followed by a fast increase slightly disturbed in 2007 and 2011 (Figure 35). Variability observed within class 1 demonstrated lower scores and diminished values between 2002 and 2007 and a gradual overall rise. Especially strong drops were detected in 2003 and 2007, where the former had the greatest absolute value, while the latter was a global minimum in both envelopes. Both profiles showed a significant linear tendency (Table 52). $NDVI_{HS}$ defined for class 6 depicted abruptly decreased greenness between 2003 and 2007 with higher but unsteady signal afterwards. Conversely, the opposite drought response indicated lower $NDVI_{HS}$ scores with strong decrease before 2007 when a global minimum was reached, and higher, but still suppressed values until 2012. SBD observed for both impact classes showed comparable responses with sooner vegetation onset detected between 2003 and 2007, and later phenology incept for 2008-2010. Class 1 was more prone to earlier start of the season whereas class 6 showed wider change

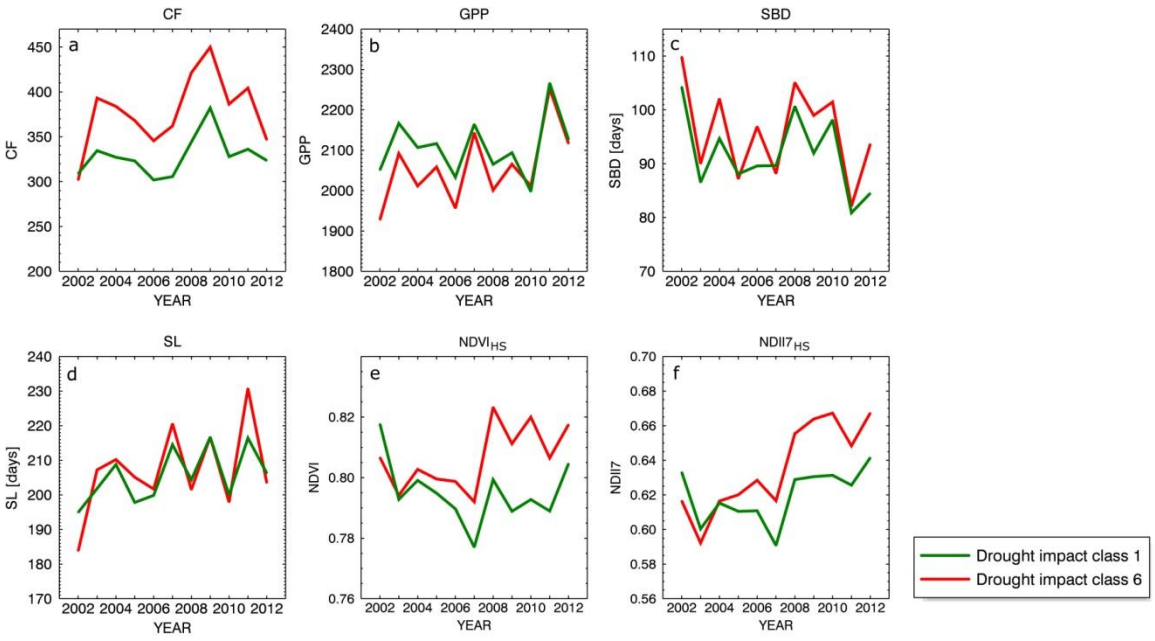

Figure 35 Year-to-year variability observed within drought impact classes 1 and 6 of the $1COR_{L250}NBRI$ spatial representation of the $1COR_LNBRI$ PC: a) CF, b) GPP, c) SBD, d) SL, e) $NDVI_{HS}$ and f)$NDII7_{HS}$.

spectrum with statistically more robust linearity (Table 52). SL differences were very limited between both analyzed responses with, in general, slightly shorter SL observed for class 1. Both showed linear tendencies only for class 6 (Table 52). GPP revealed better diversification between classes with lower but leveled productivity in class 6, and higher but gradually decreasing scores depicted within class 1. Both time profiles comprised serried of rises and drops with GPP increase in 2003, 2005, 2007 and 2011, and two more robust downs in 2006 and 2010. Also in this case only class 6 reported significant linearity of changes. Seasonal vegetation growth approximated by CF showed higher productivity within class 6. Although both strata rendered alike responses of productivity increase in 2003 and 2008, separated by the index loss centered on 2006, absolute changes observed within class 1 were smaller, and supported no linearity assumption (Table 52).

Table 52 Strength of overall linear trends observed for phenology and productivity indicators within response classes 1 and 6 derived for the $1COR_{L250}NBRI$ spatial representation. Assessment done using the within subject contrasts test of repeated ANOVA

	Class 1		**Class 6**	
	F	p	F	p
CF	1.739	0.188	4.411	0.036
GPP	2.429	0.119	38.519*	0.000
SBD	2.948	0.086	6.791	0.009
SL	3.335	0.068	11.634	0.001
$NDVI_{HS}$	0.088	0.767	128.511	0.000
$NDII7_{HS}$	78.553*	0.000	400.225*	0.000

* - the strongest trend of all tested contrast orders

Further focus was put on the $1COR_{L250}NBRI$ response class 6. The within-subjects effects test of repeated ANOVA measures run with Hujnh-Feldt correction revealed significant impact of time on observed phenological changes within class 6 (Table A10 3). Moreover, a detailed investigation accounting on combined impact of time and four environmental factors indicated for CF and $NDVI_{HS}$ meaningful but weak diversification within elevation classes (Table 53).

Table 53 Effect of elevation factor in time on distinction between productivity indices tested for the response class 6 derived for the $1COR_{L250}NBRI$ spatial representation. Analyses performed using subjects effects test of repeated ANOVA. Only measures with significant statistics are shown ($p<0.001$).

	time*elevation	
indicator	df	F
CF	30.000	2.935
$NDVI_{HS}$	34.189	4.316

An investigation of drought governed phenology and productivity variability within forest type, aspect, elevation and slope levels, was achieved through repeated ANOVA measures run for area of class 6 (Figure A11 3). Differences between forest types, where

broadleaved stands were excluded due to limited representation, were distinct and showed for coniferous woodland lower $NDVI_{HS}$ and GPP scores, as well as surprisingly high CF values. Hardly any divergence was observed for SL, whereas SBD derived for mixed stands revealed a strong tendency towards earlier vegetation onset. Interestingly, although CF temporal profiles were much alike for both forest types, coniferous trees reported an increase in 2003. Phenological indices were reported to be exposition-dependent, where the south exposition showed lower $NDVI_{HS}$ and $NDII7_{HS}$, but higher CF and SL comparing with other levels. SBD revealed for north facing regions intense changes with the earliest vegetation onset in 2005 and 2011. Although the latter drop was present also for other aspects, the former seemed to be site specific phenomenon. Moreover, SL showed substantial differences between all four strata in the first part of the analyses time-window, with uniform variability beyound 2006. Elevation impact on phenology was rather complex and nonlinear. Interestingly the highest $NDVI_{HS}$, $NDII7_{HS}$ and GPP scores were derived for 700-1400 m asl strata. Contrasting observation was made for CF and partly also SL. The third altitudinal zone (the forth was excluded due to insufficient area), demonstrated in 2003 a contrasting response of increased productivity. An inclination increase revealed minor negative impact on all phenology and productivity measures but CF. Moreover, temporal profiles observed for areas with the lowest steepness showed a bit diverse variability than the rest of the investigated region ,demonstrating for SL isolated peaks in 2005, as well as CF decrease in 2007.

5.4.4. $2COR_{L250}NBRI$ spatial pattern

Although the $2COR_{L250}NBRI$ (Figure 36) originated from the spatial response to the $2COR_{L}NBRI$ PC (Figure 27), its allocation within factors levels was altered due to a different resolution and spatial aggregation principles governing exclusion of some regions (Table 41). Areas recognized as inclined with the $2COR_{L}NBRI$ variability were represented in response class 6, and showed only small dominance of coniferous stands and definitively stronger share of mixed woodland (Table 41) comparing with the $2COR_{L}NBRI$ footprint. Moreover, almost all discussed area was located below 1400 m asl with a substantial part belonging to the lowest elevation class (Table 41). Furthermore, west and east exposed slopes were the most common location for class 6, which indicated a change in relation to the $2COR_{L}NBRI$ impact representation. On the contrary, class 1 addressed almost exclusively coniferous forest stands frequently growing on north facing locations and on elevation between 1400 and 2100 m asl. The latter revealed a clear shift towards the higher altitudes comparing with the $2COR_{L}NBRI$ footprint. Sloping preferences suggested this response to be the most prominent at sides with moderate to high inclination (10-40 degrees).

Significance of time dependent phenology and productivity changes observed for the $2COR_{L250}NBRI$ pattern were tested with the within-subjects effects test of the repeated measures ANOVA performed with the Hujnh-Feldt adjustment. Statistics confirmed significance of time governed forest status differences (Table 54), as well as valid influence of combined factors of time and impact class within all six considered indices. Independently, a relation between forest response and site specific features of forest type, aspect, slope and elevation were looked upon. Analyses demonstrated the biggest disparity between elevation levels (Table 55). Three remaining factors revealed less

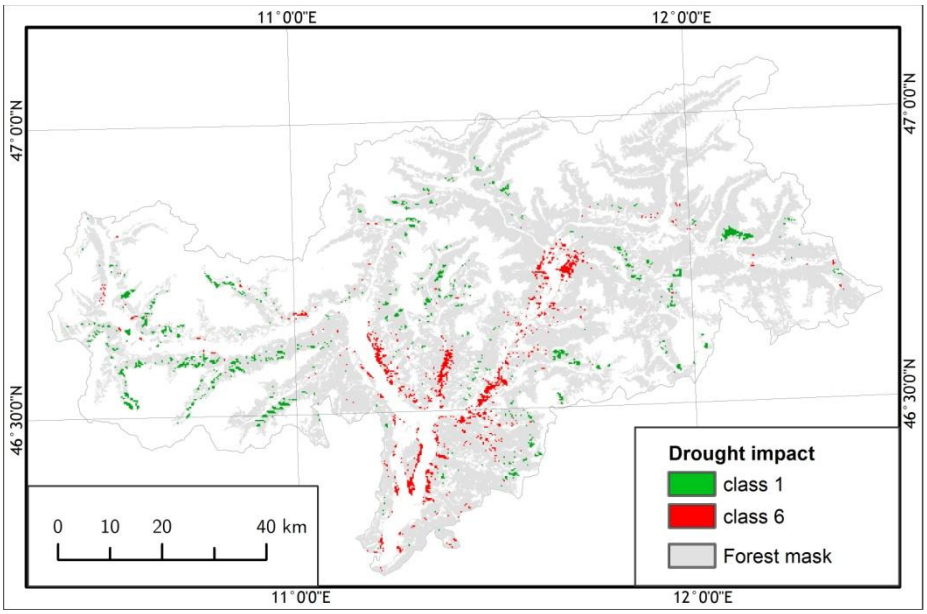

Figure 36 Spatial representation of the $2COR_L$NBRI PC converted into MODIS-like response $2COR_{L250}$NBRI. Only response class 1 (green) and 6 (red) are plotted. The forest mask is marked in gray.

Table 54 Within-subjects effects test of repeated measures ANOVA performed for the $2COR_{L250}$NBRI spatial representation. Test run with the Hujnh-Feldt adjustment returning results for the factor of time, and time combined with response class within selected phenology and productivity indicators.

	time			**time*correlation class**			**Error**
	df	F	p	df	F	p	df
CF	9.236	1239.76	0.000	46.181	91.465	0.000	194718.746
GPP	9.448	417.819	0.000	47.238	18.308	0.000	199173.184
SBD	9.353	407.660	0.000	46.765	14.298	0.000	197178.703
SL	9.573	358.874	0.000	47.864	17.830	0.000	201815.692
$NDVI_{HS}$	8.845	2909.55	0.000	44.223	175.681	0.000	186461.801
$NDII7_{HS}$	9.615	4673.46	0.000	48.077	59.046	0.000	200537.469

Table 55 Effects of forest type, aspect, elevation and slope factors evaluated for phenology and productivity indices within the $2COR_{L250}$NBRI spatial representation using the test of between subjects effects of repeated ANOVA.

	Forest type (df=2)		**Aspect (df=3)**		**Elevation (df=4)**		**Slope (df=4)**	
indicator	F	p	F	p	F	p	F	p
CF	40.500	0.000	1.162	0.323	57.699	0.000	0.450	0.773
GPP	1.663	0.190	1.087	0.353	96.301	0.000	4.847	0.001
SBD	8.6990	0.000	3.930	0.008	13.741	0.000	0.532	0.712
SL	1.376	0.253	5.265	0.001	4.020	0.003	2.188	0.068
$NDVI_{HS}$	28.084	0.000	10.359	0.000	64.375	0.000	7.733	0.000
$NDII7_{HS}$	0.655	0.519	1.548	0.200	40.344	0.000	10.415	0.000

apparent impact on forest growth. Areas indicated by the $2COR_{L250}NBRI$ response class 6 revealed in 2003 an intense drop in $NDVI_{HS}$ and $NDII7_{HS}$ envelopes, which was next followed by gradual scores increase culminated in 2008 (Figure 37). Consecutive years indicated high values of both indices with a minor decrease in 2011. Moreover, the 2003-2008 increase was interrupted in 2007 by another abrupt decrease in both envelopes. An increasing trend was much stronger for the $NDII7_{HS}$ (Table 56). Regions associated with class 1 showed $NDII7_{HS}$ response similar to the one observed for class 6, however with less intense decrease in 2003. $NDVI_{HS}$ reported for locations following the decreasing $2COR_{L}NDVI$ PC phase demonstrated an overall decline until 2007 with an increase episode in 2004. The following years revealed a leveled $NDVI_{HS}$ signal concluded in a 2011 drop and 2012 peak (Figure 37). The area associated with response class 6 revealed between 2002 and 2007 a steady and intense trend for the earlier vegetation onset. Although the consecutive years broke this trend demonstrating an

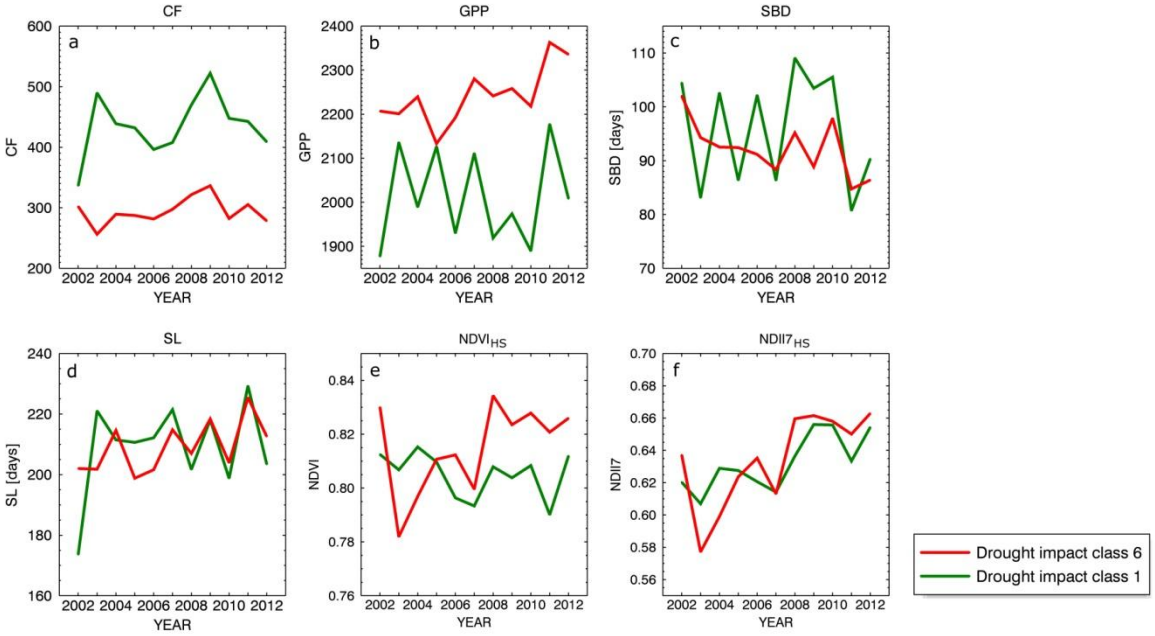

Figure 37 Year-to-year variability observed within drought impact classes 1 and 6 of the $2COR_{L250}NBRI$ spatial representation of the $2COR_{L}NBRI$ PC: a) CF, b) GPP, c) SBD, d) SL, e) $NDVI_{HS}$ and f) $NDII7_{HS}$.

Table 56 Strength of overall linear trends observed for phenology and productivity indicators within response classes 1 and 6 derived for the $2COR_{L250}NBRI$ spatial representation. Assessment done using the within subject contrasts test of repeated ANOVA.

	Class 1		**Class 6**	
	F	p	F	p
CF	0.070	0.791	28.495	0.000
GPP	1.632	0.202	17.458*	0.000
SBD	1.809	0.179	13.368*	0.000
SL	0.104	0.747	11.235*	0.001
$NDVI_{HS}$	4.938	0.026	149.581	0.000
$NDII7_{HS}$	47.399*	0.000	414.768*	0.000

* - the strongest trend of all tested contrast orders

increase, the overall tendency was sound and significant (Table 56). Accordingly, coupled SL showed some fluctuation of the signal, dominated by inclination to season prolongation (Table 56). In contrast, SBD observed within class 1 revealed a very shaky signal of wide amplitude and no meaningful trend (Table 56). SL derived for this stratum revealed, alike for class 6, no clear coupling with the vegetation onset neither any prolongation tendency. SL within class 1 suggested for 2003-2007 slightly longer vegetation period. Following the SBD tendency, CF observed for class 6 reported gradual increase between 2003 and 2009, with CF decrease in 2003. Despite CF drop after 2009, the overall increasing tendency was statistically significant (Table 56). Conversely, class 1 not only had higher CF, but also revealed an intense increase in 2003, which was followed by a productivity decline culminated in 2007. Another increase was commenced in 2008 and reached its maximum in 2009. GPP demonstrated limited correlation to CF. Drought impact class 6 obtained here the highest productivity scores, with a moderate, but clear increasing trend (Table 56). Years 2005, 2008 and 2011 brought index drop. Area of reversed NBRI temporal behavior showed unsteady GPP evolution of high amplitude of changes and hazy decreasing tendency between 2005 and 2010, and a consecutive abrupt increase.

Subsequently, response within the drought impact class 6 was investigated deeper through the within-subjects effects test of repeated ANOVA measures with Hujnh-Feldt correction. Significance of time governed changes was confirmed for all measures (Table A10 4). Further analyses performed for time combined with factors of slope, aspect and elevation revealed limited significance only for CF, $NDVI_{HS}$ and $NDII7_{HS}$ (Table 57).

Table 57 Effect of elevation, aspect and slope factors in time on distinction between productivity indices tested for the response class 6 derived for the $2COR_{L250}NBRI$ spatial representation. Analyses performed using subjects effects test of repeated ANOVA. Only measures with significant statistics are shown ($p<0.001$).

	time*elevation		**time*aspect**		**time*slope**	
indicato	df	F	df	F	df	F
CF	20.000	4.533	30.000	2.713	40.000	2.359
$NDVI_{HS}$	-	-	33.265	3.020	44.354	2.304
$NDII7_{HS}$	22.864	2.967	34.295	2.134	45.727	2.688

Comprehensive information on drought governed forest status variability within regions of class 6 inspected for forest type, aspect, elevation and slope classes was ensured through repeated ANOVA measures plots (Figure A11 4). Following the obtained results coniferous stands, as expected, showed the lowest CF, GPP and $NDVI_{HS}$ scores. Importantly, they also reported GPP increase for 2002 and 2003, as well as the slowest $NDVI_{HS}$ and CF increase between 2003 and 2007. 2008 and 2009 brought a robust rise of coniferous forest productivity, making it equal with mixed and broadleaved. Together with mixed stands, coniferous woodland demonstrated a clear SBD decrease between 2002/2003 and 2006/2007. SL seemed to be species independent though. North facing slopes revealed the highest $NDVI_{HS}$ and $NDII7_{HS}$. On the other hand, these locations demonstrated outstanding and the lowest CF, SBD and SL

scores. SL was particularly strongly diminished between 2003 and 2005, with a gradual increase reported afterwards. Moreover, despite an initial GPP rise, north oriented forest stands experienced an intense productivity drop in 2005, as well as massive depression cantered at 2008. Elevation increase resulted in linear $NDII7_{HS}$ rise, as well as $NDVI_{HS}$ and GPP decrease, although the latter revealed also more complex variability. The highest considered elevation class (1400-2100 m asl), unlike the lower regions, demonstrated a strong, positive CF increase which was additionally coupled with prolongation of the vegetation season. On the contrary, forest growing below 1400 m asl reported productivity drop in 2003. Interestingly, these woodlands seemed to experience a lower change amplitude. Elevation governed differences in vegetation onset were very subtle. An inspection of phenological changes related to inclination suggested rather negative impact of slope increase on GPP, SL and $NDVI_{HS}$. However, no clear tendency was detected as differences between slope classes were very limited.

5.5. Comparison with MODIS-based drought impact results

Appealing similarity between identified MODIS and Landsat PCs identified as fostering forest drought impact response, called upon examination. As expected, the time-domain based comparison coupled the $3COVnNDVI_{8\text{-}18}$, $2COR_LNDVI$ and $1COR_LNBRI$ principal components; $1CORNDII7_{8\text{-}18}$ with $2COR_LNBRI$ as well as $4CONnNDII7_{8\text{-}18}$ and $1COR_LNBRI$ PCs, where the latter correspondence was negative (Table 58). Following analyses of appropriate footprints showed however no meaningful connection between spatial representation (Table 59).

Table 58 Correlation between MODIS and Landsat PCs fostering forest response to drought meteorological conditions. Comparison was done with MODIS scores averaged to yearly values and truncated to the 2002-2011 period.

Landsat based PCs	**MODIS derived drought related PCs**		
	$3COVnNDVI_{8\text{-}18}$	$1CORNDII7_{8\text{-}18}$	$4COVnNDII7_{8\text{-}18}$
$1COR_LNDVI$	0.444, p=0.172	0.506, p=0.113	0.090, p=0.793
$2COR_LNDVI$	0.694, p=0.020	0.317, p=0.342	-0.560, p=0.073
$1COR_LNBRI$	0.809, p=0.003	0.438, p=0.177	-0.652, p=0.030
$2COR_LNBRI$	0.480, p=0.135	0.689, p=0.019	0.402, p=0.220

Table 59 Correlation between spatial representations of MODIS and Landsat PCs fostering forest response to drought meteorological conditions. Analysis was done for synthetic, MODIS-like spatial representations of the original Landsat derived PCs.

Landsat based PCs	**MODIS derived drought related PCs**		
	$3COVnNDVI_{8\text{-}18}$	$1CORNDII7_{8\text{-}18}$	$4COVnNDII7_{8\text{-}18}$
$1COR_{L250}NDVI$	0.301, p=0.000	-0.217, p=0.000	-0.009, p=0.000
$2COR_{L250}NDVI$	0.100, p=0.000	0.114, p=0.000	-0.165, p=0.000
$1COR_{L250}NBRI$	-0.229, p=0.000	0.034, p=0.000	0.168, p=0.000
$2COR_{L250}NBRI$	0.363, p=0. 000	-0.160, p=0.000	0.073, p=0.000

5.6. Summary and discussion

Results of the S-mode PCA of Landsat derived NDVI and NBRI 2001-2011 time series of annual composites ($_{L}$NDVI and $_{L}$NBRI respectively) approximated forest condition in South Tyrol. Four selected principal components related to the scPDSI temporal patterns (Figure 14) were examined further. Since drought impact inspection was based on phenology and productivity indices derived from MODIS time series, all Landsat-based spatial representations were converted into MODIS-like footprints. Analyses ensured a detailed insight into forest variability under meteorological stress condition as well as assessed capability of Landsat data for vegetation status studies in a complex alpine region. Moreover, a comparison with MODIS results shed some light on capacity of both data sources.

5.6.1. S-mode PCA of Landsat time series

The four PCs resulting from the correlation-matrix based S-mode PCA of the $_{L}$NDVI and $_{L}$NBRI time series were recognized as related to the scPDSI approximated meteorological variability of drought (Figure 23). In order to match the temporal resolution of Landsat PCs, scPDSI profiles were averaged into yearly values, which inhibited perception of the intra-annual weather variability. Possible disparity could originate from a fact that all scPDSI values within a given year were used to calculate mean yearly score, whereas Landsat images adopted for the compositing process were restricted to the June-September annual time-window. On the other hand, vegetation growth is strongly governed by the weather conditions prior to the summer period coincided with acquisition of used Landsat scenes. Since scPDSI PCs showed narrow intra-annual, seasonal-dependent variability, used approximation could not undermine aptness of the comparison.

The $_{L}$NDVI derived PCs focused on forest 'greenness' status. The 1COR$_{L}$NDVI highlighted high score for 2001-2002, deteriorated values in 2003 and 2004, and a strong isolated peak in 2008 (Figure 23A). All three were in line with consecutive meteorological events of elevated rainfall sums observed in central Europe in 2002 (Eqecat, 2002), the 2003 heat-wave conditions (e.g Rebetez *et al.*, 2006) and the impact of 'Emma' cyclone in 2008. On the other hand, the 2COR$_{L}$NDVI depicted steady increase of the forest status (Figure 23B) with a small positive anomaly in 2008. Although in contrast with the recognized by Auer *et al.* (2007) regional drying tendencies, the response reflected results of the 3COVnNDVI$_{8\text{-}18}$ score from the MODIS oriented analyses (Chapter 4).

Alike for the $_{L}$NDVI PCA results, the $_{L}$NBRI based decomposition revealed a potential physical meaning in the two first principal components. Since the NBRI index approximates plant foliage water content, emerging PCs demonstrated higher correlation with the scPDSI profiles (Table 37). The 1COR$_{L}$NBRI score demonstrated a monotonous increasing/decreasing tendency which strongly contrasted/followed (depending on the assumed phase of the signal) the 4scPDSI. Although the $_{L}$NBRI decrease was in accordance with some global and regional trends (Auer *et al.*, 2007), both tendencies were assumed a possible vegetation development scenarios. This decision was supported by analyses performed for the MODIS time series (Chapter 4). Finally, the 2COR$_{L}$NBRI PC depicted deteriorate index between 2003 and 2007

followed by a positive anomaly in 2008, which mirrored not only the 1scPDSI pattern, but also findings of Ivits *et al.* (2014).

Despite restricted temporal resolution as well as spatial coverage, both Landsat-derived time series enabled identification of sound temporal patterns, which were strongly related to the local and continental meteorological variability, hence stood for potential forest response to observed drought conditions.

5.6.2. MODIS-like dataset modeled on Landsat derived spatial representations

Conversion of four spatial representations of Landsat derived forest drought impact responses into MODIS-like footprints was essential for further analyses using MODIS-based phenology and productivity information as well as direct comparison with MODIS results. The transformation employed MODIS PSF model adjusted to work on 30 m resolution scenes and integrated additional spatial aggregation conditions, which aimed to increase convolution accuracy and exclude regions with limited spatial representation. The convolution was performed directly on PCs correlation footprints with no p-value threshold, as this additional condition would severely limit available data, hence obscure spatial understanding of results.

Because the main purpose of the analysis was not to model MODIS-like dataset based on Landsat scenes, but to inspect capacity of Landsat data for detection of drought impact on forest stands, it was more appropriate to convert Landsat-derived PCs impact footprints to MODIS resolution, than to model MODIS time series using Landsat acquisitions, and then determine drought vegetation response using PCA. Moreover, the former concept is loaded with smaller statistical uncertainty, in some cases is assumed as linear (Liang, 2004, chap. 12.3.1) and produces smaller statistical errors (Jarihani *et al.*, 2014).

Although Landsat footprints upscaled to 250 m preserved original spatial distribution, emerging geographical patterns of 'synthetic' correlation values (Table 38 vs. Table 40) were somewhat altered comparing with the original Landsat impact maps (Appendix 8 vs. Appendix 9). Moreover, environmental characteristics of PCs' response classes were further modified due to the rescaling of the forest type, elevation, aspect and slope datasets (Table 39 vs. Table 41). This shows how the resolution adjustment impacts the environmental feature of the study site and blurs analysis results, which is especially striking for complex and diverse region, such as the Alps. On the other hand, spatial generalization is unavoidable in synthesis-oriented studies, but should be handled with care and understanding.

Since the PSF-based conversion was run under spatially limited coverage of the forest mask, accuracy of results could be questioned due to not always complete PSF-kernel coverage. This particular aspect was addressed by the thresholds set for the entire kernel and its core. The kernel's core 80% cut-off value presented a good compromise between reliable outcome and consistent coverage. Because the area outside the kernel's-core accounts on less than 40% of the PSF signal, the 50% criterion was chosen to allow on reliable estimation, but without severe restriction on a spatial extend of a final result. In other words, synthetic MODIS-like pixel was modeled using minimum 68% of its potential signal, where 48% originated from the core area.

Although, both values were selected based on an 'expert's judgment' and were not supported by any additional analysis, they ensured reasonable compromise.

The MODIS PSF governed impact of non-forest regions on MODIS pixels within the forest mask was ignored.

5.6.3. Forest vegetation response to drought

Four Landsat derived spatial representations of drought forest impact upscaled to the MODIS resolution were further analyzed using the time series of phenology and productivity indicators. A comprehensive identification and understanding of changes was ensured through repeated ANOVA measures.

5.6.3.1. $1COR_{L250}NDVI$ spatial pattern

Regions coincident with the $1COR_{L}NDVI$ PC (Figure 23A) showing a $_{L}NDVI$ decrease in 2003 with a following incline peaked in 2008 were represented in the $1COR_{L250}NDVI$ spatial pattern by class 6. They were located mostly in the central part of South Tyrol, at medium elevations of the Eisack and Etschtal Valleys slopes (Figure 30). A primary habitat of these locations accounts on Sessile Oak, Downy Oak, Hop Hornbeam, Manna Ash and Sweet Chestnut with Norway Spruce, Common Beech as well as Scots Pine growing in the driest places. Although an initial response to the inception of drought condition was negative for these forest stands, presumably due to wilting, an overall productivity rise was observed from 2004 onwards. The strongest increase of seasonal growth and a steady SBD decline was noted on south facing locations. This observation can be explained by the forest structure dominated by hardwood species that are better adjusted to arid conditions and outperform coniferous trees growth (Scherrer *et al.*, 2011; Rigling *et al.*, 2013). Although the earlier vegetation start is presumably not connected to drought conditions (Swidrak *et al.*, 2013), analogus observations were made at other alpine sites (EEA, 2009; Theurillat & Guisan, 2001), as well as on the continental scale (Ahas *et al.*, 2002) and are being linked with climate change (IPCC, 2013).

The $_{L}NDVI$ decreasing response marked by the $1COR_{L250}NDVI$ impact class 1 related mainly to Norway Spruce and European Larch of subalpine and alpine forest formations growing in the Vinschgau, Wipp and Puster valleys (Figure 30). Phenology development revealed here diminished gross productivity paired with rising CF that showed two strong local maxima in 2003 and 2009. Both peaks were detected one year after wet years of 2002 and 2008. This suggests that combined temperature increase and moisture supply present in rich silt and carbonate soils prompted trees growth (Castagneri *et al.*, 2014), but was soon halted by running out water supplies, which is in line with findings of Theurillat & Guisan (2001) and Jump & Penuelas (2005). Importantly, regardless CF rise, GPP decline suggests forest structural changes with depleting permanent vegetation fraction.

Despite demonstrated meteorological aridity, both inspected response classes reported increasing $NDII7_{HS}$ (Figure 30).

5.6.3.2. $2COR_{L250}NDVI$ spatial pattern

Forest variability recognized using the $2COR_{L}NDVI$ PC (Figure 23B) and related to its increasing (class 6) and decreasing (class 1) patterns, demonstrated mutually similar phenology and productivity changes (Figure 32). Both showed an abrupt $NDII7_{HS}$ decrease in 2003, with a steady envelope rise, briefly interrupted in 2007 and 2011. Although an intense drop was also detected for both response classes in $NDVI_{HS}$, class 1 revealed much stronger decrease of forest 'greenness' between 2001 and 2007. On the contrary, class 6 demonstrated lower $NDVI_{HS}$ between 2001 and 2007, with two negative anomalies in 2003 and 2007, and elevated scores beyound 2008. Regions characterized by PC increase were associated with alpine and subalpine stands, located sparsely along the Eisack and Puster Valleys as well as at a crossing of the Vinschgau and Etschtal regions (Figure 32). Species structure consists there mainly of Norway Spruce and Silver Fir as well as European Larch, Scots Pine and Arolla Pine trees growing on more arid sites and forming the upper forest line. On the contrary, a decreasing $_{L}NDVI$ tendency, identified due to massive 2001-2007 $NDVI_{HS}$ decline, was revealed in the central part of South Tyrol, the Vinschgau Valley as well as Wipp region (Figure 32). It highlighted mainly coniferous forest of Norway Spruce and Silver Fir, with essential share of mixed and broadleaved stands with Downy Oak and Manna Ash near the valley floor. Moreover the response indicated the Eisack and Etschtal Valleys where woodland structure comprises Downy Oak, Sessile Oak, Hop Hornbeam, Manna Ash and Sweet Chestnut, substituted on more arid locations by Common Beech.

Observed accordance of phenology and productivity changes within both classes is surprising regarding differences in abovementioned species structure. However, since share of hardwood and mixed stands within class 1 was less than 18% and 9,5% respectively (Table 41), an impact of broadleaved-specific on mean phenology response could be suppressed. Although 2003 brought $NDVI_{HS}$ and $NDII7_{HS}$ drop, productivity reported for this year was elevated comparing with 2002. Even higher scores were observed in 2004, when only GPP within class 1 revealed decline between 2003 and 2006, suggesting potential change in forest stand structure. Moreover, another, even stronger, CF increase was detected in 2008-2009, but this time was not reflected in GPP, neither SI. The observed productivity rise can be explained by a short-lived combined impact of elevated temperature and excess of soil moisture after rainy 2002 and 2008. Especially the former stimulates temperature governed vegetation growth at high elevations (Theurillat & Guisan, 2001; Jolly *et al.*, 2005; Primicia *et al.*, 2015). However, prolonged dry spell soon depleted moisture accessibility and leaded to decline of vegetation status for 2005-2007. Unfortunately, the depicted positive feedback is representative only for coniferous forest at high altitudes and leaves unresolved decreasing phenology of broadleaved and mixed stands growing near valleys floors. Because hardwood tree species are anticipated to take advantage of increasing aridity (Hanewinkel *et al.*, 2013; Zimmermann *et al.*, 2013b), it is assumed that coniferous-specific response dominated the overall signal.

Interestingly, despite scPDSI suggested arising aridity, strong increasing trend in $NDII7_{HS}$, and less dominant linear tendencies of productivity rise were depicted.

5.6.3.3. $1COR_{L250}$NBRI spatial pattern

In spite of the increasing aridity thread (Auer et al., 2005) supported by the local scPDSI tendencies (Figure 14), ANOVA run for the $1COR_{L250}$NDVI spatial representation of the $1COR_{L}$NBRI PC (Figure 23C) suggested within response class 6 increasing vegetation water capacity. The recognized $_{L}$NBRI rise was observed in the central part of South Tyrol in mixed stands of Sessile Oak, Downy Oak, Sweet Chestnut and Norway Spruce as well as in Vinschgau, where forest structure was represented by Norway Spruce, European Larch and Arolla Pine trees. Although the $NDII7_{HS}$ demonstrated an overall intense increase, $NDVI_{HS}$ indicated diminished greenness between 2003 and 2007, with elevated scores only since 2008. Despite suppressed $NDVI_{HS}$ and $NDII7_{HS}$, CF in 2003 was strongly elevated. A similar brief productivity increase was observed also in 2008-2009. Both can be explained by a short-term beneficial combination of moisture excess and reduced temperature gradient limitations (Jolly *et al.*, 2005; Primicia *et al.*, 2015) that stimulated growth of coniferous stands (Figure A11 3).

A comparable, although statistically less certain, response of the $1COR_{L250}$NBRI impact class 1 was observed for coniferous forests in Vinschgau Valley as well as coniferous and mixed woodland of the central part of South Tyrol (Figure 34). Tree species recognition indicated here Norway Spruce, Common Beech, Down Oak, Scots Pine and European Larch presence. Interestingly, despite the suggested $_{L}$NBRI decrease, $NDII7_{HS}$ revealed deteriorated scores only between 2003 and 2007 with rising values from 2008 onward. This variability was accompanied by an intense $NDVI_{HS}$ decrease culminated in strong anomaly in 2007. Remaining phenological indices showed temporal profiles being in accordance with class 6. Moderate differences were spotted for CF and GPP. Although seasonal productivity measure followed described above pattern of elevated growth in 2003 and 2008-2009, observed changes were smaller comparing with class 6. Also in this case CF increase was attributed on reduction of temperature imposed growth limitations (Jolly *et al.*, 2005; Primicia *et al.*, 2015). Noticeably, although initially higher, GPP observed within class 1 showed gradual decrease until 2010, which implies decreasing permanent vegetation fraction hence also alternation of forest structure.

5.6.3.4. $2COR_{L250}$NBRI spatial pattern

The $2COR_{L}$NBRI PC rigidly followed the 1scPDSI temporal pattern, and depicted $_{L}$NBRI decrease between 2003 and 2007 (Figure 23D). Forest stands being the most prone to this temporal variability grow at medium and low elevation in the Eisack and Etschtal Valleys (Figure 36), where species distribution accounts on Downy Oak, Sessile Oak, Common Beech, Sweet Chestnut, Hop Hornbeam and Manna Ash, with addition of Norway Spruce, Scots Pine and European Larch on the north as well as higher elevations. Initial response to the dry spell accounted on productivity decrease in 2003, where CF showed the strongest, while GPP the smallest drop. Given that the hardwood tree species compose a substantial part of discussed forest, depicted drop could be attributed on leaves wilting. The productivity increase in the following years is potentially resulting from a better adaptation to drought conditions. Interesting is also GPP decreases in 2005-2006 that not reflected in CF, suggests depleted permanent vegetation fraction represented by evergreen vegetation, as well as even a potential

transition between needle leaved and hardwood species (Bigler *et al.*, 2006; Rigling *et al.*, 2013). The overall CF increase until 2009 with leveled GPP imply expanding broadleaved species productivity governed by temperature increase (Hanewinkel *et al.*, 2013; Rigling *et al.*, 2013; Zimmermann *et al.*, 2013b). Although earlier vegetation onset, is not directly related to drought conditions (Swidrak *et al.*, 2013) elevated temperature could accelerated the shift, which was particularly apparent for coniferous stands (Figure A11 4) and is often accounted on climate changes (IPCC, 2013).

A response contrasting with the $2COR_{L}NBRI$ temporal pattern was depicted in the $2COR_{L250}NBRI$ impact class 1 and exposed various sites placed in majority in the Vinschgau, Puster and Wipp Valleys (Figure 36). Highlighted forest formations belong to the subalpine vegetation zone and comprise mainly Norway Spruce, European Larch and Arolla Pine, where the two latter are especially common in the Vinschgau region. The reported $NDII7_{HS}$ increase coupled with the $NDVI_{HS}$ decrease is noteworthy and could refer to possible vegetation transfer processes, which is further supported by simultaneously decreasing GPP. Independently, CF demonstrated strong dynamism in 2003 and 2009, likely explained by a catalytic effect of elevated temperature and soil moisture surplus from 2002 and 2008, on coniferous trees growth at higher altitudes (Jolly *et al.*, 2005; Coppola *et al.*, 2012; Primicia *et al.*, 2015). A CF enhancement noted one year after wet years demonstrates a lagged physiological relation of trees growth and status to meteorological conditions.

5.6.3.5. Drought impact within elevation, slope, aspect and forest type

Among all factors, elevation demonstrated the strongest impact on phenology and productivity within four Landsat based drought patterns (Table 43, Table 47, Table 51 and Table 55). GPP revealed the most robust altitudinal-dependent diversification, whereas SL was the least influenced indicator. CF and $NDVI_{HS}$ showed lower, but still strong relation to elevation zones, with $NDII7_{HS}$ following closely behind. Governance of altitude on SBD was moderate but still clear and significant. Combination of time and elevation factors for the response class 6 regions, implied weak influence on CF (all four spatial patterns), $NDVI_{HS}$ ($1COR_{L250}NDVI$, $2COR_{L250}NDVI$ and $1COR_{L250}NBRI$), as well as $NDII7_{HS}$ ($2COR_{L250}NDVI$, and $2COR_{L250}NBRI$) (Table 45, Table 49, Table 53 and Table 57). Detailed analyses performed for the same areas (Appendix 11) were limited mainly to 700-1400 m asl, and 1400-2100 m asl elevation zones, which was the effect of spatial representation (Table 41). Relying on this restricted information altitude increase promoted CF, but had a reversed relationship to $NDVI_{HS}$, and GPP. SBD and SL showed no clear response pattern. Interestingly, $NDII7_{HS}$ had positive connection to elevation for $1COR_{L250}NDVI$ and $1COR_{L250}NBRI$, but inversed for $2COR_{L250}NDVI$ and $2COR_{L250}NBRI$. A diversification between CF initial drought response was observed among elevation strata, where response of the forest at higher altitudes was in line with observations of Dobbertin *et al.* (2005), Jolly *et al.* (2005), Vacchiano *et al.* (2012), Gebetsroither *et al.* (2013) and Rigling *et al.* (2013).

The factor of aspect demonstrated low overall influence on phenology (Table 43, Table 47, Table 51 and Table 55). F-statistics were the highest for $NDVI_{HS}$, which is presumably attributed on natural species diversity among expositions. These differences were however not supported by CF, GPP nor $NDII7_{HS}$ results. SL was mildly related to aspect, with lower, but still significant results observed for SBD.

Phenology and productivity differences observed within class 6 responses for combined factors of aspect and time were rarely significant (Table 45, Table 49, Table 53 and Table 57). Very limited relation was observed for $NDII7_{HS}$ ($1COR_{L250}NDVI$ and $2COR_{L250}NBRI$), $NDVI_{HS}$ ($1COR_{L250}NDVI$ and $2COR_{L250}NBRI$), as well as CF ($1COR_{L250}NDVI$). According to marginal means analyses done within class 6 responses, south exposed regions tend to reveal lower $NDVI_{HS}$ and $NDII7_{HS}$ coupled with the highest CF and the latest vegetation onset (Appendix 11). A disparity between north and south exposed forest stands were usually apparent which is in line with Rigling *et al.* (2013) and Lévesque *et al.* (2014). Moreover, SBD observed within north facing areas in the $1COR_{L250}NDVI$, $1COR_{L250}NBRI$ and $2COR_{L250}NBRI$ responses revealed between 2003 and 2004/2005 a prompt shift towards earlier vegetation onset. Apparently, neither GPP nor SI indicated alike variability among aspect classes.

Inclination governed the strongest relation with $NDII7_{HS}$ and $NDVI_{HS}$, which reflected also on GPP (Table 43, Table 47, Table 51 and Table 55). Among the remaining phenology and productivity indices, only SL demonstrated a significant but limited influence of slope. CF and SBD variability showed no relation to inclination. Despite this, CF demonstrated significant, but scarcely meaningful diversification for the combination of slope and time factors for the $1COR_{L250}NDVI$ and $2COR_{L250}NBRI$ class 6 responses (Table 45 and Table 57). Furthermore, the same factors' combination was relevant for $NDVI_{HS}$ and $NDII7_{HS}$ observed within the class 6 associated areas of the $2COR_{L250}NDVI$ and $2COR_{L250}NBRI$ footprints (Table 49 and Table 57). Precise insight into this variability assured through marginal means (Appendix 11) showed limited differences between phenology of inclination levels.

Not surprisingly, forest type demonstrated the highest control over CF and $NDVI_{HS}$ (Table 43, Table 47, Table 51 and Table 55). Moreover, SBD also revealed moderate influence of forest structure. No other phenology or productivity measure showed significant relation to forest type, which is unexpected with respect to anticipated GPP disparity. Drought affected sites (class 6 responses) showed no significant changes for a combination of forest type and time, but for CF within the $1COR_{L250}NDVI$ footprint (Table 45). This observation was further supported by the marginal means calculated for this area, where a clear diversification between coniferous and broadleaved-mixed stands was observed (Figure A11 1). Interestingly, needle-leaved forest formations demonstrated the highest CF values for the $1COR_{L250}NDVI$ and $2COR_{L250}NBRI$ class 6 spatial representations. Coniferous stands shown usually the lowest $NDVI_{HS}$ and $NDII7_{HS}$, but a distinction among forest types was not always apparent. Despite insignificant statistics for the whole region, GPP analyzed only within class 6 revealed a good separation.

The most distinguish differences between temporal profiles of phenology and productivity indices derived for each drought impact response, and dissolved into diverse factors levels, were usually noticeable before 2008, with more mutually alike responses afterwards. This indicates diverse responses and adaptation strategies to prolonged drought spell governed by the local environment (Pasho *et al.*, 2011; Scherrer *et al.*, 2011; Rigling *et al.*, 2013).

5.6.4. General remarks on Landsat derived forest drought response

All four identified Landsat based principal components revealed sound and physically probable temporal patterns. Remarkably, each remotely sensed index depicted two alike temporal behaviors of decreasing/increasing long-term tendency supported by 3scPDSI and 4scPDSI ($2COR_{L}$NDVI and $1COR_{L}$NBRI) as well as drought induced diminished scores followed by a 2008 positive anomaly, which is in accordance to the 1scPDSI ($1COR_{L}$NDVI and $2COR_{L}$NBRI). Further analyses revealed that the former are more statistically sound when interpreted as an increment in forest condition. In addition to similarity of PCs, also their footprints and MODIS-scale representations bear considerable similarity to one another (Appendix 9; Figure 30 and Figure 37, Figure 32 and Figure 34).

While $2COR_{L250}$NDVI and $1COR_{L250}$NBRI scores demonstrated considerable mutual resemblance with limited phenology and productivity differences between drought impact classes 1 and 6 (Figure 33 and Figure 35), $1COR_{L250}$NDVI and $2COR_{L250}$NBRI revealed sound disparity between two extreme drought classes (Figure 32 and Figure 37). Furthermore, responses of two latter patterns were found in accord with each other. This diversification was governed mainly by species distribution within identified drought responses. The $1COR_{L250}$NDVI drought impact class 6 and $2COR_{L250}$NBRI class 6 indicated forest sites located in the central part of South Tyrol (Figure 30 and Figure 37) and composed of all three forest types with significant share of hardwood species such as: Sessile Oak, Downy Oak, Common Beech, Hop Hornbeam, Manna Ash and Sweet Chestnut. An analogy in the space distribution transfers into affinity of phenology and productivity responses registered for both drought representations. The common pattern indicated an overall $NDII7_{HS}$ increase, a $NDVI_{HS}$ depression between 2003 and 2007, sound and statistically significant CF and GPP increases as well as 2002-2007 tendencies for earlier vegetation onset. At first, these finding seems to be in strong contradiction with climate-oriented projections suggesting progressing aridity (Auer *et al.*, 2007). However, species composition of discussed sites comprises stenothermal tree species, that according to Hanewinkel *et al.*, (2013) and Zimmermann *et al.* (2013a) benefit from increasing temperature and adapt to aridity, and in the long way run will substitute dying out coniferous woodland. Consequently, observed temporal variability renders local response to alternation of climate conditions, where hardwood trees demonstrate increasing productivity. On the contrary, both class 6 responses of the $2COR_{L250}$NDVI and $1COR_{L250}$NBRI, as well as $1COR_{L250}$NDVI class 1 and $2COR_{L250}$NBRI class 1 regions highlighted Norway Spruce, European Larch, Scots Pine and Arolla Pine habitats. Recognized vegetation variability accounted on deteriorated $NDVI_{HS}$, dynamic but rather leveled SBD, SL and GPP scores, as well as increasing modulate CF response with two local maxima in 2003 and 2009. Although $NDII7_{HS}$ showed always moderate values between 2002 and 2007, the following years revealed an intense index increase, which translated into exceptional an overall increasing trend. As showen, coniferous trees adopted diverse from hardwood species response to raised aridity in South Tyrol. Observed long-term $_{L}$NDVI and $_{L}$NBRI changes suggested vegetation status decline, which was however only partly confirmed by forest phenology and productivity. On the one hand, this resistance, can be somewhat attributed on allocation of aforementioned coniferous species on more favorable, shaded and fertile locations. On the other hand, as Norway

Spruce under a dry spell tend to decrease crown density and status (Bréda & Badeau, 2008), a response from forest floor can potentially corrupt remotely sensed signal. Moreover, unlike productivity bust, negative drought impact can occur even several years after a drought stress event (Bigler *et al.*, 2006), therefore it is probable that consequences of the 2003-2007 drought spell in South Tyrol are still not recognized fully.

Next to the long-term trends, a site- and index-specific variability was detected. Regardless the drought pattern nor impact class, all inspected $NDVI_{HS}$ and $NDII7_{HS}$ temporal profiles emphasize three local minima in 2003, 2007 and 2011, as well as an abrupt and strong peak in 2008 (Figure 31, Figure 33, Figure 35 and Figure 37). It is out of a question the 2003 decline is related to the pan-European heat wave (e.g. Rebetez *et al.*, 2006) and was also depicted by the scPDSI analysis (Chapter 3). The 2007 response harmonizes in South Tyrol with extremely hot conditions during spring and summer 2007 that could be associated with a drought event observed that year in central Europe (EEA, 2012). Although 2006 is considered in Europe also a summer heat wave year (e.g. Rebetez *et al.*, 2008) forest $NDVI_{HS}$ and $NDII7_{HS}$ suffered then less comparing with 2007, when extreme temperatures were reported much earlier in the year. Subsequently, the 2011 drop resulted from extremely hot beginning of September, followed by exceptionally reach in precipitation second half of the month (Hydrographic Office of the Autonomous Province of Bolzano-Südtirol, 2011). Although both records balanced well in the scPDSI, above normal temperatures advanced senescence and depleted vegetation condition. Vegetation surplus dated on 2008 is clearly governed by a rainy and warm summer resulted from the 'Emma' cyclone impact and is the most compelling in the $NDVI_{HS}$ response.

Remarkably, phenology and productivity indicators did not always follow the $NDVI_{HS}$ and $NDII7_{HS}$ scores, or reacted with a certain delay, which is, among others, a result of vegetation resistance and growth strategies (Scherrer *et al.*, 2011). CF response to the 2003 heatwave revealed instantly diminished productivity for $1COR_{L250}NDVI$ and $2COR_{L250}NBRI$ class 6 regions. Conversely, sites associated with class 1 as well as both strata within the $2COR_{L250}NDVI$ and $1COR_{L250}NBRI$ pattern revealed relevant CF increase. This disparity arises most probably from altitudinal allocation of sites where vegetation growth at lower elevations is constrained by precipitation, while the higher regions are limited by temperature (Theurillat & Guisan, 2001; Castagneri *et al.*, 2014). Consequently, the overall temperature increase and precipitation decrease stressed vegetation in valley floors and on lower slopes (Gebetsroither *et al.*, 2013) but stimulated phenology at higher altitudes (Jolly *et al.*, 2005). However, under prolonged dry-spell conditions, species specific resistance and adaptation strategies started to govern forest response, with hardwood species showing an enhance growth rate (Hanewinkel *et al.*, 2013; Zimmermann *et al.*, 2013b).

Delay was also observed in phenology response to moist spring and summer of 2008. Although the $NDVI_{HS}$ and $NDII7_{HS}$ noted immediate rise which was reflected also in the CF productivity, the superior growth conditions including GPP increase, were observed in 2009, which is in line with observations of Lévesque *et al.* (2014).

Interestingly, CF, GPP and SL depicted in 2010 a decrease, which was not supported in the corresponding $NDVI_{HS}$ and $NDII7_{HS}$ temporal profiles. A possible explanation of the phenomena can be attributed on late SBD. Although the weather conditions during

the spring 2010 were good, April 14th brought an eruption of Eyjafjallajökull. Exhaust ashes that contaminated for the following weeks the atmosphere over Europe (Pappalardo *et al.*, 2013) were likely to affect the NDVI composites, resulting in falsely late vegetation onset. Moreover, this anomaly was frequently coupled with delayed SBD in 2008 and 2009, as well as GPP decline (1COR$_L$NDVI class 1, 2COR$_L$NDVI class 1 and 6, 1COR$_L$NBRI class 1 and 6, and 2COR$_L$NBRI class 1). Since aforementioned regions are characterized in majority by coniferous stands growing at higher elevation, it is likely that depicted variability originated from lower temperature conditions and restoration of growth restrictions of temperature gradient. However more advanced investigation is required to fully support this hypothesis.

Although four considered environmental factors combined with time revealed a weak or insignificant effect on forest phenology within regions of drought impact class 6, observed trends and relations suggest direct and indirect influence of elevation, aspect, slope and forest type on stands productivity. The most robust, but not linear differences between considered levels were noted for elevation. This observation is in line with anticipated influence of the elevation gradient, temperature-moisture balance (Affolter *et al.*, 2009), vegetation belts as well as emerging species distribution and their impact on forest productivity (Pellerin *et al.*, 2012). A diversification of response within sites of different exposition was also recognized rather positively, with particularly strong CF differences between the south and north facing regions. This behavior was already reported in some drought related examinations (e.g. Dobbertin *et al.*, 2005; Vacchiano *et al.*, 2012; Rigling *et al.*, 2013). Slope showed the smallest contrast between strata. Interestingly, regions with the lowest inclination not always demonstrated the highest productivity indicators. Forest type, although was expected to be the strongest cause of phenology and productivity diversification among sites, revealed mild or even limited differences between coniferous, mixed and broadleaved woodland.

In the light of the progressing aridity thread (Auer *et al.*, 2007) and confirmed precipitation rainfall decrease (Chapter 3) robust and statistically significant NDII7$_{HS}$ increase noted within all identified patterns and drought impact classes is unexpected. Interestingly, corresponding NDVI$_{HS}$ temporal responses do not reveal alike tendencies, suggesting either reverse trends or highlighting the 2003-2007 decrease. A long trend perception can be however influenced by indices increase in 2008 and high NDVI$_{HS}$ and NDII7$_{HS}$ values observed in 2012. The other cause of NDII7$_{HS}$ increase could originates from the sensor degradation adjustment (Wang *et al.*, 2012), but is unlikely since the NDVI$_{HS}$ demonstrated no increasing trend.

Taking together, the 1COR$_L$NDVI and 2COR$_L$NBRI and their derivative footprints 1COR$_{L250}$NDVI and 2COR$_{L250}$NBRI shed some more light on complexity of drought related weather variability in the alpine forest.

5.6.5. Utility of Landsat time series for investigation of vegetation drought stress in the Alps, and further comments

The main hindrance in the drought related forest monitoring in South Tyrol between 2001 and 2011 was a restricted amount of Landsat data. Although the study incorporated all available 192-028 and 192-027 scenes acquired between June and September with a maximum cloud cover of 80% (24 and 23 datasets respectively) and

even used tiles overlap, intra-annual vegetation analyses were beyond any means. Furthermore derived yearly composites still presented incomplete coverage of the province. As a result, the entire 2001-2011 Landsat time series of yearly composites was available for only 42% of the forested area in South Tyrol. Consequently, although the S-mode PCA returned four reliable temporal profiles of vegetation development, those responses represent only a portion of the South Tyrolean woodland, and will change with an increased data coverage.

Although time series of yearly observations can approximate vegetation trends in a long time series of data, or capture main or well-timed short-term changes, they are limited in addressing intra-annual growth variability governed by seasonal extreme weather events. Despite the fact that the extensive data preprocessing with a specific impact put on the data normalization between acquisitions was conducted, reflectance value could still be a function of acquisition day and vegetation development phase, which obviously corrupts time series interpretation. This is not an issue while analyzing a time series comprising bigger amount of scenes registered at comparable time, or with constant intervals along a year.

Despite aforementioned limitations, yearly $_{L}$NDVI and $_{L}$NBRI time series introduced to the S-mode PCA decomposition resulted in robust and physically probable patterns. Furthermore, both indices addressed diverse but complementary forest vegetation variability aspects.

The not questioned asset of the TM and ETM+ data is their spatial resolution of 30 m, which allows on precise identification of landscape features and further detailed investigation. It is particularly desirable in complex and diverse mountainous regions, such as the Alps. On the other hand, restricted data availability induces a need for ancillary information, or fusion with other remote-sensed datasets when a study implies high temporal resolution (Gao *et al.*, 2006; Gao, 2013). In order to provide a deeper understanding of investigated problem, the Landsat analysis was supplemented with the MODIS based 2002-2012 time series of phenology and productivity indicators, as well as 2001-2012 yearly $NDVI_{HS}$ and $NDII7_{HS}$ MODIS derived scores. An imposed need for resampling of the Landsat based results to 250 meters leaded to generalization of the outcomes. Consequently, the analyses were conducted at 250 m resolution, which implies generalization of reference datasets of elevation, aspect, slope and forest type distribution, hence blurs any site-specific response and obstructs detailed interpretation of drought induced forest feedback. The differences between information quality and quantity became particularly clear when comparing original Landsat drought impact patterns with their MODIS-alike equivalents. Furthermore, the design of the fundamental GEOLAND forest mask, additionally resampled to the 250 m resolution, incorporated additional uncertainty and obscured detailed understanding of inspected processes.

Presented results confirm a great capacity of Landsat data for vegetation stress monitoring, however reveal also a burning issue of data scarcity and cloud contamination. Despite a careful design and performance of the compositing process, resulting time series comprises limited information pool. On the other hand, even with restricted annual datasets, a general forest vegetation response to drought weather conditions was successfully detected using the S-mode PCA approach.

Obtained temporal Landsat-based profiles alone provided limited understanding of environmental changes and required ancillary MODIS-based dataset to explore underlying variability. Importantly, this synergy worked out well, but revealed some disparities between the NDVI and NDII7/NBRI responses derived for MODIS and Landsat datasets. The latter can be however attributed on applied compositing method and difference in data acquisition time.

6. SYNTHESIS AND CONCLUSIONS

The main objective of this thesis was to comprehend alpine forest response to drought variability, which is a still unsatisfied demand (Standing Forestry Committee Ad Hoc Working Group III on Climate Change and Forestry, 2010) and a great hindrance not only for the sustainable resource management and silviculture (Schoene & Bernier, 2012), but also for carbon sink efficiency modeling (Ma *et al.*, 2012; He *et al.*, 2014) and resulting climate change scenarios (Bonan, 2008).

The study was conducted for the alpine region of South Tyrol and accounted on a coupling between the 2001-2012 scPDSI defined weather variability and coinciding forest condition investigated with the NDVI and NDII7/NBRI MODIS and Landsat derived time series. The S-mode PCA decomposition was proposed and evaluated as a versatile approach for remote-sensed time series analysis, and a robust method for identification of dominant temporal changes in forest status.

Performed analyses not only produced detailed information on meteorology induced drought condition in the region, but also identified aridity affected forest sites and ensured extensive insight on resultant forest productivity and phenology changes. The utility of MODIS and Landsat data for alpine forest status monitoring was evaluated, the same as functionality and efficiency of the S-mode PCA approach. Presented results shed light on diversity and complexity of the alpine mountain forest in South Tyrol, providing a detailed insight into the ongoing long- to medium-term changes as well as, shorter stress-induced alternation of forest status.

6.1. Drought conditions in South Tyrol and associated forest stress responses

The scPDSI-based weather variability in South Tyrol was characterized by heavily diminished moisture conditions between 2003 and 2007 as well as progressing aridity trend initiated by the 2003 summer heatwave. Both responses are not only in strong accordance with other studies conducted at a global and local scale, but also confirm intense drought impact in the region. Moreover, on top of these general weather tendencies, a regional diversification of weather conditions was identified, where sites located at low altitudes in the central part of South Tyrol experience the most severe and prolonged drought impact, whereas the Vinschgau Valley is reported to be relatively the least affected by arising aridity. Both observations are confirmed by other, independent studies. Unfortunately, due to a limited number of meteorological stations as well as their restricted spatial location, no compelling conclusions were drawn neither on elevation impact on drought strength and evolution, nor possible alternation of the temperature and precipitation gradients.

Meteorology-governed forest status was identified by the S-mode PCA performed on the NDVI and NDII7/NBRI time series derived from MODIS and Landsat datasets. Although processed independently, both approaches highlighted related leading temporal variability of forest status, which beside a direct reference to the scPDSI weather related information, accounted also on vegetation resistance and adaptation strategies to the percept water stress.

Even though, the progressing aridity pattern was recognized in the $3COVnNDVI_{8\text{-}18}$, $2COR_{L}NDVI$ and $1COR_{L}NBRI$ PCs observed changes suggested increasing productivity, and alternation in the forest structure. PC that followed the 1scPDSI

meteorological changeability (namely: $4COVnNDII7_{8\text{-}18}$, $1COR_LNDVI$ and $2COR_LNBRI$) also suggested rise in forest status, but in all the cases improvement was smaller and steadier in its tendency. Furthermore, areas associated with the inversed forest response revealed decrease in GPP and strong CF variability.

Identified changes in forest status vary between diverse environment characteristics and most importantly tree species structure. Moreover, drought stress conditions intensified pre-existing differences among regions and local environmental factors id est. exposition, forest types and elevation.

Even though, each identified principal component embraced unique conditions of the forest of South Tyrol, a considerable overleap among responses and resulting footprints was identified. Despite apparent simplicity, they provided insight into complex variability of the alpine forest. Given no local ground-truth information, observed phenology and productivity changes were related to other studies and known forest drought responses. Irrespectively of considerable disparity between tree/trees community scale of referred surveys, and stand/region scale of this study, identified patterns fit well to observations made at other sites. The following drought feedback responses were singled out:

- influence of the elevation gradient on vegetation growth, where plants at higher altitudes are limited by temperature, while phenology of lower placed regions is subjected to precipitation (Primicia *et al.*, 2015);
- catalytic effect of moisture surplus in 2002 and 2008, combined with elevated temperature that boosted forest productivity in 2003 and 2008-2009 respectively (Theurillat & Guisan, 2001; Jolly *et al.*, 2005; Castagneri *et al.*, 2014);
- persistent aridity conditions of 2003-2007 that drained soil moisture and negatively affected growth of coniferous trees (Coppola *et al.*, 2012; Rigling *et al.*, 2013; Lévesque *et al.*, 2014);
- lower susceplibility of hardwood drought-resistant Mediterranean species to dry conditions (Hanewinkel *et al.*, 2013; Zimmermann *et al.*, 2013a).

Although all aforementioned ensured general explanation of the observed forest variability, it is important to keep in mind the size and complexity of the analyzed area. The orography determines aspect, inclination, insolation, local climate and even soil formation, resulting in variety of site-specific conditions that shape species allocation, trees growth or trees competition. Furthermore, history of local silviculture and natural or artificial character of forest structure as well as, genetic variations on species and population level (Brunner *et al.*, 2015) are also of great importance. These properties become the most critical during stress conditions that sway the natural balance (e.g. Pasho *et al.*, 2011; Scherrer *et al.*, 2011b; Rigling *et al.*, 2013; Lévesque *et al.*, 2014). Consequently, the shown results demonstrate generalized perception of the phenomena. A great diversity of forest ecosystem and drought responses is recognized through disconnected and 'patchy' spatial projections of PCs correlation footprints. Moreover, derived phenology and productivity indices suggest diverse forest formations characterized by various GPP and CF productivity.

In spite of encouraging results, the presented approach has some flaws. Firstly, the scPDSI model does not account on snow retention and snowmelt, potentially providing inaccurate spring moisture conditions. Moreover, merger of temperature and

precipitation into one measure inhibits investigation of their independent influence on trees growth (e.g. Coppola *et al.*, 2012; Castagneri *et al.*, 2014; Lévesque *et al.*, 2014). Secondly, the adopted spatial resolution of 250 m could produce some uncertainty, particularly when analyzing complex and diverse alpine environment. Pixel size determines signal generalization not only in terms of captured forest response, but also environmental features adopted during interpretation of results. Furthermore, frequently low alpine forest canopy closure implies that registered reflectance can originate not only from the top-most stand canopy, but also understory, undergrowth or other background. This naturally corrupts the signal obscuring genuine trees response. On the other hand, adopted remotely sensed datasets reflect only on the top most layer of the forest, usually plant crowns, ensuring approximated, but restricted information of forest condition. Finally, a lack of ground truth data on real forest drought impact or phenology status, disables straightforward verification of the PCA outcomes, and quantitative analyses of forest drought impact. Consequently, time series of phenology and productivity measures are treated as an indicator of relative changes, whereas validation of identified temporal patterns is conducted indirectly against the scPDSI variability and confronted with research published on the topic. In addition satellite data are *pre-se* burden with uncertainty of geolocation, as well as registration and preprocessing-errors.

Nevertheless, considering known studies and climatic projections, presented meteorologically induced forest response is in strong accordance with other published analyses and state of the art. Although the study covers only 11 years, captured long-term tendencies are consistent with trends depicting already ongoing transformation of the alpine environment. Moreover, also more site-specific phenology changes highlighted in the study are supported by observations made by other researchers.

6.2. S-mode PCA decomposition and datasets evaluation

The presented investigation confirms high utility of the PCA for analyses of remote-sensed time series. Identified results are characterized by high physical meaning and ensure comprehensive understanding of drought induced forest response. Moreover, implemented time series truncating to the vegetation-season period combined with the adequate z-score normalization scheme and S-mode PCA setup, allowed to exclude redundant information and target analysis only on relevant portion of data variance. Consequently, although as presented, the PCA can be conducted on diverse datasets, the method requires a deep understanding of processed information and properties of anticipated resulting variability. Despite utterly statistical nature of PCA, the S-mode decomposition allowed on robust identification of desired temporal patterns and associated spatial representations, even when coping with very subtle variance variability.

Despite the fact that the PCA underlying orthogonality assumption can be physically unrealistic, performed secondary rotation did not always improve recognition and understanding of investigated variability. However, the rotation is oriented on identification of simple structures, which is not a genuine characteristic of temporal evolution patterns.

Certainly, the performed relative evaluation of resulting PCA patterns could obscure the actual limitation and inaccuracy of the method, however considering wellness of derived results, potential severe hindrances are at this point imperceptible.

Regardless some limitations (Gao, 1996; Huete *et al.*, 2002) both NDVI and NDII7/NBRI indices provided a reliable estimation of alpine forest condition ensuring detection of subtle changes. While the NDVI focuses on 'greenness' rendering a straightforward canopy status, the NDII7/NBRI addresses plant water content and cell structure. Consequently, NDII7 is correlated with net ecosystem carbon exchange (Cheng *et al.*, 2007), hence provides a better approximation for carbon cycle models. Due to application of the far infrared spectrum range, NDII7/NBRI is insensitive to soil moisture and experiences lower saturation effect (de Beurs & Townsend, 2008). Moreover, according to DeVries *et al.* (2015) application of far infrared signal makes the index more sensitive to regrowth comparing to NDVI. Although Landsat based analyses revealed limited differences between NDVI and NBRI derived results, MODIS founded investigation exposed diverse potential of both measures. Even though, the utility of the NDII7/NBRI could be considered for some applications superior to NDVI, when possible, it is beneficial to apply both measures together, exploiting their divergence and complementary properties.

Because the TM and ETM+ as well as MODIS scanners share considerable similarity in spectral bands ranges, the most distinct and crucial differences between datasets acquired with Landsat and Terra platforms originate from data spatial and temporal resolution. Presented results suggest that despite lower spatial resolution MODIS based analyses provided better identification and understanding of drought affected forest stands. Daily data acquisitions combined in 16-day CV-MVC composites ensure high quality datasets with limited cloud cover contamination, which is especially important for mountainous regions. Moreover, a whole-year observation allows on continuous monitoring, providing data not only on drought induced stress, but also on recovery process. Furthermore, extended time series allows on more realistic inspection as some tree species, such as Common Beech, have a lagged reaction to meteorological changes (Castagneri *et al.*, 2014). In addition, approximately constant interval between datasets enable straightforward modeling of phenology and productivity changes, which, as demonstrated, sheds additional light on the perceived variability.

In spite of extensive data collection and further processing, Landsat obtained results provided only a general overview of the weather and drought governed forest response. Although the Landsat-derived results were in line with the MODIS analyses, limited spatial coverage as well as temporal resolution restricted to only one composition per year, leaded to diminished or even insufficient diversification between inspected indices, identified temporal responses and hence their spatial representations. Moreover, data scarcity disables comprehensive monitoring of a complete vegetation period, excluding important influence of the increasing spring drought risk (Beniston, 2012).

Taking together, MODIS derived NDVI and NDII7 time series showed higher utility for forest drought related studies in the alpine region. The most essential advantage provided by these data is high data quality and temporal resolution, which balance coarse spatial resolution.

6.3. Perspectives

This thesis presents a robust and versatile approach for forest monitoring under weather stress conditions. Observed climate alternation determines constantly increasing need for comprehensive understanding of environmental processes, and improvement in survey techniques and data collection.

Although the demonstrated approach was shown to be successful and the selected datasets provided sufficient scientific input, potential of the approach was not fully exploited, and offers room for improvement. The main issue to be addressed is enhancing of spatial resolution without sacrificing, or even better with an increase in temporal resolution. Drawing from the made experience as well as literature based state of the art, MODIS-Landsat synergy would address this aspect well (e.g. Roy *et al.*, 2008; Hilker *et al.*, 2009; Zhu *et al.*, 2010). However, taking under consideration current status of the Landsat and EOS satellite programs, such solution is not really conclusive for the future. Natural successor in the Landsat enterprise is the Landsat Data Continuity Mission (LDCM; Irons *et al.*, 2012). Despite preserved temporal and spatial resolution LDCM acquired data are no longer a genuine extension of the TM/ETM+ time series as the OLI (Operational Land Imaginer) sensor have a bit different band wavelength configuration. Conversely, MODIS scanner does not have a true follower at the moment. A potential replacement is the Visible Infrared Imaging Radiometer Suite (VIIRS) onboard on Suomi NPP platform, but the sensor provides data with resolution of 375 m, which could be insufficient for the complex alpine environment.

It is out of a question that already initiated Sentinel-2A/-2B missions supplemented by the Sentinel-3A/-3B satellites will provide excellent environmental information source for the alpine forest condition monitoring (Malenovský *et al.*, 2012). Importantly, missions have been planned for at least 15 years of service, which combining with already available Landsat and MODIS archives will assemble extraordinary data collection. In contrast, recently experienced limited amount of high resolution Landsat or Landsat-like acquisitions attributed on Landsat 5 shutdown in 2013 and Landsat 7 SLC failure in 2003, is a serious limitation not only for the further time series analyses, but also current surveys. It hampers a reliable assessment of observed tendencies in a broader perspective of global changes.

Independently of the great outlook for the future remote-sensed forest monitoring, it is important to collect ground truth data and carry out extensive forest campaigns objected on comprehensive investigation of physiological changes triggered or enhanced by dry conditions, including also secondary damages threats. Essentially, field campaigns should address regions of all elevations and multiple tree species. Moreover, surveying should not be limited only to extreme events and stress affected sites, nor regions particularly endangered by climate change, but also collect information on 'normal' forest status and 'typical' woodland. Only reflection on a disparity between regular and extreme conditions provides adequate understanding of trees responses to stress, correct change interpretation, assessment of physiological limits and consequently mitigation and further modeling. However, under revealed ongoing change of global and local climate patterns, normality of meteorological conditions could be very illusive. Furthermore, an additional concern should be given to

monitoring of other forest damages agents, which combined with drought stress can increase trees mortality.

Subsequently, use of additional information on CO_2 levels or more local temperature and precipitation variability, will definitively allow to enhance interpretation of obtained results.

Furthermore, application of other statistical variance oriented approaches remains still open and needs further investigation. Independent Component Analysis (ICA) presents itself as a promising solution, however its primary appealing fundamental restriction of nongaussian distribution of resulting components could be difficult to meet.

Last but not least, it is essential to better implement knowledge established through the environmental research into the policy and decision-making processes at the local, regional and global scale. Only such integrated approach can ensure proper actions and mitigation strategies of the ongoing climate alternation. It is particularly important for unique and already endangered regions such as the Alps.

APPENDIX 1

While considering drought related vegetation stress monitoring the biggest impact is put on the vegetation water content. For this reason, most of relevant indices employ a portion of the 1 µm – 2.5 µm spectrum, which is sensitive to the plant water content. According to Tucker (1980) 1.55-1.75µm range is the best-suited spectral interval for the monitoring plant canopy water status.

Mainly due to multiple monitoring objectives as well as diverse satellite sensor specifications and spectral resolution, vegetation water content oriented indices employ various portions of the infrared spectrum. Unfortunately, it results in some confusion, as the same name can represent ratios with diverse wavelength spectra, or the other way round, the same mathematical equation stands under multiple names. Although this issue was already briefly addressed by Ji et al. (2009) and Yilmaz et al. (2008), the topic deserves further attempt for systematization.

An application of normalized difference between near- and medium-infrared spectra was firstly investigated by Kimes et al. (1981) who used Landsat TM bands 4 and 5 (0.76-0.90 µm and 1.55-1.75 µm respectively) and called the resulting index ND45. Later, this formulation was specified by Hardisky et al. (1983) as a sensor independent relation called Normalized Difference Infrared Index (NDII):

$$\mathrm{NDII} = \frac{\rho 0.85\mu\mathrm{m} - \rho 1.65\mu\mathrm{m}}{\rho 0.85\mu\mathrm{m} + \rho 1.65\mu\mathrm{m}} \qquad [\mathrm{A}\,1]$$

The ratio between NIR and SWIR (or MIR following the Landsat convention) spectral channels presents itself as a robust approximation of vegetation condition and found application in diverse monitoring approaches (e.g. Yilmaz et al., 2008). This recognition resulted in minor, sensor driven differences of applied bandwidth of near and medium infrared bands as well as sometimes also in diverse names. For example, deriving it from Landsat data Jin and Sader (2005) as well as Wilson and Sader (2002) called it Normalized Difference Moisture Index (NDMI). Its MODIS based equivalent (calculated using band 2 (0.841-876 µm) and 6 (1.628-1.652 µm)) is referred to as: Normalized Difference Infrared Index band 6 (NDII6, Rahimzadeh Bajgiran et al., 2009); Normalized Difference Water Index band 6 (NDWI6; Chakraborty and Sehgal, 2010); Normalized Difference Water Index$_{1640}$ (NDWI$_{1640}$; Chen *et al.*, 2005); or Land Surface Water Index (LSWI; Xiao et al., 2005). Moreover, Delbart et al. (2005) applied the same formula to Band 3 (0.78–0.89µm) and SWIR (1.58–1.75µm) of the SPOT VEGETATION sensor, titling it Normalized Difference Water Index (NDWI). The latter name can leads to further confusion.

Because the whole infrared spectrum carries vegetation water content information, also further portions of the electromagnetic spectrum are used in plant condition studies. A good example is MODIS based modification of the original NDII that employs reflectance from Short Wavelength Infrared (SWIR) band 7 instead of band 6 (Xiao *et al.*, 2005; Rahimzadeh Bajgiran *et al.*, 2009; Verbesselt *et al.*, 2009):

$$NDII7 = \frac{\rho 0.86\mu m - \rho 2.2\mu m}{\rho 0.86\mu m + \rho 2.2\mu m} \qquad [\mathrm{A}\,2]$$

Also in this case the index appears under multiple names of: NDII7 (Rahimzadeh Bajgiran *et al.*, 2009), NDII (Verbesselt *et al.*, 2009), NDWI (Gu *et al.*, 2007) or $NDWI_{2130}$ (Chen *et al.*, 2005).

Interestingly, when comparing NDII7 with Landsat based indices, it becomes clear that this relation is known also as Normalized Burn Ratio (NBR; van Wagtendonk et al., 2004) or Normalized Burn Ratio Index (NBRI; Huang et al., 2010).

Another index providing proxy of vegetation status and vegetation water content is formulated by Gao (1996) Normalized Difference Water Index (NDWI):

$$\mathrm{NDWI} = \frac{\rho 0.86\mu\mathrm{m} - \rho 1.24\mu\mathrm{m}}{\rho 0.86\mu\mathrm{m} + \rho 1.24\mu\mathrm{m}} \qquad [A3]$$

Alike NDII, it uses normalized rationing of two infrared bands, taking advantage of their similar scattering properties. Also in this case naming convention differs and for example Chakraborty and Sehgal (2010) who based their study on MODIS data referred to it as NDWI5 (Normalized Difference Water Index band 5).

As previously mentioned, some confusion can arise from the fact that NDWI name is used for indices employing diverse infrared electromagnetic spectrum. Moreover, the same name is applied to indices used for surface water mapping. Although also oriented on water identification, they foster disparate water characteristics basing on combination of infrared and green spectra (Ji *et al.*, 2009).

Because the naming convention of some remote-sensed indices is subjective and can lead to some ambiguity, it is important not to take an index name for granted and always inspect wavelengths employed in the computation.

APPENDIX 2

A.2. Forest condition indicated by PCA

A.2.1. NDVI time series

Full year time series: $NDVI_{1\text{-}23}$, $NDVI_{SG1\text{-}23}$, $nNDVI_{1\text{-}23}$ and $nNDVI_{SG1\text{-}23}$

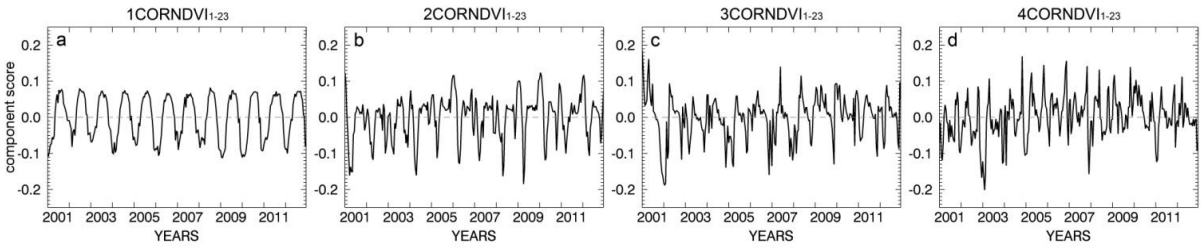

Figure A2 1 First four PCs resulted from the S-mode correlation-matrix based PCA of the $NDVI_{1\text{-}23}$ (full year NDVI) time series, herein: (a) $1CORNDVI_{1\text{-}23}$, (b) $2CORNDVI_{1\text{-}23}$, (c) $3CORNDVI_{1\text{-}23}$ and (d) $4CORNDVI_{1\text{-}23}$. Temporal patterns explained 63.23%, 3.29%, 2.68% and 1.69% of the total $NDVI_{1\text{-}23}$ time series variance respectively.

Table A2 1 Correlation between the scPDSI scores and first four PCs obtained through the S-mode correlation-matrix based PCA of the $NDVI_{1\text{-}23}$ (full year NDVI) time series. Due to inconsistent length of scPDSI and $NDVI_{1\text{-}23}$ datasets all time evolution patterns were converted into yearly average time series.

	$CORNDVI_{1\text{-}23}$			
	1PC	2PC	3PC	4PC
1scPDSI	0.179	0.215	0.664*	-0.205
2scPDSI	-0.268	0.476	-0.112	-0.461
3scPDSI	-0.008	0.584*	-0.460	-0.290
4scPDSI	-0.397	0.215	-0.124	-0.491

* - significant at the level $p<0.05$

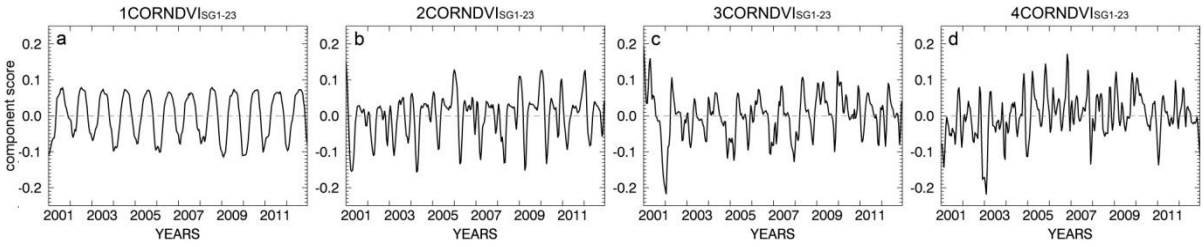

Figure A2 2 First four PCs resulted from the S-mode correlation-matrix based PCA of the $NDVI_{SG1\text{-}23}$ (full year $NDVI_{SG}$) time series, herein: (a) $1CORNDVI_{SG1\text{-}23}$, (b) $2CORNDVI_{SG1\text{-}23}$, (c) $3CORNDVI_{SG1\text{-}23}$ and (d) $4CORNDVI_{SG1\text{-}23}$. Temporal patterns explained 70.86%, 3.51%, 2.71% and 1.77% of the total $NDVI_{SG1\text{-}23}$ time series variance respectively.

Table A2 2 Correlation between the scPDSI scores and first four PCs obtained through the S-mode correlation-matrix based PCA of the $NDVI_{SG1-23}$ (SG filtered full year NDVI) time series. Due to inconsistent length of scPDSI and $NDVI_{SG1-23}$ datasets all time evolution patterns were converted into yearly average time series.

	$CORNDVI_{SG1-23}$			
	1PC	2PC	3PC	4PC
1scPDSI	0.174	0.144	0.644*	-0.279
2scPDSI	-0.268	0.446	-0.113	-0.466
3scPDSI	-0.022	0.620*	-0.444	-0.281
4scPDSI	-0.417	0.197	-0.169	-0.485

* - significant at the level $p<0.05$

Table A2 3 Correlation between corresponding four first PCs derived for correlation-matrix based S-mode PCA of $NDVI_{1-23}$ and $NDVI_{SG1-23}$ datasets

PCs	correlation	p
$1CORNDVI_{1-23}$ vs.$1CORNDVI_{SG1-23}$	0.991	0.000
$2CORNDVI_{1-23}$ vs. $2CORNDVI_{SG1-23}$	0.971	0.000
$3CORNDVI_{1-23}$ vs. $3CORNDVI_{SG1-23}$	0.934	0.000
$4CORNDVI_{1-23}$ vs. $4CORNDVI_{SG1-23}$	0.945	0.000

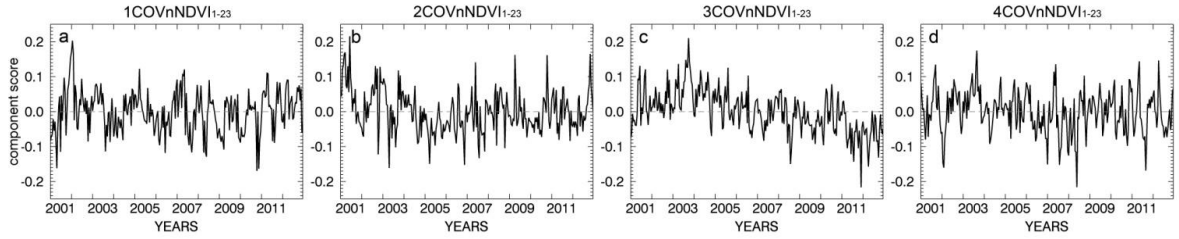

Figure A2 3 First four PCs resulted from the S-mode covariance-matrix based PCA of the $nNDVI_{1-23}$ (z-score normalized full year NDVI) time series, herein: (a) $1COVnNDVI_{1-23}$, (b) $2COVnNDVI_{1-23}$, (c) $3COVnNDVI_{1-23}$ and (d) $4COVnNDVI_{1-23}$. Temporal patterns explained 18.55%, 5.35%, 2.31% and 1.79% of the total $nNDVI_{1-23}$ time series variance respectively.

Table A2 4 Correlation between the scPDSI scores and first four PCs obtained through the S-mode covariance-matrix based PCA of the $nNDVI_{1-23}$ (z-score normalized full year NDVI) time series. Due to inconsistent length of scPDSI and $nNDVI_{1-23}$ datasets all time evolution patterns were converted into yearly average time series.

	$COVnNDVI_{1-23}$			
	1PC	2PC	3PC	4PC
1scPDSI	0.031	-0.712*	0.456	-0.070
2scPDSI	-0.263	-0.517	-0.265	0.181
3scPDSI	0.033	-0.195	-0.731*	0.024
4scPDSI	-0.535	0.278	-0.086	0.414

* - significant at the level $p<0.05$

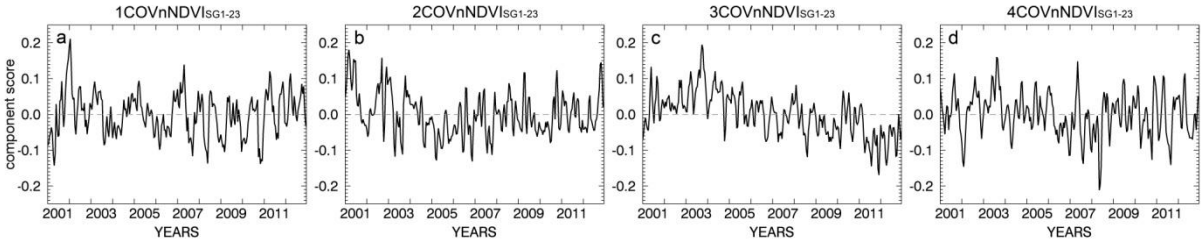

Figure A2 4 First four PCs resulted from the S-mode covariance-matrix based PCA of the $nNDVI_{SG1\text{-}23}$ (z-score normalized full year $NDVI_{SG}$) time series, herein: (a) $1COVnNDVI_{SG1\text{-}23}$, (b) $2COVnNDVI_{SG1\text{-}23}$, (c) $3COVnNDVI_{SG1\text{-}23}$ and (d) $4COVnNDVI_{SG1\text{-}23}$. Temporal patterns explained 22.48%, 6.50%, 3.03% and 2.26% of the total $nNDVI_{SG1\text{-}23}$ time series variance respectively.

Table A2 5 Correlation between the scPDSI scores and first four PCs obtained through the S-mode covariance-matrix based PCA of the $nNDVI_{SG1\text{-}23}$ (z-score normalized full year $NDVI_{SG}$) time series. Due to inconsistent length of scPDSI and $nNDVI_{SG1\text{-}23}$ datasets all time evolution patterns were converted into yearly average time series.

	$COVnNDVI_{SG1\text{-}23}$			
	1PC	2PC	3PC	4PC
1scPDSI	0.098	-0.722*	0.446	0.060
2scPDSI	-0.221	-0.509	-0.273	-0.215
3scPDSI	0.059	-0.141	-0.739*	-0.025
4scPDSI	-0.539	-0.308	-0.127	-0.448

* - significant at the level $p<0.05$

Table A2 6 Correlation based comparison between corresponding four first PCs derived for covariance-matrix based S-mode PCA of $nNDVI_{1\text{-}23}$ and $nNDVI_{SG1\text{-}23}$ datasets

PCs	correlation	p
$1COVnNDVI_{1\text{-}23}$ vs. $1COVnNDVI_{SG1\text{-}23}$	0.867	0.000
$2COVnNDVI_{1\text{-}23}$ vs. $2COVnNDVI_{SG1\text{-}23}$	0.865	0.000
$3COVnNDVI_{1\text{-}23}$ vs. $3COVnNDVI_{SG1\text{-}23}$	0.914	0.000
$4COVnNDVI_{1\text{-}23}$ vs. $4COVnNDVI_{SG1\text{-}23}$	0.883	0.000

Vegetation season time series: $NDVI_{8\text{-}18}$, $NDVI_{SG8\text{-}18}$, $nNDVI_{8\text{-}18}$ and $nNDVI_{SG8\text{-}18}$

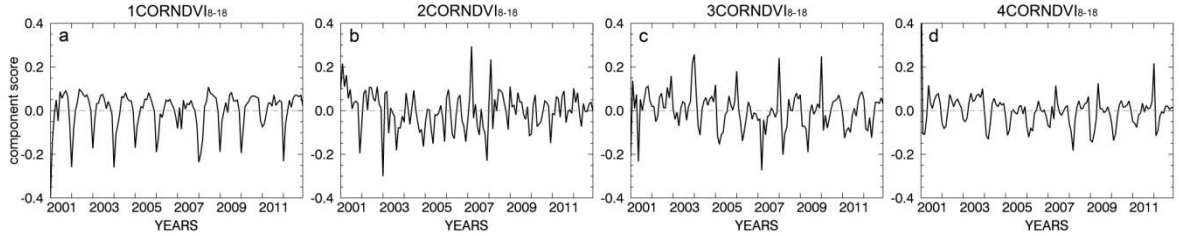

Figure A2 5 First four PCs resulted from the S-mode correlation-matrix based PCA of the $NDVI_{8\text{-}18}$ (vegetation season NDVI) time series, herein: (a) $1CORNDVI_{8\text{-}18}$, (b) $2CORNDVI_{8\text{-}18}$, (c) $3CORNDVI_{8\text{-}18}$ and (d) $4CORNDVI_{8\text{-}18}$. Temporal patterns explained 41.94%, 4.77%, 3.04% and 2.68% of the total $NDVI_{8\text{-}18}$ time series variance respectively.

Table A2 7 Correlation between the scPDSI scores and first four PCs obtained through the S-mode correlation-matrix based PCA of the $NDVI_{8\text{-}18}$ (vegetation season NDVI) time series. Due to inconsistent length of scPDSI and $NDVI_{8\text{-}18}$ datasets all time evolution patterns were converted into yearly average time series.

	$CORNDVI_{8\text{-}18}$			
	1PC	2PC	3PC	4PC
1scPDSI	0.062	0.825*	0.213	-0.384
2scPDSI	0.082	0.450	0.420	-0.392
3scPDSI	-0.474	0.120	0.457	-0.195
4scPDSI	0.309	0.054	0.364	-0.423

* - significant at the level $p<0.05$

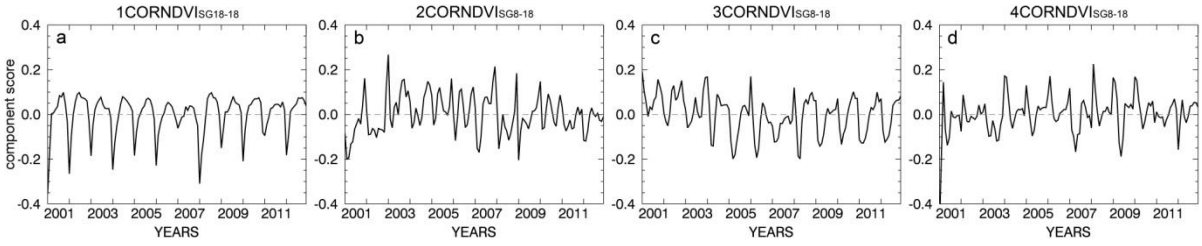

Figure A2 6 First four PCs resulted from the S-mode correlation-matrix based PCA of the $NDVI_{SG8\text{-}18}$ (vegetation season $NDVI_{SG}$) time series, herein: (a) $1CORNDVI_{SG8\text{-}18}$, (b) $2CORNDVI_{SG8\text{-}18}$, (c) $3CORNDVI_{SG8\text{-}18}$ and (d) $4CORNDVI_{SG8\text{-}18}$. Temporal patterns explained 52.88%, 5.03%, 3.23% and 2.26% of the total $NDVI_{8\text{-}18}$ time series variance respectively.

Table A2 8 Correlation between the scPDSI scores and first four PCs obtained through the S-mode correlation-matrix based PCA of the $NDVI_{SG8\text{-}18}$ (SG filtered vegetation season NDVI) time series. Due to inconsistent length of scPDSI and $NDVI_{SG8\text{-}18}$ datasets all time evolution patterns were converted into yearly average time series.

	$CORNDVI_{SG8\text{-}18}$			
	1PC	2PC	3PC	4PC
1scPDSI	0.134	-0.837*	0.548	0.241
2scPDSI	0.058	-0.382	0.582*	0.341
3scPDSI	-0.509	0.027	0.432	0.149
4scPDSI	0.403	-0.035	0.384	0.256

* - significant at the level $p<0.05$

Table A2 9 Correlation based comparison between corresponding four first PCs derived for correlation-matrix based S-mode PCA of $NDVI_{8\text{-}18}$ and $NDVI_{SG8\text{-}18}$ datasets

PCs	correlation	p
$1CORNDVI_{8\text{-}18}$ vs. $1CORNDVI_{SG8\text{-}18}$	0.980	0.000
$2CORNDVI_{8\text{-}18}$ vs. $2CORNDVI_{SG8\text{-}18}$	0.731	0.000
$3CORNDVI_{8\text{-}18}$ vs. $3CORNDVI_{SG8\text{-}18}$	0.710	0.000
$4CORNDVI_{8\text{-}18}$ vs. $4CORNDVI_{SG8\text{-}18}$	0.668	0.000

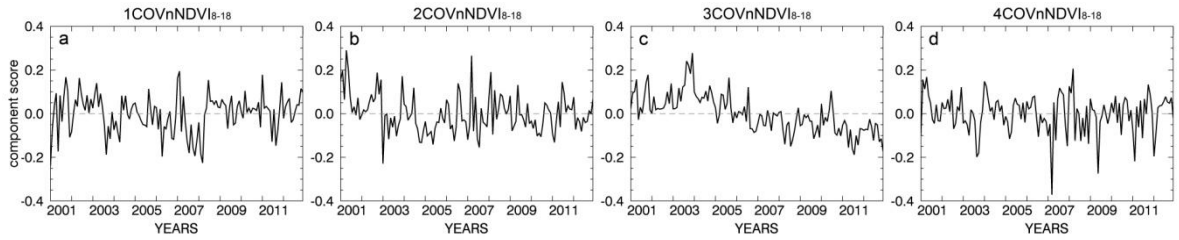

Figure A2 7 First four PCs resulted from the S-mode covariance-matrix based PCA of the $nNDVI_{8\text{-}18}$ (z-score normalized vegetation season NDVI) time series, herein: (a) $1COVnNDVI_{8\text{-}18}$, (b) $2COVnNDVI_{8\text{-}18}$, (c) $3COVnNDVI_{8\text{-}18}$ and (d) $4COVnNDVI_{8\text{-}18}$. Temporal patterns explained 15.25%, 5.65%, 3.37% and 2.28% of the total $nNDVI_{8\text{-}18}$ time series variance respectively.

Table A2 10 Correlation between the scPDSI scores and first four PCs obtained through the S-mode covariance-matrix based PCA of the $nNDVI_{8\text{-}18}$ (z-score normalized vegetation season NDVI) time series. Due to inconsistent length of scPDSI and $nNDVI_{8\text{-}18}$ datasets all time evolution patterns were converted into yearly average time series.

	$COVnNDVI_{8\text{-}18}$			
	1PC	2PC	3PC	4PC
1scPDSI	0.573	-0.713*	0.310	0.374
2scPDSI	0.321	-0.608*	-0.360	0.349
3scPDSI	-0.155	-0.337	-0.632*	0.160
4scPDSI	0.489	0.013	-0.257	0.261

* - significant at the level $p<0.05$

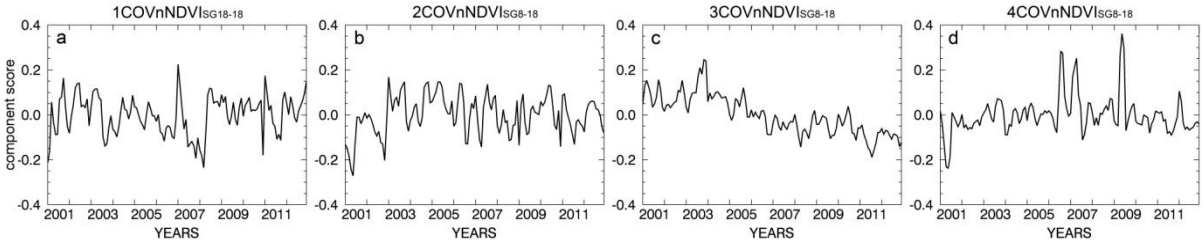

Figure A2 8 First four PCs resulted from the S-mode covariance-matrix based PCA of the $nNDVI_{SG8\text{-}18}$ (z-score normalized vegetation season $NDVI_{SG}$) time series, herein: (a) $1COVnNDVI_{SG8\text{-}18}$, (b) $2COVnNDVI_{SG8\text{-}18}$, (c) $3COVnNDVI_{SG8\text{-}18}$ and (d) $4COVnNDVI_{SG8\text{-}18}$. Temporal patterns explained 18.15%, 6.82%, 4.42% and 3.09% of the total $nNDVI_{SG8\text{-}18}$ time series variance respectively.

Table A2 11 Correlation between the scPDSI scores and first four PCs obtained through the S-mode covariance-matrix based PCA of the $nNDVI_{SG8\text{-}18}$ (z-score normalized vegetation season $NDVI_{SG}$) time series. Due to inconsistent length of scPDSI and $nNDVI_{SG8\text{-}18}$ datasets all time evolution patterns were converted into yearly average time series.

	$COVnNDVI_{SG8\text{-}18}$			
	1PC	2PC	3PC	4PC
1scPDSI	0.432	-0.791*	0.234	-0.522
2scPDSI	0.204	-0.581*	-0.427	-0.502
3scPDSI	-0.216	-0.183	-0.667*	0.047
4scPDSI	0.546	0.045	-0.272	-0.514

* - significant at the level $p<0.05$

Table A2 12 Correlation based comparison between corresponding four first PCs derived for covariance-matrix based S-mode PCA of $nNDVI_{8\text{-}18}$ and $nNDVI_{SG8\text{-}18}$ datasets

PCs	correlation	p
$1COVnNDVI_{1\text{-}18}$ vs. $1COVnNDVI_{SG1\text{-}18}$	0.810	0.000
$2COVnNDVI_{1\text{-}18}$ vs. $2COVnNDVI_{SG1\text{-}18}$	0.795	0.000
$3COVnNDVI_{1\text{-}18}$ vs. $3COVnNDVI_{SG1\text{-}18}$	0.919	0.000
$4COVnNDVI_{1\text{-}18}$ vs. $4COVnNDVI_{SG1\text{-}18}$	0.544	0.000

High season time series: $nNDVI_{14\text{-}17}$

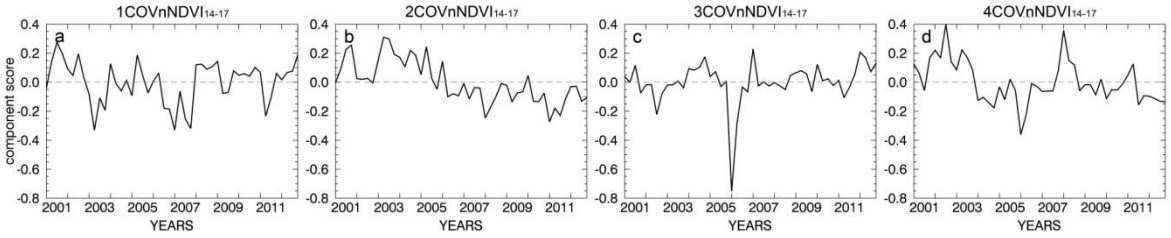

Figure A2 9 First four PCs resulted from the S-mode covariance-matrix based PCA of the $nNDVI_{14\text{-}17}$ (z-score normalized high-season NDVI) time series, herein: (a) $1COVnNDVI_{14\text{-}17}$, (b) $2COVnNDVI_{14\text{-}17}$, (c) $3COVnNDVI_{14\text{-}17}$ and (d) $4COVnNDVI_{14\text{-}17}$. Temporal patterns explained 15.85%, 6.43%, 5.03% and 4.36% of the total $nNDVI_{14\text{-}17}$ time series variance respectively.

Table A2 13 Correlation between the scPDSI scores and first four PCs obtained through the S-mode covariance-matrix based PCA of the $nNDVI_{14\text{-}17}$ (z-score normalized high-season NDVI) time series. Due to inconsistent length of scPDSI and $nNDVI_{14\text{-}17}$ datasets all time evolution patterns were converted into yearly average time series.

	$COVnNDVI_{14\text{-}17}$			
	1PC	2PC	3PC	4PC
1scPDSI	0.662*	-0.336	0.224	0.356
2scPDSI	0.268	0.164	-0.271	0.623*
3scPDSI	0.142	0.530	-0.255	0.512
4scPDSI	0.242	0.384	0.327	-0.016

* - significant at the level $p<0.05$

A.2.2. NDII7 time series

Vegetation season time series: NDII7$_{8\text{-}18}$, nNDII7$_{8\text{-}18}$

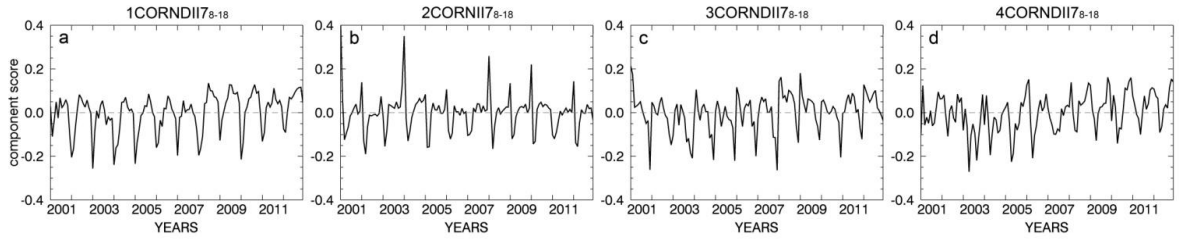

Figure A2 10 First four PCs resulted from the S-mode correlation-matrix based PCA of the NDII7$_{8\text{-}18}$ (vegetation season NDII7) time series, herein: (a) 1CORNDII7$_{8\text{-}18}$, (b) 2CORNDII7$_{8\text{-}18}$, (c) 3CORNDII7$_{8\text{-}18}$ and (d) 4CORNDII7$_{8\text{-}18}$. Temporal patterns explained 22.55%, 8.66%, 4.40% and 2.68% of the total NDII7$_{8\text{-}18}$ time series variance respectively.

Table A2 14 Correlation between the scPDSI scores and first four PCs obtained through the S-mode correlation-matrix based PCA of the NDII7$_{8\text{-}18}$ (vegetation season NDII7) time series. Due to inconsistent length of scPDSI and NDII7$_{8\text{-}18}$ datasets all time evolution patterns were converted into yearly average time series.

	CORNDII7$_{8\text{-}18}$			
	1PC	2PC	3PC	4PC
1scPDSI	0.736*	0.153	-0.660*	-0.702*
2scPDSI	-0.172	-0.093	0.193	0.011
3scPDSI	-0.576*	0.335	0.238	0.386
4scPDSI	0.030	-0.092	0.050	0.063

* - significant at the level $p<0.05$

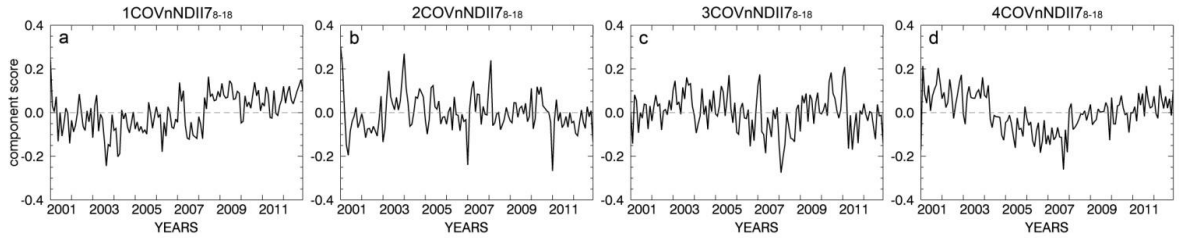

Figure A2 11 First four PCs resulted from the S-mode covariance-matrix based PCA of the nNDII7$_{8\text{-}18}$ (z-score normalized vegetation season NDII7) time series, herein: (a) 1COVnNDII7$_{8\text{-}18}$, (b) 2COVnNDII7$_{8\text{-}18}$, (c) 3COVnNDII7$_{8\text{-}18}$ and (d) 4COVnNDII7$_{8\text{-}18}$. Temporal patterns explained 11.98%, 3.39%, 2.23% and 1.66% of the total nNDII7$_{8\text{-}18}$ time series variance respectively.

Table A2 15 Correlation between the scPDSI scores and first four PCs obtained through the S-mode covariance-matrix based PCA of the $nNDII7_{8\text{-}18}$ (z-score normalized vegetation season NDII7) time series. Due to inconsistent length of scPDSI and $nNDII7_{8\text{-}18}$ datasets all time evolution patterns were converted into yearly average time series.

	$COVnNDII7_{8\text{-}18}$			
	1PC	2PC	3PC	4PC
1scPDSI	-0.717*	-0.374	0.189	0.608*
2scPDSI	0.199	-0.278	-0.260	0.502
3scPDSI	0.559	0.257	0.131	-0.023
4scPDSI	0.010	-0.243	-0.288	0.583*

* - significant at the level $p<0.05$

High-season time series: $nNDII7_{14\text{-}17}$

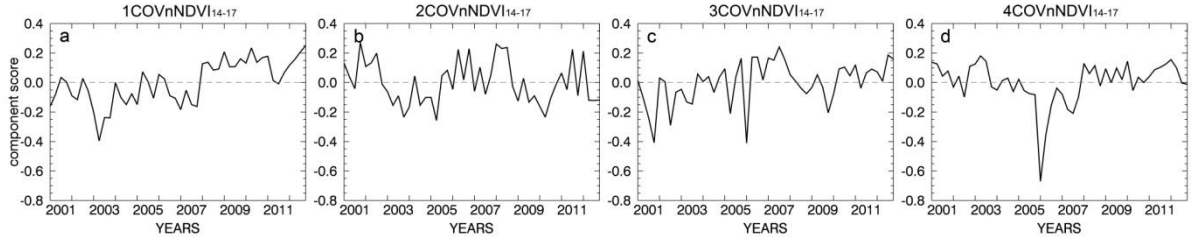

Figure A2 12 First four PCs resulted from the S-mode covariance-matrix based PCA of the $nNDII7_{14\text{-}17}$ (z-score normalized high season NDII7) time series, herein: (a) $1COVnNDII7_{14\text{-}17}$, (b) $2COVnNDII7_{14\text{-}17}$, (c) $3COVnNDII7_{14\text{-}17}$ and (d) $4COVnNDII7_{14\text{-}17}$. Temporal patterns explained 14.36%, 3.89%, 3.31% and 3.20% of the total $nNDII7_{14\text{-}17}$ time series variance respectively.

Table A2 16 Correlation between the scPDSI scores and first four PCs obtained through the S-mode covariance-matrix based PCA of the $nNDII7_{14\text{-}17}$ (z-score normalized high-season NDII7) time series. Due to inconsistent length of scPDSI and $nNDII7_{14\text{-}17}$ datasets all time evolution patterns were converted into yearly average time series.

	$COVnNDII7_{14\text{-}17}$			
	1PC	2PC	3PC	4PC
1scPDSI	-0.387	-0.521	0.122	0.490
2scPDSI	0.337	0.304	-0.513	0.185
3scPDSI	0.417	0.680	-0.811*	0.324
4scPDSI	0.578*	0.208	0.064	-0.668*

* - significant at the level $p<0.05$

APPENDIX 3

A.3.Secondary rotation of selected PCA loadings

A.3.1. $COVnNDVI_{8\text{-}18}$

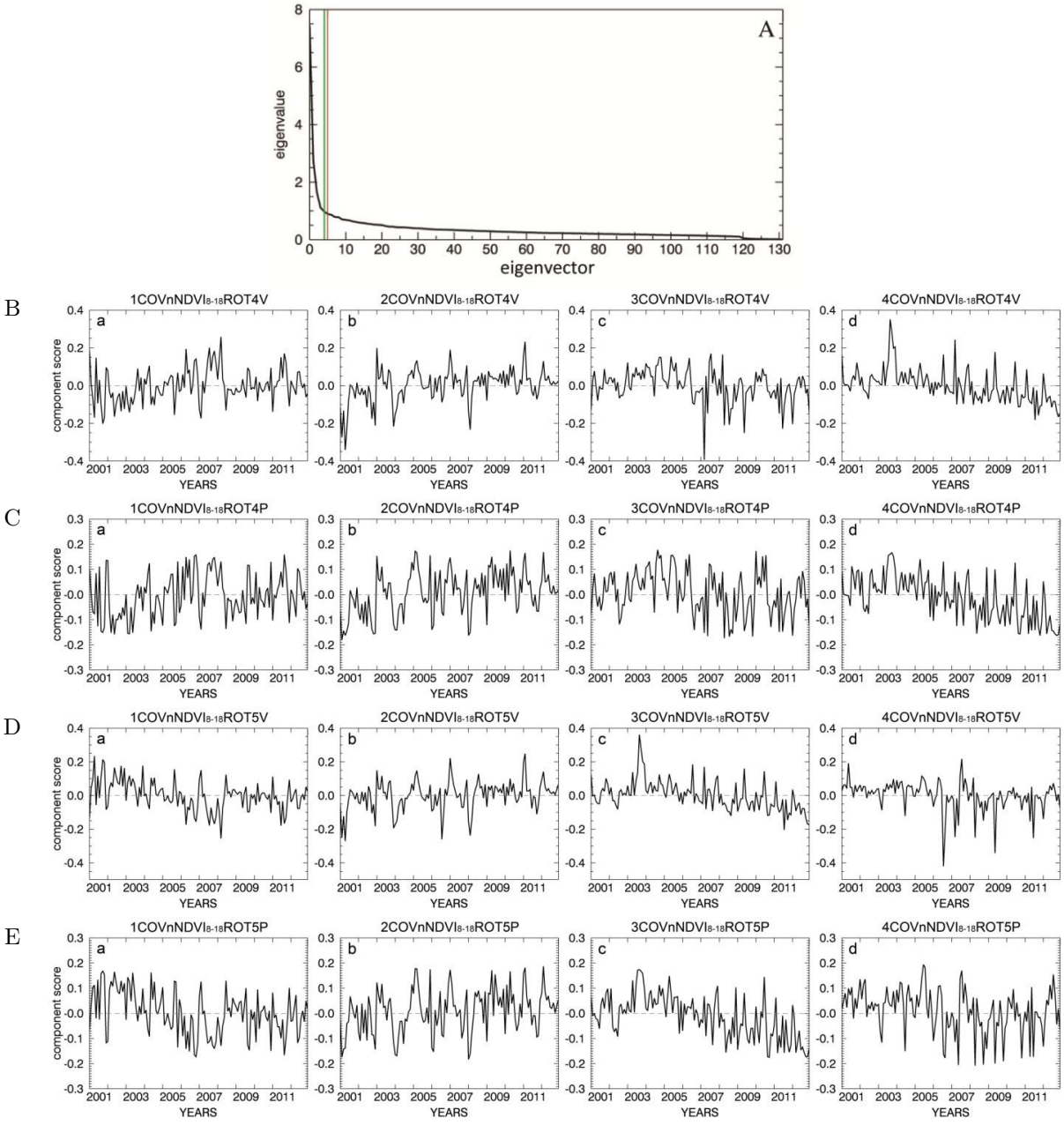

Figure A3 1 A: Plot of eigenvalues spectrum of the $COVnNDVI_{8\text{-}18}$ (covariance-matrix based decomposition of z-score normalized vegetation season NDVI time series) PCA setup. Vertical lines represent results of two stopping rules approaches: Cattell's scree test in red (5), and Kaiser's stopping rule in green (4). First four PCs resulting from the Varimax (B) and Promax (C) rotation of the first five loadings of the lowest order retained from the $COVnNDVI_{8\text{-}18}$ PCA results. First four PCs produced through the Varimax (D) and Promax (E) rotation of the first four loadings of the lowest order retained from the $COVnNDVI_{8\text{-}18}$ PCA results.

Table A3 1 Correlation based comparison between corresponding 1-4 PCs derived for Varimax and Promax rotations performed on the first five EOFs resulted from the covariance-matrix based S-mode PCA of the $nNDVI_{8\text{-}18}$ dataset

PCs	correlation	p
$1COVnNDVI_{8\text{-}18}ROT5V$ vs. $1COVnNDVI_{8\text{-}18}ROT5P$	0.904	0.000
$2COVnNDVI_{8\text{-}18}ROT5V$ vs. $2COVnNDVI_{8\text{-}18}ROT5P$	0.890	0.000
$3COVnNDVI_{8\text{-}18}ROT5V$ vs. $3COVnNDVI_{8\text{-}18}ROT5P$	0.902	0.000
$4COVnNDVI_{8\text{-}18}ROT5V$ vs. $4COVnNDVI_{8\text{-}18}ROT5P$	0.867	0.000

Table A3 2 Correlation among the scPDSI scores and first four PCs obtained from Varimax (V) and Promax (P) rotations (ROT) of the first five loadings of the $COVnNDVI_{8\text{-}18}$ dataset (covariance-matrix based S-mode PCA of the z-score normalized vegetation season NDVI time series). Due to inconsistent length of scPDSI and $nNDVI_{8\text{-}18}$ datasets all time evolution patterns were converted into yearly average time series

	$COVnNDVI_{8\text{-}18}ROT5V$				$COVnNDVI_{8\text{-}18}ROT5P$			
	1PC	2PC	3PC	4PC	1PC	2PC	3PC	4PC
1scPDSI	0.308	-0.203	0.569	-0.104	0.290	-0.124	0.590*	-0.205
2scPDSI	0.638*	-0.495	-0.107	0.353	0.615*	-0.536	-0.186	0.333
3scPDSI	0.476	-0.588*	-0.533	0.380	0.504	-0.576*	-0.607*	0.324
4scPDSI	0.503	0.057	-0.057	0.532	0.433	0.020	-0.029	0.612*

* - significant at the level $p<0.05$

Table A3 3 Correlation among four first unrotated PC of the $COVnNDVI_{8\text{-}18}$ dataset (covariance-matrix based S-mode PCA of the z-score normalized vegetation season NDVI time series) and their rotated (ROT) equivalents derived using Varimax (V; left part of the table) and Promax (P; right part of the table) algorithms applied to the first five (5) EOFs of the $COVnNDVI_{8\text{-}18}$ dataset.

	$COVnNDVI_{8\text{-}18}ROT5V$				$COVnNDVI_{8\text{-}18}ROT5P$			
	1PC	2PC	3PC	4PC	1PC	2PC	3PC	4PC
$1CONnNDVI_{8\text{-}18}$	0.978*	0.620*	0.309*	0.088	0.864*	0.409*	0.176	0.043
$2CONnNDVI_{8\text{-}18}$	-0.082	-0.276*	0.741*	0.521*	-0.114	-0.289*	0.622*	0.432*
$3CONnNDVI_{8\text{-}18}$	-0.176*	0.679*	-0.133	-0.147	-0.240*	0.714*	-0.170	-0.161
$4CONnNDVI_{8\text{-}18}$	-0.063	0.276*	0.316*	0.551*	-0.093	0.295*	0.302*	0.510*

* - significant at the level $p<0.05$

Table A3 4 Correlation based comparison between corresponding 1-4 PCs derived for Varimax and Promax rotations performed on the first four EOFs resulted from the covariance-matrix based S-mode PCA of the $nNDVI_{8\text{-}18}$ dataset.

PCs	correlation	p
$1COVnNDVI_{8\text{-}18}ROT4V$ vs. $1COVnNDVI_{8\text{-}18}ROT4P$	0.904	0.000
$2COVnNDVI_{8\text{-}18}ROT4V$ vs. $2COVnNDVI_{8\text{-}18}ROT4P$	0.891	0.000
$3COVnNDVI_{8\text{-}18}ROT4V$ vs. $3COVnNDVI_{8\text{-}18}ROT4P$	0.908	0.000
$4COVnNDVI_{8\text{-}18}ROT4V$ vs. $4COVnNDVI_{8\text{-}18}ROT4P$	0.885	0.000

Table A3 5 Correlation among the scPDSI scores and first four PCs obtained from Varimax (V) and Promax (P) rotations (ROT) of the first four loadings of the $COVnNDVI_{8\text{-}18}$ dataset (covariance-matrix based S-mode PCA of the z-score normalized vegetation season NDVI time series). Due to inconsistent length of scPDSI and $nNDVI_{8\text{-}18}$ datasets all time evolution patterns were converted into yearly average time series.

	$COVnNDVI_{8\text{-}18}ROT4V$				$COVnNDVI_{8\text{-}18}ROT4P$			
	1PC	2PC	3PC	4PC	1PC	2PC	3PC	4PC
1scPDSI	-0.072	-0.121	0.548	-0.751*	0.311	-0.330	0.573	0.482
2scPDSI	-0.614*	-0.294	-0.143	-0.301	0.534	-0.694*	0.009	-0.305
3scPDSI	-0.396	0.410	-0.200	0.331	0.411	-0.584*	-0.239	-0.658*
4scPDSI	-0.527	-0.267	-0.090	-0.466	0.405	-0.163	-0.320	-0.069

* - significant at the level $p<0.05$

Table A3 6 Correlation among four first unrotated PC of the $COVnNDVI_{8\text{-}18}$ dataset (covariance-matrix based S-mode PCA of the z-score normalized vegetation season NDVI time series) and their rotated (ROT) equivalents derived using Varimax (V; left part of the table) and Promax (P; right part of the table) algorithms applied to the first four (4) EOFs of the $COVnNDVI_{8\text{-}18}$ dataset.

	$COVnNDVI_{8\text{-}18}ROT4V$				$COVnNDVI_{8\text{-}18}ROT4P$			
	1PC	2PC	3PC	4PC	1PC	2PC	3PC	4PC
$1CONnNDVI_{8\text{-}18}$	0.994*	-0.026	0.464*	0.185*	0.892*	-0.036	0.292*	0.095
$2CONnNDVI_{8\text{-}18}$	0.024	0.840*	-0.386*	0.720*	0.007	0.714*	-0.359*	0.597*
$3CONnNDVI_{8\text{-}18}$	-0.075	0.479*	0.704*	-0.273*	-0.100	0.464*	0.706*	-0.301*
$4CONnNDVI_{8\text{-}18}$	-0.079	-0.254*	0.376*	0.610*	-0.120	-0.278*	0.368*	0.582*

* - significant at the level $p<0.05$

Table A3 7 Correlation basd comparison between corresponding 1-4 PCs derived for Varimax rotation performed on the first five and four EOFs resulted from the covariance-matrix based S-mode PCA of the $nNDVI_{8\text{-}18}$ dataset.

PCs	correlation	p
$1COVnNDVI_{8\text{-}18}ROT5V$ vs. $1COVnNDVI_{8\text{-}18}ROT4V$	0.989	0.000
$2COVnNDVI_{8\text{-}18}ROT5V$ vs. $2COVnNDVI_{8\text{-}18}ROT4V$	0.924	0.000
$3COVnNDVI_{8\text{-}18}ROT5V$ vs. $3COVnNDVI_{8\text{-}18}ROT4V$	0.975	0.000
$4COVnNDVI_{8\text{-}18}ROT5V$ vs. $4COVnNDVI_{8\text{-}18}ROT4V$	0.820	0.000

Table A3 8 Correlation based comparison between corresponding 1-4 PCs derived for Promax rotation performed on the first five and four EOFs resulted from the covariance-matrix based S-mode PCA of the $nNDVI_{8\text{-}18}$ dataset.

PCs	correlation	p
$1COVnNDVI_{8\text{-}18}ROT5P$ vs. $1COVnNDVI_{8\text{-}18}ROT4P$	0.976	0.000
$2COVnNDVI_{8\text{-}18}ROT5P$ vs. $2COVnNDVI_{8\text{-}18}ROT4P$	0.940	0.000
$3COVnNDVI_{8\text{-}18}ROT5P$ vs. $3COVnNDVI_{8\text{-}18}ROT4P$	0.982	0.000
$4COVnNDVI_{8\text{-}18}ROT5P$ vs. $4COVnNDVI_{8\text{-}18}ROT4P$	0.789	0.000

A.3.2. COVnNDVI$_{14\text{-}17}$

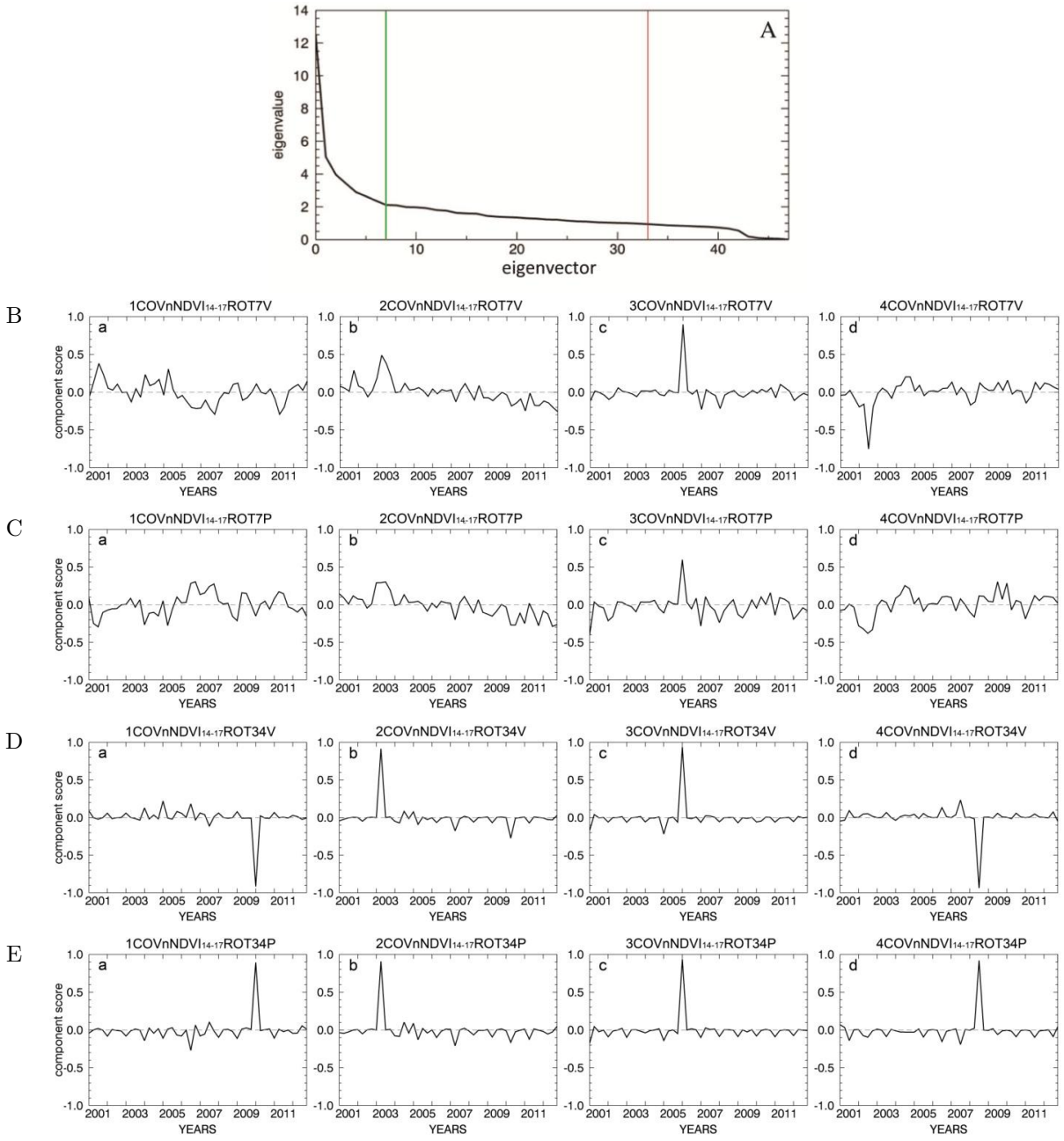

Figure A3 2 A: Plot of eigenvalues spectrum of the COVnNDVI$_{14\text{-}17}$ (covariance-matrix based decomposition of the z-score normalized high-season NDVI time series) PCA setup. Vertical lines represent results of two stopping rules approaches: Cattell's scree test in green (7), and Kaiser's stopping rule in red (34). First four PCs resulting from the Varimax (B) and Promax (C) rotation of the first seven loadings of the lowest order retained from the COVnNDVI$_{14\text{-}17}$ PCA results. First four PCs produced through the Varimax (D) and Promax (E) rotation of the first 34 loadings of the lowest order retained from the COVnNDVI$_{14\text{-}17}$ PCA results.

Table A3 9 Correlation between corresponding 1-4 PCs derived for Varimax and Promax rotations performed on the first seven EOFs resulted from the covariance-matrix based S-mode PCA of the $nNDVI_{14\text{-}17}$ dataset.

PCs	correlation	p
$1COVnNDVI_{14\text{-}17}$ ROT7V vs. $1COVnNDVI_{14\text{-}17}$ ROT7P	0.937	0.000
$2COVnNDVI_{14\text{-}17}$ ROT7V vs. $2COVnNDVI_{14\text{-}17}$ ROT7P	0.909	0.000
$3COVnNDVI_{14\text{-}17}$ ROT7V vs. $3COVnNDVI_{14\text{-}17}$ ROT7P	0.883	0.000
$4COVnNDVI_{14\text{-}17}$ ROT7V vs. $4COVnNDVI_{14\text{-}17}$ ROT7P	0.872	0.000

Table A3 10 Correlation among the scPDSI scores and first four PCs obtained from Varimax (V) and Promax (P) rotations (ROT) of the first seven loadings of the $COVnNDVI_{14\text{-}17}$ dataset (covariance-matrix based S-mode PCA of the z-score normalized high-season NDVI time series). Due to inconsistent length of scPDSI and$nNDVI_{14\text{-}17}$ datasets all time evolution patterns were converted into yearly average time series.

	$COVnNDVI_{14\text{-}17}$ROT7V				$COVnNDVI_{14\text{-}17}$ROT7P			
	1PC	2PC	3PC	4PC	1PC	2PC	3PC	4PC
1scPDSI	0.119	0.542	0.043	-0.849*	0.196	0.513	-0.169	-0.839*
2scPDSI	0.577*	-0.024	0.562	-0.110	0.565	-0.122	0.474	-0.040
3scPDSI	0.286	-0.179	0.557	0.462	0.148	-0.218	0.601*	0.563
4scPDSI	0.690*	-0.569	0.044	-0.208	0.755*	-0.633*	0.100	-0.195

* - significant at the level $p<0.05$

Table A3 11 Correlation among four first unrotated PC of the $COVnNDVI_{14\text{-}17}$ dataset (covariance-matrix based S-mode PCA of the z-score normalized high-season NDVI time series) and their rotated (ROT) equivalents derived using Varimax (V; left part of the table) and Promax (P; right part of the table) algorithms applied to the seven (7) first EOFs of the $COVnNDVI_{14\text{-}17}$ dataset.

	$COVnNDVI_{14\text{-}17}$ROT7V				$COVnNDVI_{14\text{-}17}$ROT7P			
	1PC	2PC	3PC	4PC	1PC	2PC	3PC	4PC
$1CONnNDVI_{14\text{-}17}$	-0.154	0.120	0.198	0.334*	-0.164	0.013	0.148	0.342*
$2CONnNDVI_{14\text{-}17}$	-0.050	0.072	-0.048	0.207	-0.036	0.028	-0.061	0.199
$3CONnNDVI_{14\text{-}17}$	0.130	0.075	-0.105	0.069	0.133	0.056	-0.059	0.066
$4CONnNDVI_{14\text{-}17}$	-0.168	-0.098	0.220	-0.035	-0.217	0.062	0.195	0.036

* - significant at the level $p<0.05$

Table A3 12 Correlation between corresponding 1-4 PCs derived for Varimax and Promax rotations performed on the first 34 scores resulted from the covariance-matrix based S-mode PCA of the $nNDVI_{14\text{-}17}$ dataset.

PCs	correlation	p
$1COVnNDVI_{14\text{-}17}$ ROT34V vs. $1COVnNDVI_{14\text{-}17}$ ROT34P	0.906	0.000
$2COVnNDVI_{14\text{-}17}$ ROT34V vs. $2COVnNDVI_{14\text{-}17}$ ROT34P	0.951	0.000
$3COVnNDVI_{14\text{-}17}$ ROT34V vs. $3COVnNDVI_{14\text{-}17}$ ROT34P	0.984	0.000
$4COVnNDVI_{14\text{-}17}$ ROT34V vs. $4COVnNDVI_{14\text{-}17}$ ROT34P	0.944	0.000

Table A3 13 Correlation among the scPDSI scores and first four PCs obtained from Varimax (V) and Promax (P) rotations (ROT) of the first 34 loadings of the $COVnNDVI_{14\text{-}17}$ dataset (covariance-matrix based S-mode PCA of the normalized high-season NDVI time series). Due to inconsistent length of scPDSI and $nNDVI_{14\text{-}17}$ datasets all time evolution patterns were converted into yearly average time series.

	$COVnNDVI_{14\text{-}17}$ROT34V				$COVnNDVI_{14\text{-}17}$ROT34P			
	1PC	2PC	3PC	4PC	1PC	2PC	3PC	4PC
1scPDSI	-0.313	0.240	0.324	0.817*	0.085	0.209	0.000	0.877*
2scPDSI	0.338	-0.248	0.081	0.153	0.639*	-0.271	0.192	0.138
3scPDSI	0.496	-0.031	0.036	-0.457	0.582*	-0.019	0.381	-0.217
4scPDSI	-0.420	-0.652*	0.113	0.255	-0.130	-0.661*	0.054	0.028

* - significant at the level $p<0.05$

Table A3 14 Correlation among four first unrotated PC of the $COVnNDVI_{14\text{-}17}$ dataset (covariance-matrix based S-mode PCA of the z-score normalized high-season NDVI time series) and their rotated (ROT) equivalents derived using Varimax (V; left part of the table) and Promax (P; right part of the table) algorithms applied to the 34 first EOFs of the $COVnNDVI_{14\text{-}17}$ dataset.

	$COVnNDVI_{14\text{-}17}$ROT34V				$COVnNDVI_{14\text{-}17}$ROT34P			
	1PC	2PC	3PC	4PC	1PC	2PC	3PC	4PC
$1CONnNDVI_{14\text{-}17}$	0.817*	-0.313*	-0.156	0.507*	0.575*	-0.161	-0.078	0.290*
$2CONnNDVI_{14\text{-}17}$	0.374*	0.499*	-0.173	0.030	0.357*	0.374*	-0.157	0.037
$3CONnNDVI_{14\text{-}17}$	0.116	0.011	0.823*	-0.258	0.143	0.015	0.797*	-0.226
$4CONnNDVI_{14\text{-}17}$	- 0.067	0.262	0.337*	0.414*	-0.070	0.194	0.357*	0.411*

* - significant at the level $p<0.05$

Table A3 15 Correlation based comparison between corresponding 1-4 PCs derived for Varimax rotation performed on the first seven and 34 scores resulted from the covariance-matrix based S-mode PCA of the $nNDVI_{14\text{-}17}$ dataset.

PCs	correlation	p
$1COVnNDVI_{14\text{-}17}$ ROT7V vs. $1COVnNDVI_{14\text{-}17}$ ROT34V	0.571	0.000
$2COVnNDVI_{14\text{-}17}$ ROT7V vs. $2COVnNDVI_{14\text{-}17}$ ROT34V	0.615	0.000
$3COVnNDVI_{14\text{-}17}$ ROT7V vs. $3COVnNDVI_{14\text{-}17}$ ROT34V	0.958	0.000
$4COVnNDVI_{14\text{-}17}$ ROT7V vs. $4COVnNDVI_{14\text{-}17}$ ROT34V	0.765	0.000

Table A3 16 Correlation based comparison between corresponding 1-4 PCs derived for Promax rotation performed on the first 7 and 34 scores resulted from the covariance-matrix based S-mode PCA of the $nNDVI_{14\text{-}17}$ dataset.

PCs	correlation	p
$1COVnNDVI_{14\text{-}17}$ ROT7P vs. $1COVnNDVI_{14\text{-}17}$ ROT34P	0.402	0.000
$2COVnNDVI_{14\text{-}17}$ ROT7P vs. $2COVnNDVI_{14\text{-}17}$ ROT34P	0.384	0.000
$3COVnNDVI_{14\text{-}17}$ ROT7P vs. $3COVnNDVI_{14\text{-}17}$ ROT34P	0.810	0.000
$4COVnNDVI_{14\text{-}17}$ ROT7P vs. $4COVnNDVI_{14\text{-}17}$ ROT34P	0.466	0.000

A.3.3. COVnNDII7$_{8\text{-}18}$

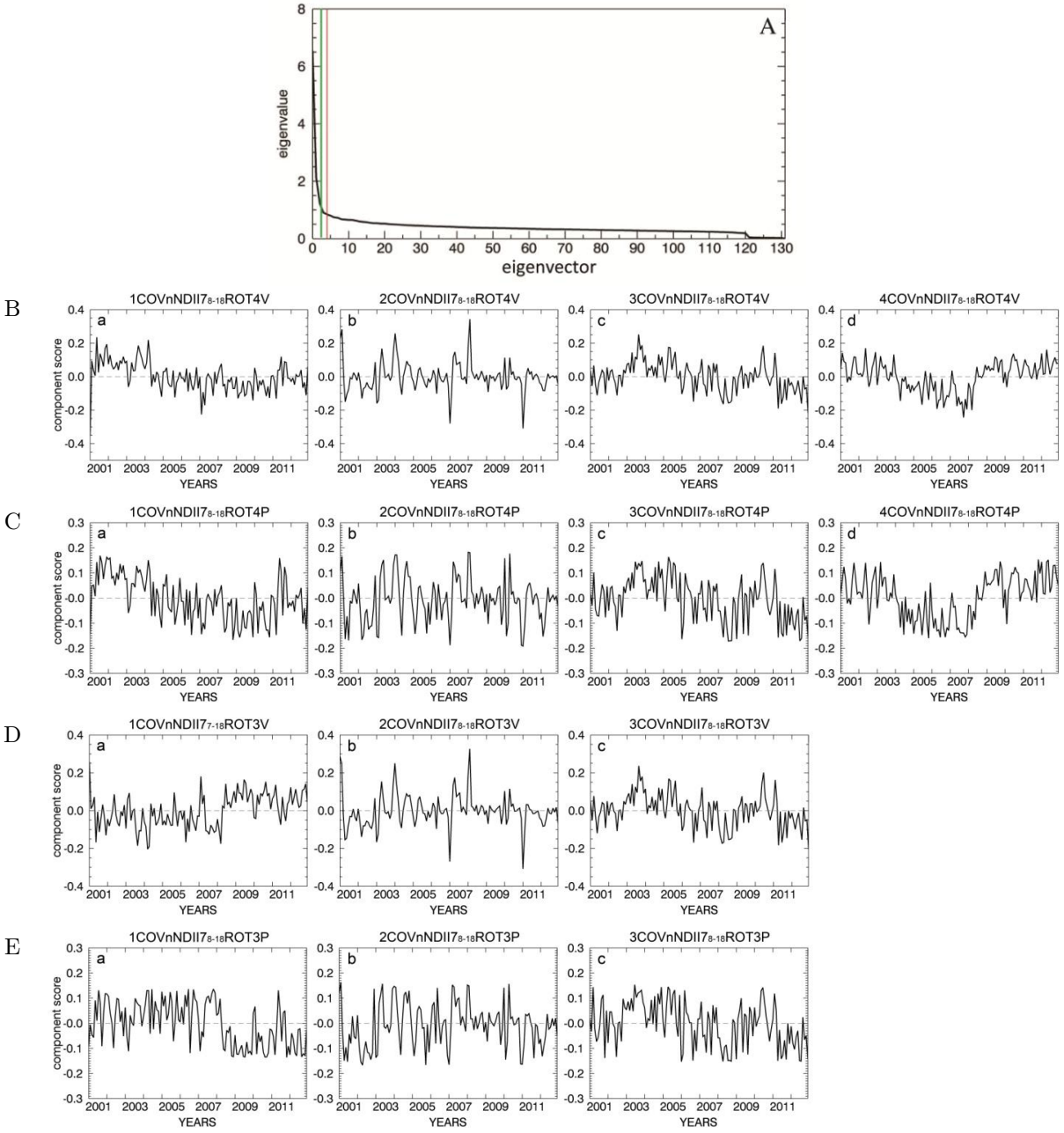

Figure A3 3 A: Plot of eigenvalues spectrum of the COVnNDII7$_{8\text{-}18}$ (covariance-matrix based decomposition of z-score normalized vegetation season NDII7 time series) PCA setup. Vertical lines represent results of two stopping rules approaches: Cattell's scree test in red (4), and Kaiser's stopping rule in green (3). First four PCs resulting from the Varimax (B) and Promax (C) rotation of the first four loadings of the lowest order retained from the COVnNDII7$_{8\text{-}18}$ PCA results. First three PCs produced through the Varimax (D) and Promax (E) rotation of the first four loadings of the lowest order retained from the COVnNDII7$_{8\text{-}18}$ PCA results.

Table A3 17 Correlation based comparison between corresponding 1-4 PCs derived for Varimax and Promax rotations performed on the first four EOFs resulted from the covariance-matrix based S-mode PCA of the nNDII7$_{8\text{-}18}$ dataset.

PCs	correlation	p
1COVnNDII7$_{8\text{-}18}$ ROT4V vs. 1COVnNDII7$_{8\text{-}18}$ ROT4P	0.910	0.000
2COVnNDII7$_{8\text{-}18}$ ROT4V vs. 2COVnNDII7$_{8\text{-}18}$ ROT4P	0.897	0.000
3COVnNDII7$_{8\text{-}18}$ ROT4V vs. 3COVnNDII7$_{8\text{-}18}$ ROT4P	0.919	0.000
4COVnNDII7$_{8\text{-}18}$ ROT4V vs. 4COVnNDII7$_{8\text{-}18}$ ROT4P	0.924	0.000

Table A3 18 Correlation among the scPDSI scores and first four PCs obtained from Varimax (V) and Promax (P) rotations (ROT) of the first four loadings of the COVnNDII7$_{8\text{-}18}$ dataset (covariance-matrix based S-mode PCA of the z-score normalized vegetation season NDII7 time series). Due to inconsistent length of scPDSI and nNDII7$_{8\text{-}18}$ datasets all time evolution patterns were converted into yearly average time series.

	COVnNDII7$_{8\text{-}18}$ROT4V				COVnNDII7$_{8\text{-}18}$ROT4P			
	1PC	2PC	3PC	4PC	1PC	2PC	3PC	4PC
1scPDSI	-0.072	-0.121	0.548	0.751*	-0.061	-0.254	0.550	0.772*
2scPDSI	-0.614*	-0.294	-0.143	0.301	-0.689*	-0.427	-0.172	0.241
3scPDSI	-0.396	0.410	-0.200	-0.331	-0.365	0.172	-0.260	-0.397
4scPDSI	-0.527	-0.267	-0.090	0.466	-0.515	-0.321	-0.066	0.400

* - significant at the level $p<0.05$

Table A3 19 Correlation among four first unrotated PC of the COVnNDII7$_{8\text{-}18}$ dataset (covariance-matrix based S-mode PCA of the z-score normalized vegetation season NDII7 time series) and their rotated (ROT) equivalents derived using Varimax (V; left part of the table) and Promax (P; right part of the table) algorithms applied to the five four (4) EOFs of the COVnNDII7$_{8\text{-}18}$ dataset.

	COVnNDII7$_{8\text{-}18}$ROT4V				COVnNDII7$_{8\text{-}18}$ROT4P			
	1PC	2PC	3PC	4PC	1PC	2PC	3PC	4PC
1CONnNDII7$_{8\text{-}18}$	0.994*	-0.026	0.464*	0.185*	0.892*	-0.036	0.292*	0.095
2CONnNDII7$_{8\text{-}18}$	0.024	0.840*	-0.386*	0.720*	0.007	0.714*	-0.359*	0.597*
3CONnNDII7$_{8\text{-}18}$	-0.075	0.479*	0.704*	-0.273*	-0.100	0.464*	0.706*	-0.301*
4CONnNDII7$_{8\text{-}18}$	-0.079	-0.254*	0.376*	0.610*	-0.120	-0.278*	0.368*	0.582*

* - significant at the level $p<0.05$

Table A3 20 Correlation based comparison between corresponding 1-4 PCs derived for Varimax and Promax rotations performed on the first three EOFs resulted from the covariance-matrix based S-mde PCA of the nNDII7$_{8\text{-}18}$ dataset.

PCs	correlation	p
1COVnNDII7$_{8\text{-}18}$ ROT3V vs. 1COVnNDII7$_{8\text{-}18}$ ROT3P	0.907	0.000
2COVnNDII7$_{8\text{-}18}$ ROT3V vs. 2COVnNDII7$_{8\text{-}18}$ ROT3P	0.873	0.000
3COVnNDII7$_{8\text{-}18}$ ROT3V vs. 3COVnNDII7$_{8\text{-}18}$ ROT3P	0.915	0.000

Table A3 21 Correlation among the scPDSI scores and first four PCs obtained from Varimax (V) and Promax (P) rotations (ROT) of the first three loadings of the COVnNDII7$_{8\text{-}18}$ dataset (covariance-matrix based S-mode PCA of the z-score normalized vegetation season NDVI time series). Due to inconsistent length of scPDSI and nNDII7$_{8\text{-}18}$ datasets all time evolution patterns were converted into yearly average time series.

	COVnNDII7$_{8\text{-}18}$ROT3V			COVnNDII7$_{8\text{-}18}$ROT3P		
	1PC	2PC	3PC	1PC	2PC	3PC
1scPDSI	0.693*	-0.243	0.438	0.658*	-0.375	0.435
2scPDSI	-0.164	-0.447	-0.182	-0.257	-0.584*	-0.213
3scPDSI	-0.609*	0.316	-0.124	-0.539	0.115	-0.223
4scPDSI	0.046	-0.418	-0.158	0.023	-0.413	-0.137

* - significant at the level $p<0.05$

Table A3 22 Correlation among four first unrotated PC of the COVnNDII7$_{8\text{-}18}$ dataset (covariance-matrix based S-mode PCA of the z-score normalized vegetation season NDII7 time series) and their rotated (ROT) equivalents derived using Varimax (V; left part of the table) and Promax (P; right part of the table) algorithms applied to the three first (3) EOFs of the COVnNDII7$_{8\text{-}18}$ dataset.

	COVnNDiI7$_{8\text{-}18}$ROT3V			COVnNDII7$_{8\text{-}18}$ROT3P		
	1PC	2PC	3PC	1PC	2PC	3PC
1CONnNDII7$_{8\text{-}18}$	0.960*	0.027	0.278*	0.867*	0.008	0.269*
2CONnNDII7$_{8\text{-}18}$	0.086	0.919*	-0.384*	0.069	0.810*	-0.383*
3CONnNDII7$_{8\text{-}18}$	-0.266*	0.393*	0.880*	-0.234*	0.321*	0.807*

* - significant at the level $p<0.05$

Table A3 23 Correlation based comparison between corresponding 1-3 PCs derived for Varimax rotation performed on the first four and three EOFs resulted from the covariance-matrix based S-mode PCA of the nNDII7$_{8\text{-}18}$ dataset.

PCs	correlation	p
1COVnNDII7$_{8\text{-}18}$ ROT4V vs. 1COVnNDII7$_{8\text{-}18}$ ROT3V	0.990	0.000
2COVnNDII7$_{8\text{-}18}$ ROT4V vs. 2COVnNDII7$_{8\text{-}18}$ ROT3V	0.972	0.000
3COVnNDII7$_{8\text{-}18}$ ROT4V vs. 3COVnNDII7$_{8\text{-}18}$ ROT3V	0.738	0.000

Table A3 24 Correlation based comparison between corresponding 1-3 PCs derived for Promax rotation performed on the first four and three scores resulted from the covariance-matrix based S-mode PCA of nNDII7$_{8\text{-}18}$ dataset.

PCs	correlation	p
1COVnNDII7$_{8\text{-}18}$ ROT4P vs. 1COVnNDII7$_{8\text{-}18}$ ROT3P	0.968	0.000
2COVnNDII7$_{8\text{-}18}$ ROT4P vs. 2COVnNDII7$_{8\text{-}18}$ ROT3P	0.947	0.001
3COVnNDII7$_{8\text{-}18}$ ROT4P vs. 3COVnNDII7$_{8\text{-}18}$ ROT3P	0.755	0.000

APPENDIX 4

A.4. Spatial representations of MODIS derived drought impact patterns

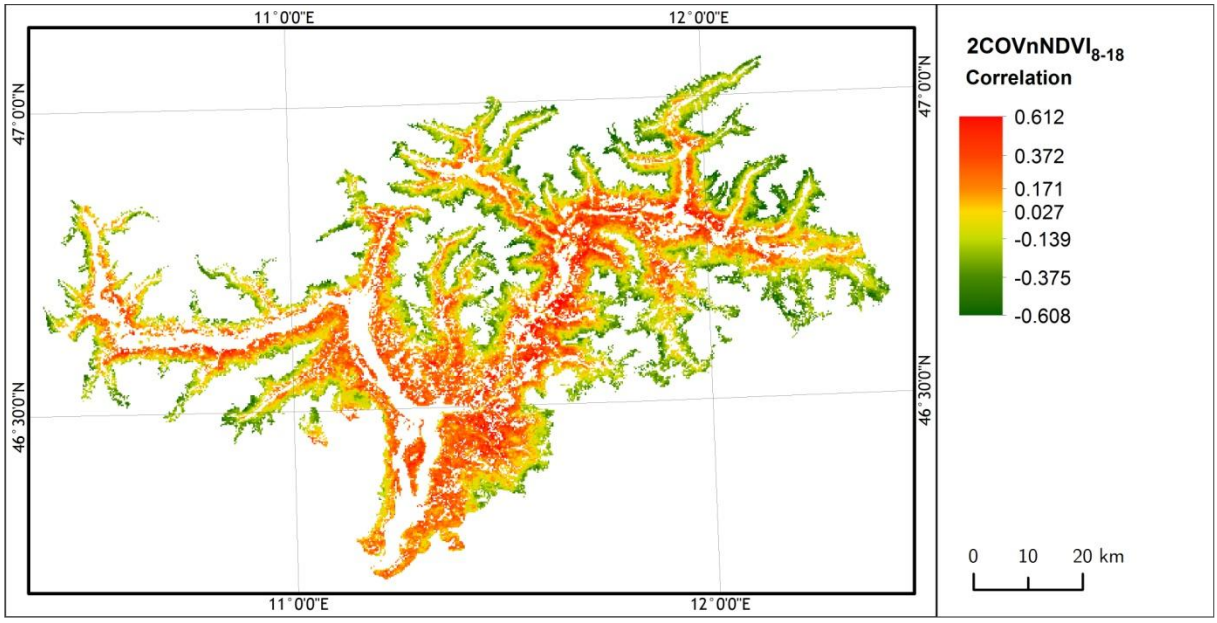

Figure A4 1 Spatial representation of forest potential drought response identified by the $2COVnNDVI_{8\text{-}18}$ PC. Correlation footprint refers to the score presented in the Figure 16A. Values next to the color ramp represents in the increasing order 0^{th}, 5^{th}, 30^{th}, 50^{th}, 70^{th} 95^{th} and 100^{th} percentiles of the correlation distribution.

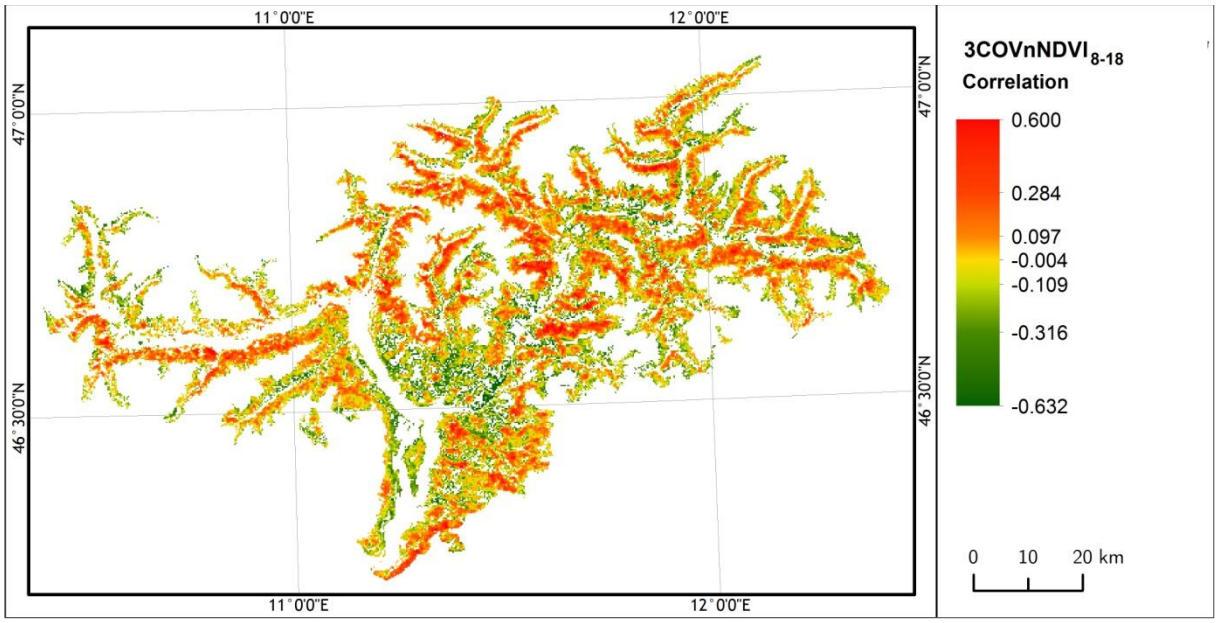

Figure A4 2 Spatial representation of forest potential drought response identified by the $3COVnNDVI_{8\text{-}18}$. Correlation footprint refers to the score presented in the Figure 16B. Values next to the color ramp represents in the increasing order 0^{th}, 5^{th}, 30^{th}, 50^{th}, 70^{th} 95^{th} and 100^{th} percentiles of the correlation distribution.

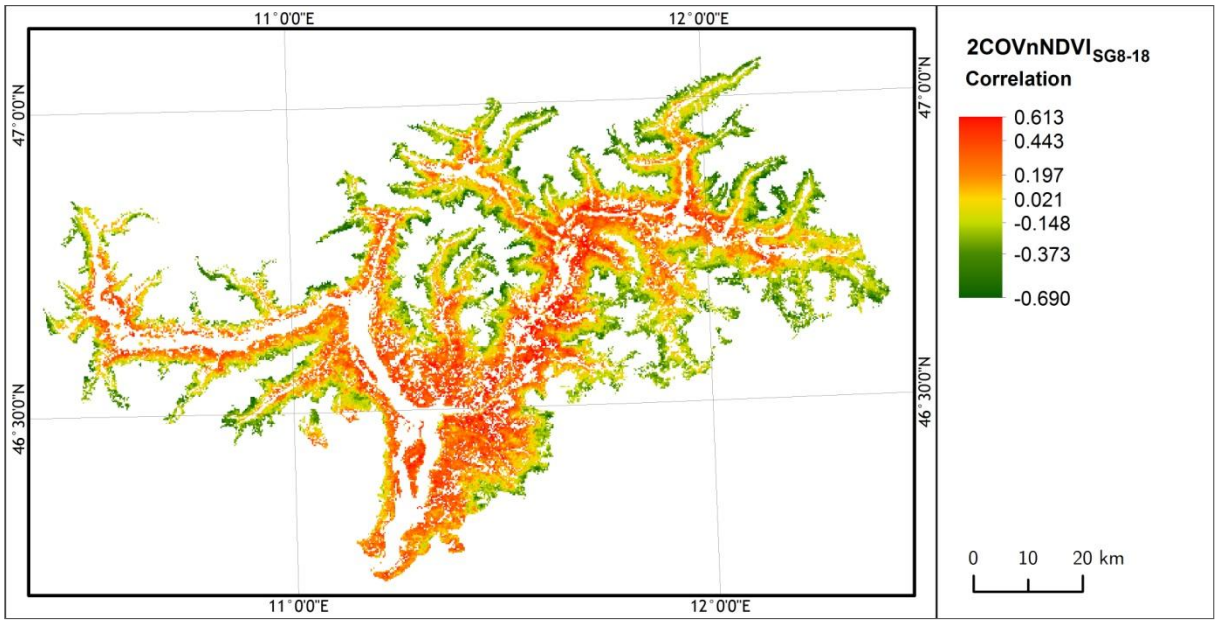

Figure A4 3 Spatial representation of forest potential drought response identified by the $2COVnNDVI_{SG8\text{-}18}$. Correlation footprint refers to the score presented in the Figure 16C. Values next to the color ramp represents in the increasing order 0^{th}, 5^{th}, 30^{th}, 50^{th}, 70^{th} 95^{th} and 100^{th} percentiles of the correlation distribution.

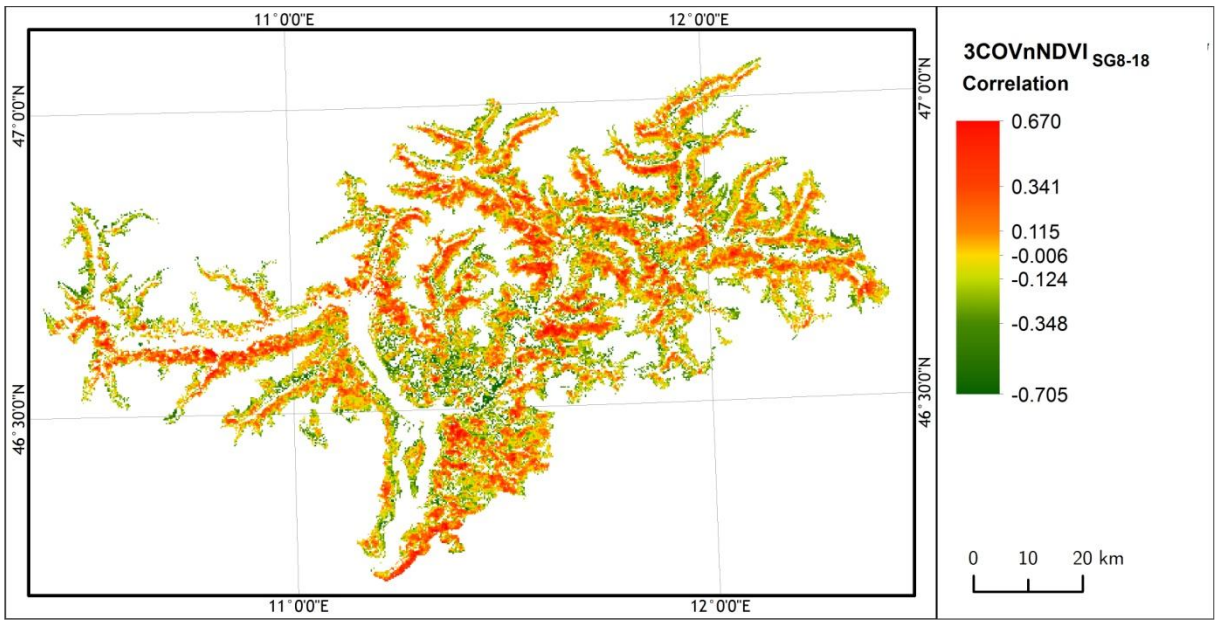

Figure A4 4 Spatial representation of forest potential drought response identified by the $3COVnNDVI_{SG8\text{-}18}$. Correlation footprint refers to the score presented in the Figure 16D. Values next to the color ramp represents in the increasing order 0^{th}, 5^{th}, 30^{th}, 50^{th}, 70^{th} 95^{th} and 100^{th} percentiles of the correlation distribution.

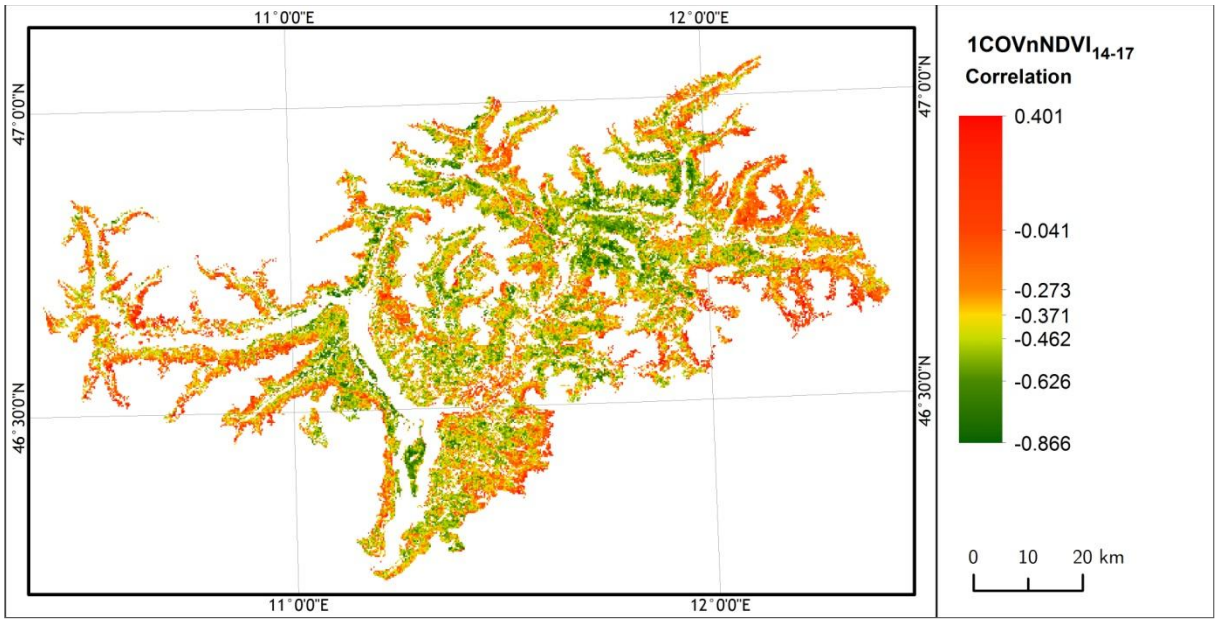

Figure A4 5 Spatial representation of forest potential drought response identified by the $1COVnNDVI_{14\text{-}17}$. Correlation footprint refers to the score presented in the Figure 16E. Values next to the color ramp represents in the increasing order 0^{th}, 5^{th}, 30^{th}, 50^{th}, 70^{th} 95^{th} and 100^{th} percentiles of the correlation distribution.

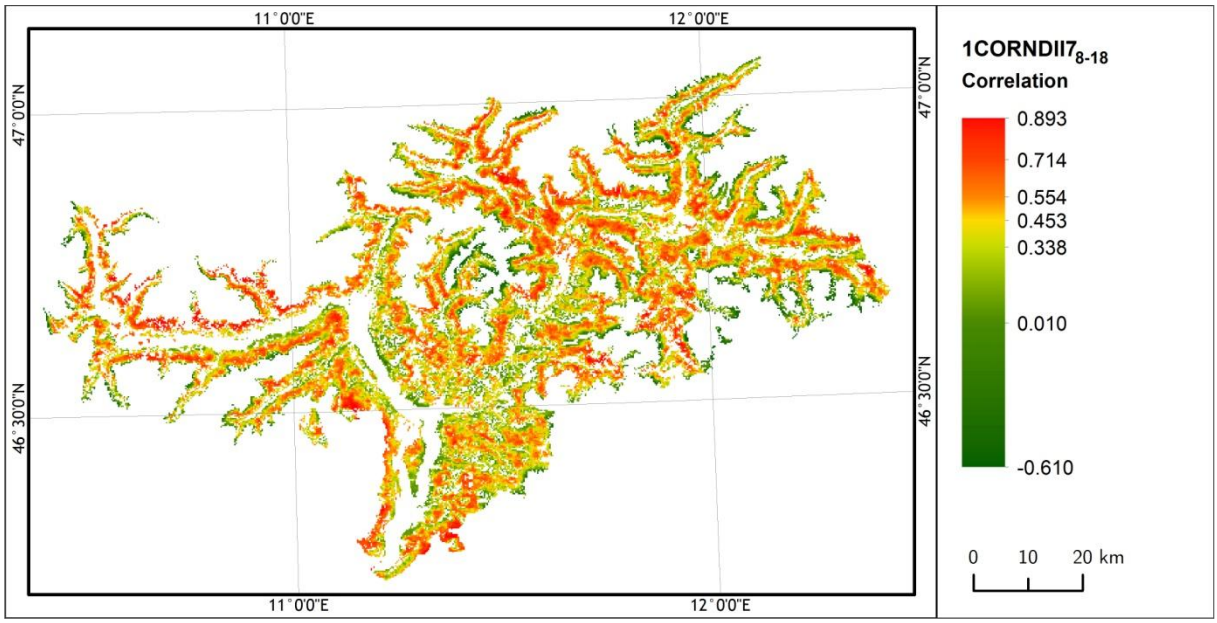

Figure A4 6 Spatial representation of forest potential drought response identified by the $1CORNDII7_{8\text{-}18}$. Correlation footprint refers to the score presented in the Figure 16F. Values next to the color ramp represents in the increasing order 0^{th}, 5^{th}, 30^{th}, 50^{th}, 70^{th} 95^{th} and 100^{th} percentiles of the correlation distribution.

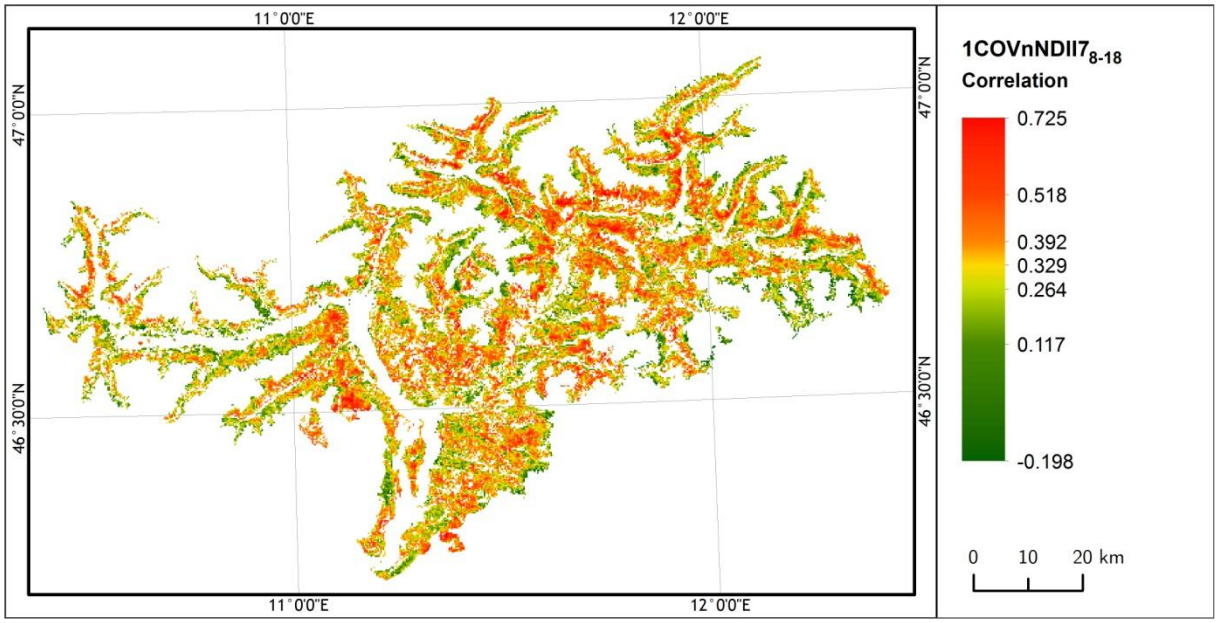

Figure A4 7 Spatial representation of forest potential drought response identified by the 1COVnNDII7$_{8\text{-}18}$. Correlation footprint refers to the score presented in the Figure 16G. Values next to the color ramp represents in the increasing order 0th, 5th, 30th, 50th, 70th 95th and 100th percentiles of the correlation distribution.

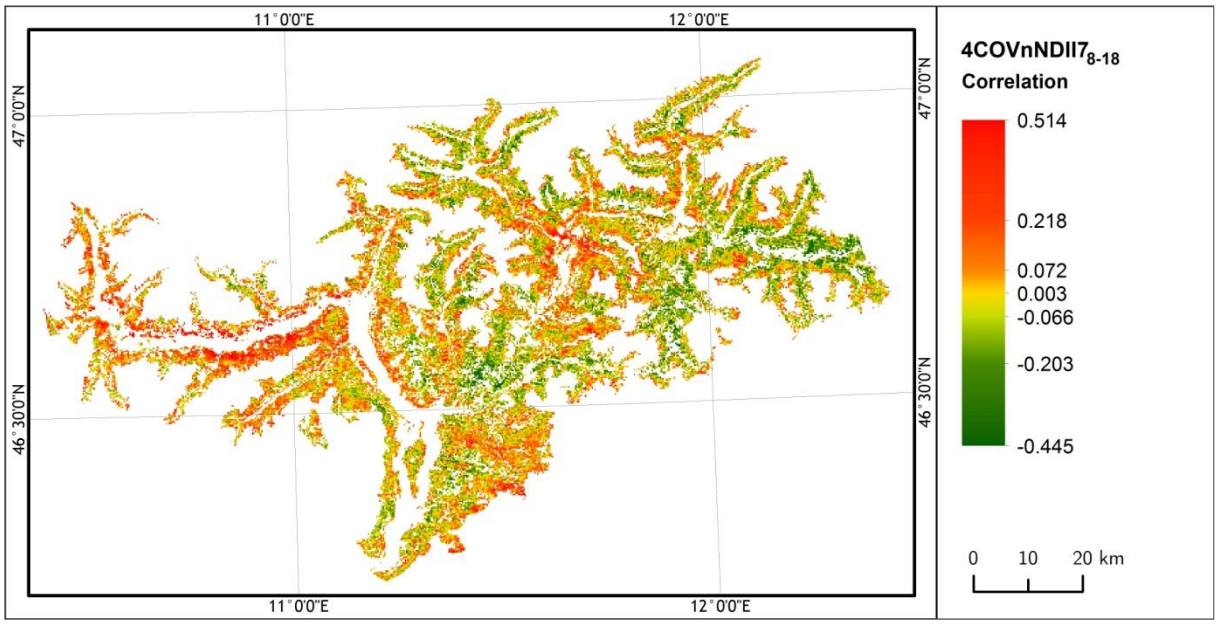

Figure A4 8 Spatial representation of forest potential drought response identified by the 4COVnNDII7$_{8\text{-}18}$. Correlation footprint refers to the score presented in the Figure 16H. Values next to the color ramp represents in the increasing order 0th, 5th, 30th, 50th, 70th 95th and 100th percentiles of the correlation distribution.

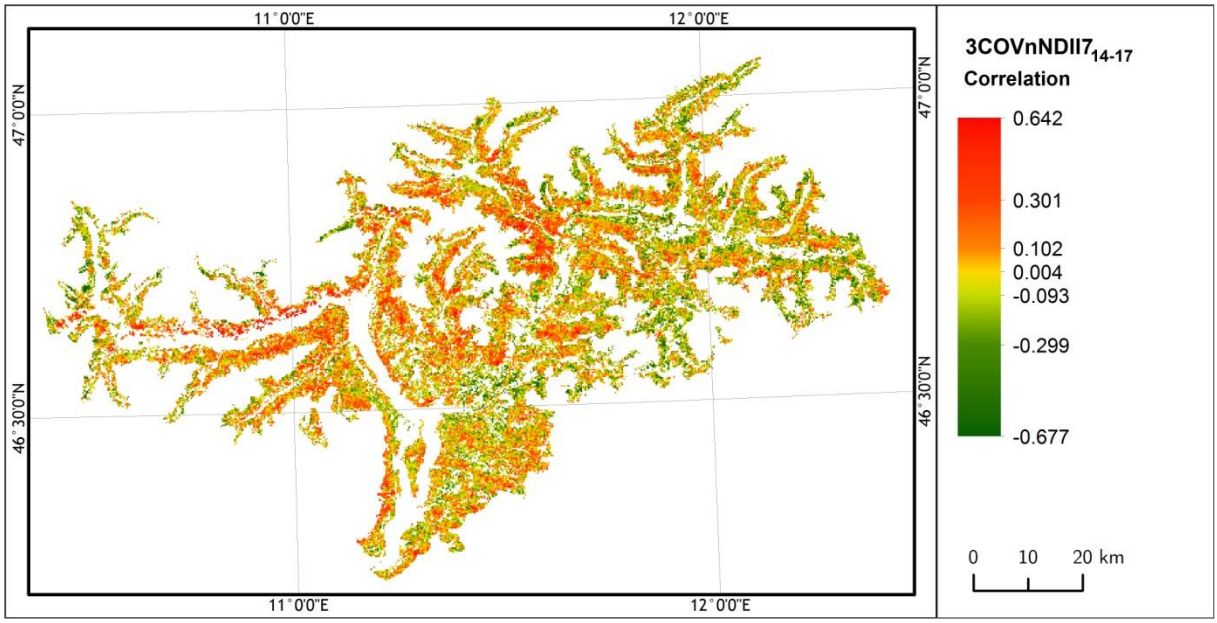

Figure A4 9 Spatial representation of forest potential drought response identified by the 3COVnNDII7$_{14\text{-}17}$. Correlation footprint refers to the score presented in the Figure 16I. Values next to the color ramp represents in the increasing order 0th, 5th, 30th, 50th, 70th 95th and 100th percentiles of the correlation distribution.

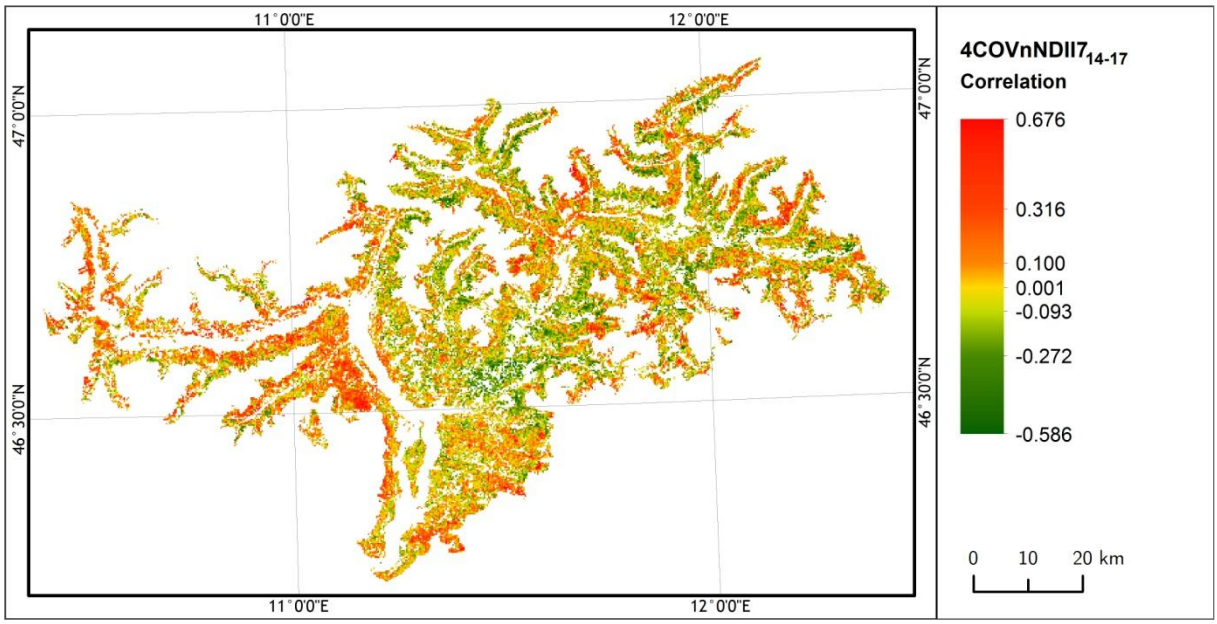

Figure A4 10 Spatial representation of forest potential drought response identified by the 4COVnNDII7$_{14\text{-}17}$. Correlation footprint refers to the score presented in the Figure 16J. Values next to the color ramp represents in the increasing order 0th, 5th, 30th, 50th, 70th 95th and 100th percentiles of the correlation distribution.

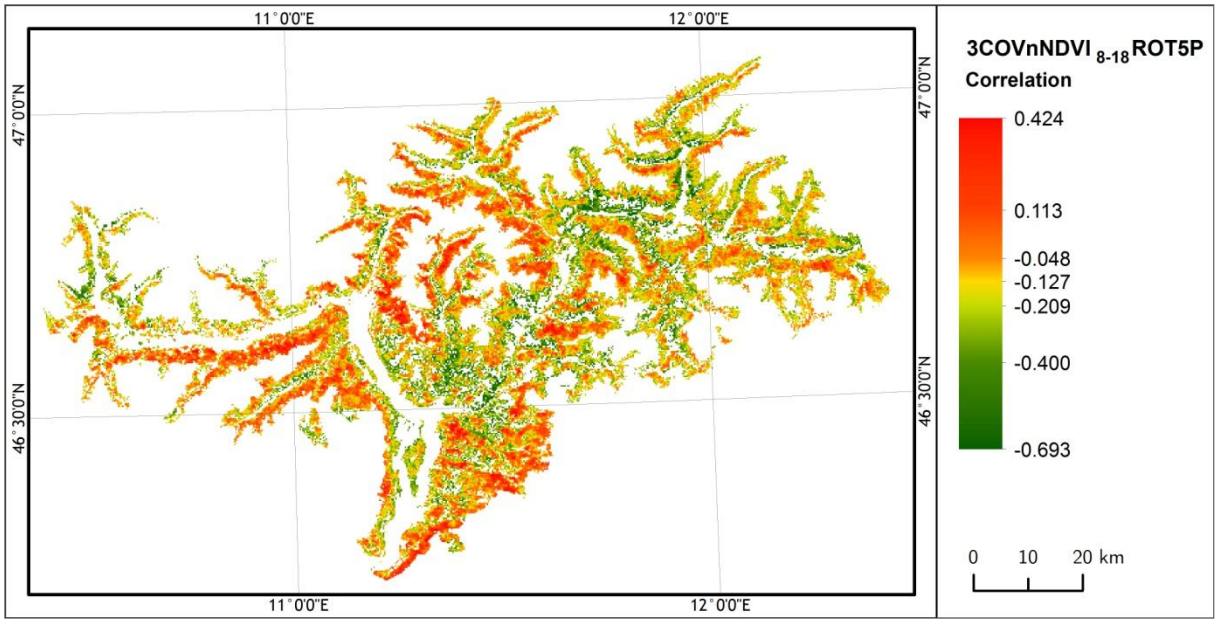

Figure A4 11 Spatial representation of forest potential drought response identified by the 3COVnNDVI$_{8\text{-}18}$ROT5P. Correlation footprint refers to the score presented in the Figure 16K. Values next to the color ramp represents in the increasing order 0th, 5th, 30th, 50th, 70th 95th and 100th percentiles of the correlation distribution.

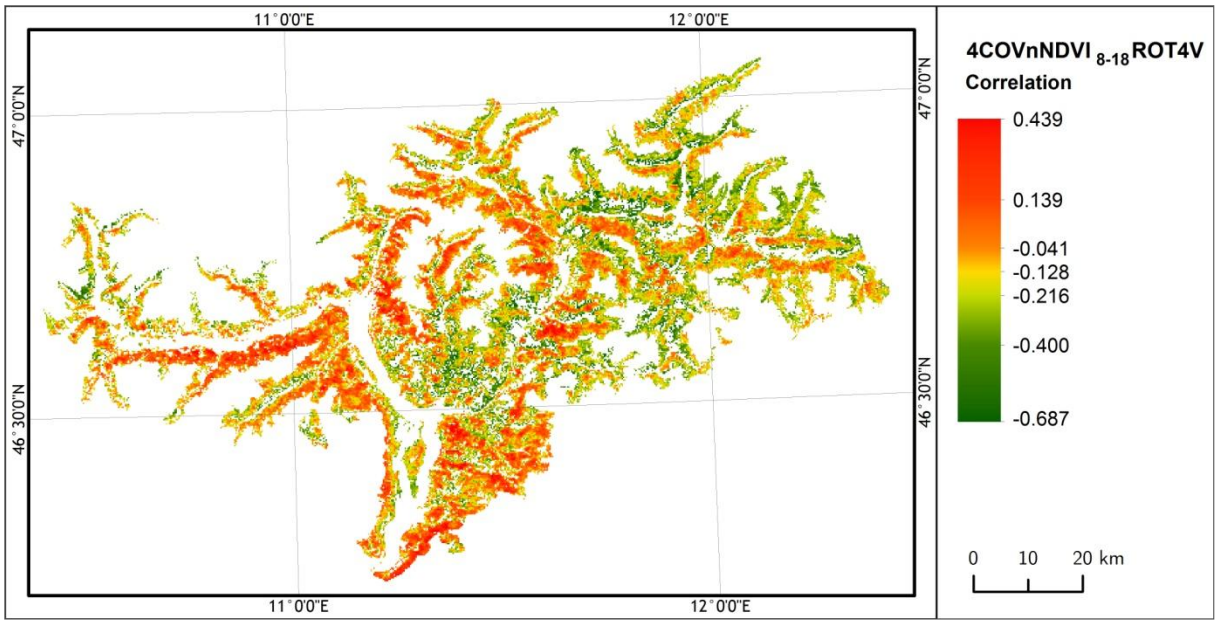

Figure A4 12 Spatial representation of forest potential drought response identified by the 4COVnNDVI$_{8\text{-}18}$ROT4V. Correlation footprint refers to the score presented in the Figure 16L. Values next to the color ramp represents in the increasing order 0th, 5th, 30th, 50th, 70th 95th and 100th percentiles of the correlation distribution.

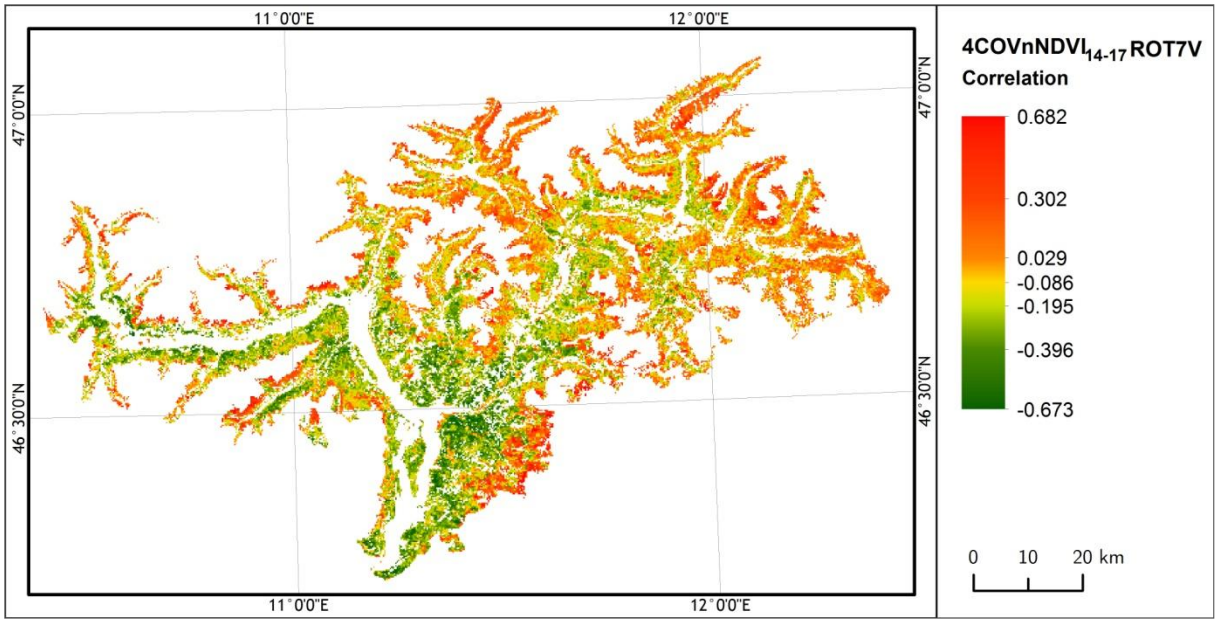

Figure A4 13 Spatial representation of forest potential drought response identified by the 4COVnNDVI$_{14\text{-}17}$ROT7V. Correlation footprint refers to the score presented in the Figure 16M. Values next to the color ramp represents in the increasing order 0th, 5th, 30th, 50th, 70th 95th and 100th percentiles of the correlation distribution.

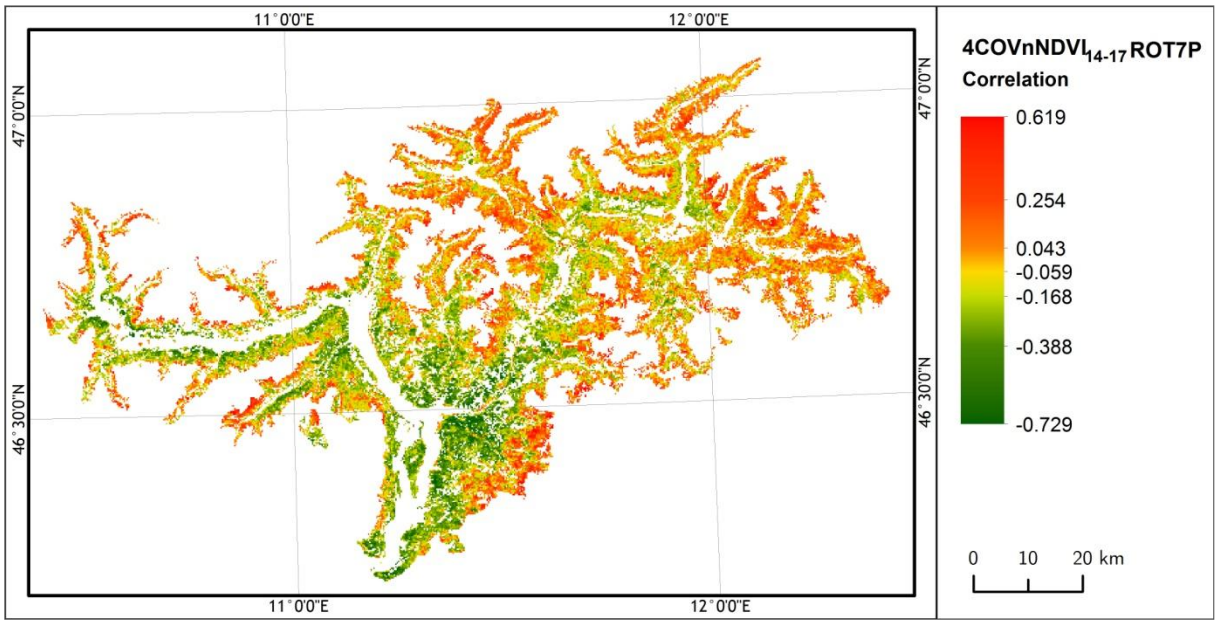

Figure A4 14 Spatial representation of forest potential drought response identified by the 4COVnNDVI$_{14\text{-}17}$ROT7P. Correlation footprint refers to the score presented in the Figure 16N. Values next to the color ramp represents in the increasing order 0th, 5th, 30th, 50th, 70th 95th and 100th percentiles of the correlation distribution.

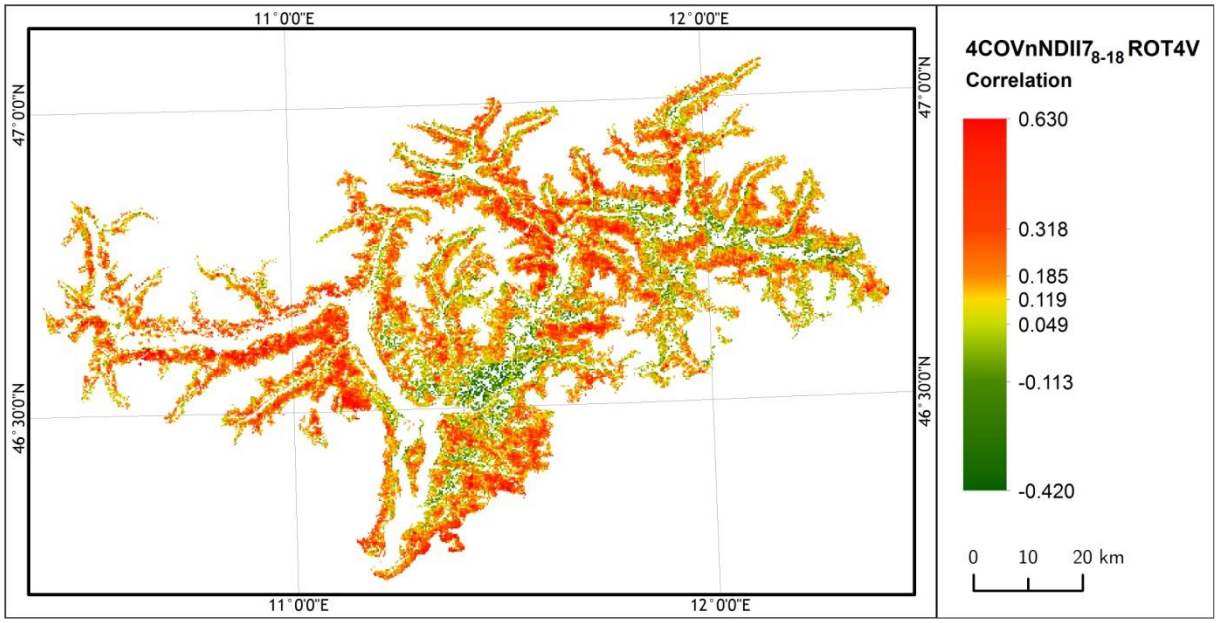

Figure A4 15 Spatial representation of forest potential drought response identified by the 4COVnNDII7$_{8-18}$ROT4V. Correlation footprint refers to the score presented in the Figure 16O. Values next to the color ramp represents in the increasing order 0th, 5th, 30th, 50th, 70th 95th and 100th percentiles of the correlation distribution.

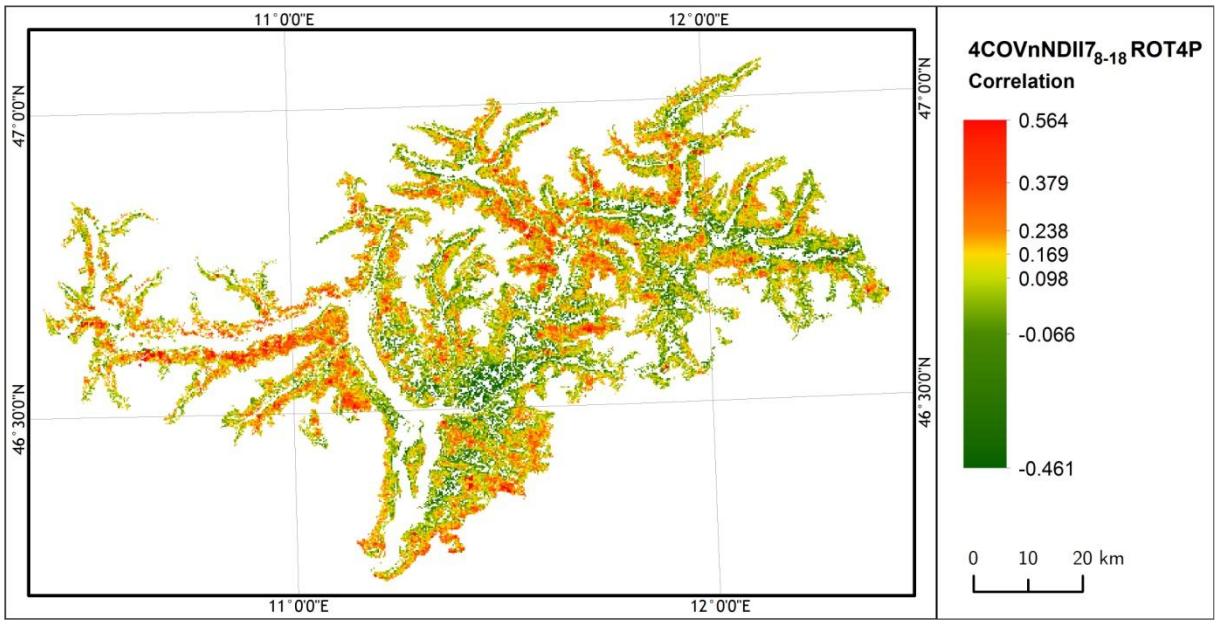

Figure A4 16 Spatial representation of forest potential drought response identified by the 4COVnNDII7$_{8-18}$ROT4P. Correlation footprint refers to the score presented in the Figure 16P. Values next to the color ramp represents in the increasing order 0th, 5th, 30th, 50th, 70th 95th and 100th percentiles of the correlation distribution.

APPENDIX 5

A.5. The within-subjects effect test or repeated ANOVA

Table A5 1 The within-subjects effects test of repeated measures ANOVA performed for class 6 of the 1CORNDII7$_{8\text{-}18}$ PC spatial representation. Test run with the Hujnh-Feldt adjustment returning results for the factor of time within selected phenology and productivity indicators.

	time			**Error**
	df	F	p	df
CF	9.098	17.596	0.000	21298.408
GPP	9.090	5.424	0.000	21279.372
SBD	8.642	4.166	0.000	20230.441
SL	9.022	3.238	0.001	21119.430
NDVI$_{HS}$	9.506	25.226	0.000	22254.618
NDII7$_{HS}$	11.447	50.952	0.000	2341.000

Table A5 2 The within-subjects effects test of repeated measures ANOVA performed for class 6 of the 4COVnNDII7$_{8\text{-}18}$ PC spatial representation. Test run with the Hujnh-Feldt adjustment returning results for the factor of time within selected phenology and productivity indicators.

	time			**Error**
	df	F	p	df
CF	10.000	13.859	0.000	6340.000
GPP	10.000	5.080	0.000	6340.000
SBD	10.000	3.895	0.000	6340.000
SL	10.000	3.218	0.000	6340.000
NDVI$_{HS}$	10.587	53.721	0.000	6711.859
NDII7$_{HS}$	12.000	95.769	0.000	7608.000

Table A5 3 The within-subjects effects test of repeated measures ANOVA performed for class 6 of the 3COVnNDVI$_{8\text{-}18}$ PC spatial representation. Test run with the Hujnh-Feldt adjustment returning results for the factor of time within selected phenology and productivity indicators.

	time			**Error**
	df	F	p	df
CF	9.821	4.124	0.000	11225.627
GPP	9.891	0.604	0.810	11305.458
SBD	9.205	0.523	0.862	10521.605
SL	10.000	1.846	0.048	11430.000
NDVI$_{HS}$	10.465	32.421	0.000	11961.012
NDII7$_{HS}$	11.662	6.420	0.000	13469.839

Table A5 4 The within-subjects effects test of repeated measures ANOVA performed for class 1 of the 3COVnNDVI$_{8\text{-}18}$ PC spatial representation. Test run with the Hujnh-Feldt adjustment returning results for the factor of time within selected phenology and productivity indicators.

	time			**Error**
	df	F	p	df
CF	8.486	38.342	0.000	9309.011
GPP	9.695	23.771	0.000	10635.826
SBD	8.335	15.525	0.000	9143.595
SL	9.252	14.318	0.000	10149.226
NDVI$_{HS}$	10.615	92.926	0.000	11644.694
NDII7$_{HS}$	10.700	80.944	0.000	12165.411

APPENDIX 6

A.6. Estimated marginal means plots of repeated ANOVA preformed for MODIS derived drought impact patterns

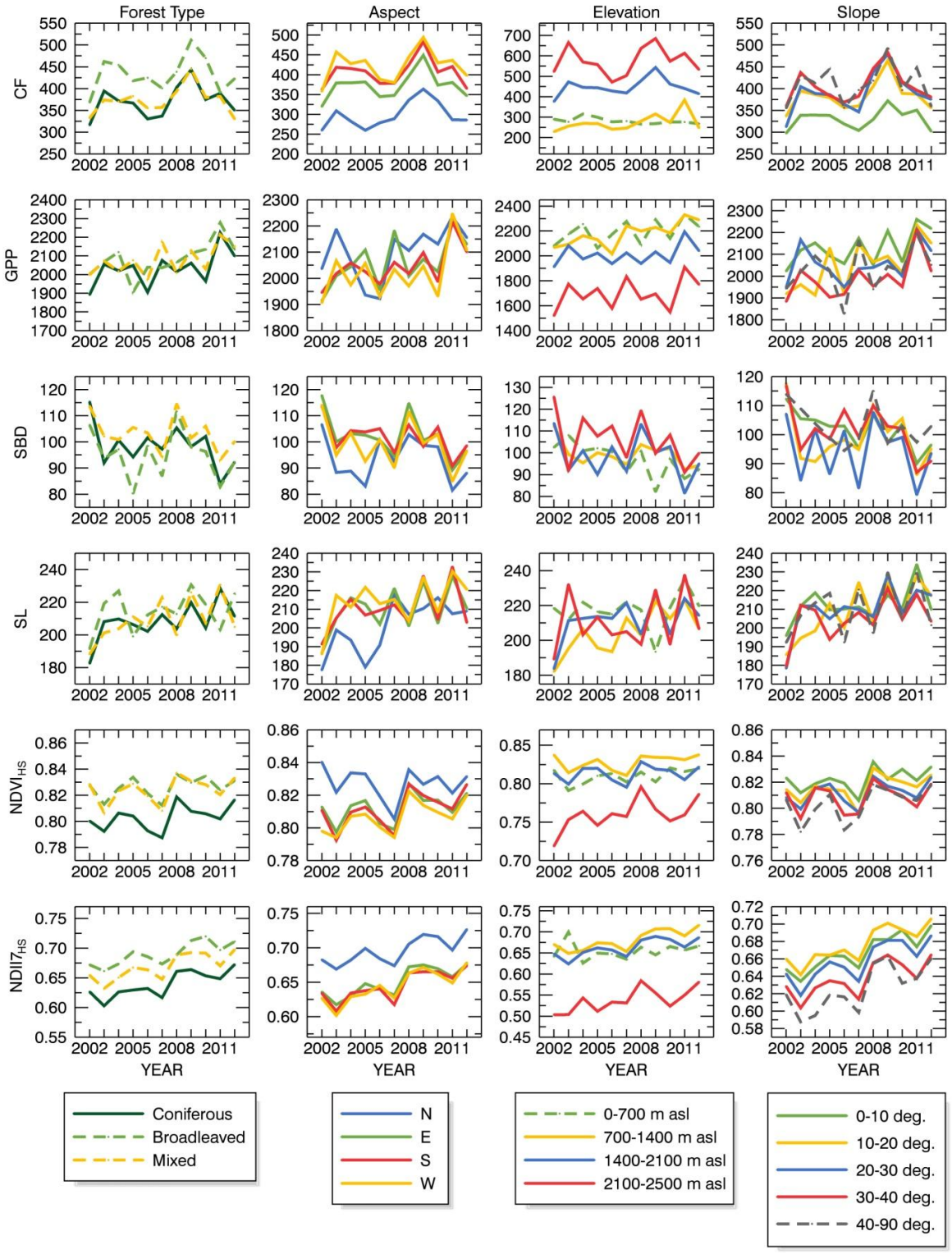

Figure A6 1 Marginal means plots of repeated ANOVA derived for (in rows) CF, GPP, SBD, SL, $NDVI_{HS}$ and $NDII7_{HS}$ analyzed within the $1CORNDII7_{8\text{-}18}$ drought impact class 6. Values are presented within four multilevel-factors (in columns) of forest type, aspect, elevation and slope. Profiles plotted in dashed line are based on less than 50 observations.

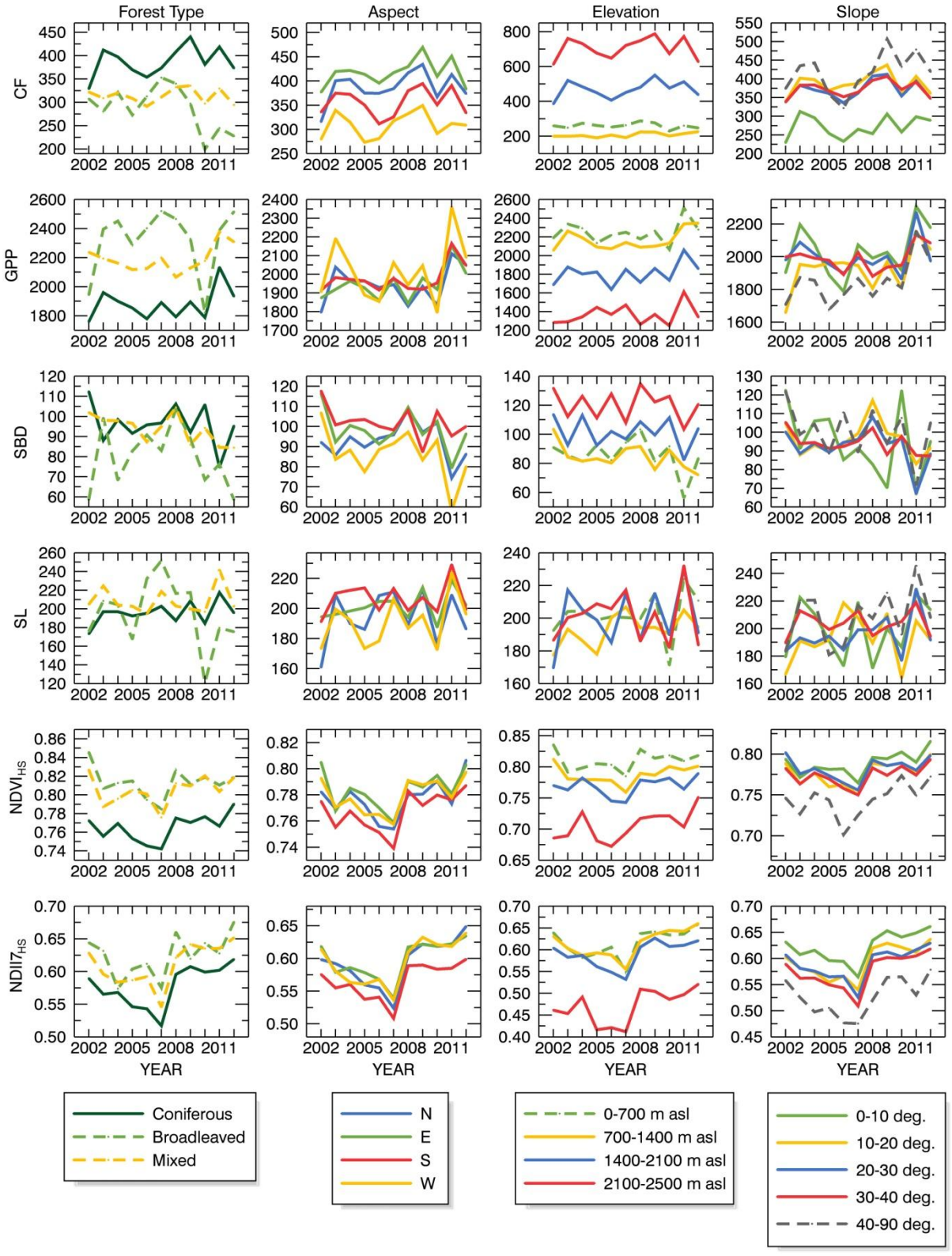

Figure A6 2 Marginal means plots of repeated ANOVA derived for (in rows) CF, GPP, SBD, SL, $NDVI_{HS}$ and $NDII7_{HS}$ analyzed within the $4COVnNDII7_{8\text{-}18}$ response class 6. Values are presented within four multilevel-factors (in columns) of forest type, aspect, elevation and slope. Profiles plotted in dashed line are based on less than 50 observations.

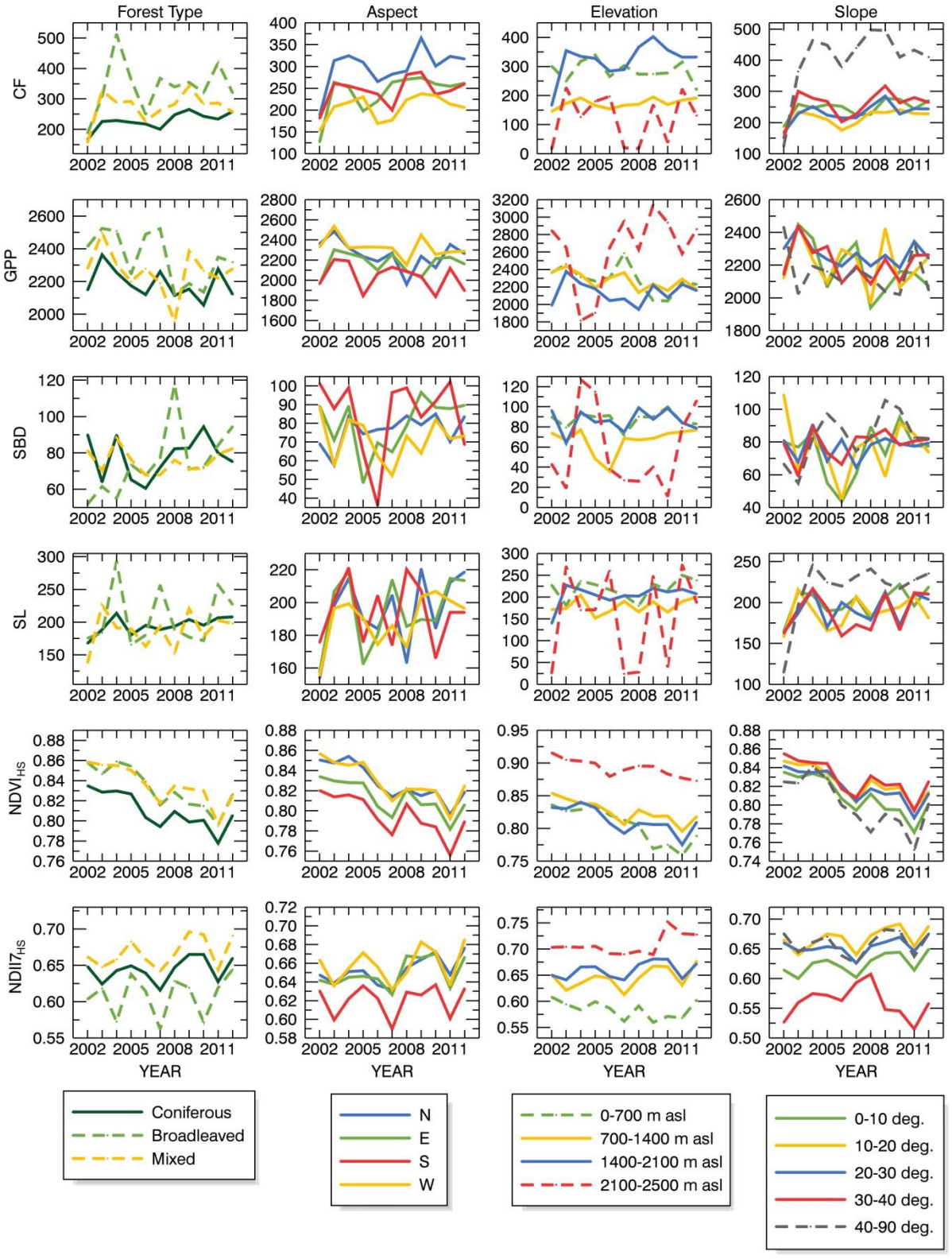

Figure A6 3 Marginal means plots of repeated ANOVA derived for (in rows) CF, GPP, SBD, SL, $NDVI_{HS}$ and $NDII7_{HS}$ analyzed within the $3COVnNDVI_{8\text{-}18}$ response class 6. Values are presented within four multilevel-factors (in columns) of forest type, aspect, elevation and slope. Profiles plotted in dashed line are based on less than 50 observations.

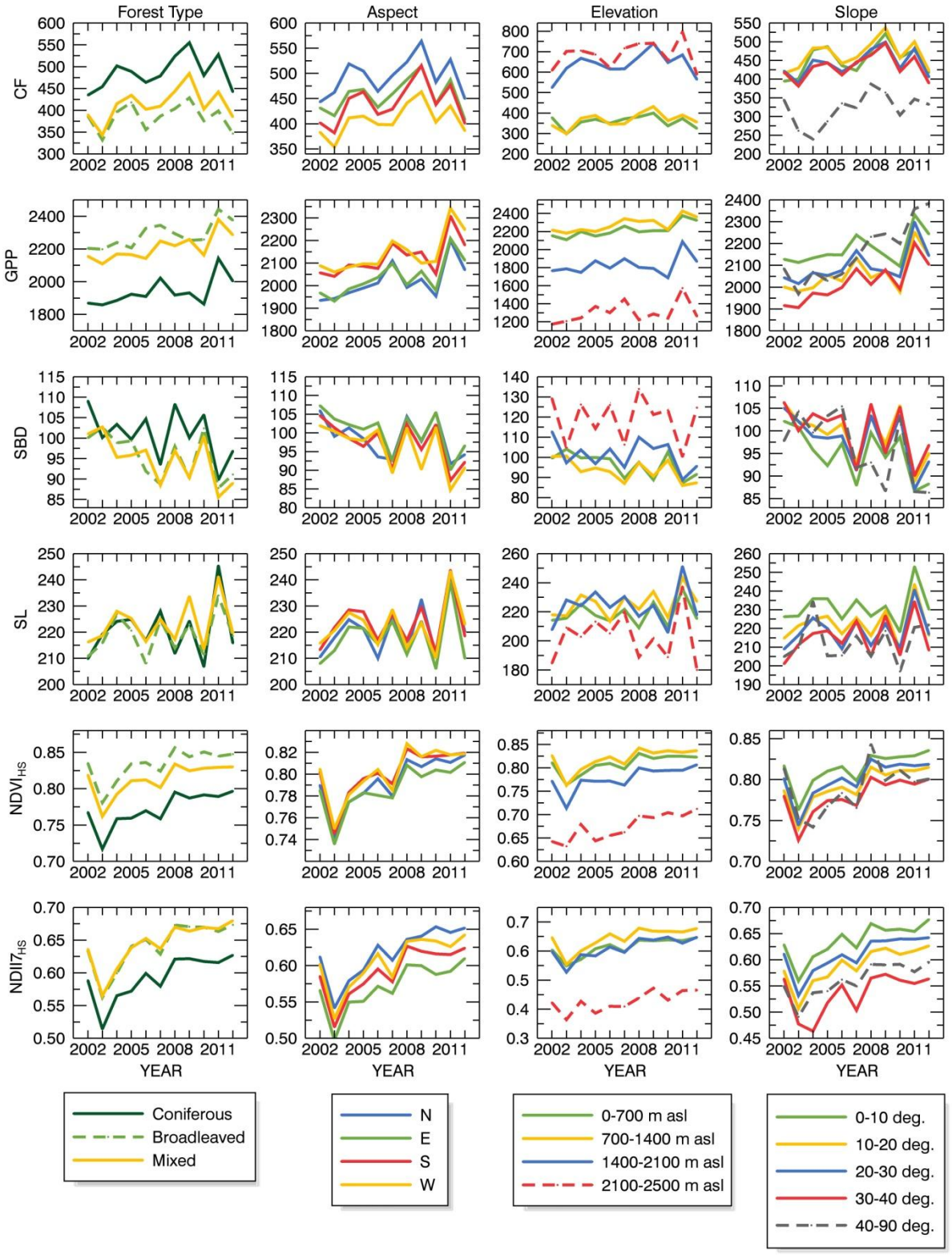

Figure A6 4 Marginal means plots of repeated ANOVA derived for (in rows) CF, GPP, SBD, SL, $NDVI_{HS}$ and $NDII7_{HS}$ analyzed within the $3COVnNDVI_{8\text{-}18}$ response class 1. Values are presented within four multilevel-factors (in columns) of forest type, aspect, elevation and slope. Profiles plotted in dashed line are based on less than 50 observations.

APPENDIX 7

A.7. PCA analyses of Landsat derived $_{L}$NDVI and $_{L}$NBRI time series – identification of drought related temporal patterns

A.7.1. Correlation-matrix based PCA of $_{L}$NDVI 2001-2011 time series

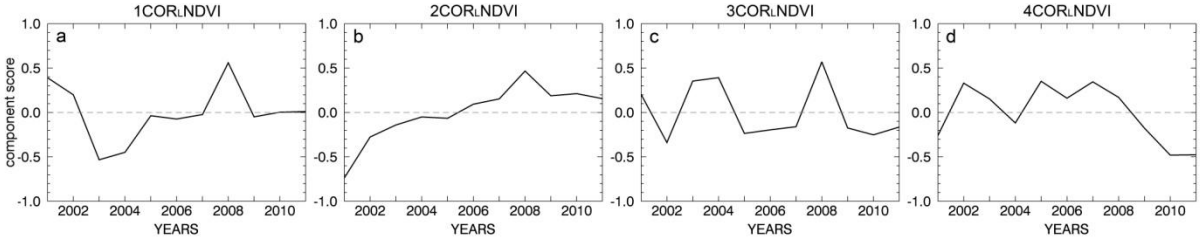

Figure A7 1 First four PCs resulting from the S-mode correlation-matrix based PCA decomposition of the $_{L}$NDVI time series.

Table A7 1 Total variability explained by first four PCs resulting from the S-mode correlation-matrix based PCA decomposition of the $_{L}$NDVI time series.

PC	Explained variability
1COR$_{L}$NDVI	16.43%
2COR$_{L}$NDVI	14.81%
3COR$_{L}$NDVI	12.85%
4COR$_{L}$NDVI	10.74%

A.7.2. Correlation-matrix based PCA of $_{L}$NBRI 2001-2011 time series

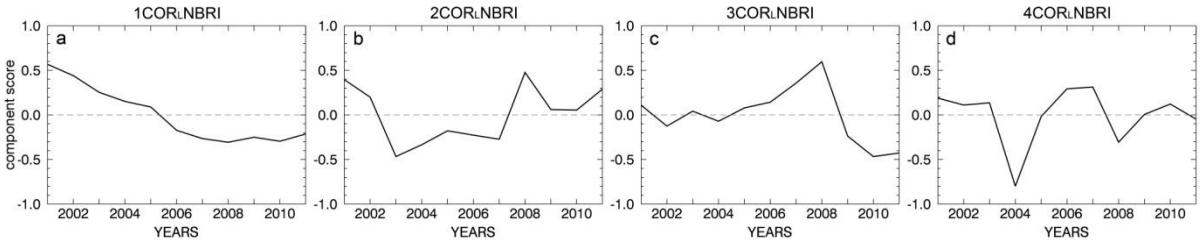

Figure A7 2 First four PCs resulting from the S-mode correlation-matrix based PCA decomposition of the $_{L}$NBRI time series.

Table A7 2 First four PCs resulting from the S-mode correlation-matrix based PCA decomposition of the $_{L}$NBRI time series.

PC	Explained variability
1COR$_{L}$NBRI	14.80%
2COR$_{L}$NBRI	13.55%
3COR$_{L}$NBRI	11.45%
4COR$_{L}$NBRI	10.70%

APPENDIX 8

A.8. Spatial representations of Landsat derived drought impact patterns

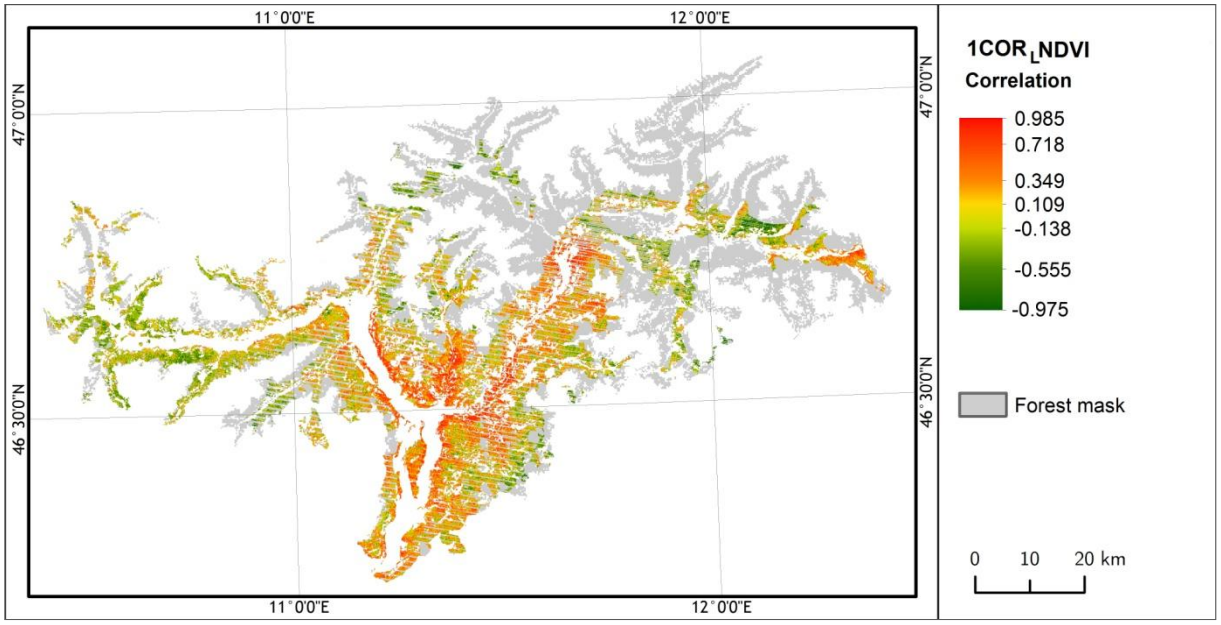

Figure A8 1 Spatial representation of forest potential drought response identified by the 1COR$_L$NDVI PC. Correlation footprint refers to the score presented in the Figure 23A. Values next to the color ramp represents in the increasing order 0th, 5th, 30th, 50th, 70th 95th and 100th percentiles of the correlation distribution.

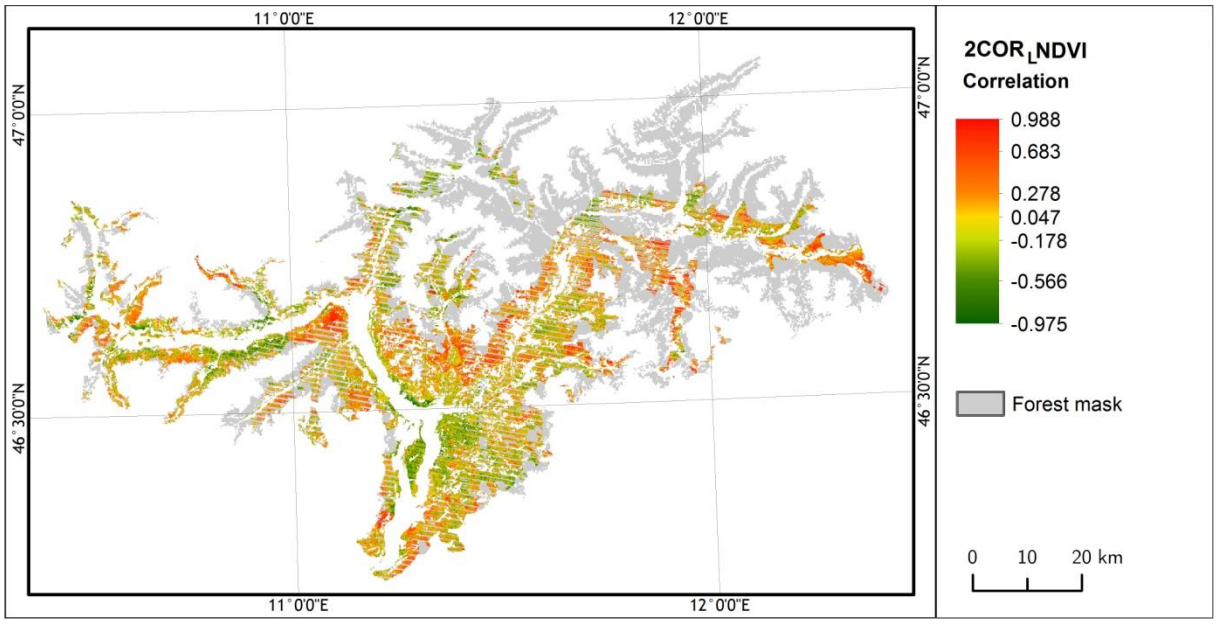

Figure A8 2 Spatial representation of forest potential drought response identified by the 2COR$_L$NDVI PC. Correlation footprint refers to the score presented in the Figure 23B. Values next to the color ramp represents in the increasing order 0th, 5th, 30th, 50th, 70th 95th and 100th percentiles of the correlation distribution.

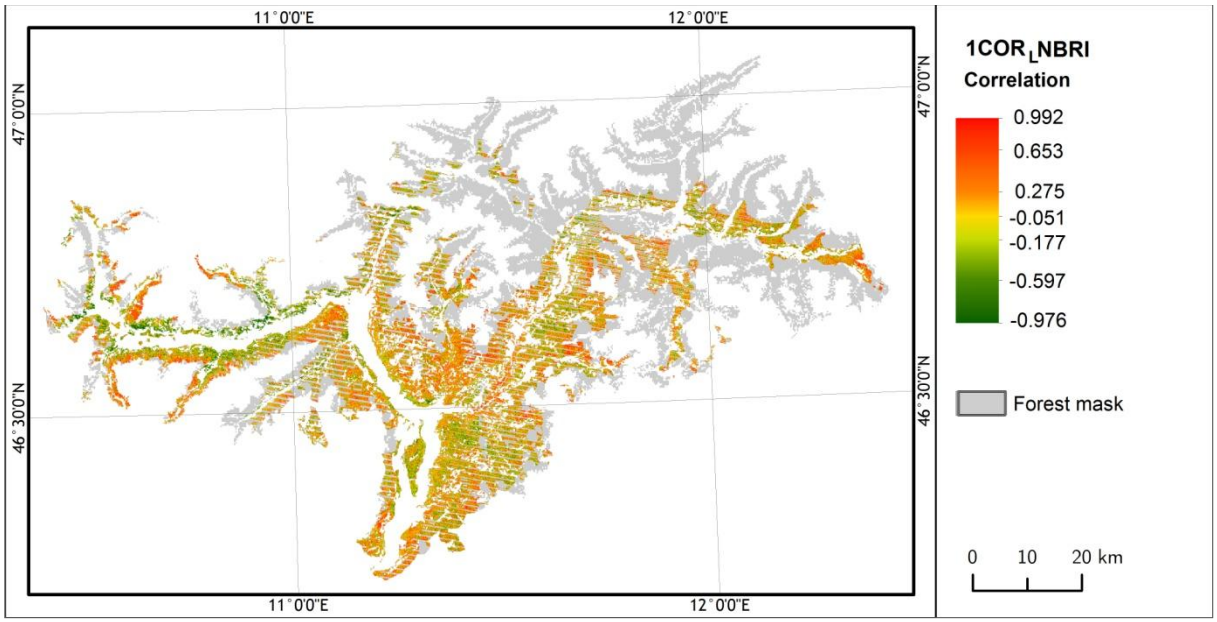

Figure A8 3 Spatial representation of forest potential drought response identified by the 1COR$_L$NBRI PC. Correlation footprint refers to the score presented in the Figure 23C. Values next to the color ramp represents in the increasing order 0th, 5th, 30th, 50th, 70th 95th and 100th percentiles of the correlation distribution.

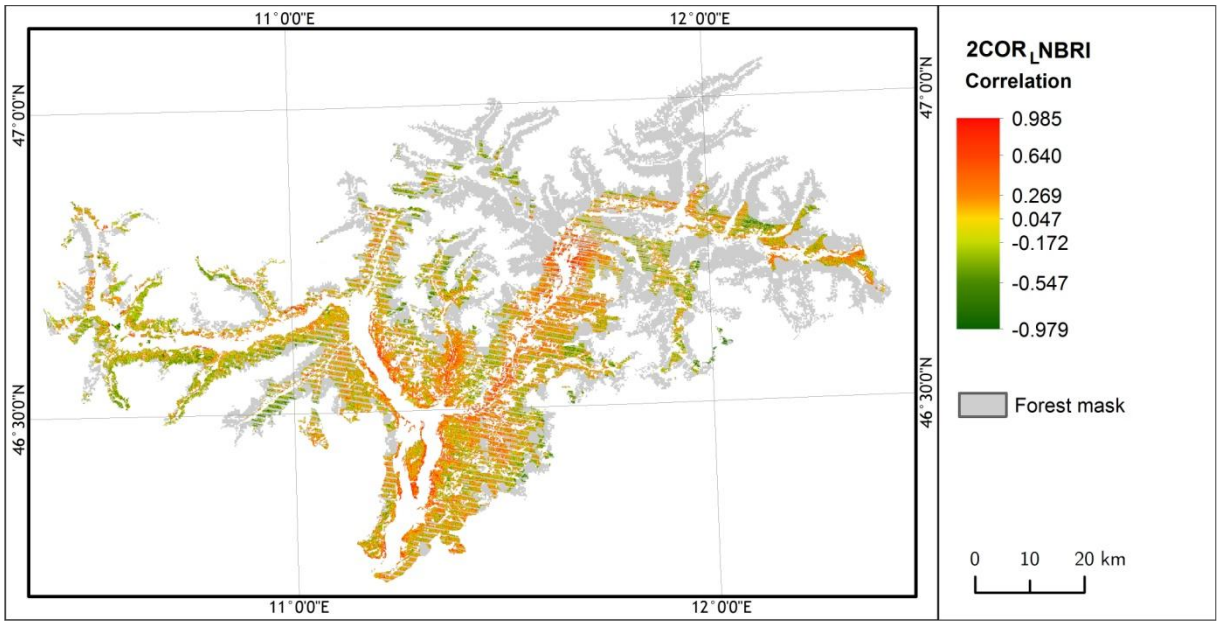

Figure A8 4 Spatial representation of forest potential drought response identified by the 2COR$_L$NBRI PC. Correlation footprint refers to the score presented in the Figure 23D. Values next to the color ramp represents in the increasing order 0th, 5th, 30th, 50th, 70th 95th and 100th percentiles of the correlation distribution.

APPENDIX 9

A.9. Synthetic MODIS-like spatial representations of Landsat derived drought impact patterns

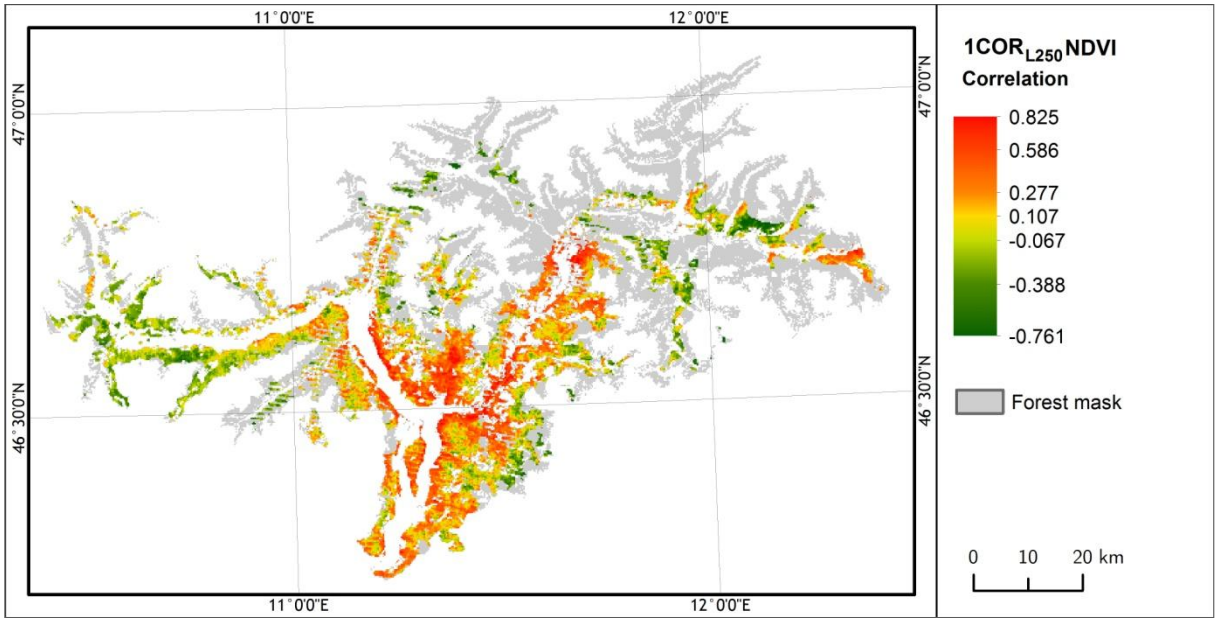

Figure A9 1 Spatial representation of forest potential drought response identified by the 1COR$_L$NDVI PC and represented as synthetic MODIS-like maps. Correlation footprint refers to the score presented in the Figure 23A. Values next to the color ramp represents in the increasing order 0th, 5th, 30th, 50th, 70th 95th and 100th percentiles of the correlation distribution.

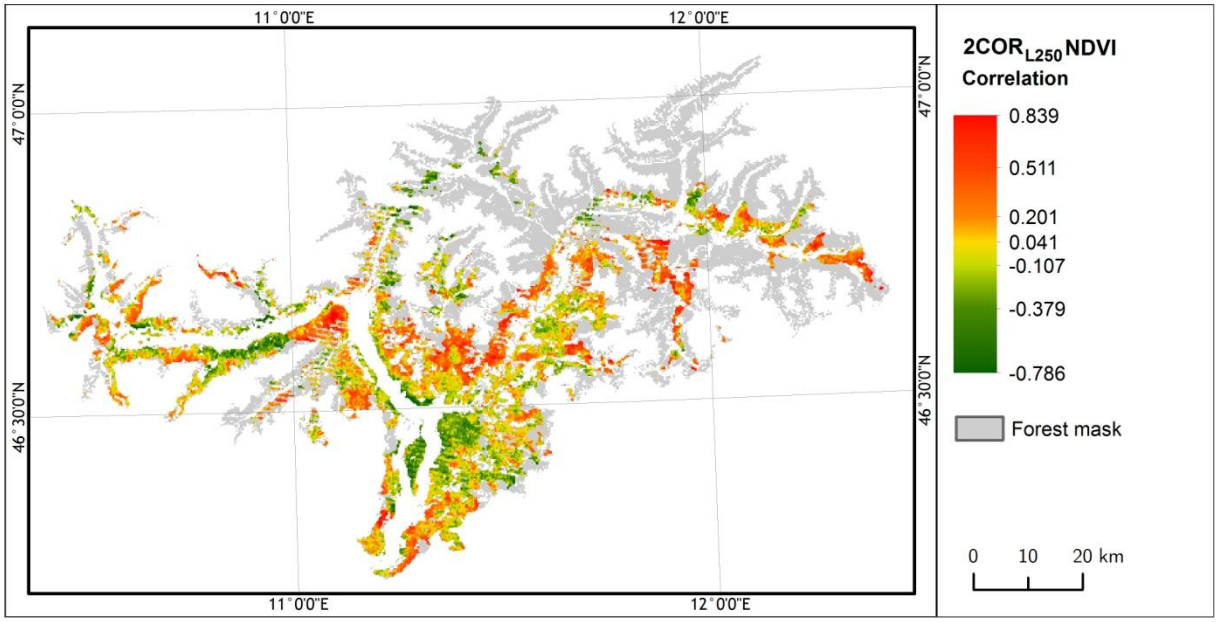

Figure A9 2 Spatial representation of forest potential drought response identified by the 2COR$_L$NDVI PC and represented as synthetic MODIS-like maps. Correlation footprint refers to the score presented in the Figure 23B. Values next to the color ramp represents in the increasing order 0th, 5th, 30th, 50th, 70th 95th and 100th percentiles of the correlation distribution.

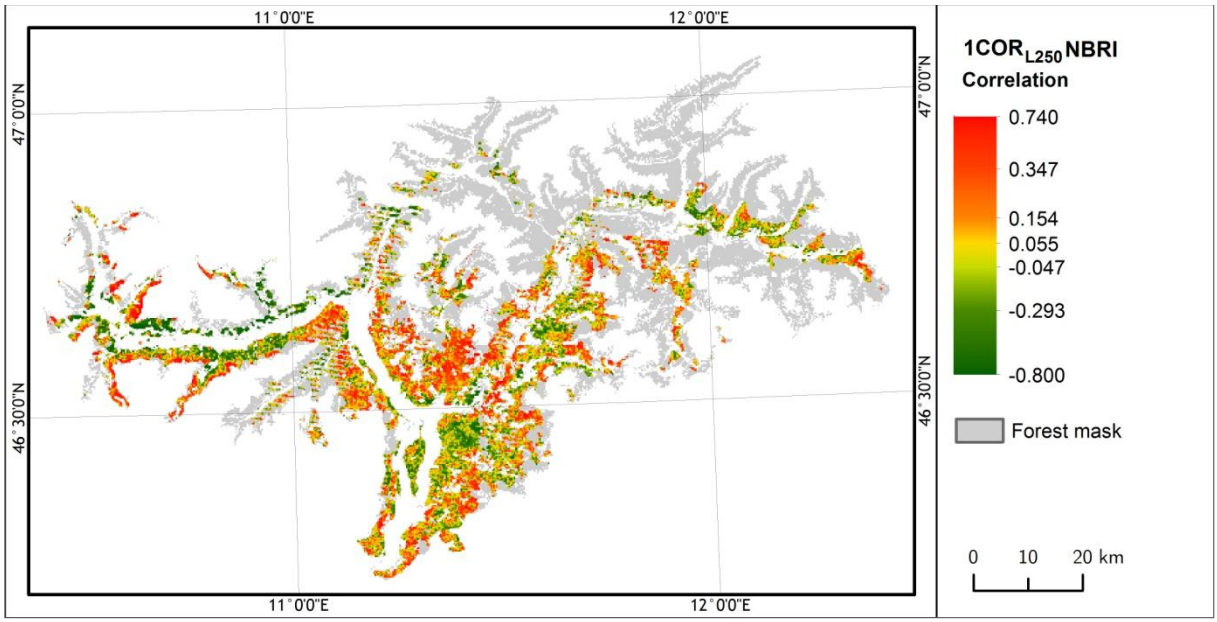

Figure A9 3 Spatial representation of forest potential drought response identified by the 1COR$_L$NBRI PC and represented as synthetic MODIS-like maps. Correlation footprint refers to the score presented in the Figure 23C. Values next to the color ramp represents in the increasing order 0th, 5th, 30th, 50th, 70th 95th and 100th percentiles of the correlation distribution.

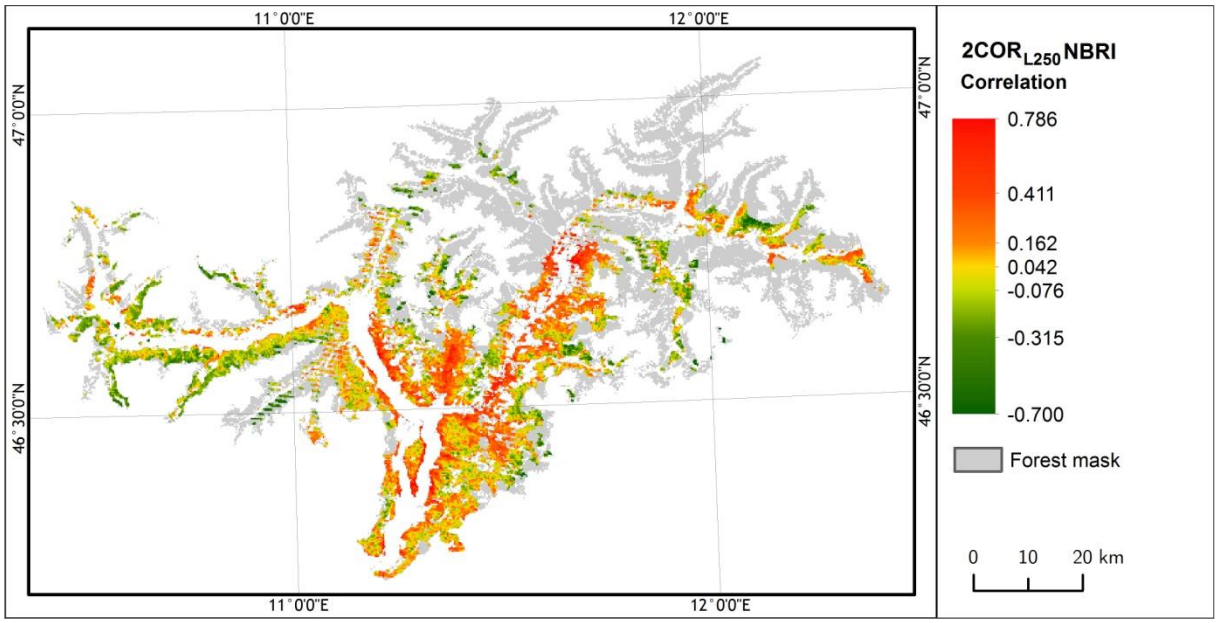

Figure A9 4 Spatial representation of forest potential drought response identified by the 2COR$_L$NBRI PC and represented as synthetic MODIS-like maps. Correlation footprint refers to the score presented in the Figure 23D. Values next to the color ramp represents in the increasing order 0th, 5th, 30th, 50th, 70th 95th and 100th percentiles of the correlation distribution.

APPENDIX 10

A.10. The within-subjects effect test or repeated ANOVA

Table A10 1 The within-subjects effects test of repeated measures ANOVA performed for the class 6 of the $1COR_{L250}$NDVI spatial representation. Test run with the Hujnh-Feldt adjustment returning results for the factor of time within selected phenology and productivity indicators.

	time			Error
	df	F	p	df
CF	9.218	1168.83	0.000	194535.862
GPP	9.447	417.107	0.000	195807.460
SBD	9.348	424.326	0.000	193758.122
SL	9.572	363.261	0.000	198408.155
$NDVI_{HS}$	10.354	3961.42	0.000	214610.770
$NDII7_{HS}$	11.474	5431.58	0.000	241654.896

Table A10 2 The within-subjects effects test of repeated measures ANOVA performed for the class 6 of the $2COR_{L250}$NDVI spatial representation. Test run with the Hujnh-Feldt adjustment returning results for the factor of time within selected phenology and productivity indicators.

	time			Error
	df	F	p	df
CF	9.109	104.587	0.000	192236.359
GPP	9.433	447.711	0.000	199085.480
SBD	9.346	425.088	0.000	197254.942
SL	9.566	383.409	0.000	201896.726
$NDVI_{HS}$	10.105	3814.02	0.000	213276.115
$NDII7_{HS}$	11.45	5201.05	0.000	241206.303

Table A10 3 The within-subjects effects test of repeated measures ANOVA performed for the class 6 of the $1COR_{L250}$NBRI spatial representation. Test run with the Hujnh-Feldt adjustment returning results for the factor of time within selected phenology and productivity indicators.

	time			Error
	df	F	p	df
CF	10.000	8.949	0.000	9350.000
GPP	10.000	6.362	0.000	9350.000
SBD	9.796	3.572	0.000	9159.112
SL	10.000	3.916	0.000	9350.000
$NDVI_{HS}$	11.396	32.373	0.000	10655.456
$NDII7_{HS}$	12.000	50.161	0.000	11100.000

Table A10 4 The within-subjects effects test of repeated measures ANOVA performed for the class 6 of the $2COR_{L250}NBRI$ spatial representation. Test run with the Hujnh-Feldt adjustment returning results for the factor of time within selected phenology and productivity indicators.

	time			**Error**
	df	F	p	df
CF	9.236	1239.764	0.000	194718.746
GPP	9.448	417.819	0.000	199173.184
SBD	9.353	407.660	0.000	197178.703
SL	9.573	358.874	0.000	201815.692
$NDVI_{HS}$	10.352	3975.383	0.000	218238.871
$NDII7_{HS}$	11.494	5389.982	0.000	239720.170

APPENDIX 11

A.11. Estimated marginal means plots of repeated ANOVA preformed for synthetic MODIS-like Landsat derived drought impact patterns

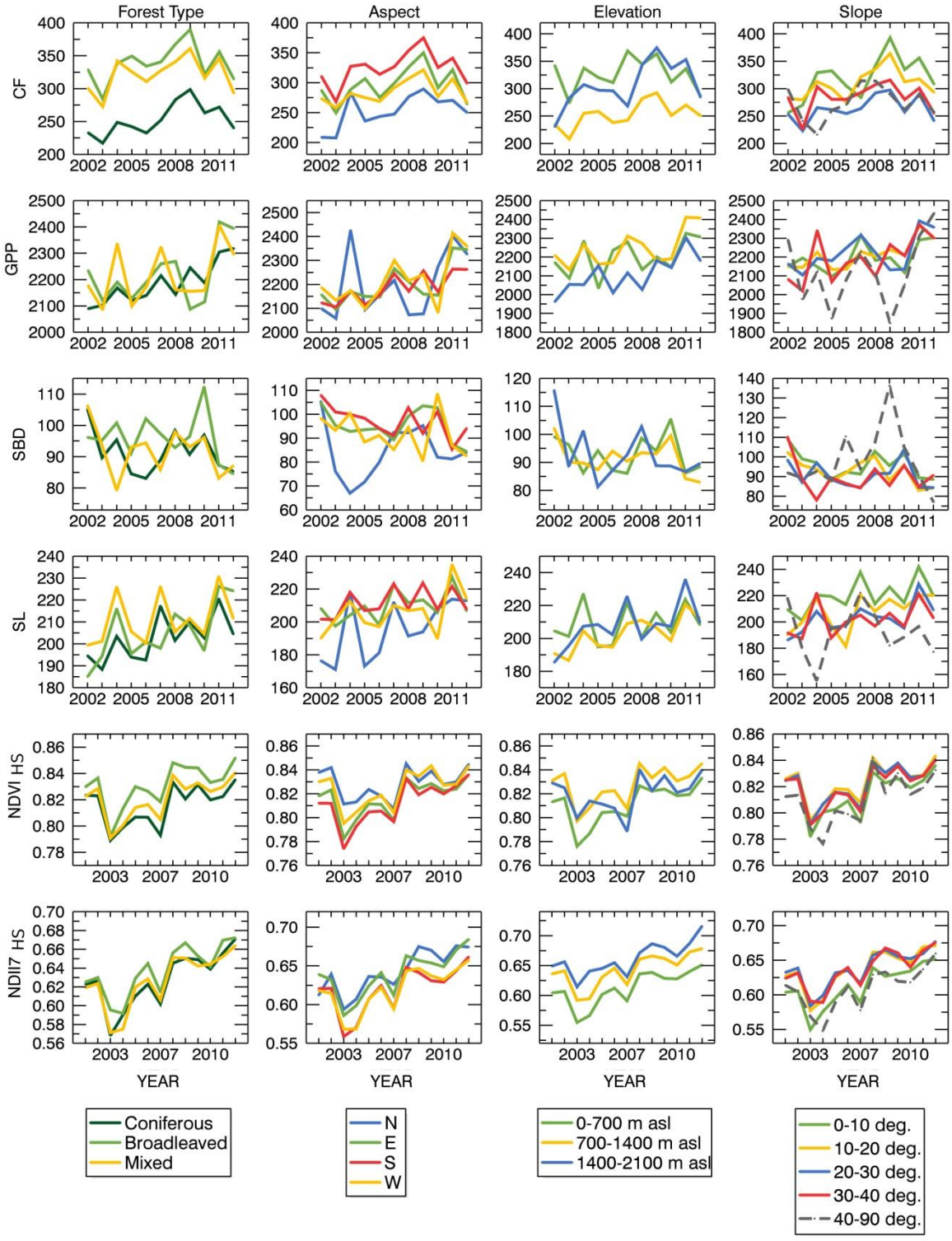

Figure A11 1 Marginal means plots of repeated ANOVA derived for (in rows) CF, GPP, SBD, SL, $NDVI_{HS}$ and $NDII7_{HS}$ analyzed within the $1COR_{L250}NDVI$ response class 6. Values are presented within four multilevel-factors (in columns) of forest type, aspect, elevation and slope. Profiles plotted in dashed line are based on less than 50 observations.

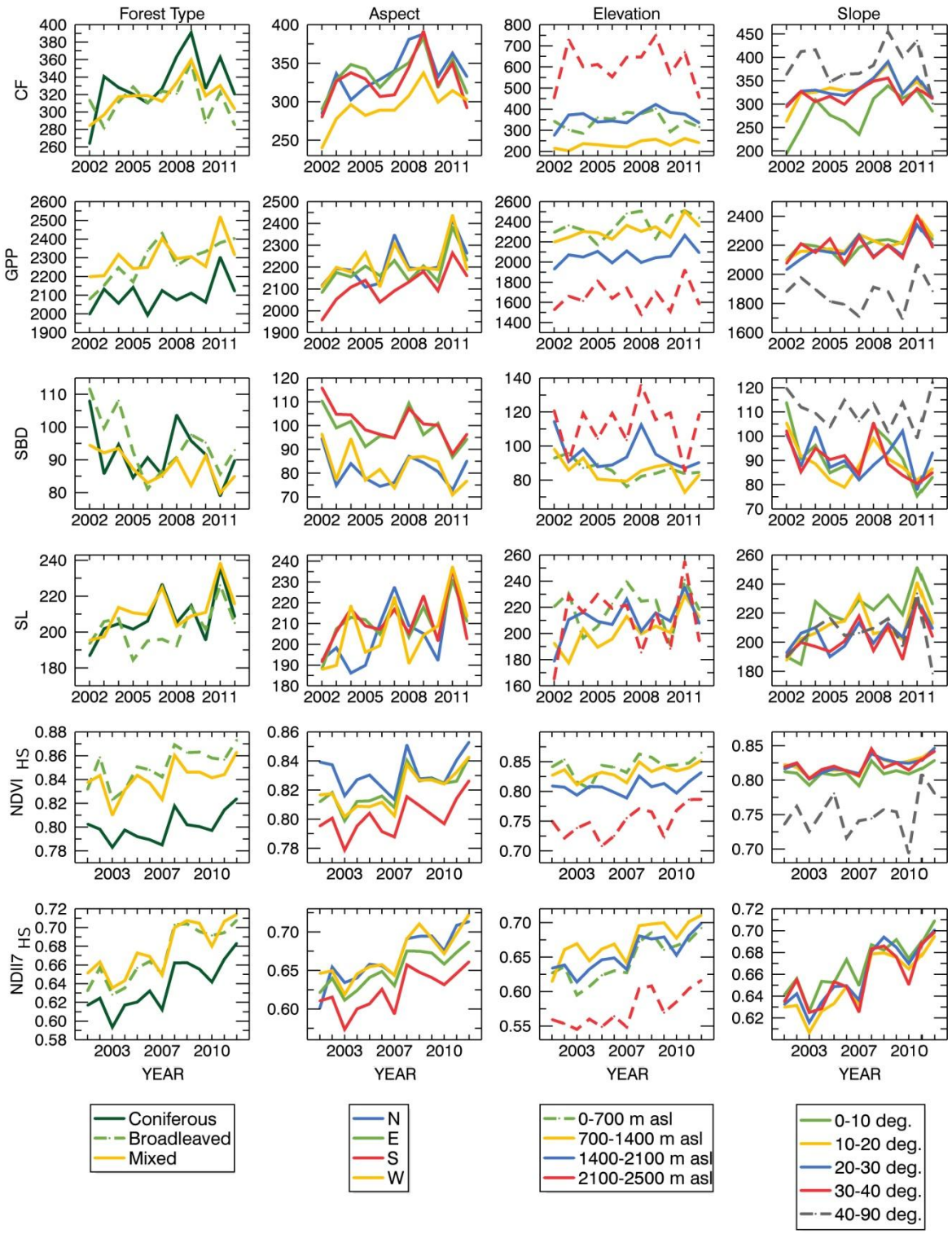

Figure A11 2 Marginal means plots of repeated ANOVA derived for (in rows) CF, GPP, SBD, SL, $NDVI_{HS}$ and $NDII7_{HS}$ analyzed within the $2COR_{L250}NDVI$ response class 6. Values are presented within four multilevel-factors (in columns) of forest type, aspect, elevation and slope. Profiles plotted in dashed line are based on less than 50 observations.

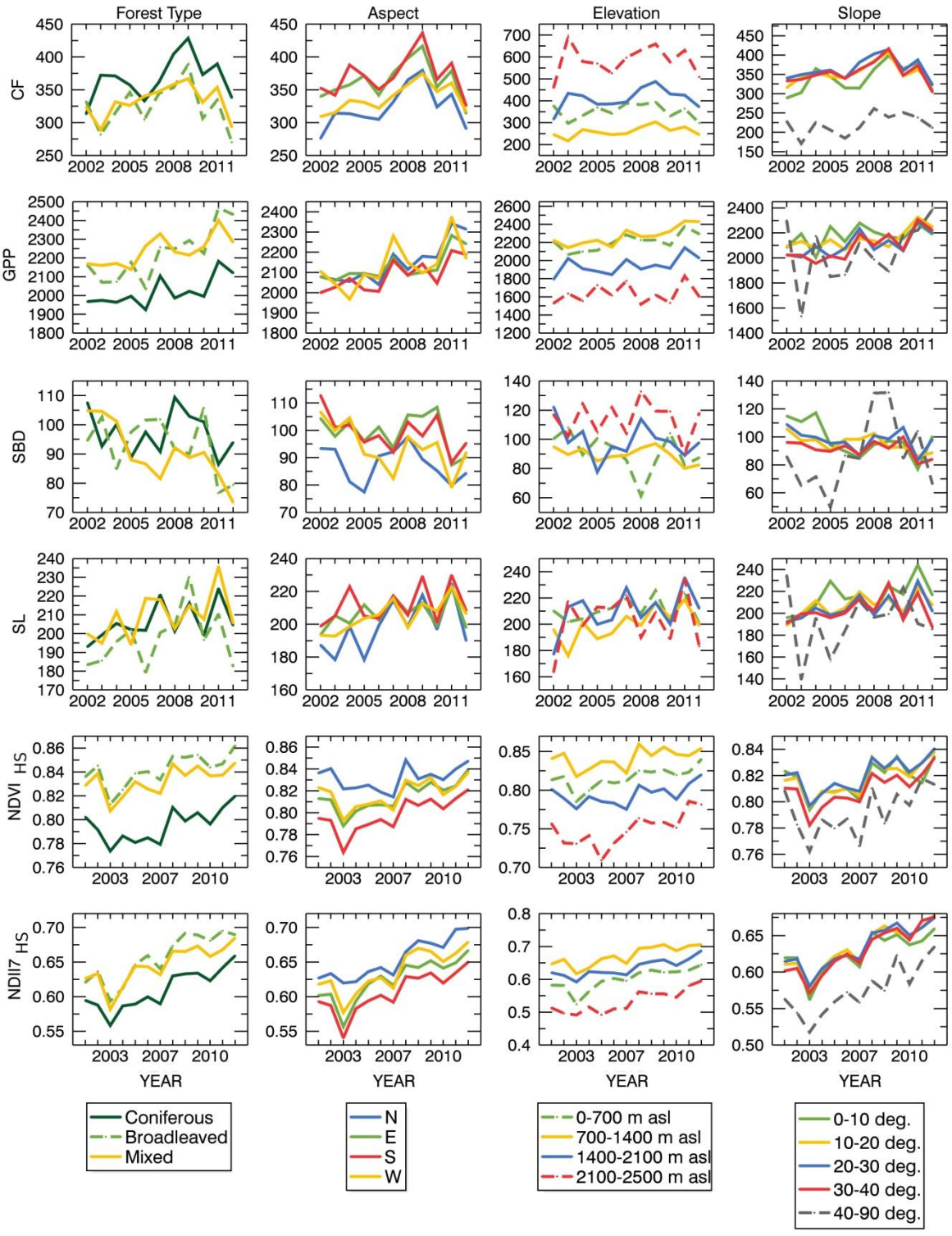

Figure A11 3 Marginal means plots of repeated ANOVA derived for (in rows) CF, GPP, SBD, SL, $NDVI_{HS}$ and $NDII7_{HS}$ analyzed within the $1COR_{L250}NBRI$ response class 6. Values are presented within four multilevel-factors (in columns) of forest type, aspect, elevation and slope. Profiles plotted in dashed line are based on less than 50 observations.

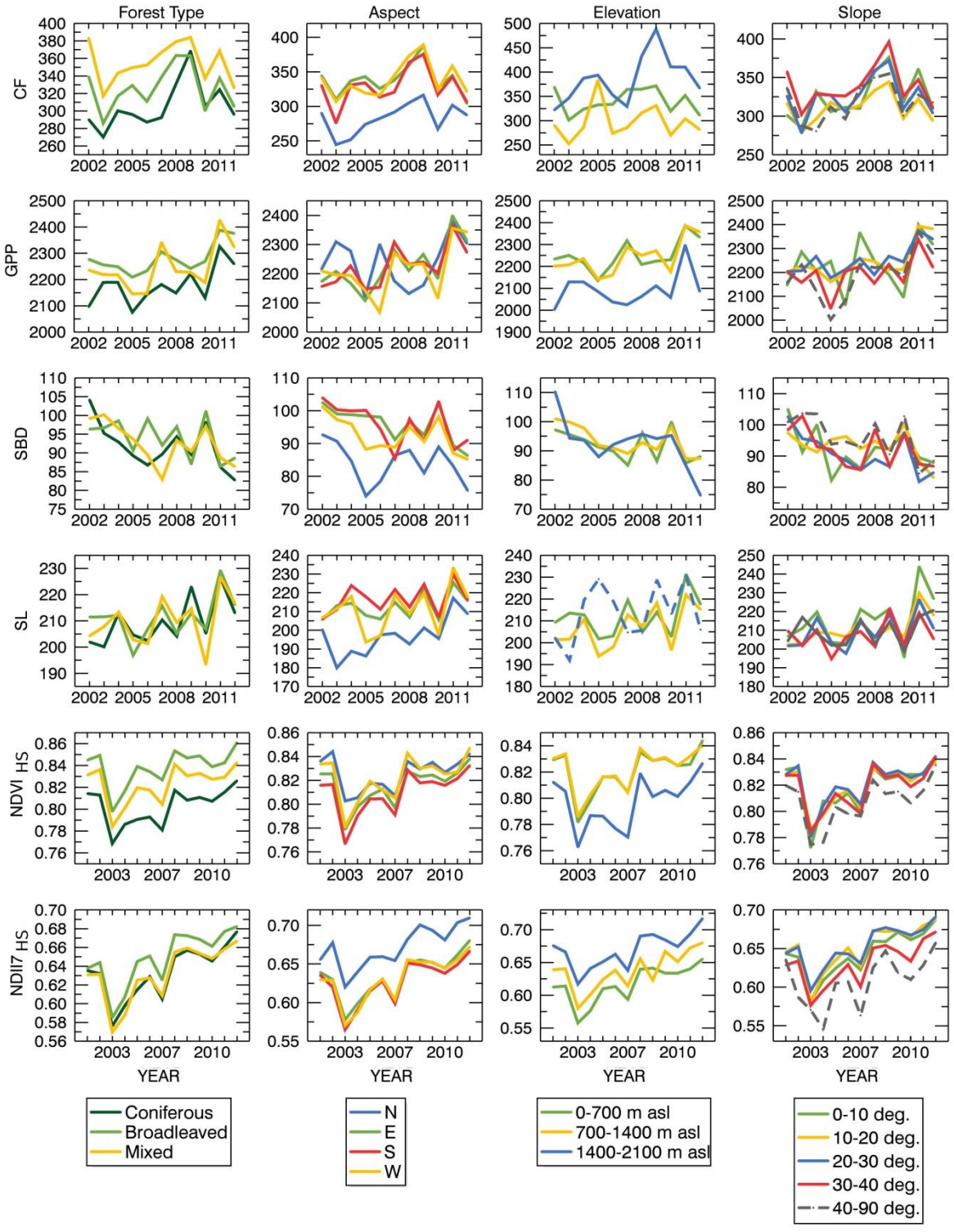

Figure A11 4 Marginal means plots of repeated ANOVA derived for (in rows) CF, GPP, SBD, SL, $NDVI_{HS}$ and $NDII7_{HS}$ analyzed within the $2COR_{L250}NBRI$ response class 6. Values are presented within four multilevel-factors (in columns) of forest type, aspect, elevation and slope. Profiles plotted in dashed line are based on less than 50 observations.

REFERENCES

Affolter P, Büntgen U, Esper J, Rigling A, Weber P, Luterbacher J, Frank D (2009) Inner Alpine conifer response to 20th century drought swings. European Journal of Forest Research, 129, 289–298.

Ahas R, Aasa A, Menzel A, Fedotova VG, Scheifinger H (2002) Changes in European spring phenology. International Journal of Climatology, 22, 1727–1738.

Alley WM (1984) The Palmer Drought Severity Index: Limitations and Assumptions. Journal of Climate and Applied Meteorology, 23.

Ascoli D, Castagneri D, Valsecchi C, Conedera M, Bovio G (2013) Post-fire restoration of beech stands in the Southern Alps by natural regeneration. Ecological Engineering, 54, 210–217.

Auer I, Bühm R, Jurković A et al. (2005) A new instrumental precipitation dataset for the greater alpine region for the period 1800-2002. International Journal of Climatology, 25, 139–166.

Auer I, Reinhard B, Jurkovic A et al. (2007) HISTALP – historical instrumental climatological surface time series of the Greater Alpine Region. International Journal of Climatology, 27, 17–46.

August D, Geiger M (2008) Drought in the Mediterranean, Recent Developments. Frankfurt am Main.

Barriopedro D, Fischer EM, Luterbacher J, Trigo RM, García-Herrera R (2011) The hot summer of 2010: redrawing the temperature record map of Europe. Science (New York, N.Y.), 332, 220–4.

Battisti A, Stastny M, Buffo E, Larsson S (2006) A rapid altitudinal range expansion in the pine processionary moth produced by the 2003 climatic anomaly. Global Change Biology, 12, 662–671.

Beniston M (2005) Mountain Climates and Climatic Change: An Overview of Processes Focusing on the European Alps. Pure and Applied Geophysics, 162, 1587–1606.

Beniston M (2012) Impacts of climatic change on water and associated economic activities in the Swiss Alps. Journal of Hydrology, 412-413, 291–296.

Beniston M (2013) Exploring the behaviour of atmospheric temperatures under dry conditions in Europe: evolution since the mid-20th century and projections for the end of the 21st century. International Journal of Climatology, 33, 457–462.

de Beurs K, Townsend P (2008) Estimating the effect of gypsy moth defoliation using MODIS. Remote Sensing of Environment, 112, 3983–3990.

Bigler C, Bräker OU, Bugmann H, Dobbertin M, Rigling A (2006) Drought as an Inciting Mortality Factor in Scots Pine Stands of the Valais, Switzerland. Ecosystems, 9, 330–343.

Björnsson H, Venegas S. (1997) A manual for EOF and SVD. Analyses of Climatic Data.

BMU (2007) Climate change in the Alps Facts - Impacts - Adaptation. Berlin.

Boccardo P, Borgogno Mondino E, Perez F, Claps P (2006) Co-Registration and Inter-Sensor Comparison of MODIS and Landsat 7 ETM+ Data Aimed At NDVI Calculation. Revue Française de Photogrammétrie et de Télédétection, 182, 74–79.

Bonan GB (2008) Forests and climate change: forcings, feedbacks, and the climate benefits of forests. Science (New York, N.Y.), 320, 1444–9.

Bordi I, Fraedrich K, Petitta M, Sutera A (2006) Large-Scale Assessment of Drought Variability Based on NCEP/NCAR and ERA-40 Re-Analyses. Water Resources Management, 20, 899–915.

Bréda N, Badeau V (2008) Forest tree responses to extreme drought and some biotic events: Towards a selection according to hazard tolerance? Comptes Rendus Geoscience, 340, 651–662.

Bréda N, Huc R, Granier A, Dreyer E (2006) Temperate forest trees and stands under severe drought: a review of ecophysiological responses, adaptation processes and long-term consequences. Annals of Forest Science, 63, 625–644.

Breshears DD, Cobb NS, Rich PM et al. (2005) Regional vegetation die-off in response to global-change-type drought. Proceedings of the National Academy of Sciences of the United States of America, 102, 15144–8.

Briffa KR, Schrier G Van Der, Jones PD (2009) Wet and dry summers in Europe since 1750: evidence of increasing drought. International Journal of Climatology, 29, 1894–1905.

Brown J (2009) Choosing the Right Type of Rotation in PCA and EFA. JALT Testing & Evaluating SIG Newsletter, 13, 20–25.

Brown JF, Wardlow BD, Tadesse T, Hayes MJ, Reed BC (2008) The Vegetation Drought Response Index (VegDRI): A New Integrated Approach for Monitoring Drought Stress in Vegetation. GIScience & Remote Sensing, 45, 16–46.

Brunner I, Herzog C, Dawes M, Arend M, Sperisen C (2015) How tree roots respond to drought. Frontiers in plant science, 6, 1–16.

Büntgen U, Trouet V, Frank D, Leuschner HH, Friedrichs D, Luterbacher J, Esper J (2010) Tree-ring indicators of German summer drought over the last millennium. Quaternary Science Reviews, 29, 1005–1016.

Bussotti F, Pollastrini M, Holland V, Brüggemann W (2014) Functional traits and adaptive capacity of European forests to climate change. Environmental and Experimental Botany, 111, 91–113.

Caccamo G, Chisholm L a., Bradstock R a., Puotinen ML (2011) Assessing the sensitivity of MODIS to monitor drought in high biomass ecosystems. Remote Sensing of Environment, 115, 2626–2639.

Calanca P (2007) Climate change and drought occurrence in the Alpine region: How severe are becoming the extremes? Global and Planetary Change, 57, 151–160.

Canty MJ, Nielsen A a, Schmidt M (2004) Automatic radiometric normalization of multitemporal satellite imagery. Remote Sensing of Environment, 91, 441–451.

Castagneri D, Nola P, Motta R, Carrer M (2014) Summer climate variability over the last 250 years differently affected tree species radial growth in a mesic Fagus-Abies–Picea old-growth forest. Forest Ecology and Management, 320, 21-29.

Cattell RB (1966) The Scree Test For The Number Of Factors. Multivariate Behavioral Research, 1, 245–276.

Chakraborty A, Sehgal VK (2010) Assessment of Agricultural Drought Using MODIS Derived Normalized Difference Water Index. Journal of Agricultural Physics, 10, 28–36.

Chauchard S, Beilhe F, Denis N, Carcaillet C (2010) An increase in the upper tree-limit of silver fir (Abies alba Mill.) in the Alps since the mid-20th century: A land-use change phenomenon. Forest Ecology and Management, 259, 1406–1415.

Chen CH, Peter Ho P-G (2008) Statistical pattern recognition in remote sensing. Pattern Recognition, 41, 2731–2741.

Chen JM, Rich PM, Gower ST, Norman JM, Plummer S (1997) Leaf area index of boreal forests: Theory, techniques, and measurements. Journal of Geophysical Research, 102, 29429.

Chen J, Jönsson P, Tamura M, Gu Z, Matsushita B, Eklundh L (2004) A simple method for reconstructing a high-quality NDVI time-series data set based on the Savitzky–Golay filter. Remote Sensing of Environment, 91, 332–344.

Chen D, Huang J, Jackson TJ (2005) Vegetation water content estimation for corn and soybeans using spectral indices derived from MODIS near- and short-wave infrared bands. Remote Sensing of Environment, 98, 225–236.

Cheng Y-B, Wharton S, Ustin SL, Zarco-Tejada PJ, Falk M, Paw U KT (2007) Relationships between Moderate Resolution Imaging Spectroradiometer water indexes and tower flux data in an old growth conifer forest. Journal of Applied Remote Sensing, 1, 013513.

Ciais P, Reichstein M, Viovy N et al. (2005) Europe-wide reduction in primary productivity caused by the heat and drought in 2003. Nature, 437, 529–533.

Cohen WB, Yang Z, Kennedy R (2010) Detecting trends in forest disturbance and recovery using yearly Landsat time series: 2. TimeSync — Tools for calibration and validation. Remote Sensing of Environment, 114, 2911–2924.

Colditz RR, Conrad C, Wehrmann T, Schmidt M, Dech S (2008) TiSeG: A Flexible Software Tool for Time-Series Generation of MODIS Data Utilizing the Quality Assessment Science Data Set. IEEE Transactions on Geoscience and Remote Sensing, 46, 3296–3308.

Coppola A, Leonelli G, Salvatore MC, Pelfini M, Baroni C (2012) Weakening climatic signal since mid-20th century in European larch tree-ring chronologies at different altitudes from the Adamello-Presanella Massif (Italian Alps). Quaternary Research, 77, 344–354.

Costello AB, Osborne JW (2005) Best Practices in Exploratory Factor Analysis: Four Recommendations for Getting the Most From Your Analysis. Practical Assessment, Research & Ealuation, 10.

Courbaud B, Kunstler G, Morin X (2010) What is the future of the ecosystem services of the Alpine forest against a backdrop of climate change? Journal of Alpine Research | Revue de géographie alpine, 98.

Dai A (2011a) Drought under global warming: a review. Wiley Interdisciplinary Reviews: Climate Change, 2, 45–65.

Dai A (2011b) Characteristics and trends in various forms of the Palmer Drought Severity Index during 1900–2008. Journal of Geophysical Research, 116, D12115.

Delbart N, Kergoat L, Le Toan T, Lhermitte J, Picard G (2005) Determination of phenological dates in boreal regions using normalized difference water index. Remote Sensing of Environment, 97, 26–38.

DeVries B, Decuyper M, Verbesselt J, Zeileis A, Herold M, Joseph S (2015) Tracking disturbance-regrowth dynamics in tropical forests using structural change detection and Landsat time series. Remote Sensing of Environment, 169, 320–334.

Dobbertin M, Mayer P, Wohlgemuth T, Feldmeyer-Christe E, Graf U, Zimmermann NE, Rigling A (2005) The Decline of Pinus sylvestris L . Forests in the Swiss Rhone Valley - a Result of Drought Stress? Phyton, 45, 153–156.

Doesken NJ, McKee TB, Kleist J (1991) Developement of a Surface Water Supply Index for the Western United States. Fort Collins, Colorado.

Dorman M, Svoray T, Perevolotsky A, Sarris D (2013) Forest performance during two consecutive drought periods: Diverging long-term trends and short-term responses along a climatic gradient. Forest Ecology and Management, 310, 1–9.

Drobyshev I, Niklasson M, Linderholm HW (2012) Forest fire activity in Sweden: Climatic controls and geographical patterns in 20th century. Agricultural and Forest Meteorology, 154-155, 174–186.

Dubrovsky M, Svoboda MD, Trnka M, Hayes MJ, Wilhite D a., Zalud Z, Hlavinka P (2009) Application of relative drought indices in assessing climate-change impacts on drought conditions in Czechia. Theoretical and Applied Climatology, 96, 155–171.

Eastman RJ, Fulk M (1993) Long Sequence Time Series Evaluation Using Standardized Principal Components. Photogrammetric Engineering & Remote Sensing, 59, 991–996.

EEA (2009a) Regional climate change and adaptation. EEA, Copenhagen.

EEA (2009b) Water resources across Europe — confronting water scarcity and drought. Copenhagen.

EEA (2010a) Europe's ecological backbone: recognising the true value of our mountains. EEA, Copenhagen.

EEA (2010b) Corine Land Cover 2006.

EEA (2012) Climate change, impacts and vulnerability in Europe 2012. EEA, Copenhagen.

Eilmann B, Weber P, Rigling A, Eckstein D (2006) Growth reactions of Pinus sylvestris L. and Quercus pubescens Willd. to drought years at a xeric site in Valais, Switzerland. Dendrochronologia, 23, 121–132.

Engler R, Randin CF, Thuiller W et al. (2011) 21st century climate change threatens mountain flora unequally across Europe. Global Change Biology, 17, 2330–2341.

Eqecat (2002) Central European Flooding, August 2002, An EQECAT Technical Report. 1-21 pp.

ESRI (2011) ArcGIS Desktop 10.1.

Etzold S, Waldner P, Thimonier A, Schmitt M, Dobbertin M (2014) Tree growth in Swiss forests between 1995 and 2010 in relation to climate and stand conditions: Recent disturbances matter. Forest Ecology and Management, 311, 41–55.

EU (2009) White Paper. Adapting to climate change: Towards a European framework for action.

Fang K, Gou X, Chen F et al. (2012) Tree-ring based reconstruction of drought variability (1615–2009) in the Kongtong Mountain area, northern China. Global and Planetary Change, 80-81, 190–197.

Feichtinger LM, Eilmann B, Buchmann N, Rigling A (2014) Growth adjustments of conifers to drought and to century-long irrigation. Forest Ecology and Management, 334, 96–105.

Feng M, Huang C, Channan S, Vermote EF, Masek JG, Townshend JR (2012) Quality assessment of Landsat surface reflectance products using MODIS data. Computers & Geosciences, 38, 9–22.

Feyen L, Dankers R (2009) Impact of global warming on streamflow drought in Europe. Journal of Geophysical Research, 114, D17116.

Gallaun H, Schardt M, Linser S (2007) Remote Sensing Based Forest Map Of Austria And Derived Environmental Indicators. In: Plenary Session: Large area forest monitoring using RS data. ForestSat 2007 Conference. November 5-7 Montpeller, France.

Gao B (1996) NDWI A Normalized Difference Water Index for Remote Sensing of Vegetation Liquid Water From Space. 266, 257–266.

Gao F (2013) Integrating Landsat with MODIS Products for Vegetation Monitoring. In: Satellite-based Applications on Climate Change SE - 16 (eds Qu J, Powell A, Sivakumar MVK), pp. 247–261. Springer Netherlands.

Gao F, Masek J, Schwaller M, Hall F (2006) On the blending of the landsat and MODIS surface reflectance: Predicting daily landsat surface reflectance. IEEE Transactions on Geoscience and Remote Sensing, 44, 2207–2218.

García-Herrera R, Hernández E, Barriopedro D, Paredes D, Trigo RM, Trigo IF, Mendes M a. (2007) The Outstanding 2004/05 Drought in the Iberian Peninsula: Associated Atmospheric Circulation. Journal of Hydrometeorology, 8, 483–498.

Gebetsroither E, Züger J, Loibl W (2013) Drought in Alpine Areas Under Changing Climate Conditions. In: Management Strategies to Adapt Alpine Space Forests to Climate Change Risks. InTech.

Gehrig-Fasel J, Guisan A, Zimmermann, Niklaus E (2007) Tree line shifts in the Swiss Alps: Climate change or land abandonment? Journal of Vegetation Science, 18, 571–582.

geoland2 (2012) Technical Note on HR Forest Layer Product Specification, Issue 1.4. Publication of the FP7 geoland2 project. 11.

Gevaert CM, García-Haro FJ (2015) Remote Sensing of Environment A comparison of STARFM and an unmixing-based algorithm for Landsat and MODIS data fusion. Remote Sensing of Environment, 156, 34–44.

Ghulam A, Qin Q, Zhan Z (2006) Designing of the perpendicular drought index. Environmental Geology, 52, 1045–1052.

Ghulam A, Qin Q, Zhan Z (2007) Modified perpendicular drought index (MPDI): a real-time drought monitoring method. Environmental Geology, 52, 1045–1052.

Gillner S, Vogt J, Roloff A (2013) Climatic response and impacts of drought on oaks at urban and forest sites. Urban Forestry and Urban Greening, 12, 597–605.

Giorgi F (2006) Climate change hot-spots. Geophysical Research Letters, 33, L08707.

Giuggiola A, Bugmann H, Zingg A, Dobbertin M, Rigling A (2013) Reduction of stand density increases drought resistance in xeric Scots pine forests. Forest Ecology and Management, 310, 827–835.

Gobiet A, Kotlarski S, Beniston M, Heinrich G, Rajczak J, Stoffel M (2014) 21st century climate change in the European Alps--a review. The Science of the total environment, 493, 1138–51.

Gobron N, Pinty B, Taberner M, Mélin F, Verstraete MM, Widlowski J-L (2006) Monitoring the photosynthetic activity of vegetation from remote sensing data. Advances in Space Research, 38, 2196–2202.

Gouveia C, Trigo RM, DaCamara CC (2009) Drought and vegetation stress monitoring in Portugal using satellite data. Natural Hazards and Earth System Science, 9, 185–195.

Granier A, Reichstein M, Bréda N et al. (2007) Evidence for soil water control on carbon and water dynamics in European forests during the extremely dry year: 2003. Agricultural and Forest Meteorology, 143, 123–145.

Gruber A, Strobl S, Veit B, Oberhuber W (2010) Impact of drought on the temporal dynamics of wood formation in Pinus sylvestris. Tree physiology, 30, 490–501.

Gu Y, Brown JF, Verdin JP, Wardlow B (2007) A five-year analysis of MODIS NDVI and NDWI for grassland drought assessment over the central Great Plains of the United States. Geophysical Research Letters, 34, L06407.

Guenther B, Xiong X, Salomonson V V, Barnes WL, Young J (2002) On-orbit performance of the Earth Observing System Moderate Resolution Imaging Spectroradiometer; first year of data. 83, 16–30.

Hanewinkel M, Cullmann DA, Schelhaas M-J, Nabuurs G-J, Zimmermann NE (2013) Climate change may cause severe loss in the economic value of European forest land. Nature Clim. Change, 3, 203–207.

Hannachi A (2004) A Primer for EOF Analysis of Climate Data. 1–33.

Hardisky MA, Klemas V, Smart R. (1983) The Influence of Soil Salinity, Growth Form, and Leaf Moisture on the Spectral Radiance of Spartina alterniflora Canopies. American Society of Photogramethry, 49, 77–83.

Hartl-Meier C, Dittmar C, Zang C, Rothe A (2014) Mountain forest growth response to climate change in the Northern Limestone Alps. Trees, 28, 819–829.

He B, Cui X, Wang H, Chen A (2014) Drought: The most important physical stress of terrestrial ecosystems. Acta Ecologica Sinica, 34, 179–183.

Helmer EH, Ruefenacht B (2007) A comparison of radiometric normalization methods when filling cloud gaps in Landsat imagery. Canadian Journal of Remote Sensing, 33, 325–340.

Hendrickson AE, White PO (1964) PROMAX: A Quick Method for Rotation to Oblique Simple Structure. British Journal of Statistical Psychology, 17, 65–70.

Hilker T, Wulder M a., Coops NC et al. (2009) Generation of dense time series synthetic Landsat data through data blending with MODIS using a spatial and temporal adaptive reflectance fusion model. Remote Sensing of Environment, 113, 1988–1999.

Horion S, Cornet Y, Erpicum M, Tychon B (2013) Studying interactions between climate variability and vegetation dynamic using a phenology based approach. International Journal of Applied Earth Observation and Geoinformation, 20, 20–32.

Huang C, Townshend JRG, Liang S, Kalluri SN V, DeFries RS (2002) Impact of sensor's point spread function on land cover characterization: Assessment and deconvolution. Remote Sensing of Environment, 80, 203–212.

Huang C, Goward SN, Masek JG, Thomas N, Zhu Z, Vogelmann JE (2010) An automated approach for reconstructing recent forest disturbance history using dense Landsat time series stacks. Remote Sensing of Environment, 114, 183–198.

Huete AR, Justice C, van Leeuwen W (1999) MODIS Vegetation Index (MOD13) Algorithm Theoretical Basis Document.

Huete A, Didan K, Miura T, Rodriguez E., Gao X, Ferreira L. (2002) Overview of the radiometric and biophysical performance of the MODIS vegetation indices. Remote Sensing of Environment, 83, 195–213.

Hwang T, Song C, Bolstad P V., Band LE (2011) Downscaling real-time vegetation dynamics by fusing multi-temporal MODIS and Landsat NDVI in topographically complex terrain. Remote Sensing of Environment, 115, 2499–2512.

Hydrographic Office of the Autonomous Province of Bolzano-Südtirol (2006) Climareport - Südtirol - Alto Adige. Bolzano.

Hydrographic Office of the Autonomous Province of Bolzano-Südtirol (2011) Climatereport. Bolzano.

Hydrographic Office of the Autonomous Province of Bolzano-Südtirol (2013) Climatereport. Bolzano.

IPCC (2000) Emissions Scenarios. Summary for Policymakers.

IPCC (2013) Climate Change 2013: The Physical Science Basis. Contribution of Working Group I to the Fifth Assessment Report of the Intergovernmental Panel on Climate Change (eds Stocker TF, Qin D, Plattner G-K, Tignor MMB, Allen SK, Boschung J, Nauels A, Xia Y, Bex V, Midgley PM). Cambridge University Press, Cambridge, United Kingdom and New York, NY, USA, 1535 pp.

Irons JR, Dwyer JL, Barsi J a. (2012) The next Landsat satellite: The Landsat Data Continuity Mission. Remote Sensing of Environment, 122, 11–21.

Ivits E, Cherlet M, Tóth T, Lewińska KE, Tóth G (2011) Characterisation of productivity limitation of salt-affected lands in different climatic regions of Europe using remote sensing derived productivity indicators. Land Degradation & Development, 24, 438–452.

Ivits E, Cherlet M, Mehl W, Sommer S (2013a) Ecosystem functional units characterized by satellite observed phenology and productivity gradients: A case study for Europe. Ecological Indicators, 27, 17–28.

Ivits E, Cherlet M, Sommer S, Mehl W (2013b) Addressing the complexity in non-linear evolution of vegetation phenological change with time-series of remote sensing images. Ecological Indicators, 26, 49–60.

Ivits E, Horion S, Fensholt R, Cherlet M (2014) Drought footprint on European ecosystems between 1999 and 2010 assessed by remotely sensed vegetation phenology and productivity. Global Change Biology, 20, 581–593.

Jarihani A, McVicar T, Van Niel T, Emelyanova I, Callow J, Johansen K (2014) Blending Landsat and MODIS Data to Generate Multispectral Indices: A Comparison of "Index-then-Blend" and "Blend-then-Index" Approaches. Remote Sensing, 6, 9213–9238.

Ji L, Peters AJ (2003) Assessing vegetation response to drought in the northern Great Plains using vegetation and drought indices. Remote Sensing of Environment, 87, 85–98.

Ji L, Zhang L, Wylle B (2009) Analysis of dynamic thresholds for the normalized difference water index. Photogrammetric engineering and remote sensing, 75, 1307–1317.

Jin S, Sader SA (2005) Comparison of time series tasseled cap wetness and the normalized difference moisture index in detecting forest disturbances. Remote Sensing of Environment, 94, 364–372.

Jolly WM, Dobbertin M, Zimmermann NE, Reichstein M (2005) Divergent vegetation growth responses to the 2003 heat wave in the Swiss Alps. Geophysical Research Letters, 32.

Jönsson a. M, Eklundh L, Hellström M, Bärring L, Jönsson P (2010) Annual changes in MODIS vegetation indices of Swedish coniferous forests in relation to snow dynamics and tree phenology. Remote Sensing of Environment, 114, 2719–2730.

Jump AS, Penuelas J (2005) Running to stand still: adaptation and the response of plants to rapid climate change. Ecology Letters, 8, 1010–1020.

Justice C., Townshend JR., Vermote E. et al. (2002) An overview of MODIS Land data processing and product status. Remote Sensing of Environment, 83, 3–15.

Kaiser H (1958) The varimax criterion for analytic rotation in factor analysis. Psychometrika, 23, 187–200.

Kaiser HF (1960) The Application of Electronic Computers to Factor Analysis. Educational and Psychological Measurement, 20, 141–151.

Kapos V, Iremonger S. (1998) Achieving Global and Regional Perspectives on Forest Biodiversity and Conservation. In: Assessment of Biodiversity for Improved Forest Planning; Proceedings of the Conference on Assessment of Biodiversity for Improved Planning, 7–11 October 1996, held in Monte Verità, Switzerland (eds Bachmann P, Köhl M, Päivinen R), pp. 3–13. Springer Netherlands.

Kennedy RE, Yang Z, Cohen WB (2010) Detecting trends in forest disturbance and recovery using yearly Landsat time series: 1. LandTrendr — Temporal segmentation algorithms. Remote Sensing of Environment, 114, 2897–2910.

Kennedy RE, Andréfouët S, Cohen WB et al. (2014) Bringing an ecological view of change to Landsat-based remote sensing. Frontiers in Ecology and Environment.

Kharuk VI, Im ST, Oskorbin PA, Petrov IA, Ranson KJ (2013) Siberian pine decline and mortality in southern siberian mountains. Forest Ecology and Management, 310, 312–320.

Kim DH, Yoo C, Kim T-W (2011) Application of spatial EOF and multivariate time series model for evaluating agricultural drought vulnerability in Korea. Advances in Water Resources, 34, 340–350.

Kimes D., Markham B., Tucker C., McMurtrey J. (1981) Temporal relationships between spectral response and agronomic variables of a corn canopy. Remote Sensing of Environment, 11, 401–411.

Knight JF, Lunetta RS, Ediriwickrema J (2006) Regional Scale Land Cover Characterization using MODIS NDVI 250 m Multi-Temporal Imagery : A Phenology-Based Approach Regional Scale Land-Cover Characterization using MODIS-NDVI 250 m Multi-Temporal Imagery: A Phenology Based Approach. 43, 1–23.

Körner C (2003) Alpine Plant Life. Springer Berlin Heidelberg, Berlin, Heidelberg.

Kottek M, Grieser J, Beck C, Rudolf B, Rubel F (2006) World Map of the Köppen-Geiger climate classification updated. Meteorologische Zeitschrift, 15, 259–263.

Kramer PJ (1983) Water relations of plants. Academic Press.

Lévesque M, Rigling A, Bugmann H, Weber P, Brang P (2014) Growth response of five co-occurring conifers to drought across a wide climatic gradient in Central Europe. Agricultural and Forest Meteorology, 197, 1–12.

Lasaponara R (2006) On the use of principal component analysis (PCA) for evaluating interannual vegetation anomalies from SPOT/VEGETATION NDVI temporal series. Ecological Modelling, 194, 429–434.

Lawley EF, Lewis MM, Ostendorf B (2011) Environmental zonation across the Australian arid region based on long-term vegetation dynamics. Journal of Arid Environments, 75, 576–585.

Leuzinger S, Zotz G, Asshoff R, Körner C (2005) Responses of deciduous forest trees to severe drought in Central Europe. Tree physiology, 25, 641–50.

Lévesque M, Rigling A, Bugmann H, Weber P, Brang P (2014) Growth response of five co-occurring conifers to drought across a wide climatic gradient in Central Europe. Agricultural and Forest Meteorology, 197, 1–12.

Liang S (2004) Quantitative Remote Sensing of Land Surfaces (ed Wiley & Sons). Wiley & Sons, 536 pp.

Lloyd-Hughes B, Saunders MA (2002) A drought climatology for Europe. International Journal of Climatology, 22, 1571–1592.

Lorenz EN (1956) Empirical Orthogonal Functions and Satistical Weather Prediction. Cambridge, Massachusette.

Lotsch A, Friedl MA, Anderson BT, Tucker CJ (2005) Response of Terrestrial Ecosystems to Recent Northern Hemispheric Drought. Geophysical Research Letters, 32.

Loveland TR, Dwyer JL (2012) Landsat: Building a strong future. Remote Sensing of Environment, 122, 22–29.

Ma Z, Peng C, Zhu Q et al. (2012) Regional drought-induced reduction in the biomass carbon sink of Canada's boreal forests. Proceedings of the National Academy of Sciences of the United States of America, 109, 2423–7.

Machado-Machado EA, Neeti N, Eastman JR, Chen H (2011) Implications of space-time orientation for Principal Components Analysis of Earth observation image time series. Earth Science Informatics, 4, 117–124.

Malenovský Z, Rott H, Cihlar J, Schaepman ME, García-Santos G, Fernandes R, Berger M (2012) Sentinels for science: Potential of Sentinel-1, -2, and -3 missions for scientific observations of ocean, cryosphere, and land. Remote Sensing of Environment, 120, 91–101.

Manusch C, Bugmann H, Heiri C, Wolf A (2012) Tree mortality in dynamic vegetation models – A key feature for accurately simulating forest properties. Ecological Modelling, 243, 101–111.

Mao F, Duan M, Min Q, Gong W, Pan Z, Liu G (2015) Investigating the impact of haze on MODIS cloud detection. Journal of Geophysical Research: Atmospheres, 120, 12,212–237,247.

Masek JG, Vermote EF, Saleous NE et al. (2006) A Landsat Surface Reflectance Dataset for North America, 1990-2000. IEEE Geoscience and Remote Sensing Letters, 3, 68–72.

Matulla C, Schöner W, Alexandersson H, Storch H, Wang XL (2007) European storminess: late nineteenth century to present. Climate Dynamics, 31, 125–130.

McKee TB, Doesken NJ, Kleist J (1993) The relationship of drought frequency and duration to time scales. In: Eighth Conference on Applied Climatology, pp. 17–22. Anaheim.

Migliavacca M, Cremonese E, Colombo R et al. (2008) European larch phenology in the Alps: can we grasp the role of ecological factors by combining field observations and inverse modelling? International journal of biometeorology, 52, 587–605.

Mika J, Horváth S, Makra L, Dunkel Z (2005) The Palmer Drought Severity Index (PDSI) as an indicator of soil moisture. Physics and Chemistry of the Earth, Parts A/B/C, 30, 223–230.

Minerbi S, Cescatti A, Cherubini P (2006) Scots Pine dieback in the Isarco Valley due to severe drought in the summer of 2003. 2, 89–143.

Mishra AK, Singh VP (2010) A review of drought concepts. Journal of Hydrology, 391, 202–216.

Moser D, Norbert S, Willner W (2011) Generalisation of drought effects on ecosystem goods and services over the Alps. Alp-Water-Scarce Internal Project Report, 1–20.

NASA Landsat 7 Science Data Users Handbook. 186.

Neeti N, Ronald Eastman J (2014) Novel approaches in Extended Principal Component Analysis to compare spatio-temporal patterns among multiple image time series. Remote Sensing of Environment, 148, 84–96.

Niemeyer S (2008) New drought indices. Options Méditerranéennes, 267–274.

Ozenda P (1988) Die Vegetation der Alpen in europäischen Gebirgsraum. Fischer, Stuttgart/New York.

Palmer WC (1965) Meteorological Drought. U.S. Department of Commerce, Weather Bureau, 58 pp.

Palmer WC (1968) Keeping Track of Crop Moisture Conditions, Nationwide: The New Crop Moisture Index. Weatherwise, 21, 156–161.

Pappalardo G, Mona L, D'Amico G et al. (2013) Four-dimensional distribution of the 2010 Eyjafjallajökull volcanic cloud over Europe observed by EARLINET. Atmospheric Chemistry and Physics, 13, 4429–4450.

Pasho E, Camarero JJ, de Luis M, Vicente-Serrano SM (2011) Impacts of drought at different time scales on forest growth across a wide climatic gradient in north-eastern Spain. Agricultural and Forest Meteorology, 151, 1800–1811.

Pecher C, Tasser E, Tappeiner U (2011) Definition of the potential treeline in the European Alps and its benefit for sustainability monitoring. Ecological Indicators, 11, 438–447.

Pellerin M, Delestrade A, Mathieu G, Rigault O, Yoccoz NG (2012) Spring tree phenology in the Alps: effects of air temperature, altitude and local topography. European Journal of Forest Research, 131, 1957–1965.

Peters AJ, Waltershea EA, Ji L, Vliia A, Hayes M, Svoboda MD, Nir RED (2002) Drought Monitoring with NDVI-Based Standardized Vegetation Index. 68, 71–75.

Philipona R, Behrens K, Ruckstuhl C (2009) How declining aerosols and rising greenhouse gases forced rapid warming in Europe since 1980s. Geophysical Research Letters, 36.

Pichler P, Oberhuber W (2007) Radial growth response of coniferous forest trees in an inner Alpine environment to heat-wave in 2003. Forest Ecology and Management, 242, 688–699.

Potapov P, Hansen MC, Stehman S V., Loveland TR, Pittman K (2008) Combining MODIS and Landsat imagery to estimate and map boreal forest cover loss. Remote Sensing of Environment, 112, 3708–3719.

Potop V, Možný M, Soukup J (2012) Drought evolution at various time scales in the lowland regions and their impact on vegetable crops in the Czech Republic. Agricultural and Forest Meteorology, 156, 121–133.

Preisendorfer RW (1988) Principal Component Analysis in Meteorology and Oceanography. Elsevier.

Price JC (2003) Comparing MODIS and ETM+ data for regional and global land classification. Remote Sensing of Environment, 86, 491–499.

Primicia I, Camarero JJ, Janda P et al. (2015) Age, competition, disturbance and elevation effects on tree and stand growth response of primary Picea abies forest to climate. Forest Ecology and Management, 354, 77–86.

Provincia Autonomica di Bolzano (2010) Tipologie forestali dell ' Alto Adige Vol. 1, Provincia edn, Vol. 1 tipi for. Provincia Autonomica di Bolzano - Alto Adige, Bolzano.

Pütz M, Kruse S, Casanova E, Butterling M (2011) CLISP - Climate Change Adaptation by Spatial Planning in the Alpine Space Climate Change Fitness of Spatial Planning WP5 Synthesis report.

Rahimzadeh Bajgiran P, Shimizu Y, Hosoi F, Omasa K (2009) MODIS vegetation and water indices for drought assessment in semi-arid ecosystems of Iran. Journal of Agricultural Meteorology, 65, 349–355.

Ram S (2012) Tree growth–climate relationships of conifer trees and reconstruction of summer season Palmer Drought Severity Index (PDSI) at Pahalgam in Srinagar, India. Quaternary International, 254, 152–158.

Rammig A, Jonas T, Zimmermann NE, Rixen C (2010) Changes in alpine plant growth under future climate conditions. Biogeosciences, 7, 2013–2024.

Rebetez M, Mayer H, Dupont O (2006) Heat and drought 2003 in Europe: a climate synthesis. Annals of Forest Science, 63, 569–577.

Rebetez M, Dupont O, Giroud M (2008) An analysis of the July 2006 heatwave extent in Europe compared to the record year of 2003. Theoretical and Applied Climatology, 95, 1–7.

Reed BC, Brown JF, VanderZee D, Loveland TR, Merchant JW, Ohlen DO (1994) Measuring phenological variability from satellite imagery. Journal of Vegetation Science, 5, 703–714.

Reichstein M, Ciais P, Papale D et al. (2007) Reduction of ecosystem productivity and respiration during the European summer 2003 climate anomaly: a joint flux tower, remote sensing and modelling analysis. Global Change Biology, 13, 634–651.

Riano D, Chuvieco E, Salas J, Aguado I (2003) Assessment of different topographic corrections in landsat-TM data for mapping vegetation types. IEEE Transactions on Geoscience and Remote Sensing, 41, 1056–1061.

Richman Michael B. (1986) Rotation of principal components. Journal of Climatology, 6, 293–335.

Rigling A, Waldner PO, Forster T, Bräker OU, Pouttu A (2001) Ecological interpretation of tree-ring width and intraannual density fluctuations in Pinus sylvestris on dry sites in the central Alps and Siberia. Canadian Journal of Forest Research, 31, 18–31.

Rigling A, Bigler C, Eilmann B et al. (2013) Driving factors of a vegetation shift from Scots pine to pubescent oak in dry Alpine forests. Global change biology, 19, 229-40.

Roy DP, Ju J, Lewis P, Schaaf C, Gao F, Hansen M, Lindquist E (2008) Multi-temporal MODIS–Landsat data fusion for relative radiometric normalization, gap filling, and prediction of Landsat data. Remote Sensing of Environment, 112, 3112–3130.

Ruffini F V, Renner K, Hoffmann C, Streifeneder T (2007) Policies to Promote Cross - Border Cooperation in the Alps Cross - border cooperation in mountain areas. 1-17.

Schär C, Vidale PL, Lüthi D, Frei C, Häberli C, Liniger M a, Appenzeller C (2004) The role of increasing temperature variability in European summer heatwaves. Nature, 427, 332–336.

Scharnweber T, Manthey M, Criegee C, Bauwe A, Schröder C, Wilmking M (2011) Drought matters - Declining precipitation influences growth of Fagus sylvatica L. and Quercus robur L. in north-eastern Germany. Forest Ecology and Management, 262, 947–961.

Scherrer D, Bader MK-F, Körner C (2011) Drought-sensitivity ranking of deciduous tree species based on thermal imaging of forest canopies. Agricultural and Forest Meteorology, 151, 1632–1640.

Schmidli J, Schmutz C, Frei C, Wanner H, Schär C (2002) Mesoscale precipitation variability in the Alpine region during the 20th century. International Journal of Climatology, 22, 1049–1074.

Schoene DHF, Bernier PY (2012) Adapting forestry and forests to climate change: A challenge to change the paradigm. Forest Policy and Economics, 24, 12–19.

van der Schrier G, Briffa KR, Jones PD, Osborn TJ (2006) Summer moisture variability across Europe. Journal of Climate, 19, 2818–2834.

van der Schrier G, Efthymiadis D, Briffa KR, Jones PD (2007) European Alpine moisture variability for 1800 – 2003. 427, 415–427.

Van Der Schrier G, Jones PD, Briffa KR (2011) The sensitivity of the PDSI to the Thornthwaite and Penman-Monteith parameterizations for potential evapotranspiration. Journal of Geophysical Research: Atmospheres, 116, 1–16.

van der Schrier G, Barichivich J, Briffa KR, Jones PD (2013) A scPDSI-based global data set of dry and wet spells for 1901-2009. Journal of Geophysical Research: Atmospheres, 118, 4025–4048.

Sheffield J, Wood EF (2007) Projected changes in drought occurrence under future global warming from multi-model, multi-scenario, IPCC AR4 simulations. Climate Dynamics, 31, 79–105.

Sheffield J, Wood EF, Roderick ML (2012) Little change in global drought over the past 60 years. Nature, 491, 435–8.

Singleton T An Empirical Orthogonal Function (EOF) Analysis of Sea Surface Temperature. 1-9 pp.

Small C (2012) Spatiotemporal dimensionality and Time-Space characterization of multitemporal imagery. Remote Sensing of Environment, 124, 793–809.

Solano R, Didan K, Jacobson A, Huete A (2010) MODIS Vegetation Indices (MOD13) C5 User's Guide. 2.

South Tyrol in figures (2012) , Rep. no 8 edn. Provincial Statistics Institute of Autonomous Province Of South Tyrol, Bolzano.

Spinoni J, Naumann G, Vogt J V., Barbosa P (2015) The biggest drought events in Europe from 1950 to 2012. Journal of Hydrology: Regional Studies, 3, 1–16.

Spruce JP, Sader S, Ryan RE et al. (2011) Assessment of MODIS NDVI time series data products for detecting forest defoliation by gypsy moth outbreaks. Remote Sensing of Environment, 115, 427–437.

Standing Forestry Committee Ad Hoc Working Group III on Climate Change and Forestry (2010) Climate Change and Forestry. Report to the Standing Forestry Committee by.

Stingl V, Mair V (2005) An introduction to the geology of South Tyrol. Autonomous Province of Bolzano-South Tyrol, Office of geology and material testing, Caldaro (BZ).

Studer S, Appenzeller C, Defila C (2005) Inter-Annual Variability and Decadal Trends in Alpine Spring Phenology: A Multivariate Analysis Approach. Climatic Change, 73, 395–414.

Studer S, Stöckli R, Appenzeller C, Vidale P. L (2007) A comparative study of satellite and ground-based phenology. International journal of biometeorology, 51, 405–14.

Swidrak I, Schuster R, Oberhuber W (2013) Comparing growth phenology of co-occurring deciduous and evergreen conifers exposed to drought. Flora - Morphology, Distribution, Functional Ecology of Plants, 208, 609–617.

Tan B, Woodcock CE, Hu J et al. (2006) The impact of gridding artifacts on the local spatial properties of MODIS data: Implications for validation, compositing, and band-to-band registration across resolutions. Remote Sensing of Environment, 105, 98–114.

Tatli H, Türkeş M (2011) Empirical Orthogonal Function analysis of the palmer drought indices. Agricultural and Forest Meteorology, 151, 981–991.

Theurillat J-P, Guisan A (2001) Potential Impact of Climate Change on Vegetation in the European Alps: A Review. Climatic Change, 50, 77–109.

Thornthwaite C. (1948) An Approach toward a Rational Classification of Climate. Geographical Review, 38, 55–94.

Tucker CJ (1979) Red and Photograpic Infrared Linear combinations for Monitoring Vegetation. Remote Sensing of Environment, 8, 127–150.

Tucker CJ (1980) Remote Sensing of Leaf Water Content in the Near Irdrared. Remote Sensing of Environment, 10, 23–32.

Udelhoven T (2011) TimeStats: A Software Tool for the Retrieval of Temporal Patterns From Global Satellite Archives. Selected Topics in Applied Earth Observations and Remote Sensing, IEEE Journal of, 4, 310–317.

USGS (2003) Preliminary Assessment of the Value of Landsat 7 ETM + Data following Scan Line Corrector Malfunction. Sioux Falls, 86 pp.

USGS EROS Data Center (2002) MODIS Reprojection Tool (MRT).

Vacchiano G, Garbarion M, Borgogno Mondino E, Renzo M (2012) Evidences of drought stress as a predisposing factor to Scots pine decline in Valle d'Aosta. European Journal of Forest Researh, 131, 989–1000.

Vanonckelen S, Lhermitte S, Van Rompaey A (2013) The effect of atmospheric and topographic correction methods on land cover classification accuracy. International Journal of Applied Earth Observation and Geoinformation, 24, 9–21.

Venegas SA (2001) Statistical Methods for Signal Detection in Climate. Copenhagen.

Verbesselt J, Robinson A, Stone C, Culvenor D (2009) Forecasting tree mortality using change metrics derived from MODIS satellite data. Forest Ecology and Management, 258, 1166–1173.

Vermote EFF, Vermeulen A (1999) Atmospheric correction algorithm: spectral reflectances (MOD09). Algorithm Technical Background Document (ATBD). 1-107 pp.

Vermote EF, El Saleous NZ, Justice CO (2002) Atmospheric correction of MODIS data in the visible to middle infrared: first results. Remote Sensing of Environment, 83, 97–111.

Vicente-Serrano SM, Beguería S, López-Moreno JI (2010) A Multiscalar Drought Index Sensitive to Global Warming: The Standardized Precipitation Evapotranspiration Index. Journal of Climate, 23, 1696–1718.

Vicente-Serrano SM, Schrier G Van Der, Beguería S, Azorin-Molina C, Lopez-Moreno J (2014) Contribution of precipitation and reference evapotranspiration to drought indices under different climates. Journal of Hydrology.

Vittoz P, Rulence B, Largey T, Freléchoux F (2008) Effects of Climate and Land-Use Change on the Establishment and Growth of Cembran Pine (Pinus cembra L.) over the Altitudinal Treeline Ecotone in the Central Swiss Alps. Arctic, Antarctic, and Alpine Research, 40, 225–232.

Vittoz P, Cherix D, Gonseth Y, Lubini V, Maggini R, Zbinden N, Zumbach S (2013) Climate change impacts on biodiversity in Switzerland: A review. Journal for Nature Conservation, 21, 154–162.

Volcani A, Karnieli A, Svoray T (2005) The use of remote sensing and GIS for spatio-temporal analysis of the physiological state of a semi-arid forest with respect to drought years. Forest Ecology and Management, 215, 239–250.

van Wagtendonk JW, Root RR, Key CH (2004) Comparison of AVIRIS and Landsat ETM+ detection capabilities for burn severity. Remote Sensing of Environment, 92, 397–408.

Wang L, Qu JJ (2009) Satellite remote sensing applications for surface soil moisture monitoring: A review. Frontiers of Earth Science in China, 3, 237–247.

Wang J, Rich PM, Price KP (2003) Temporal responses of NDVI to precipitation and temperature in the central Great Plains, USA. International Journal of Remote Sensing, 24, 2345–2364.

Wang D, Morton D, Masek J et al. (2012) Impact of sensor degradation on the MODIS NDVI time series. Remote Sensing of Environment, 119, 55–61.

Wastl C, Schunk C, Leuchner M, Pezzatti GB, Menzel A (2012) Recent climate change: Long-term trends in meteorological forest fire danger in the Alps. Agricultural and Forest Meteorology, 162-163, 1–13.

Weber P, Bugmann H, Rigling A (2007) Radial growth responses to drought of Pinus sylvestris and Quercus pubescens in an inner-Alpine dry valley. Journal of Vegetation Science, 18, 777–792.

Weber P, Bugmann H, Pluess a. R, Walthert L, Rigling a. (2012) Drought response and changing mean sensitivity of European beech close to the dry distribution limit. Trees, 27, 171–181.

Wells N (2003) PDSI. National Agricultural Decision Support System, University of Nebraska-Lincoln.

Wells N, Steve G, Hayes, Michael J (2004) A Self-Calibrating Palmer Drought Severity Index. Journal of Climate, 17, 2335–2351.

Wilhite DA, Glantz MH (1985) Understanding: the Drought Phenomenon: The Role of Definitions. Water International, 10, 111–120.

Wilks DS (2006) Statistical Methods in the Atmospheric Science, Second edn (eds Dmowska R, Hartmann D, Rossby TH). Elsevier.

Williams DL, Goward S, Arvidson T (2006) Landsat : Yesterday , Today , and Tomorrow. Photogrammetric Engineering & Remote Sensing, 72, 1171–1178.

Wilson EH, Sader S a (2002) Detection of forest harvest type using multiple dates of Landsat TM imagery. Remote Sensing of Environment, 80, 385–396.

Wolfe RE, Nishihama M, Fleig AJ, Kuyper J a., Roy DP, Storey JC, Patt FS (2002) Achieving sub-pixel geolocation accuracy in support of MODIS land science. Remote Sensing of Environment, 83, 31–49.

Wulder M a., Masek JG, Cohen WB, Loveland TR, Woodcock CE (2012) Opening the archive: How free data has enabled the science and monitoring promise of Landsat. Remote Sensing of Environment, 122, 2–10.

Wulder MA, White JC, Loveland TR et al. (2015) The global Landsat archive: Status, consolidation, and direction. Remote Sensing of Environment.

Xiao X, Boles S, Liu J et al. (2005) Mapping paddy rice agriculture in southern China using multi-temporal MODIS images. Remote Sensing of Environment, 95, 480--492.

Yilmaz MT, Hunt ER, Jackson TJ (2008) Remote sensing of vegetation water content from equivalent water thickness using satellite imagery. Remote Sensing of Environment, 112, 2514–2522.

Zhang A, Jia G (2013) Monitoring meteorological drought in semiarid regions using multi-sensor microwave remote sensing data. Remote Sensing of Environment, 134, 12–23.

Zhu Z, Woodcock CE (2012) Object-based cloud and cloud shadow detection in Landsat imagery. Remote Sensing of Environment, 118, 83–94.

Zhu X, Chen J, Gao F, Chen X, Masek JG (2010) An enhanced spatial and temporal adaptive reflectance fusion model for complex heterogeneous regions. Remote Sensing of Environment, 114, 2610–2623.

Zimmermann NE, Gebetsroither E, Züger J, Schmatz D, Psomas A (2013a) Future Climate of the European Alps. In: Management Strategies to Adapt Alpine Space Forests to Climate Change Risks (ed Zimmermann NE), pp. 27–36. InTech.

Zimmermann NE, Jandl R, Hanewinkel M et al. (2013b) Potential Future Ranges of Tree Species in the Alps. In: Management Strategies to Adapt Alpine Space Forests to Climate Change Risks (eds Cerbu GA, Hanewinkel M, Gerosa G, Jandl R), pp. 37–48. InTech.

ACRONYMS AND ABBREVIATIONS

asl – above sea level
ANOVA – Analysis of Variance
AVHRR – Advanced Very High Resolution Radiometer
CF – Cyclic Fraction
CFA - Common Factor Analysis
CLC2006 – CORINE Land Cover 2006
CMI – Crop Moisture Index
CORINE – Coordinate Information on the Environment
CV-MVC – Constrained View angle – Maximum Value Composite
CZCS – Coastal Zone Color Scanner
DEM – Digital Elevation Model
DOY – Day Of the Year
ENVI - Environment for Visualizing Images
EOF – Empirical Orthogonal Function
EOS – Earth Observing System
EVI – Enhanced Vegetation Index
ETM – Enhanced Thematic Mapper
ETM+ – Enhanced Thematic Mapper Plus
EU – European Union
FAPAR – Fraction of Absorbed Photosynthetically Active Radiation
FP7 – The Seventh Framework Programme
GPP – Gross Primary Productivity
HDF – Hierarchical Data Format
HIRS – High-resolution Infrared Sounder
ICA - Independent Components Analysis
IDL – Interactive Data Language
iMAD – Iteratively Reweighted Multivariate Alteration Detection
ISIN – Integrated Sinusoidal
LAEA - Lambert Azimuthal Equal-Area
LAI – Leaf Area Index
Landsat – Land Remote Sensing Satellite
LEDAPS – Landsat Ecosystem Disturbance Adaptive Processing System
LDCM – Landsat Data Continuity Mission
$_{L}$NBRI - 2001-2011 time series of Landsat NBRI yearly composites
$_{L}$NDVI – 2001-2011 time series of Landsat NDVI yearly composites
LST – Land Surface Temperature
LSWI – Land Surface Water Index
MBD – Minimum Begin Day

MED – Minimum End Day

MIDI – Microwave Integrated Drought Index

MIR – Mid-Infrared

MOD13Q1 – MODIS-Terra 16-day Vegetation Index product of 250 m resolution

MODIS – Moderate-Resolution Imaging Spectroradiometer

MRT – MODIS Reprojection Tool

MSS – Multi-Spectral Scanner

MV – Maximum Value

NBR – Normalized Burn Ratio

NBRI – Normalized Burn Ratio Index

NDII – Normalized Difference Infrared Index

NDII6 – Normalized Difference Infrared Index derived using MODIS band 6

NDII7 – Normalized Difference Infrared Index derived using MODIS band 7

$NDII7_{HS}$ – 2001-2013 MODIS high-season (14^{th}-17^{th}) NDII7 mean time series

NDMI - Normalized Difference Moisture Index

NDVI – Normalized Difference Vegetation Index

$NDVI_{1-23}$ – Complete 2001-2013 MODIS NDVI time series

$NDVI_{8-18}$ – Vegetation season 2001-2013 MODIS NDVI time series

$NDVI_{HS}$ – 2001-2013 MODIS high-season (14^{th}-17^{th}) NDVI mean time series

$NDVI_{SG1-23}$ – Complete 2001-2013 MODIS NDVI time series after Savitzky-Golay filtering

$NDVI_{SG8-18}$ – Vegetation season 2001-2013 MODIS NDVI time series after Savitzky-Golay filtering

NDWI – Normalized Difference Water Index

NDWI5 – Normalized Difference Water Index derived using MODIS band 5

NDWI6 – Normalized Difference Water Index derived using MODIS band 6

$NDWI_{1640}$ – Normalized Difference Water Index derived using MODIS band 6

NIR – Near-infrared

$nNDII7_{14-17}$ – z-score normalized high-season season 2001-2013 MODIS NDII7 time series

$nNDII7_{8-18}$ – z-score normalized vegetation season 2001-2013 MODIS NDII7 time series

$nNDVI_{1-23}$ – z-score normalized 2001-2013 MODIS NDVI time series

$nNDVI_{14-17}$ – z-score normalized high-season 2001-2013 MODIS NDVI time series

$nNDVI_{8-18}$ – z-score normalized vegetation season 2001-2013 MODIS NDVI time series

$nNDVI_{SG1-23}$ – z-score normalized 2001-2013 MODIS NDVI time series after Savitzky-Golay filtering

$nNDVI_{SG8-18}$ – z-score normalized vegetation season 2001-2013 MODIS NDVI time series after Savitzky-Golay filtering

OLI – Operational Land Imager

PAN - Panchromatic
PC – Principal Component
PCA – Principal component Analysis
PDSI – Palmer Drought Severity Index
PSF – Point Spread Function
QA – Quality Assessment/Assurance
SBD – Season Begin Day
scPDSI – self-calibrated Palmer Drought Severity Index
Sea-WIFS – Sea-Viewing Wide Field-of-View Sensor
SED – Season End Day
SG – Savitzky-Golay filter
SI – Seasonal Integral
SL – Season Length
SLC - Scan-Line Corrector
SPEI – Standardized Precipitation-Evapotranspiration Index
SPI – Standardized Precipitation Index
Suomi NPP - Suomi National Polar-orbiting Partnership
SVD - Signal Value Decomposition
SWI – Soil Water Index
SWIR – Short-wavelength Infrared
SWSI – Surface Water Supply Index
TM – Thematic Mapper
USGS – United States Geological Survey
UTM – Universal Transverse Mercator
VegDRI – Vegetation Drought Response Index
VIIRS - Visible Infrared Imaging Radiometer Suite
WRS-2 – World Reference System 2
YA – Year Ago